



UNIVERSIDAD DE MÁLAGA

TESIS DOCTORAL

María Irene Badía Domínguez

Málaga, 2022

Understanding the diradical character,  
cyclophane formation and molecular  
properties of carbazole-based systems



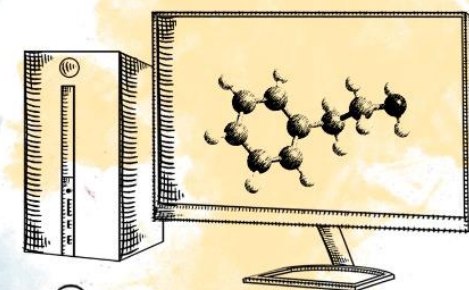
UNIVERSIDAD  
DE MÁLAGA

M<sup>a</sup> Irene Badía Domínguez

TESIS DOCTORAL

2022

Understanding the diradical character,  
cyclophane formation and molecular  
properties of carbazole-based systems



TESIS DOCTORAL

María Irene Badía Domínguez

Málaga, 2022

Directores: María del Carmen Ruiz Delgado y Víctor Hernández Jolín  
Doctorado en Química y Tecnología Química y Materiales y Nanotecnología  
Departamento de Química Física, Facultad de Ciencias, Universidad de Málaga

Universidad de Málaga  
Facultad de Ciencias



**Understanding the diradical character,  
cyclophane formation and molecular  
properties of carbazole-based systems**


Memoria de Tesis Doctoral presentada por  
María Irene Badía Domínguez

Málaga, 2022



UNIVERSIDAD  
DE MÁLAGA

AUTOR: María Irene Badía Domínguez

 <https://orcid.org/0000-0002-2736-8943>

EDITA: Publicaciones y Divulgación Científica. Universidad de Málaga



Esta obra está bajo una licencia de Creative Commons Reconocimiento-NoComercial-SinObraDerivada 4.0 Internacional:

<http://creativecommons.org/licenses/by-nc-nd/4.0/legalcode>

Cualquier parte de esta obra se puede reproducir sin autorización pero con el reconocimiento y atribución de los autores.

No se puede hacer uso comercial de la obra y no se puede alterar, transformar o hacer obras derivadas.

Esta Tesis Doctoral está depositada en el Repositorio Institucional de la Universidad de Málaga (RIUMA): [riuma.uma.es](http://riuma.uma.es)



## DECLARACIÓN DE AUTORÍA Y ORIGINALIDAD DE LA TESIS PRESENTADA PARA OBTENER EL TÍTULO DE DOCTOR

D./Dña. MARÍA IRENE BADÍA DOMÍNGUEZ

Estudiante del programa de doctorado QUÍMICA Y TECNOLOGÍAS QUÍMICAS, MATERIALES Y NANOTECNOLOGÍA de la Universidad de Málaga, autor/a de la tesis, presentada para la obtención del título de doctor por la Universidad de Málaga, titulada: "UNDERSTANDING THE DIRADICAL CHARACTER, CYCLOPHANE FORMATION AND MOLECULAR PROPERTIES OF CARBAZOLE-BASED SYSTEMS"

Realizada bajo la tutorización de MARÍA DEL CARMEN RUIZ DELGADO y dirección de MARÍA DEL CARMEN RUIZ DELGADO Y VÍCTOR HERNÁNDEZ JOLÍN

DECLARO QUE:

La tesis presentada es una obra original que no infringe los derechos de propiedad intelectual ni los derechos de propiedad industrial u otros, conforme al ordenamiento jurídico vigente (Real Decreto Legislativo 1/1996, de 12 de abril, por el que se aprueba el texto refundido de la Ley de Propiedad Intelectual, regularizando, aclarando y armonizando las disposiciones legales vigentes sobre la materia), modificado por la Ley 2/2019, de 1 de marzo.

Igualmente asumo, ante a la Universidad de Málaga y ante cualquier otra instancia, la responsabilidad que pudiera derivarse en caso de plagio de contenidos en la tesis presentada, conforme al ordenamiento jurídico vigente.

En Málaga, a 12 de SEPTIEMBRE de 2022

Fdo.: M <sup>a</sup> IRENE BADÍA DOMÍNGUEZ Doctorando/a	Fdo.: M <sup>a</sup> CARMEN RUIZ DELGADO Tutor/a
Fdo.: M <sup>a</sup> CARMEN RUIZ DELGADO y VÍCTOR HERNÁNDEZ JOLÍN Director/es de tesis	



Dña. María del Carmen Ruiz Delgado, Profesora Titular del Departamento de Química-Física de la Universidad de Málaga y D. Víctor Hernández Jolín, Catedrático del Departamento de Química Física de la Universidad de Málaga,

Certifican:

Que la memoria presentada por María Irene Badía Domínguez bajo el título "UNDERSTANDING THE DIRADICAL CHARACTER, CYCLOPHANE FORMATION AND MOLECULAR PROPERTIES OF CARBAZOLE-BASED SYSTEMS" para optar al grado de Doctora en Ciencias Químicas por la Universidad de Málaga, ha sido realizada bajo nuestra dirección en los laboratorios del Departamento de Química Física y en el Servicio de Espectroscopía Vibracional del Servicio Central de Apoyo a la Investigación de la Universidad de Málaga.

Considerando que constituye una investigación de alta calidad, se autoriza mediante este escrito su presentación y defensa como Tesis Doctoral en la Facultad de Ciencias de la Universidad de Málaga.

Y para que así conste, firman el presente certificado en Málaga a 12 de SEPTIEMBRE de 2022

Fdo.: M<sup>a</sup> Carmen Ruiz Delgado

Fdo.: Víctor Hernández Jolín



D. Juan Carlos Otero Fernández de Molina, Catedrático de la Universidad de Málaga y Director del Departamento de Química Física de la Universidad de Málaga,

Certifica:

Que la Tesis Doctoral titulada "UNDERSTANDING THE DIRADICAL CHARACTER, CYCLOPHANE FORMATION AND MOLECULAR PROPERTIES OF CARBAZOLE-BASED SYSTEMS", que constituye la memoria que presenta Dña. María Irene Badía Domínguez para optar al título de Doctora en Ciencias Químicas por la Universidad de Málaga, ha sido realizada bajo la dirección de Dña. María del Carmen Ruiz Delgado y D. Víctor Hernández Jolín, en el Departamento de Química Física de la Universidad de Málaga.

Y para que así conste, firma el presente certificado en Málaga a 12 de SEPTIEMBRE de 2022

Fdo.: Juan Carlos Otero Fernández de Molina



## Agradecimientos

Poner punto final a esta etapa de mi vida no hubiese sido posible sin el apoyo desinteresado de todas y cada una de las personas que me han acompañado a lo largo de esta aventura. A pesar de lo difícil que puede llegar a ser escribir estas líneas, quiero esforzarme por decir las cosas que se piensan, pero casi nunca se dicen.

Las primeras líneas se las quería dedicar, como no podía ser de otro modo, a mis directores de Tesis, Maricarmen y Víctor. A vosotros os debo la oportunidad de crecer y ser la científica que soy hoy en día. Soy feliz de pensar que, como yo, las próximas personas con la inmensa suerte de toparse con vosotros podrán ser mejores gracias a vuestro ejemplo. Gracias, Víctor, por enseñarme que la investigación científica es muchísimo más que pulsar un botón para que aparezcan espectros; gracias por demostrarme cada día la grandísima persona que eres y la gran calidad humana que tienes; gracias por tu alegría contagiosa y por tu apoyo constante. Mi doctorado hubiera estado vacío sin erte decir “Huracán Airiín”.

Para agradecer a Maricarmen todo lo que ha hecho por mí durante tantos años me faltarían páginas. Siete años trabajando juntas no se pueden resumir en un párrafo. Sin embargo, quiero hacer especial mención a dos cosas que me hacen sentirme afortunada de trabajar contigo. A nivel laboral, no he podido tener un referente mejor; gracias por enseñarme lo que es el trabajo, el esfuerzo, la dedicación, la constancia, el sacrificio, la paciencia... Gracias por tus útiles consejos y palabras de aliento cuando no sabía cómo conseguir lo que hoy he logrado. A nivel personal, debo elevar mi agradecimiento a un nivel superior y es que, para mí, has sido mucho más que una “jefa”. Gracias por tu apoyo en uno de los momentos más difíciles de mi vida. Gracias por nuestras charlas científicas (y no tan científicas) que hacían que mi doctorado tuviera sentido. Gracias por dedicarme tiempo, aun cuando no lo tenías. Gracias por enseñarme que hay que



cuidar de uno mismo y que antes que científicos, somos personas. En fin, gracias por TODO.

Por supuesto, no puedo evitar dar las gracias a la persona que supo guiar a aquella muchacha inocente que quería formar parte de su grupo de investigación. Gracias por estar ahí, Teo.

También quiero dedicar un espacio a dos excelentes científicas que he tenido la suerte de conocer en esta enriquecedora etapa. A Rocío, gracias por aportarme una visión tan cercana de la ciencia y por demostrarme que, siguiendo el ejemplo de mujeres como tú, se pueden conseguir grandes logros. A María, gracias por ser un ejemplo de valentía y dedicación. Marta puede estar orgullosa de la madre que tiene.

Además, tengo que agradecer a mucha gente que me han acompañado en este largo camino. Gracias, Rafa, por tus sabios consejos sobre la tesis. Mis inicios en la química computacional no fueron tan duros gracias a ti. Eskerrik asko, Iratxe, por enseñarme lo que es la determinación; tu firmeza hizo que fueras un pilar del grupo. Gracias, Sara y Guzmán, por ser la pareja con la que he compartido tantas risas. Los congresos sin vosotros no son lo mismo. Gracias, Cristina y Zafra, por ser los mayores apoyos que he tenido en el laboratorio. Gracias por aguantar mis “preguntillas” y por hacer que las largas jornadas de trabajo sean tan amenas. Gracias, Raúl (el neófito del grupo), por tu disposición y por tus entradas en el despacho para preguntar cómo va todo. Estoy segura de que conseguirás todo lo que te propongas. Gracias, Alexandra, por ser la alegría de la huerta y tener siempre una frase para cada ocasión. Ha sido muy bonito compartir este camino contigo. Gracias, Sergio Moles, por ser el “*abullaor*” y hacer que el trabajo cunda. Gracias por ser tan cercano y atento.

Gracias Marivi por todo el tiempo y las palabras que me has dedicado. Esta portada no hubiera sido posible sin tus dotes en diseño gráfico.





Llegados a este punto, no quiero dejar en el tintero al Prof. Juan Carlos Sancho García de la Universidad de Alicante y a la Prof. Fabrizia Negri de la Universidad de Bolonia. Gracias, Juan Carlos, por permitirme trabajar con tu grupo y enseñarme tantas cosas que han ayudado a completar esta tesis. *One of the best experiences that PhD has given me is the time in Bologna. Thank Fabrizia for giving me the opportunity to work with you and meet your amazing town.*

Son muchas las personas que he conocido gracias al doctorado (Andrés, Jesús, Fabio, Bea, Sofia, Yazí, Daniele, Sara, Iván, Raúl...), pero quiero hacer especial mención a dos, Nadia y Ana Claudia. Ellas me enseñaron que existe “la amistad a primera vista”. Por supuesto, no se me puede olvidar mencionar a Samara, ejemplo de superación y entrega. Gracias por tus charlas motivacionales que me hacían pensar que podía con todo. Gracias por hacer que los días para olvidar se convirtiesen en desayunos con churros. Sin ti, muchos momentos hubieran sido más grises.

Cómo olvidar a las personas con la que he compartido más penas y alegrías durante estos años. Gracias, Sergio Gámez, por ser mi apoyo durante todo este tiempo. Gracias por enseñarme lo que es la confianza y por tratarme como a una hermana. No hubiera podido tener un compañero de despacho mejor. Gracias, Abel, por nuestras charlas después de trabajar. Gracias por hacerme reír hasta acabar en el suelo. Gracias por ir siempre de mi mano y ser un amigo leal. A los dos os debo muchas risas cuando todo iba bien y mucho apoyo cuando todo iba mal. Gracias por enseñarme que la amistad puede durar para siempre.

Fuera del ámbito laboral, he tenido la suerte de tener a personas que aun sin entender mi trabajo, no me han dejado sola ni un momento. Hablo de mi familia. Gracias a Toño, Maribén, Pablo y Javi, mis “siempre alegres”. Gracias por enseñarme que la familia no necesita compartir ADN. Gracias por hacerme sentir que puedo con todo. Gracias a mi hermana Beatriz, a Luis, a



Aarón y a Sira, mi “hogar”. Gracias por ser mi fuente de inspiración y darme seguridad. Sois el lugar al que volver la mirada para coger aire. Gracias a Joaquín y a Mariví, mis padres. Sin vosotros, yo no estaría aquí escribiendo estas palabras. Sois mi ejemplo a seguir, mi escuela de confianza, de autoestima y de valentía. En resumen, sois mi vida.

He querido dejar para el final a la persona que indirectamente me ha ayudado más durante estos años. Gracias a Antonio, mi marido. Gracias por ser mi mejor amigo y por enseñarme que para casarnos solo hacíamos falta tu y yo. Gracias por darme confianza para no rendirme ante nada, por ayudarme a ser mejor, por tu templanza y paciencia. Gracias por hacer que mis lagrimas sean de felicidad. Me siento muy afortunada de poder compartir mi vida contigo.

Gracias, Irene, por todas esas batallas silenciosas que luchaste.







## Contents

### Section 1: Introduction

1.1 Introduction to organic conjugated materials. ....	1
1.2 Organic electronics: historical background. ....	3
1.3 Carbazole-based organic compounds: structure and applications. 6	
1.4 Diradical systems and dynamic covalent chemistry. ....	12
1.5 Systems under study and aim of this Thesis. ....	17
1.6 Bibliography. ....	26

### Section 2: Methodology

2.1 Spectroscopic methods.....	43
2.1.1 Electronic Absorption Spectroscopy.....	45
2.1.1.1 The experimental techniques. ....	47
2.1.2 Vibrational Infrared Spectroscopy.....	49
2.1.2.1 The experimental techniques. ....	50
2.1.3 Vibrational Raman Spectroscopy. ....	51
2.1.3.1 The experimental techniques. ....	53
2.1.4 Variable temperature studies. ....	55
2.2 Quantum chemistry methods. ....	56
2.2.1 Introduction to the quantum chemistry methods.....	56
2.2.2 Density functional theory method.....	58
2.2.2.1 Time-dependent density functional theory. ....	64
2.2.2.2 Charge transport parameters. ....	64
2.2.2.3 Aromatic parameters. ....	66
2.2.2.4 Physical parameters.....	66
2.2.2.5 Frequency calculations.....	68
2.2.3 Software Details. ....	70
2.3 Fabrication and characterization of OFETs.....	71
2.3.1 The experimental techniques. ....	72
2.4 Bibliography. ....	74



## Section 3: Results and discussion

### 3.1 Chapter I: Evolution of the diradical character of dicyanomethylene substituted carbazole and indolocarbazole-based systems.

3.1.1 Introduction.....	87
3.1.2 Effect of substitution pattern and chain elongation on the diradical stability. ....	89
3.1.2.1 Ground-state electronic structure.....	89
3.1.2.2 Optical properties.....	94
3.1.2.3 Relationship between diradical character and aromaticity. ....	96
3.1.3 Influence of the structural isomerism on the diradical stability. ....	99
3.1.3.1 Ground-state electronic structure.....	101
3.1.3.2 Relationship between diradical character and aromaticity. ....	107
3.1.4 Conclusions. ....	111
3.1.5 Bibliography.....	112

### 3.2 Chapter II: Cyclophane self-assembly from carbazole and indolocarbazole-based diradicals.

3.2.1 Introduction.....	127
3.2.2 Cyclophane structural features.....	128
3.2.2.1 Carbazole-based molecules. ....	129
3.2.2.2 Indolocarbazole-based molecules. ....	131
3.2.3 Interconversion between cyclophane and monomer in solution.....	134
3.2.3.1 Carbazole-based molecules. ....	134
3.2.3.2 Indolocarbazole-based molecules. ....	139
3.2.4 Interconversion between cyclophane and monomer in solid-state.....	143
3.2.4.1 Carbazole-based molecules. ....	143



## Contents

3.2.4.2 Indolocarbazole-based molecules. ....	149
3.2.5 Conclusions. ....	154
3.2.6 Bibliography. ....	156
<b>3.3 Chapter III: Photophysical and charge transport properties of carbazole-based macrocycles.</b>	
3.3.1 Introduction. ....	165
3.3.2 Structural and photophysical properties of tetracarbazole-based macrocycles. ....	166
3.3.2.1 Effect of the substitution pattern (ortho, meta and para positions). ....	166
3.3.2.2 Effect of cyclization on the photophysical properties. ...	177
3.3.3 Charge transport properties of Cz-based macrocycles. ....	182
3.3.3.1 Tetracarbazole-based macrocycles: insertion of ethylene group. ....	182
3.3.3.2 Coronoid carbazole-based macrocycles: Influence of the isomerism. ....	195
3.3.4 Conclusions. ....	202
3.3.5 Bibliography. ....	203
<b>Section 4: Concluding observations. ....</b>	<b>215</b>
<b>Section 5: Resumen y conclusiones. ....</b>	<b>225</b>
<b>Section 6: Appendix. ....</b>	<b>257</b>
Appendix A. List of abbreviations and symbols. ....	257
Appendix B. List of publications. ....	260









# SECTION 1. Introduction

## Table of contents

---

- 1.1 Introduction to organic conjugated materials.
- 1.2 Organic electronics: historical background.
- 1.3 Carbazole-based organic compounds: structure and applications.
- 1.4 Diradical systems and dynamic covalent chemistry.
- 1.5 Systems under study and aim of this Thesis.
- 1.6 Bibliography.





### 1.1 Introduction to organic conjugated materials.

Nowadays, we are living in a world where electronic devices are becoming essential for everyday life. Some examples of electronic devices include television, smartphones, household appliances, computer processors, iPad stands, displays, office gadgets, and so on. In this sense, the scientists have been focused on the study of novel materials that can provide new structure-property relationships to design enhanced electronic devices. One of the key forms of this development has been a gradual shift away from inorganic devices towards organic and hybrid organic-inorganic devices<sup>1</sup>.

The inorganic compounds are characterized by the absence of the bonding of carbon and hydrogen atoms. All the inorganic compounds are mainly found in non-living things as minerals or geologically based-compounds (mainly metals). Also, the inorganic compounds show ionic bonds which keep atoms in very close proximity. Therefore, they are packed densely and consequently, they have high boiling as well as melting points. This fact causes high fabrication cost, low processability and hardness and strength structures. In addition, the presence of ionic bonds in inorganic compounds imply their capacity to ionize, allowing them to be good electro-conductors.

In contrast, the organic compounds are characterized by the presence of carbon and hydrogen bonds. All the organic compounds are mainly seen in living organisms as plant materials, proteins, lipids, or the DNA in our own body. When



## 1. Introduction

compared to inorganic compounds, the organic systems exhibit lower melting points due to their supramolecular architectures in the solid state which depends on weak intermolecular forces. Besides, most organic systems tend to be less dense because these compounds usually have more hydrogen atoms than inorganic systems. In summary, their low weight, low fabrication cost, structural properties or their high processability are some of the reasons why organic conjugated systems have been used as an alternative to conventional silicon-based compounds.

Recently, new promising materials known as metal-organic frameworks (MOFs) have attracted much interest during the last decades since they combine the intrinsic properties of organic systems as the processability or flexibility with the high electrical conductivity of inorganic compounds. MOFs contain metal ions or clusters coordinated to organic ligands. This class of structures are a prime example of the power of combining inorganic and organic chemistry, two disciplines which are often on opposite sides. The number of scientific publications about MOFs is considerably lower than inorganic and organic materials. Nevertheless, substantial progress has been made in recent years providing hope that MOFs could have an outstanding place in future electronic devices<sup>2-4</sup>.

As its name implies, the electrical conductivity can be described as the movement of electrons from one location to another. Thus, for organic conjugated materials, the behaviour of an electron depends directly on the energy of the highest



## 1. Introduction

occupied molecular orbital (HOMO) and lowest unoccupied molecular orbital (LUMO) levels and their proximity. The value of the HOMO-LUMO gap (HL gap) are prime connected with the position of HOMO and LUMO levels. Hence, the molecular design concept of organic conjugated systems with tuneable HOMO and LUMO levels has become a key principle to obtain high-performing materials<sup>5</sup>.

### 1.2 Organic electronics: historical background.

Historically, organic systems have been considered as insulators. Nevertheless, this concept changed with the research of new organic materials which displayed electrical conductivity. In 1948, D.D.Eley published an article entitled "*Phthalocyanines as Semiconductors*",<sup>6</sup> where the electrical conductivity of two phthalocyanines was examined (Figure 1.1a). Prof. Eley demonstrated that both copper-phthalocyanine and metal-free phthalocyanine show thermal- and photo-conductivity. In 1954, Akamatu and co-workers published an article entitled "*Electrical Conductivity of the Perylene-Bromine Complex*"<sup>7</sup> in which was found that perylene-bromine complex (Figure 1.1b) displayed good electrical conductance in solid-state and become one of the first semiconducting organic materials.

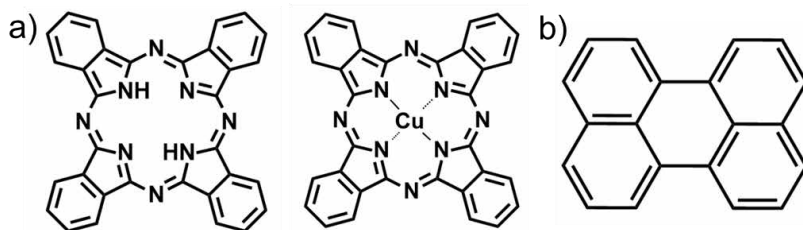


Figure 1.1 Chemical structures of (a) metal-free phthalocyanine (left) and copper-phthalocyanine (right) and (b) perylene.

Despite these relevant findings, the search for new semiconducting organic materials was not intensified up to 1970s. The first discovery was in 1973 when Ferraris *et al.* published an article entitled “*Electron transfer in a new highly conducting donor-acceptor complex*”<sup>8</sup> where the synthesis of a charge-transfer complex was reported. This complex between the electron donor tetrathiafulvalene (TTF) and the electron acceptor tetracyano-*p*-quinodimethane (TCNQ) presented a metallic electrical conductivity becoming the first organic metal (Figure 1.2a). The second discovery was in 1977 when the group of scientists formed by Alan J. Heeger, Alan MacDiarmid and Hideki Shirakawa observed that the conductivity of polyacetylene (Figure 1.2b) could be increased tremendously by chemical doping with oxidant species such as chlorine, bromine, or iodine<sup>9</sup>.<sup>10</sup> Furthermore, such increased conductivity from a traditional “insulator” promoted the development of fruitful research based on organic electronics.



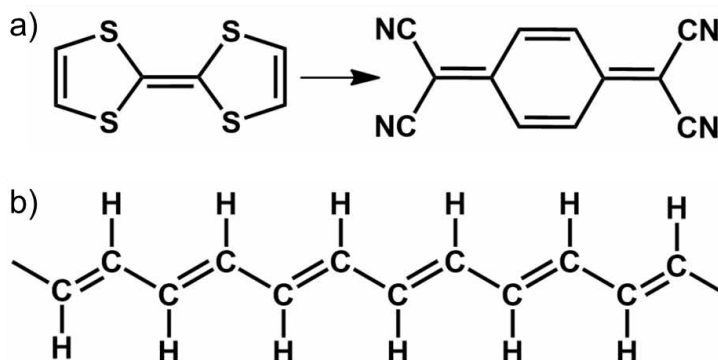


Figure 1.2 Chemical structures of (a) a complex between the electron donor tetrathiafulvalene (TTF) and the electron acceptor tetracyano-*p*-quinodimethane (TCNQ) and (b) *trans*-polyacetylene.

In fact, the Nobel Prize in Chemistry in 2000 was awarded to Heeger, MacDiarmid, and Shirakawa for “*the discovery and development of conducting polymers*”. Conducting polymers (CPs) are organic polymers with double bonds which are promising materials for electronic applications. Usually, doping transforms the CPs from insulators/semiconductors into useful conductors. Wishing to improve the properties of polyacetylene, different conjugated polymers were synthesized such as poly(*para*-phenylene) (PPP)<sup>11</sup>, poly(*para*-phenylenevinylene) (PPV)<sup>12</sup> or polyfluorene (PF)<sup>13-16</sup>, among others (Figure 1.3). These CPs presented high chemical and environmental stability (because of the introduction of heterocycles in the conjugated backbone) and are attractive derivatives for electronic applications.

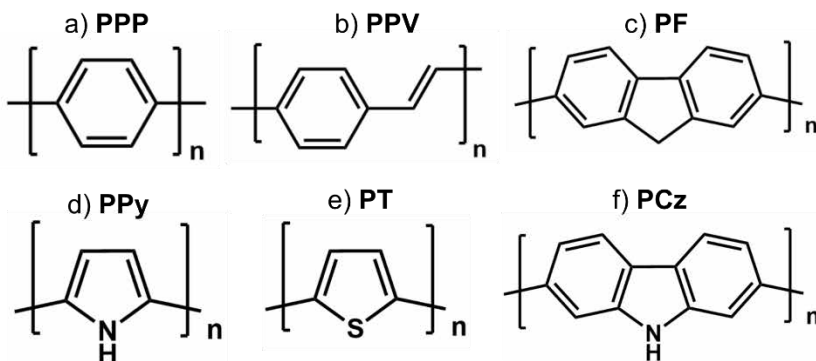


Figure 1.3 Examples of conducting polymers: (a) poly(*para*-phenylene), (b) poly(*para*-phenylenevinylene), (c) polyfluorene, (d) poly(pyrrole), (e) poly(thiophene) and (f) poly-(carbazole).

In addition, the incorporation of heteroatoms into the core of these organic conjugated materials is an effective way to modulate their electronic properties<sup>17</sup>. Sulphur and nitrogen atoms have been deeply utilized for such a purpose; for instance, poly(carbazole) (PCz)<sup>18</sup>, poly(pyrrole) (PPy)<sup>19</sup>, poly(thiophene) (PT)<sup>20, 21</sup> and so on, were successfully synthesized. In this sense, organic materials based on carbazole (Cz) and its derivatives have achieved a well-deserved status within the field of organic electronics due to their unique properties<sup>22-24</sup>.

### 1.3 Carbazole-based organic compounds: structure and applications.

In 1872, Graebe and Glaser discovered a molecule, constituting of two benzene rings fused on either side of a central pyrrole ring, named carbazole (C<sub>12</sub>H<sub>9</sub>N) or dibenzopyrrole (Figure 1.4)<sup>25</sup>.

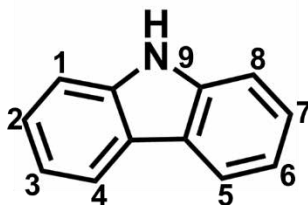


Figure 1.4 Chemical structure of a Cz unit and numeration.

The beginning of interest in Cz-based polymers (PCz) was in 1965 when H. Hoegl published an article entitled “*On Photoelectric Effects in Polymers and Their Sensitization by Dopants*”<sup>26</sup> in which was demonstrated the photoconductivity of poly(N-vinylcarbazole) (PVK). This interest has increased in the last five decades due to their good electro- and photoactive properties, such as high hole-transporting mobilities, with respect to other conducting polymers<sup>27</sup>. In fact, Cz exhibits several advantages over other heterocycles such as:

- 1) 9H-Cz is a cheap starting material available from coal-tar distillation.
- 2) Cz presents high chemical and experimental stability due to its fully aromatic unit.
- 3) The nitrogen atom can be easily functionalized with a wide variety of substituents to increase the solubility and to tune the optical and electrical properties. Also, it is possible to insert a large variety of substituents in the conjugated backbone (as in positions 3 and 6), modifying the physicochemical properties.

- 4) PCz shows a lower bandgap than traditional PPP because it possesses a bridged biphenyl unit.

These are some of the reasons why the Cz-based compounds are promising building blocks in organic electronics. There is extensive literature based on the synthesis of numerous Cz-based compounds and on the possibility to fine-tune their electronic and optical properties by chemical modifications allowing to obtain enhanced electronic devices<sup>24, 28-33</sup>. Detailed knowledge of the Cz properties together with a deep understanding of its structure/properties relationships are of large importance and represent the background to design useful systems based on Cz with desired properties. Concretely, the value of the HL gap of conjugated polymers plays a crucial role in electronic devices. The insertion of  $\pi$ -conjugated linkages or the attachment of substituents into the Cz backbone (such as electron-donating or accepting substituents) allow tuning this HL gap<sup>34</sup>.

On the one hand, Cz unit shows various active positions yielding poly(3,6-carbazole)s, poly(2,7-carbazole)s and poly(1,8-carbazole)s derivatives with different properties and applications (Figure 1.5).

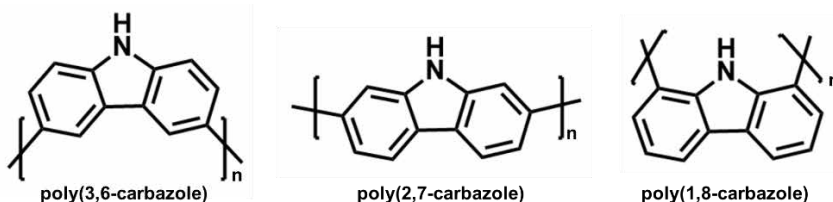


Figure 1.5 Chemical structures of PCz with different connectivity.



## 1. Introduction

During the last decade, the poly(3,6-carbazole) derivatives have been deeply investigated since they are the easiest to synthesize. Nevertheless, the N atom in this 3,6 connection is directly implicated in the conjugation which causes a conjugation break in the central core of the Cz units and consequently, a poor delocalization of the electrons in their structure. On the contrary, the 2,7 connection have longer conjugation because of their poly(p-phenylene)-like structure resulting in better applicability and properties for poly(2,7-carbazole)s<sup>18,35</sup>. Finally, the poly(1,8-carbazole) derivatives are the less stable and tend to produce the more distorted conjugated polymers because of the steric hindrance as a result of the N atom close connection compared to 3,6 and 2,7 positions<sup>36</sup>.

On the other hand, it is well-known that the Cz unit is an electron donor, and the incorporation of alkyl groups (to improve the solubility) enhances the electron-donating ability of the Cz unit since these functional groups are electron donor through inductive effect. Owing to the possibility of coupling between the Cz and other aromatic units; this can lead to molecules containing aromatic electron-withdrawing moieties and Cz electron-donating units. In this sense, the HL gap of Cz derivatives can be reduced by the insertion of an electron-withdrawing acceptor unit stimulating the intramolecular charge transfer (ICT) from the donor (D) to the acceptor (A) moiety. Thus, Cz can be linked to the acceptor moiety directly or using a  $\pi$ -linker. Accordingly, D-A small molecules based on Cz has been extensively utilized as

emitting materials over the last decades thanks to their ambipolar charge transport and their high photoluminescence efficiency<sup>37</sup>,

38.

Another way to reduce the HL gap values is to expand the  $\pi$ -conjugation upon the extension of the conjugated core (for instance, indolocarbazole (ICz) or diindolocarbazole (IICz) compounds)<sup>39</sup>. The indolo[3,2-b]carbazole is a pentacyclic fused heteroatomic compound which shows more  $\pi$ -conjugation than isolated Cz unit. Interestingly, the chemistry of indolo[3,2-b]carbazole has been reported in the literature evidencing an easy modulation of their properties by the insertion of functional groups<sup>40-45</sup>. However, note that indolo[3,2-b]carbazole is not the only member of this family but also possesses four other positional isomers with different phenyl linkages (ortho/meta/para) and different bridge structure (anti vs. syn), see Figure 1.6.

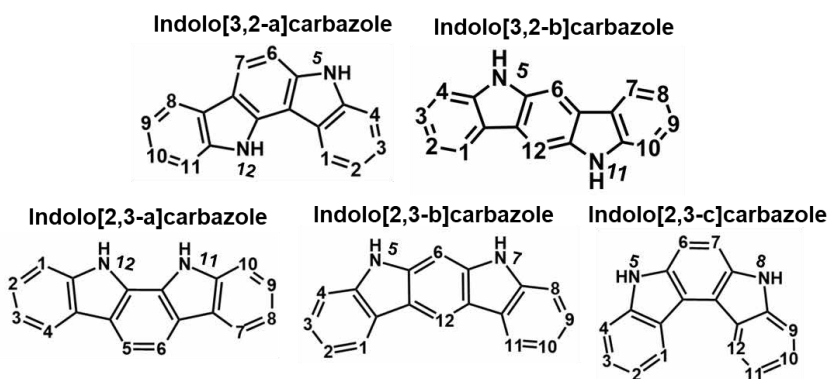


Figure 1.6 Chemical structure of five ICz isomers, with atom numbering indicated.

It is interesting to highlight that the charge mobility of organic systems is not only affected by the inherent molecular nature but

also by the supramolecular arrangement of the isolated molecules. Conjugated Cz-based macrocycles of limited size (Figure 1.7) appear in this scenario as an emerging family of materials with significant potential for electronic applications since their 2D structures allow for better electronic interactions between adjacent molecules. To this end up to now, several  $\pi$ -conjugated Cz-based macrocycles have been investigated to understand their electronic properties in order to rationally design materials with great potential for electronic applications<sup>46-</sup>

49.

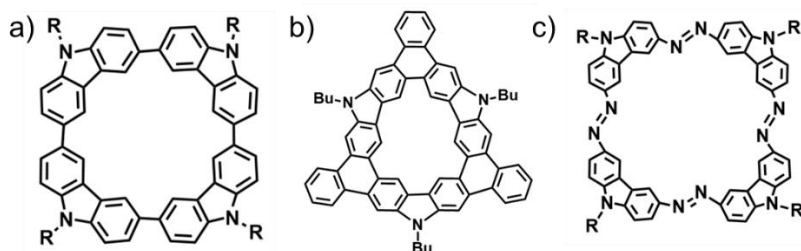


Figure 1.7 Examples of conjugated Cz-based macrocycles reported in the literature, known as (a) [4]Cyclo-N-ethyl-2,7-carbazole<sup>46</sup>, (b) Cz-fused polycyclic aromatic<sup>47</sup> and (c) tetraazocarbazole macrocycle<sup>48</sup>.

The Cz-based compounds are quite important from biological and environmental perspectives. These systems are widely used in the industry as building blocks to produce insecticides, dyes, reagents, so on<sup>50</sup>. Besides, their anti-inflammatory, antitumor, antioxidative and antimicrobial activities are some of the most important properties that present the Cz derivatives for their potential use in medicine<sup>27</sup>. Apart from biological characteristics, these compounds exhibit electrochemical, electronic, and electrical properties resulting in

various specific applications, such as photovoltaic devices, electroluminescent displays, batteries, bio(sensors), etc<sup>18,51</sup>.

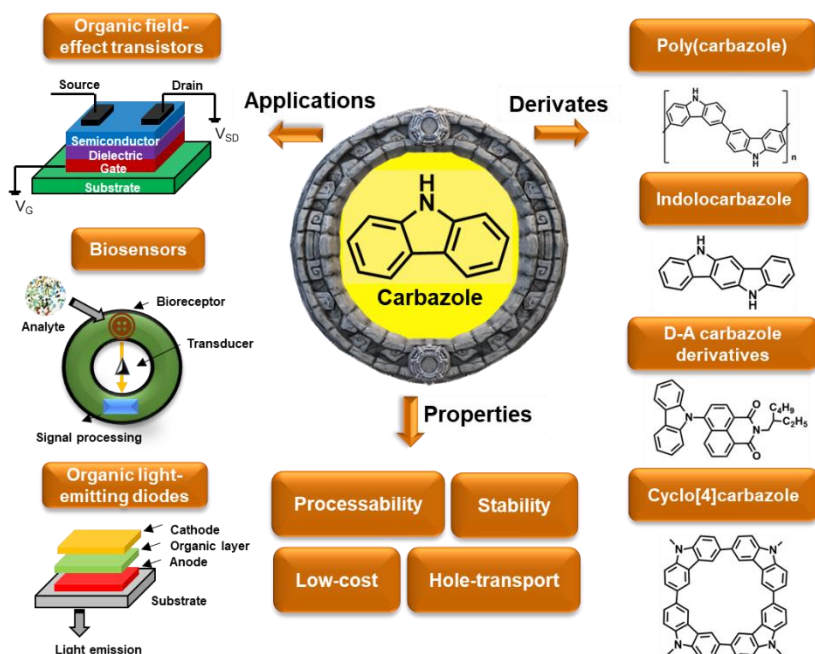


Figure 1.8 Scheme of applications, derivatives and properties of Cz systems.

## 1.4 Diradical systems and dynamic covalent chemistry.

Since the end of the last century, the development of open-shell (OS) organic conjugated materials has increased substantially because of their unique chemical and physical properties with great potential in various applications such as flexible organic electronics<sup>52,53</sup>, spintronics<sup>54,55</sup>, stimuli-responsive materials<sup>56-61</sup>, spin-crossover materials<sup>62,63</sup> or molecular self-assembly<sup>64</sup>, among others. The last few decades have witnessed the finding of OS organic conjugated diradicals increasingly stable as the result of improved synthetic strategies. According to IUPAC, "a diradical is a molecular specie having two unpaired





## 1. Introduction

*electrons, in which at least two different electronic states with different multiplicities (electron-paired (singlet state) or electron-unpaired (triplet state)) can be identified*"<sup>65</sup>. In other words, systems characterized by two unpaired electrons with a long distance between them would result in distinct singlet and triplet electronic states because of the negligible interelectronic interaction. The elucidation of the electronic configuration of these systems is fundamental to understand their electronic and structural properties<sup>66</sup>. Nevertheless, it is possible that two radical centres interact significantly, and in this case, these species are better defined as diradicaloids according to the IUPAC<sup>65</sup>. These species have two representative resonance forms in the ground singlet state (i) a closed-shell (CS) quinoid structure and (ii) an open-shell (OS) singlet diradical structure<sup>67, 68</sup>.

When the focus is on organic diradical systems, it is unavoidable to think in Thiele's and Chichibabin's hydrocarbons<sup>69,70</sup> since they have served as a basis for subsequent building a huge number of diradical systems. As seen in Figure 1.9, both possess representative resonance structures between an OS diradical state and a CS quinoid state. However, these two hydrocarbons proved to be highly unstable due to the contribution of the diradical character. Thus, the stabilization of diradical systems has become the main goal of scientists in the last decades. In this sense, the insertion of heteroatoms has played a key role in the development of new stable diradical molecules.

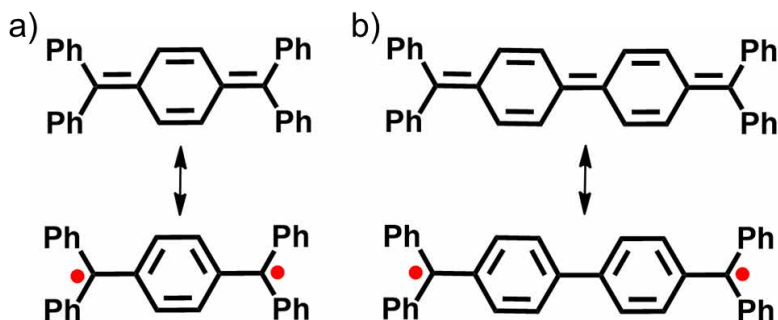


Figure 1.9 Resonant structures of (a) Thiele's hydrocarbon and (b) Chichibabin's hydrocarbon.

In 1966, Zimmerman and co-workers synthesized a bisimidazole derivative (called BDPI-2Y) with deep greenish-blue colour and a metallic lustre<sup>71</sup> (Figure 1.10a). This system showed about 0.1% of paramagnetic molecules in solution at room temperature (RT) and this percentage could be increased upon temperature rising. This leads scientists to think that there was a thermal equilibrium between a CS diamagnetic-quinoid ground state and an OS paramagnetic-diradical excited state. A noticeable finding was in 2004 when Abe and co-workers published an article entitled "*Definitive Evidence for the Contribution of Biradical Character in a Closed-Shell Molecule, Derivative of 1,4-Bis-(4,5-diphenylimidazol-2-ylidene)cyclohexa-2,5-diene*"<sup>72</sup> where it was demonstrated the contribution of a thermal excited diradical state to the ground state of a CS molecule, named as tF-BDPI-2Y, see Figure 1.10b.

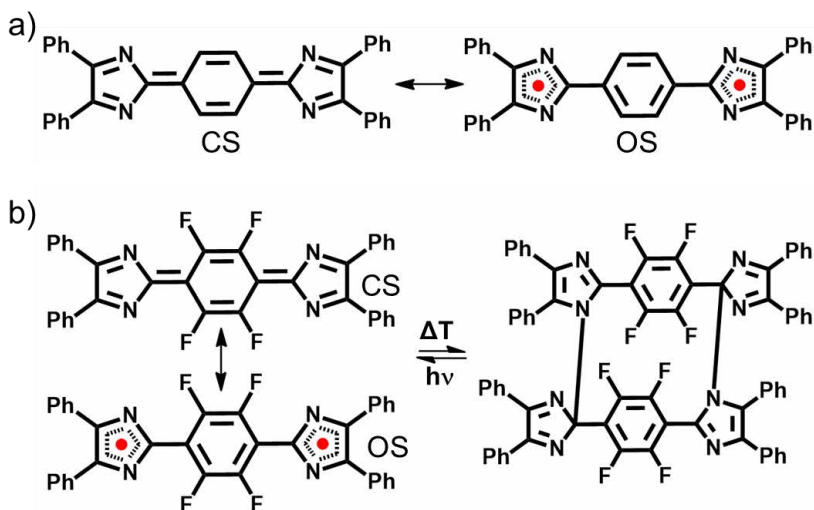


Figure 1.10 (a) Resonant structures of BDPI-2Y and (b) resonant structures of tF-BDPI-2Y and its dimeric form.

Oligothiophenes are another relevant example of the chemistry of heterocyclics with diradical character (Figure 1.11). In 2005, Otsubo and co-workers reported a family of oligothiophenequinodimethanes with terminal electron-withdrawing dicyanomethylene (DCM) groups where larger oligomers (*i.e.*, pentamer and hexamer systems) with NMR silent and ESR active, which was explained thanks to the existence of diradical species<sup>73</sup>. In this sense, Rocío Ponce and co-workers demonstrated that Raman spectroscopy is an extraordinarily powerful and versatile tool to discern the electronic and structural properties of diradical systems and the evolution from CS to OS state<sup>74, 75</sup>. All these discoveries together with many other relevant scientific contributions have given rise to very interesting diradical systems with potential material applications in different areas.

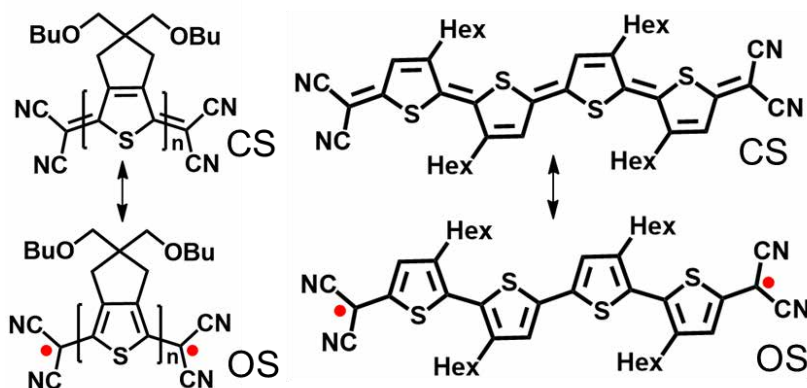


Figure 1.11 Resonant forms of oligothiophenes with terminal DCM groups.

Interestingly, it has been recently demonstrated that several diradical systems are able to form long C–C bonds between unpaired electrons from the radical centres of monomers resulting in macrocycles<sup>76</sup>, staircase oligomers<sup>77</sup>, or polymers by diradical polymerization<sup>78</sup>. Owing to this property, organic mono and diradicals have emerged as essential building blocks in dynamic covalent chemistry (DCC)<sup>79</sup>. This field is focused on the creation of structural scaffolds based on chemical components that interact through strong but reversible bonds<sup>80</sup>. Reversible homolytic covalent bond cleavage/formation involving radical species has been recently demonstrated to be an efficient strategy to obtain multi-responsive chromic soft materials<sup>59, 81-86</sup>. In addition, the rupture/formation of the long C–C bonds upon external stimuli is accompanied by a gradual colour change. These chromo-active materials have attracted much interest of the scientific community in different fields as they are able to reversibly change colour when (i) exposed to certain light



energies (photochromic switches)<sup>87, 88</sup>, (ii) slightly deformed with small compressive strain<sup>89, 90</sup> or (iii) lightly heated/cooled<sup>56, 57</sup>.

### 1.5 Systems under study and aim of this Thesis.

The main objective of this Thesis is to carry out an exhaustive study of the electronic and structural properties of certain Cz and ICz based systems using a combined experimental and theoretical approach that links electronic and vibrational spectroscopy (infrared and Raman) together with quantum-chemical calculations based on DFT theory.

In Chapter I and II, different structural modifications such as the substitution pattern, the elongation of the conjugated backbone or the isomerism of Cz and ICz based diradicals with terminal DCM groups have been investigated to explore the connection between these structural changes and the diradical character. Besides, we demonstrated that these Cz and ICz based diradicals can form long C-C  $\sigma$ -bonds between unpaired electrons resulting in cyclophane structures. Therefore, we also wanted to explore the relationship between the diradical character and the cyclophane stability and whether the transformation between the OS diradical state and the cyclophane structure is reversible or not.

In chapter III, we wanted to rationalize the structural, photophysical and charge transport properties of different families of Cz-based macrocycles which show promising characteristics in the field of organic electronics.



To clarify the exposition and discussion of the results, we classified this Thesis in two different blocks:

### **Block A. Cz and ICz-based diradical compounds.**

The main goal of this section is to rationalize how the structural changes of DCM-substituted Cz and ICz-based systems stabilize (or destabilize) the diradical character, thus affecting the formation/dissociation of stimuli-responsive cyclophanes. Concretely, we aim to establish a connection between the electronic and optical properties and chemical structural modifications providing new design guidelines for more efficient functional diradical systems. To make clear the discussion of the results, this block has been divided in two chapters (Chapter I and II).

---

Chapter I. Evolution of the diradical character of dicyanomethylene substituted carbazole and indolocarbazole-based systems.

---

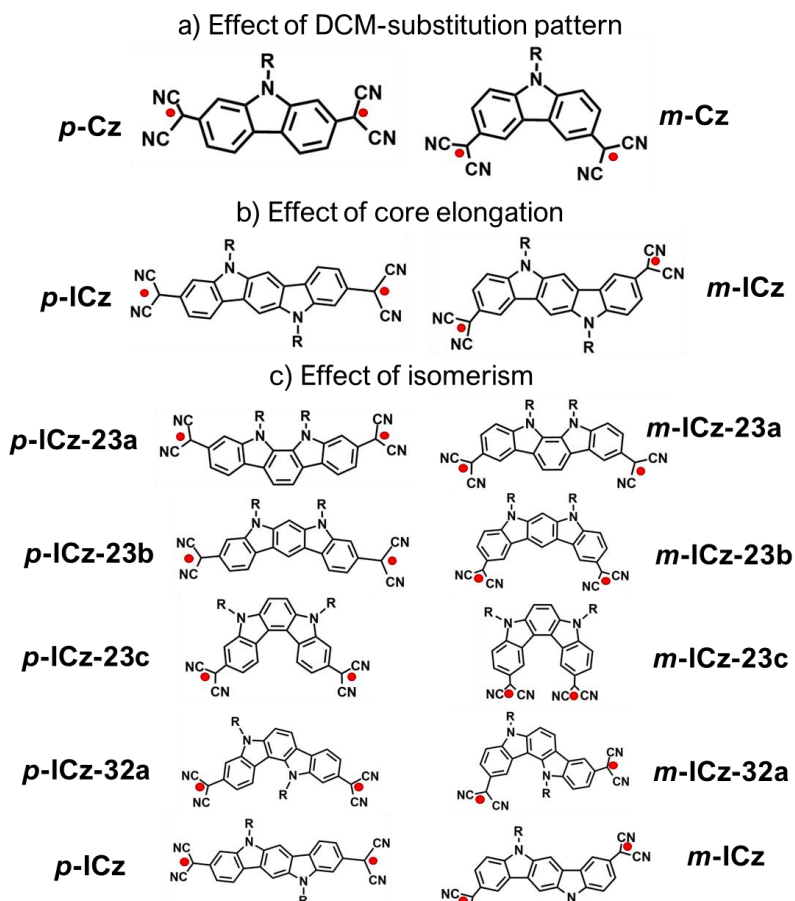


Figure 1.12 Whole set of DCM-substituted Cz and ICz-based systems studied in this section in their OS singlet state. A classification is made based on different structural modifications (a) effect of the DCM-substitution pattern, (b) effect of core elongation and (c) effect of isomerism.

Within this chapter, we carried out a purely theoretical study where the principal objective is to understand the relationship between the diradical character and the structural modifications (Figure 1.12). For this purpose, we have explored three different chemical structural changes:



## 1. Introduction

1) How the DCM-substitution pattern affects the stability of diradical species. To this end, we focused on the comparison between a para-substituted Cz compound and its meta-substituted Cz analogue. Both compounds present the same Cz core with DCM groups in para- or meta-positions (see Figure 1.12a).

2) How the elongation of the conjugated backbone affects the diradical character. To this end, we compared the previous Cz-based systems with the long chain ICz-based analogous (see Figure 1.12b).

3) How the structural isomerism influences the diradical character. Here we extend our study to the influence of isomerism for a family of ICz-based diradicals. The ICz possesses five positional isomers with different phenyl linkages (ortho/meta/para) and different bridge structure (anti vs. syn). In addition, by inserting DCM groups in different positions (para- or meta-positions), a library of ten ICz isomers is obtained, which represents a good dataset to understand the consequences of the topology changes in the diradical character (see Figure 1.12c).

---

Chapter II. Cyclophane self-assembly from carbazole and indolocarbazole-based diradicals.

---



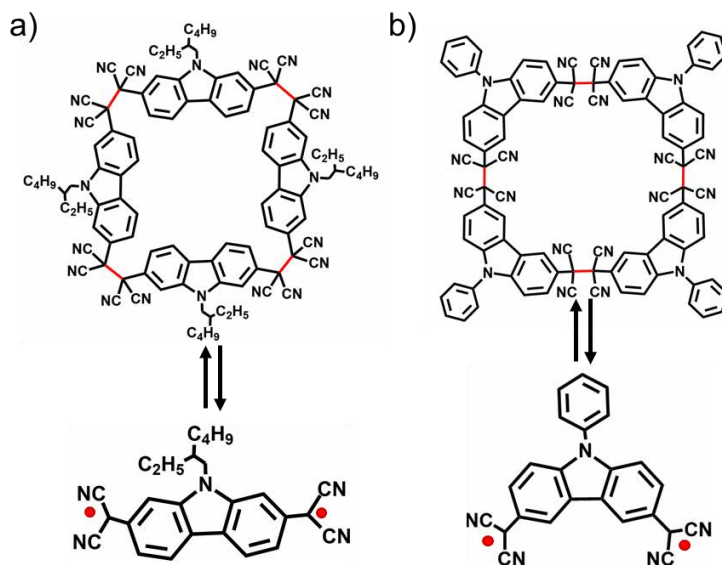


Figure 1.13 Equilibrium between the cyclophane-type oligomers and their corresponding isolated DCM-substituted *p*-Cz (a) and *m*-Cz (b) diradicals.

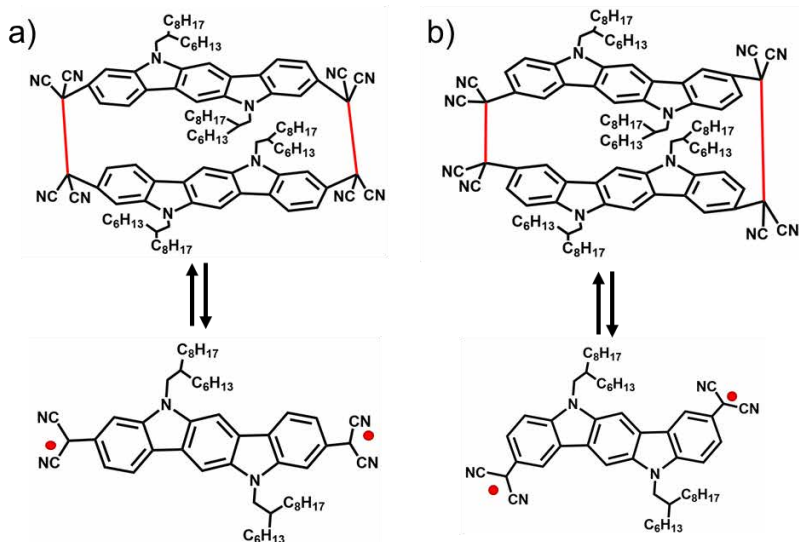


Figure 1.14 Equilibrium between the cyclophane-type oligomers and their corresponding isolated DCM-substituted *p*-ICz (a) and *m*-ICz (b) diradicals.



## 1. Introduction

As above-mentioned, several diradical systems can form cyclophane structures through the formation of long C-C  $\sigma$ -bonds between radicals which could result in strong colour changes. The aim of this chapter consists of the investigation of how external conditions affect the molecular structure and supramolecular organization of a family of Cz and ICz-based systems. Specifically, we will focus on the formation/dissociation of stimuli-responsive cyclophanes, and we will explore the dynamic and reversible transformation between  $\sigma$ -cyclophane structures and their isolated monomer diradicals upon stimuli (pressure, temperature, etc). To this purpose, we report an optical and vibrational study of a family of Cz and ICz-based diradicals (Figure 1.13-1.14) with DCM groups incorporated via para (***p*-Cz** and ***p*-ICz**) or meta positions (***m*-Cz** and ***m*-ICz**) aiming to identify potential new building blocks for stimuli-responsive materials.

The synthesis of the ***p*-Cz**<sup>84</sup>, ***p*-ICz**<sup>56</sup> and ***m*-ICz**<sup>91</sup> systems has been performed by the group of Professor Hongxiang Li, from the Shanghai Institute of Organic Chemistry of Chinese Academy of Sciences (Shanghai, China). The synthesis of the ***m*-Cz**<sup>58</sup> system has been performed by the group of Professor Shu Seki, from the Graduate School of Engineering of Kyoto University (Kyoto, Japan).

### **Block B. Cz-based macrocycles for organic electronics.**

In the previous block, we focused on how the chemical reactivity and physical properties of Cz, and ICz-based diradicals

are affected by structural changes. Now, we wanted to explore the electronic and charge transport properties of Cz-based macrocycles with potential applications in organic electronics.

In recent years, it has been demonstrated that cyclization of organic conjugated systems has numerous benefits for the development of electronic devices<sup>92,93</sup>. On the other hand, it is well known that organic conjugated systems based on Cz units have been recognized as “essential structures” due to their good electro- and photoactive properties, such as high hole-transporting mobilities, with respect to other heterocycles<sup>51,94-99</sup>. Thus, conjugated Cz-based macrocycles appear in this scenario as an emerging family of materials with large potential for electronic applications<sup>33,100</sup>. For that reason, Chapter III is focused on Cz-based macrocycles aiming at exploring their electronic, photophysical and charge transport properties.

---

Chapter III. Photophysical and charge transport properties of carbazole-based macrocycles.

---

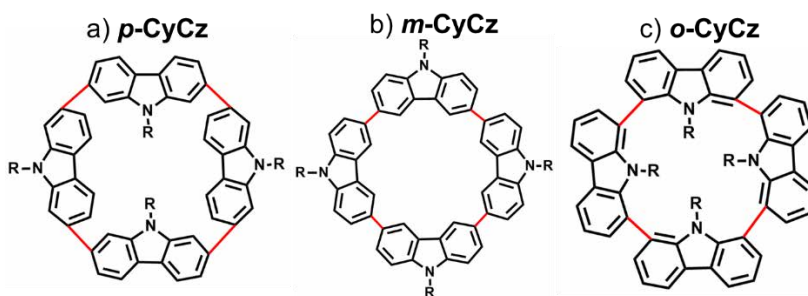


Figure 1.15 Chemical structures of tetracarbazole-based macrocycles where the Cz units are connected through para (a), meta (b) and ortho (c) positions.

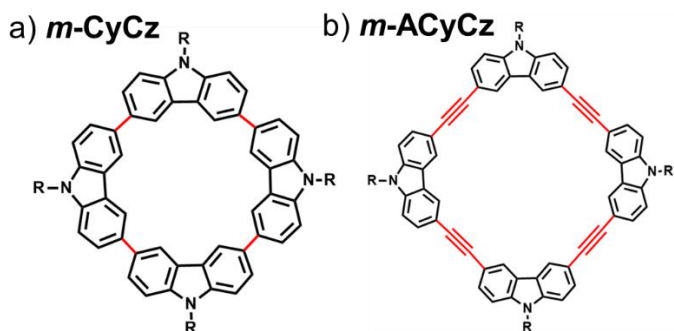


Figure 1.16 Chemical structures of tetracarbazole-based macrocycle *m-CyCz* (a) and its analogue molecule with ethylene groups *m-ACyCz*(b).

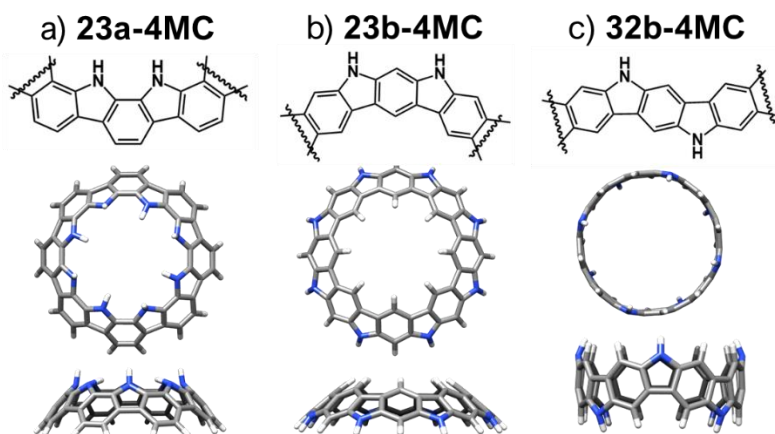


Figure 1.17 Chemical structures of the three isomers (a) **23a-4MC**, (b) **23b-4MC** and (c) **32b-4MC**, which contain four fully-fused ICz units.

In this chapter, several  $\pi$ -conjugated Cz-based macrocycles have been investigated with the aim of rationality their chemical structure and electronic properties with the resulting device performance (Figure 1.15-1.17). To this end, Chapter III has been organized in three different sections:



## 1. Introduction

1) A first section where we explored the effect of ortho, meta and para linking positions between the Cz units in tetracarbazole-based macrocycles (see Figure 1.15).

2) A second section where we investigated how the insertion of an ethylene group between the neighbouring Cz units in a tetracarbazole-based macrocycle affects the electronic communication of the conjugated backbone and thus their resulting charge transport properties (see Figure 1.16).

3) A third section where we carried out a purely theoretical study of a family of coronoid Cz-based molecules to test the usefulness of these macrostructures in organic electronics (see Figure 1.17).

At this point, it is important to note that close collaboration with different national and international research groups has been established during the development of this Thesis.

The synthesis of the ***p*-CyCz**<sup>46</sup> system has been performed by the group of Professor Cyril Poriel, from the university of Rennes (Rennes, France). ***m*-CyCz**<sup>101</sup> system has been synthesized by the group of Professor Feihe Huang, from the Centre of Chemistry of High-Performance & Novel materials (Hangzhou, China). The synthesis of the ***o*-CyCz**<sup>102</sup> system has been performed by the group of Professor Shuhei Higashibayashi, from the Institute for Molecular Science (Okazaki, Japan). ***m*-ACyCz**<sup>103</sup> system has been synthesized by the group of Professor Jeffrey Moore, from the Department of chemistry of the University of Illinois (Illinois, USA).



## 1. Introduction

Regarding the experimental results, Miriam Peña Alvarez from the University Complutense of Madrid performed the high-pressure Raman measurements; Yolanda Vida from the University of Málaga conducted the diffusion-ordered spectroscopy (DOSY) experiments; Raúl González Núñez from the University of Málaga carried out the fabrication and characterization of OFET devices. On the other hand, I performed a short research stay at the University of Alicante, under the supervision of Prof. Juan Carlos Sancho García dealing with the theoretical calculations of the diradical character presented in Chapter I. In addition, I also spent three months carrying out a research stay at the "Giacomo Ciamician" Chemistry Department of the University of Bologna, under the supervision of Prof. Fabrizia Negri. During this stay, a theoretical investigation of the low-lying excited electronic states of conjugated diradical systems, presented in Chapter I, were performed.

### 1.6 Bibliography.

1. Mir, S. H., Nagahara, L. A., Thundat, T., Mokarian-Tabari, P., Furukawa, H., and Khosla, A., Organic-inorganic hybrid functional materials: An integrated platform for applied technologies. *Journal of The Electrochemical Society* **2018**, 165, (8), B3137.
2. Feng, L.; Wang, K.Y.; Willman, J. and Zhou, H.C., Hierarchy in metal-organic frameworks. *ACS Central Science* **2020**, 6, (3), 359-367.
3. Stassen, I.; Burtch, N.; Talin, A.; Falcaro, P.; Allendorf, M. and Ameloot, R., An updated roadmap for the integration of metal-organic frameworks with electronic devices and chemical sensors. *Chemical Society Reviews* **2017**, 46, (11), 3185-3241.
4. Zhou, H.C.; Long, J.R.; Yaghi, O.M., Introduction to metal-organic frameworks. *Chemical reviews* **2012**, 112, (2), 673-674.



## 1. Introduction

5. Bendikov, M.; Wudl, F.; Perepichka, D.F., Tetrathiafulvalenes, oligoacenes, and their buckminsterfullerene derivatives: The brick and mortar of organic electronics. *Chemical Reviews* **2004**, 104, (11), 4891-4946.
6. Eley, D. D., Phthalocyanines as semiconductors. *Nature* **1948**, 162, (4125), 819-819.
7. Akamatu, H.; Inokuchi, H.; Matsunaga, Y., Electrical Conductivity of the Perylene–Bromine Complex. *Nature* **1954**, 173, (4395), 168-169.
8. Ferraris, J.; Cowan, D.; Walatka, V. t.; Perlstein, J., Electron transfer in a new highly conducting donor-acceptor complex. *Journal of the American Chemical Society* **1973**, 95, (3), 948-949.
9. Chiang, C.; Druy, M.; Gau, S.; Heeger, A.; Louis, E.; MacDiarmid, A. G.; Park, Y.; Shirakawa, H., Synthesis of highly conducting films of derivatives of polyacetylene,(CH) x. *Journal of the American Chemical Society* **1978**, 100, (3), 1013-1015.
10. Chiang, C. K.; Fincher Jr, C.; Park, Y. W.; Heeger, A. J.; Shirakawa, H.; Louis, E. J.; Gau, S. C.; MacDiarmid, A. G., Electrical conductivity in doped polyacetylene. *Physical review letters* **1977**, 39, (17), 1098.
11. Rehahn, M.; Schlüter, A.-D.; Wegner, G.; Feast, W. J., Soluble poly (para-phenylene) s. 1. Extension of the Yamamoto synthesis to dibromobenzenes substituted with flexible side chains. *Polymer* **1989**, 30, (6), 1054-1059.
12. Burroughes, J. H.; Bradley, D. D.; Brown, A.; Marks, R.; Mackay, K.; Friend, R. H.; Burns, P. L.; Holmes, A. B., Light-emitting diodes based on conjugated polymers. *Nature* **1990**, 347, (6293), 539-541.
13. Leclerc, M., Polyfluorenes: Twenty years of progress. *Journal of Polymer Science Part A: Polymer Chemistry* **2001**, 39, (17), 2867-2873.
14. Neher, D., Polyfluorene homopolymers: conjugated liquid-crystalline polymers for bright blue emission and polarized electroluminescence. *Macromolecular Rapid Communications* **2001**, 22, (17), 1365-1385.
15. Ranger, M.; Rondeau, D.; Leclerc, M., New well-defined poly (2, 7-fluorene) derivatives: photoluminescence and base doping. *Macromolecules* **1997**, 30, (25), 7686-7691.



16. Yang, Y.; Pei, Q.; Heeger, A., Efficient blue light-emitting diodes from a soluble poly (para-phenylene) internal field emission measurement of the energy gap in semiconducting polymers. *Synthetic metals* **1996**, 78, (3), 263-267.
17. Su, H.-C.; Fadhel, O.; Yang, C.-J.; Cho, T.-Y.; Fave, C.; Hissler, M.; Wu, C.-C.; Réau, R., Toward functional  $\pi$ -conjugated organophosphorus materials: design of phosphole-based oligomers for electroluminescent devices. *Journal of the American Chemical Society* **2006**, 128, (3), 983-995.
18. Bekkar, F.; Bettahar, F.; Moreno, I.; Meghabar, R.; Hamadouche, M.; Hernández, E.; Vilas-Vilela, J. L.; Ruiz-Rubio, L., Polycarbazole and its derivatives: Synthesis and applications. A review of the last 10 years. *Polymers* **2020**, 12, (10), 2227.
19. Watanabe, A.; Murakami, S.; Mori, K.; Kashiwaba, Y., Electronic properties of polypyrrole/n-Si heterojunctions and polypyrrole/metal contacts. *Macromolecules* **1989**, 22, (11), 4231-4235.
20. Leclerc, M., Optical and electrochemical transducers based on functionalized conjugated polymers. *Advanced materials* **1999**, 11, (18), 1491-1498.
21. McCullough, R. D., The chemistry of conducting polythiophenes. *Advanced materials* **1998**, 10, (2), 93-116.
22. Grazulevicius, J. V.; Strohmriegl, P.; Pielichowski, J.; Pielichowski, K., Carbazole-containing polymers: synthesis, properties and applications. *Progress in Polymer Science* **2003**, 28, (9), 1297-1353.
23. Karon, K.; Lapkowski, M., Carbazole electrochemistry: a short review. *Journal of Solid State Electrochemistry* **2015**, 19, (9), 2601-2610.
24. Sathiyam, G.; Sivakumar, E.; Ganesamoorthy, R.; Thangamuthu, R.; Sakthivel, P., Review of carbazole based conjugated molecules for highly efficient organic solar cell application. *Tetrahedron Letters* **2016**, 57, (3), 243-252.
25. Graebe, C.; Glaser, C., Ueber carbazol. *Justus Liebigs Annalen der Chemie* **1872**, 163, (3), 343-360.
26. Hoegl, H., On photoelectric effects in polymers and their sensitization by dopants. *The Journal of Physical Chemistry* **1965**, 69, (3), 755-766.





27. Nandy, B. C., Gupta, A. K., Mittal, A., and Vyas, V., Carbazole: It's biological activity. *J. Biomed. Pharm. Res*, **2014** 3, 42-48.
28. Brunner, K.; van Dijken, A.; Börner, H.; Bastiaansen, J. J.; Kikken, N. M.; Langeveld, B. M., Carbazole compounds as host materials for triplet emitters in organic light-emitting diodes: tuning the HOMO level without influencing the triplet energy in small molecules. *Journal of the American Chemical Society* **2004**, 126, (19), 6035-6042.
29. Gong, W.L.; Wang, B.; Aldred, M.P.; Li, C.; Zhang, G.F.; Chen, T.; Wang, L.; Zhu, M.Q., Tetraphenylethene-decorated carbazoles: synthesis, aggregation-induced emission, photo-oxidation and electroluminescence. *Journal of Materials Chemistry C* **2014**, 2, (34), 7001-7012.
30. Skórka, Ł.; Kurzep, P.; Wiosna-Sałyga, G.; Łuszczynska, B.; Wielgus, I.; Wróbel, Z.; Ulański, J.; Kulszewicz-Bajer, I., New diarylaminophenyl derivatives of carbazole: Effect of substituent position on their redox, spectroscopic and electroluminescent properties. *Synthetic metals* **2017**, 228, 1-8.
31. Tomkeviciene, A.; Grazulevicius, J.V.; Kazlauskas, K.; Gruodis, A.; Jursenas, S.; Ke, T.H.; Wu, C.C., Impact of linking topology on the properties of carbazole trimers and dimers. *The Journal of Physical Chemistry C* **2011**, 115, (11), 4887-4897.
32. Venkateswararao, A.; Thomas, K. R. J.; Lee, C.P.; Li, C.T.; Ho, K.C., Organic Dyes Containing Carbazole as Donor and  $\pi$ -Linker: Optical, Electrochemical, and Photovoltaic Properties. *ACS Applied Materials & Interfaces* **2014**, 6, (4), 2528-2539.
33. Zhu, H.; Badía-Domínguez, I.; Shi, B.; Li, Q.; Wei, P.; Xing, H.; Ruiz Delgado, M. C.; Huang, F., Cyclization-promoted ultralong low-temperature phosphorescence via boosting intersystem crossing. *Journal of the American Chemical Society* **2021**, 143, (4), 2164-2169.
34. Liao, L.; Pang, Y.; Ding, L.; Karasz, F. E., Blue-emitting soluble poly (m-phenylenevinylene) derivatives. *Macromolecules* **2001**, 34, (21), 7300-7305.
35. Boudreault, P.-L.T.; Beaupré, S.; Leclerc, M. Polycarbazoles for plastic electronics. *Polym. Chem.* **2010**, 1, 127-136.



36. Michinobu, T.; Osako, H.; Shigehara, K. Synthesis and Properties of 1,8-Carbazole-Based Conjugated Copolymers. *Polymers* **2010**, *2*, 159–173.
37. Ledwon, P., Recent advances of donor-acceptor type carbazole-based molecules for light emitting applications. *Organic Electronics* **2019**, *75*, 105422.
38. Zhang, H.; Wan, X.; Xue, X.; Li, Y.; Yu, A.; Chen, Y., Selective tuning of the HOMO–LUMO gap of carbazole-based donor–acceptor–donor compounds toward different emission colors. *Eur. J. Org. Chem.* **2010**, 1681–1687.
39. Janosik, T.; Rannug, A.; Rannug, U.; Wahlstrom, N.; Slatt, J.; Bergman, J., Chemistry and properties of indolocarbazoles. *Chemical Reviews* **2018**, *118*, (18), 9058-9128.
40. Irgashev, R. A.; Kazin, N. A.; Rusinov, G. L.; Charushin, V. N., A convenient synthesis of new 5,11-dihydroindolo[3,2-b]carbazoles bearing thiophene, 2,2'-bithiophene or 2,2':5',2"-terthiophene units at C-2 and C-8 positions. *Tetrahedron Letters* **2017**, *58*, (32), 3139-3142.
41. Irgashev, R. A.; Teslenko, A. Y.; Zhilina, E. F.; Schepochkin, A. V.; El'tsov, O. S.; Rusinov, G. L.; Charushin, V. N., Synthesis, photophysical and electrochemical properties of novel 6, 12-di (thiophen-2-yl) substituted indolo [3, 2-b] carbazoles. *Tetrahedron* **2014**, *70*, (31), 4685-4696.
42. Nakano, M.; Kishi, R.; Ohta, S.; Takahashi, H.; Kubo, T.; Kamada, K.; Ohta, K.; Botek, E.; Champagne, B., Relationship between third-order nonlinear optical properties and magnetic interactions in open-shell systems: a new paradigm for nonlinear optics. *Physical review letters* **2007**, *99*, (3), 033001.
43. Van Snick, S.; Dehaen, W., Synthesis of novel 2, 8-disubstituted indolo [3, 2-b] carbazoles. *Organic & Biomolecular Chemistry* **2012**, *10*, (1), 79-82.
44. Zhang, Y.; Zhang, T.; Wang, X.; Kong, L.; Yang, J., Indolo[3,2-b]carbazole derivatives with high fluorescent emission both in solution and aggregated states and mechanical-induced emission enhancement characteristic. *Dyes and Pigments* **2021**, *188*, 109230.
45. Streckaite, S.; Karpicz, R.; Gruodis, A.; Dehaen, W.; Van Snick, S.; Kirkus, M.; Grigalevicius, S.; Grazulevicius, J. V.; Gulbinas, V., Fluorescence quenching of indolo[3,2-b]carbazole



compounds by conformational motions of attached substituents. *Dyes and Pigments* **2016**, 133, 120-126.

46. Lucas, F.; Sicard, L.; Jeannin, O.; Rault-Berthelot, J.; Jacques, E.; Quinton, C.; Poriel, C., [4]Cyclo-N-ethyl-2,7-carbazole: Synthesis, Structural, Electronic and Charge Transport Properties. *Chemistry – A European Journal* **2019**, 25, (32), 7740-7748.

47. Zhao, M., Pun, S. H., Gong, Q., & Miao, Q., Carbazole-Fused Polycyclic Aromatics Enabled by Regioselective Scholl Reactions. *Angewandte Chemie* **2021**, 133, (45), 24326-24332.

48. Schweighauser, L.; Häussinger, D.; Neuburger, M.; Wegner, H. A., Symmetry as a new element to control molecular switches. *Organic & Biomolecular Chemistry* **2014**, 12, (21), 3371-3379.

49. Vehoff, T.; Baumeier, B.; Andrienko, D., Charge transport in columnar mesophases of carbazole macrocycles. *The Journal of Chemical Physics* **2010**, 133, (13), 134901.

50. Salam, L.B., Ilori, M.O. & Amund, O.O. Properties, environmental fate and biodegradation of carbazole. *Biotech* **2017**, 7, (2), 1-14.

51. Nayana, V.; Kandasubramanian, B., Polycarbazole and its derivatives: progress, synthesis, and applications. *Journal of Polymer Research* **2020**, 27, (9), 285.

52. Cui, Z., Abdurahman, A., Ai, X., & Li, F, Stable luminescent radicals and radical-based LEDs with doublet emission. *CCS chemistry* **2020**, 2, (4), 1129-1145.

53. Hu, X.; Wang, W.; Wang, D.; Zheng, Y., The electronic applications of stable diradicaloids: present and future. *Journal of Materials Chemistry C* **2018**, 6, (42), 11232-11242.

54. Chen, G.; Huang, S.; Shen, Y.; Kou, X.; Ma, X.; Huang, S.; Tong, Q.; Ma, K.; Chen, W.; Wang, P.; Shen, J.; Zhu, F.; Ouyang, G., Protein-directed, hydrogen-bonded biohybrid framework. *Chem* **2021**, 7, (10), 2722-2742.

55. Y. Gopalakrishna, T.; Zeng, W.; Lu, X.; Wu, J., From open-shell singlet diradicaloids to polyradicaloids. *Chemical Communications* **2018**, 54, (18), 2186-2199.

56. Badía-Domínguez, I.; Peña-Álvarez, M.; Wang, D.; Pérez Guardiola, A.; Vida, Y.; Rodríguez González, S.; López Navarrete, J. T.; Hernández Jolín, V.; Sancho García, J. C.; García Baonza, V.; Nash, R.; Hartl, F.; Li, H.; Ruiz Delgado, M. C., Dynamic



Covalent Properties of a Novel Indolo[3,2-b]carbazole Diradical. *Chemistry – A European Journal* **2021**, 27, (17), 5509-5520.

57. Badía-Domínguez, I.; Pérez-Guardiola, A.; Sancho-García, J. C.; López Navarrete, J. T.; Hernández Jolín, V.; Li, H.; Sakamaki, D.; Seki, S.; Ruiz Delgado, M. C., Formation of Cyclophane Macrocycles in Carbazole-Based Biradicaloids: Impact of the Dicyanomethylene Substitution Position. *ACS Omega* **2019**, 4, (3), 4761-4769.

58. Kobashi, T.; Sakamaki, D.; Seki, S., N-Substituted Dicyanomethylphenyl Radicals: Dynamic Covalent Properties and Formation of Stimuli-Responsive Cyclophanes by Self-Assembly. *Angewandte Chemie International Edition* **2016**, 55, (30), 8634-8638.

59. Zhang, R.; Peterson, J. P.; Fischer, L. J.; Ellern, A.; Winter, A. H., Effect of Structure on the Spin-Spin Interactions of Tethered Dicyanomethyl Diradicals. *Journal of the American Chemical Society* **2018**, 140, (43), 14308-14313.

60. Okino, K.; Hira, S.; Inoue, Y.; Sakamaki, D.; Seki, S., The Divergent Dimerization Behavior of N-Substituted Dicyanomethyl Radicals: Dynamically Stabilized versus Stable Radicals. *Angewandte Chemie International Edition* **2017**, 56, (52), 16597-16601.

61. Peterson, J. P.; Geraskina, M. R.; Zhang, R.; Winter, A. H., Effect of Substituents on the Bond Strength of Air-Stable Dicyanomethyl Radical Thermochromes. *The Journal of Organic Chemistry* **2017**, 82, (12), 6497-6501.

62. Geraskina, M. R.; Buck, A. T.; Winter, A. H., An Organic Spin Crossover Material in Water from a Covalently Linked Radical Dyad. *The Journal of Organic Chemistry* **2014**, 79, (16), 7723-7727.

63. Juetten, M. J.; Buck, A. T.; Winter, A. H., A radical spin on viologen polymers: organic spin crossover materials in water. *Chemical Communications* **2015**, 51, (25), 5516-5519.

64. Jin, Y.; Yu, C.; Denman, R. J.; Zhang, W., Recent advances in dynamic covalent chemistry. *Chemical Society Reviews* **2013**, 42, (16), 6634-6654.

65. Wilkinson, A. D. M. a. A., IUPAC. Compendium of Chemical Terminology, 2nd ed. (the "Gold Book"). In Publications, B. S., Ed. Oxford, 1997 Online version (2019-) created by S. J. Chalk.



66. Abe, M., Diradicals. *Chemical Reviews* **2013**, 113, (9), 7011-7088.
67. Dewar, M. J. S.; Healy, E. F., Ab initio study of the chair cope rearrangement of 1,5-hexadiene. *Chemical Physics Letters* **1987**, 141, (6), 521-524.
68. Li, Z.; Hou, Y.; Li, Y.; Hinz, A.; Chen, X., Biradicaloid and Zwitterion Reactivity of Dicarbondiphosphide Stabilized with N-Heterocyclic Carbenes. *Chemistry – A European Journal* **2018**, 24, (19), 4849-4855.
69. Thiele, J.; Balhorn, H., Ueber einen chinoïden Kohlenwasserstoff. *Berichte der deutschen chemischen Gesellschaft* **1904**, 37, (2), 1463-1470.
70. Tschitschibabin, A. E., Über das Triphenylmethyl. *Berichte der deutschen chemischen Gesellschaft* **1907**, 40, (3), 3056-3058.
71. Mayer, U.; Baumgärtel, H.; Zimmermann, H., Biradicals, Quinones, and Semiquinones of the Imidazole Series. *Angewandte Chemie International Edition in English* **1966**, 5, (3), 311-311.
72. Kikuchi, A.; Iwahori, F.; Abe, J., Definitive Evidence for the Contribution of Biradical Character in a Closed-Shell Molecule, Derivative of 1,4-Bis-(4,5-diphenylimidazol-2-ylidene)cyclohexa-2,5-diene. *Journal of the American Chemical Society* **2004**, 126, (21), 6526-6527.
73. Takahashi, T.; Matsuoka, K.-i.; Takimiya, K.; Otsubo, T.; Aso, Y., Extensive Quinoidal Oligothiophenes with Dicyanomethylene Groups at Terminal Positions as Highly Amphoteric Redox Molecules. *Journal of the American Chemical Society* **2005**, 127, (25), 8928-8929.
74. Casado, J.; Ponce Ortiz, R.; López Navarrete, J. T., Quinoidal oligothiophenes: new properties behind an unconventional electronic structure. *Chemical Society Reviews* **2012**, 41, (17), 5672-5686.
75. Ponce Ortiz, R.; Casado, J.; Hernández, V.; López Navarrete, J. T.; Viruela, P. M.; Ortí, E.; Takimiya, K.; Otsubo, T., On the Biradicaloid Nature of Long Quinoidal Oligothiophenes: Experimental Evidence Guided by Theoretical Studies. *Angewandte Chemie International Edition* **2007**, 46, (47), 9057-9061.



76. Hu, P.; Wu, J., Modern zethrene chemistry. *Canadian Journal of Chemistry* **2017**, 95, (3), 223-233.
77. Thomas, H. M.; Kumari, H.; Maddalena, J.; Mayhan, C. M.; Ellis, L. T.; Adams, J. E.; Deakyne, C. A., Conformational preference and dynamics of pyrogallol[4]arene: stability, interconversion, and solvent influence. *Supramolecular Chemistry* **2018**, 30, (5-6), 520-532.
78. Huang, J.; Kertesz, M., Intermolecular Covalent  $\pi$ - $\pi$  Bonding Interaction Indicated by Bond Distances, Energy Bands, and Magnetism in Biphenalenyl Biradicaloid Molecular Crystal. *Journal of the American Chemical Society* **2007**, 129, (6), 1634-1643.
79. Rowan, S. J.; Cantrill, S. J.; Cousins, G. R. L.; Sanders, J. K. M.; Stoddart, J. F., Dynamic Covalent Chemistry. *Angewandte Chemie International Edition* **2002**, 41, (6), 898-952.
80. Zafra, J. L.; Qiu, L.; Yanai, N.; Mori, T.; Nakano, M.; Alvarez, M. P.; Navarrete, J. T. L.; Gómez-García, C. J.; Kertesz, M.; Takimiya, K.; Casado, J., Reversible Dimerization and Polymerization of a Janus Diradical To Produce Labile C-C Bonds and Large Chromic Effects. *Angewandte Chemie International Edition* **2016**, 55, (47), 14563-14568.
81. Adinarayana, B.; Shimizu, D.; Furukawa, K.; Osuka, A., Stable radical versus reversible  $\sigma$ -bond formation of (porphyrinyl)dicyanomethyl radicals. *Chemical Science* **2019**, 10, (23), 6007-6012.
82. Chen, X.; Wang, X.; Zhou, Z.; Li, Y.; Sui, Y.; Ma, J.; Wang, X.; Power, P. P., Reversible  $\sigma$ -Dimerizations of Persistent Organic Radical Cations. *Angewandte Chemie International Edition* **2013**, 52, (2), 589-592.
83. Moshniaha, L.; Żyła-Karwowska, M.; Chmielewski, P. J.; Lis, T.; Cybińska, J.; Gońka, E.; Oschwald, J.; Drewello, T.; Rivero, S. M.; Casado, J.; Stępień, M., Aromatic Nanosandwich Obtained by  $\sigma$ -Dimerization of a Nanographenoid  $\pi$ -Radical. *Journal of the American Chemical Society* **2020**, 142, (7), 3626-3635.
84. Wang, D.; Capel Ferrón, C.; Li, J.; Gámez-Valenzuela, S.; Ponce Ortiz, R.; López Navarrete, J. T.; Hernández Jolín, V.; Yang, X.; Peña Álvarez, M.; García Baonza, V.; Hartl, F.; Ruiz Delgado, M. C.; Li, H., New Multiresponsive Chromic Soft Materials: Dynamic Interconversion of Short 2,7-Dicyanomethylenecarbazole-Based Biradicaloid and the



Corresponding Cyclophane Tetramer. *Chemistry – A European Journal* **2017**, 23, (55), 13776-13783.

85. Xiang, Q.; Xu, J.; Guo, J.; Dang, Y.; Xu, Z.; Zeng, Z.; Sun, Z., Unveiling the Hidden  $\sigma$ -Dimerization of a Kinetically Protected Olympicenyl Radical. *Chemistry – A European Journal* **2021**, 27, (31), 8203-8213.

86. Yokoi, H.; Hiroto, S.; Shinokubo, H., Reversible  $\sigma$ -Bond Formation in Bowl-Shaped  $\pi$ -Radical Cations: The Effects of Curved and Planar Structures. *Journal of the American Chemical Society* **2018**, 140, (13), 4649-4655.

87. Mutoh, K.; Miyashita, N.; Arai, K.; Abe, J., Turn-On Mode Fluorescence Switch by Using Negative Photochromic Imidazole Dimer. *Journal of the American Chemical Society* **2019**, 141, (14), 5650-5654.

88. Yamaguchi, T.; Hatano, S.; Abe, J., Multistate Photochromism of 1-Phenyl-naphthalene-Bridged Imidazole Dimer That Has Three Colorless Isomers and Two Colored Isomers. *The Journal of Physical Chemistry A* **2014**, 118, (1), 134-143.

89. Nagura, K.; Saito, S.; Yusa, H.; Yamawaki, H.; Fujihisa, H.; Sato, H.; Shimoikeda, Y.; Yamaguchi, S., Distinct Responses to Mechanical Grinding and Hydrostatic Pressure in Luminescent Chromism of Tetrathiazolylthiophene. *Journal of the American Chemical Society* **2013**, 135, (28), 10322-10325.

90. Oda, K.; Hiroto, S.; Shinokubo, H., NIR mechanochromic behaviours of a tetracyanoethylene-bridged hexa-peri-hexabenzocoronene dimer and trimer through dissociation of C–C bonds. *Journal of Materials Chemistry C* **2017**, 5, (22), 5310-5315.

91. Badía-Domínguez I., Wang D., Nash R., Hernández V., Li H., Hartl F., Ruiz Delgado M.C., Dynamic Covalent Cyclophanes Assembled from Indolo[3,2-b]carbazole-based Diradicals: Influence of Substitution Pattern. *In preparation*.

92. Ball M., Zhong Y., Fowler B., Zhang B., Li P., Etkin G., Paley D.W., Decatur J., Dalsania A.K., Li, H., Xiao S., Ng F., Steigerwald M.L. and Nuckolls, C., Macrocyclization in the design of organic n-type electronic materials. *Journal of the American Chemical Society*, **2016**, 138(39), 12861-12867.

93. Li, S., Liu, K., Feng, X. C., Li, Z. X., Zhang, Z. Y., Wang, B., and Li, C., Synthesis and macrocyclization-induced emission



enhancement of benzothiadiazole-based macrocycle. *Nature Communications*, **2022**, 13(1), 1-7.

94. Li, J.; Grimsdale, A. C., Carbazole-based polymers for organic photovoltaic devices. *Chemical Society Reviews* **2010**, 39, (7), 2399-2410.

95. Tomkeviciene, A.; Bartiuk, T.; Grazulevicius, J. V., Synthesis and properties of 2-(10,11-dihydrodibenz[b,f]azepine-5-yl)carbazole-based monomers and polymers. *Polymer Bulletin* **2012**, 68, (2), 453-464.

96. Hlel, A.; Mabrouk, A.; Chemek, M.; Ben Khalifa, I.; Alimi, K., A DFT study of charge-transfer and opto-electronic properties of some new materials involving carbazole units. *Computational Condensed Matter* **2015**, 3, 30-40.

97. Jenekhe, S. A.; Lu, L.; Alam, M. M., New Conjugated Polymers with Donor–Acceptor Architectures: Synthesis and Photophysics of Carbazole–Quinoline and Phenothiazine–Quinoline Copolymers and Oligomers Exhibiting Large Intramolecular Charge Transfer. *Macromolecules* **2001**, 34, (21), 7315-7324.

98. Peng, F.; Wang, X.; Guo, T.; Xiong, J.; Ying, L.; Cao, Y., Realizing efficient bipolar deep-blue light-emitting poly (2, 7-carbazole) derivatives by suppressing intramolecular charge transfer. *Organic Electronics* **2019**, 67, 34-42.

99. Strahan, J.; Popere, B. C.; Khomein, P.; Pointer, C. A.; Martin, S. M.; Oldacre, A. N.; Thayumanavan, S.; Young, E. R., Modulating absorption and charge transfer in bodipy-carbazole donor–acceptor dyads through molecular design. *Dalton Transactions* **2019**, 48, (23), 8488-8501.

100. Mao, L.; Zhou, M.; Niu, Y.-F.; Zhao, X.-L.; Shi, X., Aryl carbazole-based macrocycles: synthesis, their remarkably stable radical cations and host–guest complexation with fullerenes. *Organic Chemistry Frontiers* **2021**, 8, (17), 4678-4684.

101. Zhu, H., Shi, B., Chen, K., Wei, P., Xia, D., Mondal, J. H., & Huang, F., Cyclo [4] carbazole, an iodide anion macrocyclic receptor. *Organic letters*, **2016**, 18(19), 5054-5057.

102. Yamamoto, K., Pandit, P., and Higashibayashi, S., Non-Planar [n] Cyclo-1, 8-carbazolylenes (n= 3, 4, 6) and [3] Cyclo-1, 8-carbazolylenyl B, P, PO, SiPh Complexes. *Chemistry–A European Journal*, **2017**, 23(56), 14011-14016.





## 1. Introduction

103. Zhang, W., Cho, H. M., & Moore, J. S., Preparation of a carbazole-based macrocycle via precipitation-driven alkyne metathesis. *Organic Syntheses*, **2003**, 84, 177-191.







# SECTION 2. Methodology

## Table of contents

---

- 2.1 Spectroscopic methods.
    - 2.1.1 Electronic absorption spectroscopy.
      - 2.1.1.1 The experimental techniques.
    - 2.1.2 Vibrational infrared spectroscopy.
      - 2.1.2.1 The experimental techniques.
    - 2.1.3 Vibrational Raman spectroscopy.
      - 2.1.3.1 The experimental techniques.
    - 2.1.4 Variable temperature studies.
  - 2.2 Quantum chemistry methods.
    - 2.2.1 Introduction to the quantum chemistry methods.
    - 2.2.2 Density functional theory method.
      - 2.2.2.1 Time-dependent density functional theory.
      - 2.2.2.2 Charge transport parameters.
      - 2.2.2.3 Aromatic parameters.
      - 2.2.2.4 Physical parameters.
      - 2.2.2.5 Frequency calculations.
    - 2.2.3 Software details.
  - 2.3 Fabrication and characterization of OFETs.
    - 2.3.1 The experimental techniques.
  - 2.4 Bibliography.
-



## 2.1 Spectroscopic methods.

Spectroscopy is a branch of science that studies the interaction between electromagnetic radiation and matter. This interaction can afford detailed information about the structure and chemical properties of atoms and molecules<sup>1,2</sup>. This electromagnetic radiation has a dual nature:

1) Wave nature: it can be described as a form of energy that is propagated through space at the speed of light. Focusing on wave nature, electromagnetic radiation is composed of a magnetic (H) and an electric (E) field perpendicularly disposed among them and orthogonal to the propagation direction (Figure 2.1). The electromagnetic wave is defined by the wavelength ( $\lambda$ ) which is the spatial period of a periodic wave and the frequency ( $\nu$ ) which is the number of times a complete wave shape is repeated per unit of time. These two parameters are correlated with the light velocity in the vacuum,  $c$  ( $2.997 \cdot 10^8$  m·s<sup>-1</sup>), see equation [1].

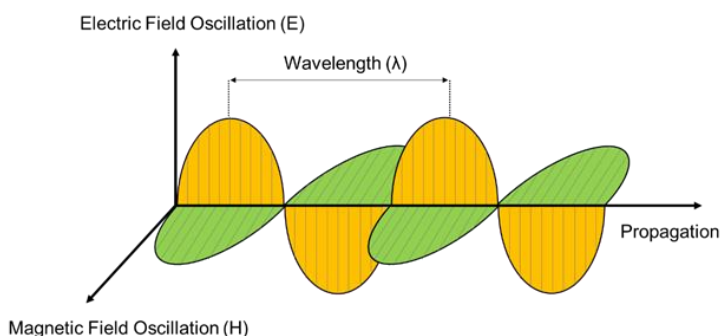


Figure 2.1 Plane-polarized electromagnetic radiation.

2) Particle nature: it can be defined as a flow of mass-less particles, named photons or light-quanta, travelling through

space at light velocity (particle properties). Each photon has a certain amount of energy. In this context, the nature of light is a key source of information about the chemical systems under study. The energy of these photons is closely linked with  $\nu$  and the Planck constant,  $h$  ( $6.62 \cdot 10^{-34}$  J·s) through the equation:

$$E = h\nu = hc/\lambda \quad [1]$$

The basic spectroscopic phenomenon is defined as the absorption or emission of quantized radiation between two different states ( $E_1$  and  $E_2$ ). According to the Einstein equation ( $\Delta E = h\nu$ ), the energy of the absorbed radiation should coincide with the energy difference between the two involved states. The different energy transitions that can take place between the energy levels of a polyatomic molecule are represented in Figure 2.2.

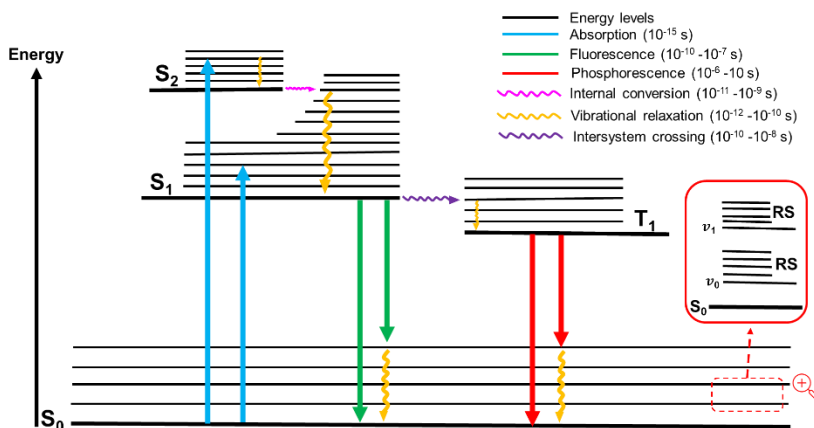


Figure 2.2. Jablonski diagram<sup>3</sup> of the energy states of a molecule together with the different possible transitions.  $S_n$ : singlet electronic states;  $T_n$ : triplet electronic states;  $\nu_n$ : vibrational states; RS: rotational states. Non-radiative transitions are indicated by squiggly arrows and radiative transitions by straight arrows.



According to the wavelength (or frequency), the use of distinct regions of electromagnetic radiation results in different kinds of spectroscopies (Figure 2.3). In this Thesis, the spectroscopic techniques employed are electronic absorption spectroscopy and vibrational IR and Raman spectroscopies, principally.


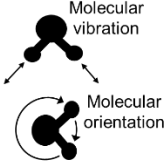
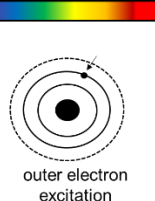
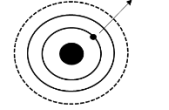
Microwaves 1 cm - 100 $\mu$ m	Infrared 100 $\mu$ m – 1000 nm	Visible/Ultraviolet 1000 nm – 10 nm	X-Rays 10 nm – 100 $\mu$ m	$\gamma$ -Rays < 100 pm
				
NMR (molecular connectivity)	IR Spectroscopy (chemical bond type) Raman Spectroscopy (molecular orientation)	UV-Vis Spectroscopy (reactivity analysis)	X-Ray Spectroscopy (elemental analysis)	

Figure 2.3 Different spectroscopies associated with the used electromagnetic radiation regions.

### 2.1.1 Electronic Absorption Spectroscopy.

Electromagnetic radiation in the UV-Vis-NIR region is used as a source of excitation for electronic absorption spectroscopy. The energy of this radiation can provoke a transition from the ground electronic state ( $S_0$ ) to a singlet excited state ( $S_n$ ). The species in charge of absorbing this radiation are named “chromophores”. Figure 2.4 displays the general components of an electronic absorption spectrophotometer<sup>2, 4</sup>: (i) the source is often several lamps that generate electromagnetic radiation in different ranges of the UV-Vis-NIR spectrum; (ii) the dispersion element is a diffraction grating that disperses the radiation into its

constituting wavelengths; (iii) the sample cell is where the sample is placed and (iv) the detector is the component that converts the radiation into an electrical signal.

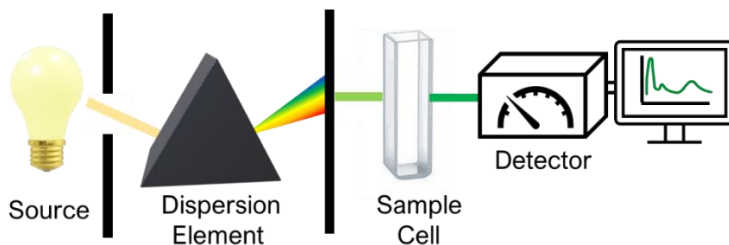


Figure 2.4 General scheme of the basic components of an electronic absorption spectrophotometer.

Thereby, an electronic absorption spectrophotometer registers the wavelengths at which absorption occurs resulting in a spectrum of absorbance versus wavelength, as in Figure 2.5. The  $\pi$ -conjugation is a relevant case of electronic spectroscopic study. In  $\pi$ -conjugated molecules, the energetically most favourable electronic transition is generally the  $\pi \rightarrow \pi^*$  excitation which commonly occurs from the HOMO to the LUMO.

As Figure 2.5 displayed, the increase of the effective  $\pi$ -conjugated length brings the HOMO and LUMO orbitals closer together causing a progressive narrowing of the HL gap. This fact provokes that the required energy to promote an electron from HOMO to LUMO levels decreases and therefore, the absorption wavelength undergoes a shifting to larger values (see equation [1])

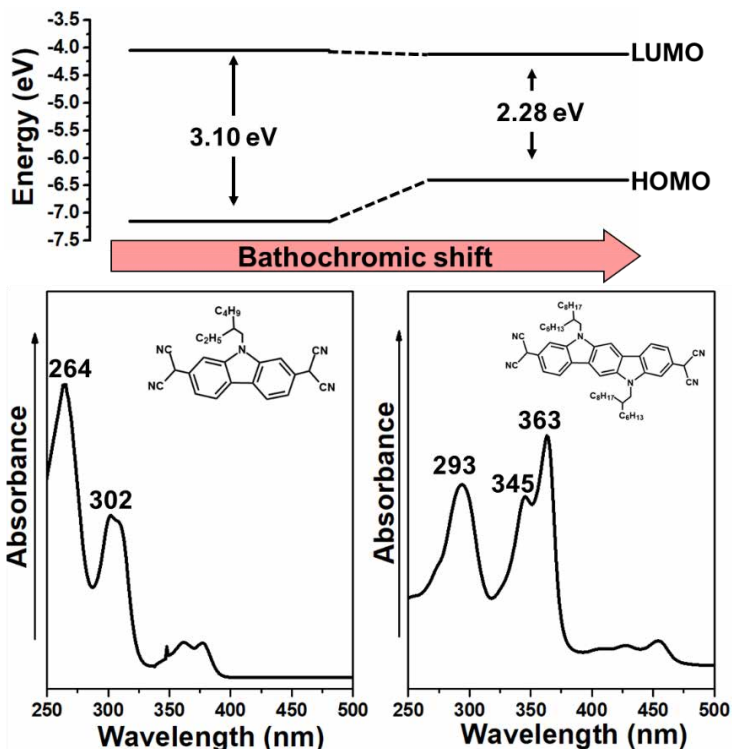


Figure 2.5. Representation of the HL gap evolution when increasing the conjugated backbone from Cz (left) to ICz (right) molecule, and its bathochromic effect on the maximum electronic absorption wavelength.

### 2.1.1.1 The experimental techniques.

The electronic absorption spectra presented in this Thesis have been measured solving the sample in dichloromethane ( $\text{CH}_2\text{Cl}_2$ ), chloroform ( $\text{CHCl}_3$ ), toluene or ortho-dichlorobenzene (*o*-DCB).  $\text{CH}_2\text{Cl}_2$  and  $\text{CHCl}_3$  solvents were mostly used for RT absorption spectra measurements meanwhile toluene and *o*-DCB were used for the registration of UV-Vis measurements at high temperatures (up to 380 and 410 K, respectively). The spectrophotometers employed in the electronic absorption measurements were:

### ❖ Agilent 8453 UV-Vis spectrophotometer.

Its radiation source is a combination of a deuterium-discharge lamp for the ultraviolet (UV) wavelength range and a tungsten lamp for the visible and near-infrared (NIR) wavelength range. The Agilent 8453 spectrophotometer consists of 1024 photodiodes, one for each nanometre, which allows very short registration times with a wavelength range of 190-1100 nm.



Figure 2.6 Agilent 8453 UV-Vis spectrophotometer.

### ❖ Cary 5000 UV-Vis-NIR spectrophotometer.

The Cary 5000 is a high-performance UV-Vis and NIR spectrophotometer with superb photometric performance in the 175–3300 nm range with a spectral resolution of 0.01 nm. The equipment consists of a light source of tungsten halogen visible and deuterium arc UV. Using a PbSmart NIR detector, the Cary 5000 extends its NIR range to 3300 nm making it a powerful tool for materials science research.



Figure 2.7 Cary 5000 UV-Vis-NIR spectrophotometer.

### 2.1.2 Vibrational Infrared Spectroscopy.

Any polyatomic molecule of  $N$  atoms has  $3N-6$  independent vibrational modes ( $3N-5$  in the case of linear systems) named normal modes. These normal modes are described as collective displacements of all the nuclei that keep the centre of mass and exhibit the same frequency. In this vibrational spectroscopy, the electric dipolar moment of the molecule must change during the relative displacement of the atoms in order to obtain an active IR vibration<sup>3, 5</sup>. This technique is usually employed in the study of  $\pi$ -conjugated molecules bearing strongly polar groups, as carbonyl or cyano groups, which possess characteristic vibrational wavenumbers in the spectral region where no other groups absorb. Comparing the behaviour of these IR bands allows determining if a strengthening (when  $\nu$  is upshifted) or a weakening (when  $\nu$  is downshifted) of the chemical bond takes place<sup>6</sup>. The most widely employed IR spectrometer is that implementing the Fourier Transform technique (FT-IR). Instead of a dispersing element, the FT-IR spectrometers use a Michelson interferometer to produce an interferogram, which is then



## 2.Methodology

transformed in the IR spectrum through a Fourier Transform mathematical treatment<sup>2,3</sup>. Through this technique, higher spectral resolution in a wider spectral range is obtained.

### 2.1.2.1 The experimental techniques.

The spectrometer employed in the Infrared absorption measurements were:

❖ Bruker Vertex FT-IR 70 spectrometer.

This spectrometer consists of a Michelson interferometer, directly joined to a KBr beam splitter and a DTGS detector. A spectral resolution of 4  $\text{cm}^{-1}$  and 64 scans was used to record the spectra. The equipment allows the recording of FT-IR spectra from 7500 to 400  $\text{cm}^{-1}$  for solid, liquid and gaseous samples. Infrared absorption measurements of the present Thesis were carried out in the spectral range of 4000-400  $\text{cm}^{-1}$ .



Figure 2.8 Bruker Vertex FT-IR 70 spectrometer.

The IR absorption studies have been performed with samples in solid-state in two different ways: (i) in a simple transmission holder of KBr pellets, or (ii) by deposition in a Specac ATR (Attenuated Total Reflectance) device called

GOLDEN GATE, which allows the recording of IR spectra of pure and opaque samples by applying a high pressure at a diamond point.

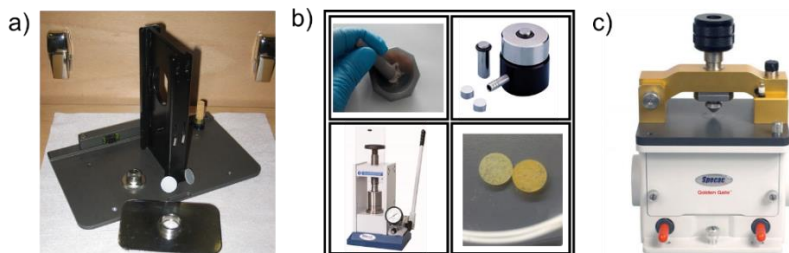


Figure 2.9 (a) Simple transmission holder of KBr pellet, (b) steps of the preparation of KBr pellets and (c) Specac Golden Gate Diamond ATR.

### 2.1.3 Vibrational Raman Spectroscopy.

Despite Raman spectroscopy being also a vibrational technique, its physical nature is different from that of IR spectroscopy. This fact is evident only considering the phenomena that are detected in each technique: light absorption in IR spectroscopy and light scattering in Raman spectroscopy. As above-mentioned, the basic spectroscopic phenomenon is defined as the absorption or emission of quantized radiation. However, photons can interact with molecules and then being re-emitted from them (called scattered light). This is the phenomenon on which Raman spectroscopy is based.

Once a photon collides with a molecule, there are two possibilities: (i) the energy of the photon is similar to the difference between the energy levels on the system and therefore it may be absorbed. (ii) The energy of the photon does not coincide with that energy difference and therefore it may be



## 2.Methodology

scattered. Such a scattering process provokes a distortion of the electron cloud around the nuclei forming a short-lived virtual state. At this point, the phonon is quickly re-radiated due to the inherent instability of this state. If the frequency of the light incident is very similar to the scattered light, the process is known as an elastic scattering called “Rayleigh scattering” where the energy is conserved (Figure 2.10). In contrast, the scattering process can imply a partial energy transfer from the photon to the molecule, in a way that this process (called “Raman scattering” in honour of its finder) is considered as an inelastic scattering because of the energy difference between the incident and scattered photon. Note that this Raman scattering is an unusual phenomenon since only one of  $10^6$ - $10^8$  photons experiments an inelastic scattering. As seen in Figure 2.10, this kind of inelastic interaction can be classified in two ways:

- Stokes Raman scattering: the molecule gains energy and consequently, the energy of scattered light is less than the incident light.
- Anti-Stokes Raman scattering: the molecule loses energy and consequently, the energy of scattered light is larger than the incident light.



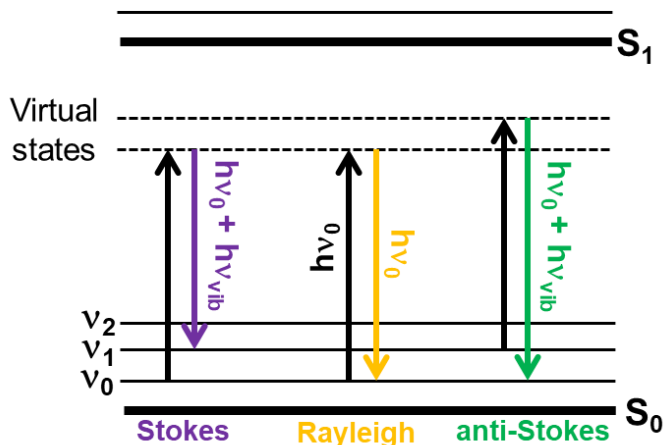


Figure 2.10 Representation of the Rayleigh and Raman scattering process.

It should be highlight that the selection rules for the Raman transitions are based on the molecular polarizability rather than in the dipole moment. A vibration will be Raman active if it produces a periodic change on the molecular polarizability. Consequently, IR inactive vibrations can present an intense Raman activity and *vice versa*, thus making both vibrational techniques highly complementary. Thus, whereas  $\pi$ -conjugated molecules do not present high IR activity, unless substitution with polar functional groups, the large polarizability of the  $\pi$ -electron density generated by the alternating double and single CC bonds, makes them suitable systems for Raman studies.

### 2.1.3.1 The experimental techniques.

Raman spectra have been measured in both, solid-state (bulk and pellet, diluted in KBr) and solution (in *o*-DCB). Several laser excitation wavelengths have been employed (described

below), indicating in the corresponding spectra if resonant effects are present. The employed vibrational Raman spectrometers are:

❖ Bruker FT-Raman Ram II.

This system makes use of a continuous-wave Nd–YAG laser working at  $\lambda_{\text{exc}} = 1064 \text{ nm}$ , and a germanium detector operating at the liquid nitrogen temperature. Raman radiation is detected in a back-scattering geometry, forming an angle of  $180^\circ$  between the incident radiation and the scattered radiation, with a standard spectral resolution of  $4 \text{ cm}^{-1}$ . 3000 Raman scans were averaged in each case to improve the signal-to-noise ratio.



Figure 2.11 Bruker FT-Raman Ram II.

❖ Bruker Micro-Raman Senterra.

This equipment makes use of two integrated lasers working at  $\lambda_{\text{exc}} = 532 \text{ nm}$  and  $785 \text{ nm}$ , respectively, in addition to a third, externally connected laser operated at  $\lambda_{\text{exc}} = 633 \text{ nm}$ . The detection system is a Charge Couple Device (CCD) that is thermoelectrically cooled to  $-65 \text{ }^\circ\text{C}$ . It also consists of an Ne lamp used for laser calibration. The resonant Raman spectra with  $785$ ,  $632$ , and  $532 \text{ nm}$  laser excitations were recorded both for bulk

and liquid samples by using the 1x1 camera of a Bruker Senterra Raman microscope with a 3-5  $\text{cm}^{-1}$  spectral resolution.



Figure 2.12 Bruker Micro-Raman Senterra.

### 2.1.4 Variable temperature studies.

These spectroscopic techniques have been used for the measurement of neutral samples at RT, but also studies as a function of temperature have been performed. Variable temperature electronic absorption spectra were obtained with an Optistat DN Oxford Instruments cryostat, which allows sample temperature variations from -196 °C to 200 °C. On the other hand, Raman spectra at different temperatures were obtained with a Linkam FTIR600 accessory for the Senterra spectrometer, operating from -196 °C to 600 °C. For variable-temperature FT-IR measurements, the Specac P / N 2100 accessory was used, which permits the recording of both solid and liquid samples. It uses a Graseby Specac automatic temperature control system working in the range of -170 to 250 °C.

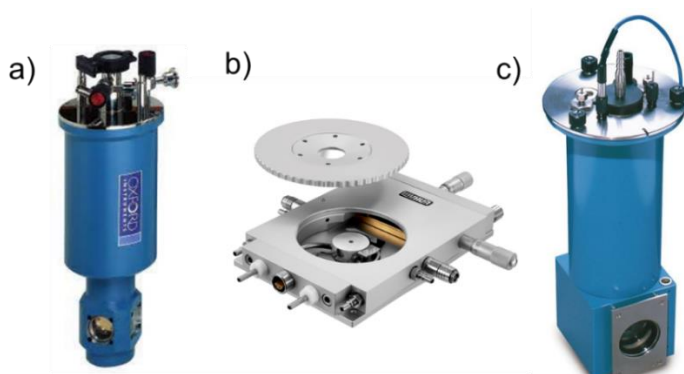


Figure 2.13 (a) Optistat DN Oxford Instruments cryostat, (b) Linkam FTIR600 accessory and (c) Specac P/N 2100 automatic temperature controller.

## 2.2 Quantum chemistry methods.

Quantum chemistry is a very powerful tool to understand the structure-property relationships of chemical systems. In this sense, numerous  $\pi$ -conjugated systems have been theoretically investigated to predict their chemical and physical properties with the aim of guiding the molecular design of materials with great potential in several research fields. In this context, throughout this Thesis, theoretical calculations have been performed not only to assist in the interpretation and provide deeper insights into the experimental results, but also to predict the physicochemical properties of the materials prior to their synthesis.

### 2.2.1 Introduction to the quantum chemistry methods.

Theoretical calculations are employed to simulate complex molecular structures and predicts their chemical and physical properties applying the theoretical principles of quantum chemistry. To this end, the solution of the time-independent



## 2. Methodology

Schrödinger equation leads to obtain the related properties of any molecular system.

$$\hat{H}\Psi = E\Psi \quad [2]$$

Where  $\hat{H}$  is the Hamiltonian operator,  $E$  is the energy and  $\Psi$  is the wavefunction that contains all the information of the molecular system. There are several methods in quantum chemistry, with different mathematical approximations, to solve this equation. These methods can be classified in three approaches:

1) Ab initio methods: when the calculations are based on quantum mechanics and do not employ other data than the fundamental physical constants (speed of light, the mass of electrons, the charge of nuclei, Planck constant, etc). The *ab initio* methods resolve approximately the Schrödinger equation by using rigorous mathematical approaches. Some of these methods can produce very accurate results although they can require enormous computational resources. The Hartree–Fock (HF) approximation was the first significant approach that allowed us to deal with molecular systems theoretically. In fact, the HF method plays a central role in quantum chemistry since more developed methods use this method as a starting point. The HF equation can be described as a set of pseudo-eigenvalue monoelectronic equations (Eq. 3).

$$\hat{f}(i)\psi_i = \varepsilon_i\psi_i \quad [3]$$

Where  $\hat{f}$  is the Fock operator acting on electron  $i$ ,  $\varepsilon_i$  is the one-electron energy of the spin-orbital  $\psi_i$ .



## 2. Methodology

2) Semi-empirical methods: these calculations introduce parameters obtained from empirical data simplifying quantum-chemical calculations and reducing the computational cost. The way the parametrization is performed characterizes the particular semi-empirical method. The most prevalent semi-empirical methods are those based on approximations of the HF approach, leading to methods such as AM1, PM3, PM6, etc. Another popular semi-empirical method derived from the DFT framework is the density functional tight binding (DFTB) approach which has become very popular in the last years and does not require large amounts of empirical parameters.

3) Density functional methods: when calculations introduce the electronic correlation effects during the solution of the electronic Schrödinger equation. This approach is an alternative to the *ab initio* method. The basic idea of DFT is to regard the ground state electron density and not the wavefunction as in *ab initio* methods, as the main variable that contains all the information about an N-electron system. Therefore, the ground state energy is a function of the electron density.

In this Thesis, all theoretical calculations have been performed within the density functional theory (DFT) methodology.

### 2.2.2 Density functional theory method.

DFT represents an alternative to conventional *ab initio* methods where the ground state electronic density ( $\rho$ ) is considered (not the wavefunction as in *ab initio* methods) as the



## 2. Methodology

main variable which contains all the information about the system<sup>7,8</sup>. The low computational costs and high accuracy make this theoretical method the most widely used for electronic structure calculations in condensed matter physics and quantum chemistry.

In 1964, Hohenberg and Kohn published a decisive paper in the physical review that proved the existence of a universal functional of the density. The Hohenberg-Kohn theorem reads: *"any observable for a non-degenerated ground state of an N-electron system, including the energy, can be calculated, in principle exactly, from the electron density of the ground state"*<sup>9</sup>. In other words, the electron density ( $\rho$ ) determines the electronic structure of the system for molecules with a non-degenerated ground state.

Thus, in the Density Functional Theory, the energy of the ground electronic state can be calculated associated to different energy terms:

$$E[\rho] = E_T[\rho] + E_V[\rho] + E_J[\rho] + E_K[\rho] + E_C[\rho] \quad [4]$$

Where  $E_T[\rho]$  is the kinetic energy,  $E_V[\rho]$  is the nucleus-electron potential energy,  $E_J[\rho]$  is the classical Coulombic electron-electron repulsion,  $E_K[\rho]$  is the electron-electron exchange energy and  $E_C[\rho]$  is the correlation energy. The analytic expressions for the  $E_V[\rho]$  and  $E_J[\rho]$  parameters are defined in equation [5] and [6]. Unfortunately, no analytical expressions were available for the others functionals.



$$E_V[\rho] = -\sum_A z_A \int \frac{\rho(r)}{R_A-r} dr \quad [5]$$

$$E_J[\rho] = \frac{1}{2} \iint \frac{\rho(r_i)\rho(r_j)}{|r_i-r_j|} dr_i dr_j \quad [6]$$

Although the DFT approach provided good energy estimations in some cases, it presents fundamental errors (for instance, atoms do not bind to form molecules). The first useful method to calculate molecular properties in the DFT framework was proposed by Kohn and Sham<sup>10</sup>. The Kohn-Sham (KS) approach consists in performing one-electron molecular orbitals as a linear combination of atomic orbitals and calculating the exact kinetic energy. Therefore, the KS method exhibits an analogous equation to the HF equation (eq. [3]) with an extra term that corresponds to the exchange-correlation functional,  $E_{xc}[\rho]$ :

$$\left[ -\frac{1}{2} \nabla_i^2 + \sum_A \frac{z_A}{|R_A-r|} + \sum_j \int \frac{|\psi_j(r_j)|^2}{|r_i-r_j|} dr_j + \frac{\delta E_{xc}[\rho]}{\delta \rho} \right] \psi_i(r_i) = \varepsilon_i \psi_i(r_i) \quad [7]$$

This new term ( $E_{xc}[\rho]$ ) is calculated from the one-electron KS orbitals according to the following equation:

$$\rho(r) = \sum_i n_i |\psi_i(r)|^2 \quad [8]$$

Where  $n_i$  is the orbital occupation number.

However, the exchange-correlation energy remains undefined and should be approximated by different ways:

1) Local Density Approach (LDA): the basic idea of LDA is to utilize the *uniform electron gas* model where the exchange-correlation energy only depends on the localized density. In this





## 2. Methodology

approach, electrons move on a positive charge distribution so that the total ensemble is electrically neutral. The *uniform electron gas* model is very detached from a realistic situation for atoms and molecules. Nevertheless, this model allows the exchange-correlation term can be split into exchange and correlation functions, which are known exactly or at least with very high accuracy. An example of these functionals is SVWN<sup>10, 11</sup>.

2) Generalized Gradient Approximation (GGA): the  $E_{xc}[\rho]$  term depends not only on the localized density but also on the gradient of the density. The GGA approach improves the resolution of several parameters (*i.e.*, harmonic frequencies or equilibrium geometries, among others) with respect to the LDA results. The most representative functionals are BLYP<sup>12-14</sup> or PBE<sup>15</sup>. However, these functionals fail in the description of weakly bounded systems (*i.e.*, van der Waals complexes). Therefore, the next step in sophistication of  $E_{xc}[\rho]$  term was to add a dependence with the kinetic energy density resulting in meta-GGA functionals<sup>16</sup>.

3) The hybrid functionals: a further step to the GGA and meta-GGA functionals is the incorporation of a new portion of exchange energy in the  $E_{xc}[\rho]$  term, giving rise to the commonly used hybrid density functionals. The most representative hybrid GGA functional is B3LYP<sup>13,17</sup>. Examples of hybrid meta-GGA functionals are M06<sup>18</sup>, M06-2X<sup>19</sup> and M06-HF<sup>20</sup>. During the last years, new functionals have emerged, among which the long-range corrected (LC) or range-separated functionals are the



## 2.Methodology

most relevant. This LC correction is needed since the exchange functionals become very inaccurate at large distances. A representative example of LC functional is  $\omega$ B97XD<sup>21,22</sup>.

DFT calculations in the present Thesis have been performed with different hybrid functionals, combining hybrid GGA, hybrid meta-GGA and LC functionals, such as

- ❖ B3LYP<sup>13,17</sup> that combines the Becke's three-parameter exchange functional (B3) with the Lee-Yang-Parr (LYP) non-local correlation functional.
- ❖ M06<sup>18</sup> and M06-2X<sup>19</sup> (both hybrid functional of Truhlar and Zhao).
- ❖  $\omega$ B97XD<sup>21,22</sup> that it is the latest functional from Head-Gordon and co-workers, which includes empirical dispersion.

Note that most of the density functionals exhibit a local or semi-local dependence on the electronic density, failing in the description of non-covalent interactions. To avoid this situation, Grimme's dispersion correction (GD3)<sup>23</sup> is essential to describe the intermolecular interactions. In this sense, the calculations of the dimeric models presented in Chapter III have been performed by using M06-2X-D3 functional.

The mathematical description of the orbitals has been computed with the 6-31G\*\*<sup>24, 25</sup> basis set as implemented in the Gaussian 09<sup>26</sup> and 16<sup>27</sup> programs. In this basis set, core atomic orbitals are defined by a contracted Gaussian function resulting from the combination of 6 primitive Gaussians. Furthermore, the



## 2.Methodology

valence orbitals are defined through two basic functions, the first one resulting from the combination of 3 primitive Gaussian functions and the second one, from only one primitive function. The double asterisk (also indicated as d,p) point that polarization functions d and p are added on heavier atoms and on the hydrogen atoms, respectively.

In this Thesis, the large alkyl chains on the *N*-substituted groups of Cz and ICz-bases systems were replaced with ethyl groups to reduce the computational cost. Also, the *N*-substituted groups of Cz-based macrocycles were replaced with methyl groups.

On the other hand, quantum chemistry methods only consider the nuclei and electrons in a vacuum making a suitable approach for gas-phase chemistry. Nevertheless, several phenomena in chemistry happen in solution, where the solvent molecules play a crucial role in many processes. Therefore, some theoretical calculations presented in Chapter II were carried out in solution by the Polarizable Continuum Model (PCM)<sup>28-30</sup> using chloroform, toluene, and *o*-dichlorobenzene as solvents.

Gibbs free energies associated with the formation of the dimer ( $\Delta G_f^0$ ) were computed based on the energies of the vibrational analysis of the isolated monomers, as well as the dimer structure, taking into account the thermal corrections<sup>31</sup>.

For several calculations presented in Chapter III, molecular symmetry was imposed by using the keyword *scf=DSymm* which



symmetrizes the density matrix at every SCF iteration to match the symmetry of the molecule.

### 2.2.2.1 Time-dependent density functional theory.

Up to now, DFT approach has proved to be a powerful tool for the definition of several properties. Nevertheless, DFT, in its original formulation, is based on a ground state theory. In 1984, Runge and Gross develop the DFT theory to include an approximation to calculate excited states. This methodology is known as the Time-Dependent DFT (TD-DFT)<sup>32</sup>. Thanks to this theory, we have calculated the properties of the excited states of the Cz-based systems under study and, consequently, the electronic vertical transitions, allowing us to predict their UV-Vis-NIR electronic absorption spectra.

### 2.2.2.2 Charge transport parameters.

In this section, we considered two key molecular charge transport parameters that have an impact on the charge mobility:

1) Reorganization energy ( $\lambda$ ): this parameter reflects the structural changes of the molecules needed to accommodate a positive or negative charge (*i.e.*, hole ( $\lambda_h$ ) or electron ( $\lambda_e$ ) reorganization energy, respectively). The  $\lambda_e$  and  $\lambda_h$  values were computed by four-points approach, extensively used for the estimation of the charge transport nature of organic electronic systems<sup>33-36</sup>, see Figure 2.14 and equations [9]-[10].

$$\lambda_e = (E_0^* - E_{-1}) + (E_{-1}^* - E_0) \quad [9]$$

$$\lambda_h = (E_0^* - E_{+1}) + (E_{+1}^* - E_0) \quad [10]$$

Where  $E_0$  is the optimized ground state energy of the neutral molecule,  $E_{-1/+1}$  is the optimized energy of the anionic/cationic molecule,  $E_{-1/+1}^*$  is the energy of the neutral molecule at the anionic/cationic geometry and  $E_0^*$  is the energy of the anionic/cationic molecule at the optimized geometry of the neutral species.

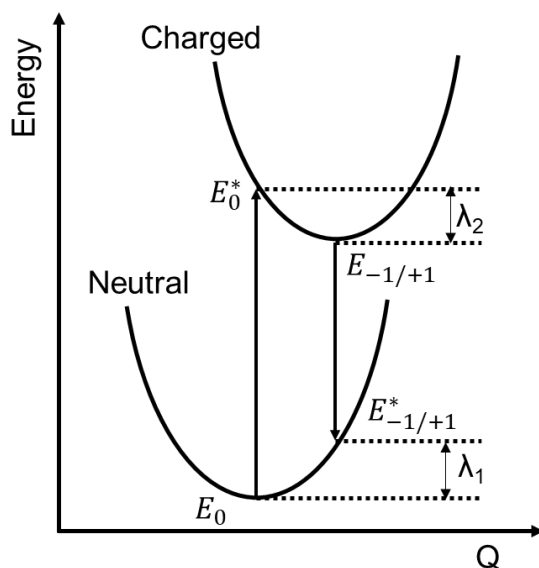


Figure 2.14 Scheme of reorganization energy

2) Transfer integral ( $t$ ): this parameter gauges the degree of intermolecular electronic interactions between nearest-neighbour molecular pairs. The transfer integrals between dimeric models of Cz-based macrocycles were computed by using a basis set orthogonalization procedure, according to the approach described by Valeev and co-workers<sup>37</sup>.



### 2.2.2.3 Aromatic parameters.

The degree of aromaticity has been evaluated by using two different ways:

1) Nucleus Independent Chemical Shifting (NICS)<sup>38-40</sup>: is a computational method that calculates the absolute magnetic shielding at the ring centre and has become the most widely used aromaticity test because of its simplicity and efficiency. These calculations were performed by using gauge-independent atomic orbital (GIAO) approach at B3LYP/6-311+G\*\* level of theory. NICS-XY scans were computed using the Aroma package<sup>41-44</sup> at the GIAO-B3LYP/6-311+G\* level. NICS-XY values were taken 1.7 Å above the molecular plane and employed the  $\sigma$ -only model to take only  $\pi$ -contributions into consideration.

2) Anisotropy current induced density (ACID)<sup>45</sup>: the anisotropy of the current density was calculated using ACID method implemented in the Gaussian program (keywords NMR=CSGT and IOp(10/93=1)). The orientation of the magnetic field is chosen to be orthogonal to the ring planes and pointing towards the viewer. The chosen isosurface value has been set up to 0.03.

### 2.2.2.4 Physical parameters.

Calculations based on diradical species have constituted an essential tool in the investigation of the DCM-substituted compounds studied in this Thesis. To this end, calculations with open-shell configurations are required. For this purpose, the Broken-Symmetry (BS) approximation in the unrestricted DFT



## 2. Methodology

methodology (BS-UDFT) was employed for the theoretical study of the energies and geometries of singlet open-shell systems. For the calculations of the triplet states, standard unrestricted calculations were also done.

The diradical stability of the compounds under study is theoretically explored by means of different physical parameters:

1) The singlet-triplet energy gap ( $\Delta E_{S-T}$ ): the spin correction for  $\Delta E_{S-T}$  was computed by using the following equation:

$$\Delta E_{S-T} = (E_{OS} - E_T) \frac{\langle S^2 \rangle_T}{\langle S^2 \rangle_T - \langle S^2 \rangle_{OS}} \quad [11]$$

Where  $E_{OS}$  and  $E_T$  correspond to the energies of the OS singlet and triplet state, with spin contamination values  $\langle S^2 \rangle_T$  and  $\langle S^2 \rangle_{OS}$  of the triplet and OS singlet state, respectively<sup>46</sup>.

2) The effective electron exchange interaction ( $J_{ab}$ ): which reflects the overlap integral between the two nearly energetically degenerate molecular orbitals. The BS method considered that spin correction is trustworthy for estimating the  $J_{ab}$  values, which were determined by using the following equation:

$$J_{ab} = \frac{(E_{OS} - E_T)}{\langle S^2 \rangle_T - \langle S^2 \rangle_{OS}} \quad [12]$$

3) The diradical character: it has been calculated by using two different methods. First, the diradical character  $y_0$  (closed-shell structure has  $y_0=0$  and pure diradical state has  $y_0=1$ ) was calculated from the occupation numbers of the highest occupied natural orbital (HONO) and the lowest unoccupied natural orbital



(LUNO) using the spin-projected formalism<sup>47</sup>. This parameter is obtained by the following equations:

$$y_0 = 1 - \frac{2T_i}{1+T_i^2} \quad [13]$$

$$T_i = \frac{n_{HONO-i} - n_{LUNO+i}}{2} \quad [14]$$

Where  $n_{HONO-i}$ ,  $n_{LUNO+i}$  are the occupation numbers of the occupied and unoccupied natural orbitals (NO). The diradical character corresponds to  $i=0$ .

Second, we have carried out an analysis based on the fractional occupation number weighted density (FOD) whose main feature is to provide a robust and cost-effective information on the localization of “hot” electrons (strongly correlated and chemically active) in a molecule<sup>48</sup>. These calculations were performed using the ORCA program<sup>49</sup>. We used the FOD analysis for a quantitative description of the OS singlet biradical character of these ground-state organic molecules. The number of hot electrons,  $N^{FOD}$ , was calculated at the FT-TPSS<sup>50</sup>/def2-TZVP<sup>51</sup> level at a default electronic temperature ( $T_{el}$ ) of 5000 K. The isocontour value of the  $\rho^{FOD}$  plots was fixed to 0.005 e·bohr<sup>-3</sup> allowing a systematic comparison.

### 2.2.2.5 Frequency calculations.

The theoretical treatment used to study molecular vibrations is considered an excellent example of the importance of theoretical chemistry to assist the interpretation of experimental observations. The theoretical methods for calculating vibrational





## 2. Methodology

frequencies have been extensively described in the scientific literature<sup>52-55</sup>. One of the most common approximations used to investigate vibrational spectroscopies is based on the double-harmonic approximation<sup>56</sup>. In this approach, molecular vibrations are defined as harmonic oscillators and the spectroscopic intensities are determined by the first-order geometric derivative of dipole moment (infrared) and polarizability (Raman) regarding a particular normal mode<sup>57</sup>.

The first step to vibrational analysis is calculating the Hessian matrix ( $3M \times 3M$  matrix, where  $M$  is the number of atoms). This matrix includes the second partial derivatives of the potential with regard to the displacement of the atoms in Cartesian coordinates. This Hessian matrix is converted from Cartesian coordinates to mass-weighted Cartesian coordinates. The translation and rotation contributions to the Hessian matrix are determined and omitted. The  $3M - 6 \times 3M - 6$  Hessian sub-matrix ( $3M - 5 \times 3M - 5$  for linear molecules), which includes only vibration contributions, is then diagonalised. The eigenvalues are converted into vibrational frequencies and finally, the force constants, reduced masses and Cartesian displacements are obtained. Note that the calculation of frequencies has been done at the same theoretical level used for geometry optimizations. In fact, all real positive vibrational frequencies confirm the minima energy of the optimized systems.

In this sense, DFT theory has demonstrated to be a useful method to calculate harmonic frequencies and to simulate the vibrational spectra of large molecules. Nevertheless, the



## 2.Methodology

calculations of harmonic frequencies by using the DFT level are usually scaled by a constant factor in order to achieve a better agreement with experimental frequencies. The comparison of theoretical harmonic frequencies and the corresponding experimental frequencies allows determining the specific scale factor for each theoretical functional (all functionals used in this Thesis are described in section 2.2.2). In the present Thesis, the scaling factors used for M06-2X functional is 0.95<sup>58</sup>.

### 2.2.3 Software Details.

The DFT calculations presented in this Thesis have been obtained using different software packages:

➤ PICASSO: supercomputer with 4016 data processing cores, 23 terabytes of RAM and 555 terabytes of storage. In addition, it contains a parallelization program which allows to share memory and processors for Gaussian calculations.

➤ GAUSSIAN 09<sup>26</sup> and 16<sup>27</sup>: this software package is the most popular within the quantum chemistry community and we used it to perform most of the DFT calculations presented in this Thesis.

➤ ORCA 5.0<sup>49</sup>: ORCA is a modern electronic structure program written by F. Neese and co-workers that we used aiming to disclose the diradical character.

To represent the data obtained from theoretical calculations, different programs were used:

➤ MobaXterm 11.0: is an ultimate toolbox for remote computing.



## 2.Methodology

- GAUSSVIEW 5.0: advanced graphical interface designed to prepare the input files for Gaussian. This also allows to graphically examine the results of the Gaussian program.
- GAUSSUM 3.0: program used to extract useful information from TD-DFT calculations.
- CHEMBIODRAW ULTRA 12.0: program used to generate the chemical structures in 2D and 3D.
- CHEMCRAFT 1.8<sup>59</sup>: graphic program used to represent theoretical data such as eigenvectors.
- ORIGINPRO 9.0: program which allows to represent data, such as absorption and Raman spectra obtained experimentally and theoretically.
- MERCURY 4.1.0: is a freeware developed by the Cambridge Crystallographic Data Centre (CCDC) designed to visualize crystal structure and analyse crystal packing and intermolecular interactions.
- UCSF CHIMERA 1.11.2<sup>60</sup>: is an extensible program for visualization and analysis of molecular structures and related data such as molecular orbitals, density maps or supramolecular assemblies.
- AVOGADRO 1.2.0<sup>61</sup>: is an advanced molecule editor and visualizer designed for cross-platform used in computational chemistry.

### 2.3 Fabrication and characterization of OFETs.

In the present Thesis, the OFET configurations used were the top contact-bottom gate (TCBG). For the fabrication of TCBG-OFETs, silicon substrates covered with a 300 nm thick thermally grown SiO<sub>2</sub> layer were employed as gate electrode and dielectric layer, respectively. These Si/300 nm SiO<sub>2</sub> substrates are commercially available, and their advantage is that they can be used as substrates achieving a high reproducibility with several organic semiconductors. To this end, the substrates should be



## 2.Methodology

first double-cleaned in an ultrasonic bath with ethanol and then dried under a flow of nitrogen. Second, self-assembly monolayers are used to modify the dielectric surface from hydrophilic to hydrophobic character, minimizing interfacial trapping sites. Hence, Si/SiO<sub>2</sub> substrates were functionalized with hexamethyldisilazane (HMDS) and octadecyltrichlorosilane (OTS). The modification of the dielectric surface is followed by the deposition of the organic semiconductor. Our semiconductors were deposited from chloroform solution (with 2.5 mg/ml concentration) by *drop casting* at room conditions.

*Drop-casting* is a simple and low-cost deposition method for the fabrication of small-area films. This method consists in dissolving the organic semiconductor in an organic solvent and dropping this solution on a target substrate allowing the evaporation of the solvent. The last step in the fabrication of OFETs is the deposition of the source and drain electrodes. For this purpose, 40 nm gold source and drain electrodes were thermally evaporated through a shadow mask.

### 2.3.1 The experimental techniques.

The OFET devices were fabricated and characterized in different instruments:

❖ Uvo cleaner 342-220: ozone surface cleaning equipment. This equipment has a low-pressure mercury vapor grid lamp as an ozone UV source that cleans surfaces in less than one minute. In addition, this process does not damage any sensitive device structures.



## 2.Methodology

❖ Oerlikon univex 250 evaporator: This evaporator has a rotary and a turbomolecular pump that allows us to reach pressure values of  $10^{-6}$  mbar in two or three hours. It also has a temperature controller, which allows the substrates to be preheated or held at a given temperature during sublimation. It allows the sublimation of organic compounds for the deposit of the semiconductor layer and metals for the manufacture of electrodes, controlling the deposit speed and the thickness of the layers by means of a quartz microbalance.

❖ Trinos vacuum probe station: this customized probe station was made by the Spanish company *Trinos Vacuum* which allows us to characterize the transistors in vacuum conditions. It reaches a pressure of  $10^{-6}$  mbar. The electrical characterization provides the output and transfer curves which define the transport properties of the organic semiconductors, as seen in Chapter III.

Finally, devices were tested at room conditions by using an EB-4 Everbeing probe station with a 4200-SCS/C Keithley semiconductor characterization system.

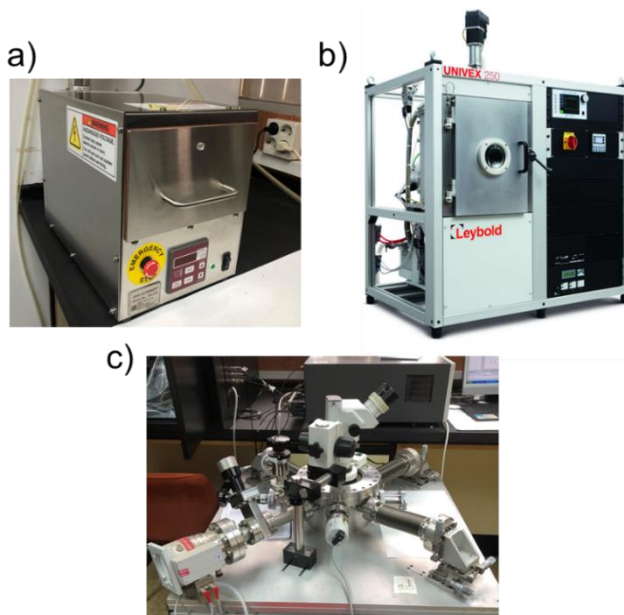


Figure 2.15 (a) Uvo cleaner 342-220, (b) oerlikon univex 250 evaporator and (c) Trinos vacuum probe station.

### 2.4 Bibliography.

1. McNaught, A. D. a. W., A, IUPAC. Compendium of Chemical Terminology, 2nd ed. (the "Gold Book"). In Blackwell Scientific Publications, O., Ed. 1997. Online version (2019) created by S. J. Chalk.
2. Douglas A. Skoog, D. M. W., F. James Holler, Stanley R. Crouch, Fundamentals of Analytical Chemistry. In Thomson Learning, U., 8th ed. (Translation of Paraninfo S. A.). Ed. 2008.
3. Drago, R. S., Physical Methods for Chemists. In Surfside Scientific Publishers, G. F., 2nd ed., Ed. 1992.
4. Hollas, J. M., Modern Spectroscopy. In John Wiley & Sons Ltd, C. E., 4th ed, Ed. 2004.
5. Paula, P. A. a. J. d., Atkin's Physical Chemistry. In Oxford University Press, U., 8th ed. (Translation of Editorial Médica Panamericana). Ed. 2006.
6. Patil, A. O.; Heeger, A. J.; Wudl, F., Optical properties of conducting polymers. *Chemical Reviews* **1988**, 88, (1), 183-200.



7. Ostlund, A. S. a. N., Modern Quantum Chemistry: Introduction to Advanced Electronic Structure Theory. In Dover Publications, I., Mineola: New York, 1st ed., Ed. 1996.
8. Levine, I. N., Quantum Chemistry. In Pearson Education S. A., L. U. K., 5th ed. , Ed. 2001.
9. Hohenberg, P.; Kohn, W., Inhomogeneous Electron Gas. *Physical Review* **1964**, 136, (3B), B864-B871.
10. Kohn, W.; Sham, L. J., Self-Consistent Equations Including Exchange and Correlation Effects. *Physical Review* **1965**, 140, (4A), A1133-A1138.
11. Vosko, S. H.; Wilk, L.; Nusair, M., Accurate spin-dependent electron liquid correlation energies for local spin density calculations: a critical analysis. *Canadian Journal of Physics* **1980**, 58, (8), 1200-1211.
12. Becke, A. D., Density-functional exchange-energy approximation with correct asymptotic behavior. *Physical Review A* **1988**, 38, (6), 3098-3100.
13. Lee, C.; Yang, W.; Parr, R. G., Development of the Colle-Salvetti correlation-energy formula into a functional of the electron density. *Physical Review B* **1988**, 37, (2), 785-789.
14. Miehlich, B.; Savin, A.; Stoll, H.; Preuss, H., Results obtained with the correlation energy density functionals of becke and Lee, Yang and Parr. *Chemical Physics Letters* **1989**, 157, (3), 200-206.
15. Perdew, J. P.; Burke, K.; Ernzerhof, M., Generalized Gradient Approximation Made Simple. *Physical Review Letters* **1996**, 77, (18), 3865-3868.
16. Tao, J.; Perdew, J.P.; Staroverov, V.N.; Scuseria, G.E.. Climbing the Density functional ladder: nonempirical meta-generalized gradient approximation designed for molecules and solids. *Physical Review Letters*. **2003**, 91, 146401.
17. Becke, A. D., Density-functional thermochemistry. III. The role of exact exchange. *The Journal of Chemical Physics* **1993**, 98, (7), 5648-5652.
18. Zhao, Y.; Truhlar, D.G. A new local density functionals for main-group thermochemistry, transition metal bonding, thermochemical kinetics, and noncovalent interactions. *Journal of chemical physics*. **2006**, 125, 194101.
19. Zhao, Y.; Truhlar, D. G., The M06 suite of density functionals for main group thermochemistry, thermochemical



kinetics, noncovalent interactions, excited states, and transition elements: two new functionals and systematic testing of four M06-class functionals and 12 other functionals. *Theoretical Chemistry Accounts* **2008**, 120, (1), 215-241.

20. Yan, Z.; Truhlar, D.G. Comparative DFT study of van der Waals complexes: Rare-gas dimers, alkaline-earth dimers, zinc dimer, and zinc-rare-gas dimers. *Journal of physical chemistry A*, **2006**, 110, 5121-5129

21. Chai, J.-D.; Head-Gordon, M., Long-range corrected hybrid density functionals with damped atom–atom dispersion corrections. *Physical Chemistry Chemical Physics* **2008**, 10, (44), 6615-6620.

22. Chai, J.-D.; Head-Gordon, M., Systematic optimization of long-range corrected hybrid density functionals. *The Journal of Chemical Physics* **2008**, 128, (8), 084106.

23. Grimme, S.; Ehrlich, S.; Goerigk, L., Effect of the damping function in dispersion corrected density functional theory. *Journal of Computational Chemistry* **2011**, 32, (7), 1456-1465.

24. Hariharan, P. C.; Pople, J. A., The influence of polarization functions on molecular orbital hydrogenation energies. *Theoretica chimica acta* **1973**, 28, (3), 213-222.

25. Hehre, W. J.; Ditchfield, R.; Pople, J. A., Self—Consistent Molecular Orbital Methods. XII. Further Extensions of Gaussian—Type Basis Sets for Use in Molecular Orbital Studies of Organic Molecules. *The Journal of Chemical Physics* **1972**, 56, (5), 2257-2261.

26. M. J. Frisch, G. W. T., H. B. Schlegel, G. E. Scuseria, M. A. Robb, J. R. Cheeseman, G. Scalmani, V. Barone, B. Mennucci, G. A. Petersson, H. Nakatsuji, M. Caricato, X. Li, H. P. Hratchian, A. F. Izmaylov, J. Bloino, G. Zheng, J. L. Sonnenberg, M. Hada, M. Ehara, K. Toyota, R. Fukuda, J. Hasegawa, M. Ishida, T. Nakajima, Y. Honda, O. Kitao, H. Nakai, T. Vreven, J. A. Montgomery, Jr., J. E. Peralta, F. Ogliaro, M. Bearpark, J. J. Heyd, E. Brothers, K. N. Kudin, V. N. Staroverov, R. Kobayashi, J. Normand, K. Raghavachari, A. Rendell, J. C. Burant, S. S. Iyengar, J. Tomasi, M. Cossi, N. Rega, J. M. Millam, M. Klene, J. E. Knox, J. B. Cross, V. Bakken, C. Adamo, J. Jaramillo, R. Gomperts, R. E. Stratmann, O. Yazyev, A. J. Austin, R. Cammi, C. Pomelli, J. W. Ochterski, R. L. Martin, K. Morokuma, V. G. Zakrzewski, G. A. Voth, P. Salvador, J. J. Dannenberg, S. Dapprich, A. D. Daniels, Ö. Farkas, J. B.



Foresman, J. V. Ortiz, J. Cioslowski, and D. J. Fox *Gaussian 09, Revision C.01*, 2009.

27. M. J. Frisch, G. W. T., H. B. Schlegel, G. E. Scuseria, M. A. Robb, J. R. Cheeseman, G. Scalmani, V. Barone, G. A. Petersson, H. Nakatsuji, X. Li, M. Caricato, A. V. Marenich, J. Bloino, B. G. Janesko, R. Gomperts, B. Mennucci, H. P. Hratchian, J. V. Ortiz, A. F. Izmaylov, J. L. Sonnenberg, D. Williams-Young, F. Ding, F. Lipparini, F. Egidi, J. Goings, B. Peng, A. Petrone, T. Henderson, D. Ranasinghe, V. G. Zakrzewski, J. Gao, N. Rega, G. Zheng, W. Liang, M. Hada, M. Ehara, K. Toyota, R. Fukuda, J. Hasegawa, M. Ishida, T. Nakajima, Y. Honda, O. Kitao, H. Nakai, T. Vreven, K. Throssell, J. A. Montgomery, Jr., J. E. Peralta, F. Ogliaro, M. J. Bearpark, J. J. Heyd, E. N. Brothers, K. N. Kudin, V. N. Staroverov, T. A. Keith, R. Kobayashi, J. Normand, K. Raghavachari, A. P. Rendell, J. C. Burant, S. S. Iyengar, J. Tomasi, M. Cossi, J. M. Millam, M. Klene, C. Adamo, R. Cammi, J. W. Ochterski, R. L. Martin, K. Morokuma, O. Farkas, J. B. Foresman, and D. J. Fox *Gaussian 16, Revision A.03*, 2016.

28. Improta, R.; Barone, V.; Scalmani, G.; Frisch, M. J., A state-specific polarizable continuum model time dependent density functional theory method for excited state calculations in solution. *The Journal of Chemical Physics* **2006**, 125, (5), 054103.

29. Improta, R.; Scalmani, G.; Frisch, M. J.; Barone, V., Toward effective and reliable fluorescence energies in solution by a new state specific polarizable continuum model time dependent density functional theory approach. *The Journal of Chemical Physics* **2007**, 127, (7), 074504.

30. Tomasi, J.; Mennucci, B.; Cammi, R., Quantum Mechanical Continuum Solvation Models. *Chemical Reviews* **2005**, 105, (8), 2999-3094.

31. Badía-Domínguez, I.; Pérez-Guardiola, A.; Sancho-García, J. C.; López Navarrete, J. T.; Hernández Jolín, V.; Li, H.; Sakamaki, D.; Seki, S.; Ruiz Delgado, M. C., Formation of Cyclophane Macrocycles in Carbazole-Based Biradicaloids: Impact of the Dicyanomethylene Substitution Position. *ACS Omega* **2019**, 4, (3), 4761-4769.

32. Runge, E.; Gross, E. K. U., Density-Functional Theory for Time-Dependent Systems. *Physical Review Letters* **1984**, 52, (12), 997-1000.



## 2. Methodology

33. Datta, A.; Mohakud, S.; Pati, S. K., Electron and hole mobilities in polymorphs of benzene and naphthalene: Role of intermolecular interactions. *The Journal of Chemical Physics* **2007**, 126, (14), 144710.
34. Datta, A.; Mohakud, S.; Pati, S. K., Comparing the electron and hole mobilities in the  $\alpha$  and  $\beta$  phases of perylene: role of  $\pi$ -stacking. *Journal of Materials Chemistry* **2007**, 17, (19), 1933-1938.
35. Mohakud, S.; Pati, S. K., Large carrier mobilities in octathio[8]circulene crystals: a theoretical study. *Journal of Materials Chemistry* **2009**, 19, (25), 4356-4361.
36. Mohan, V.; Datta, A., Structures and Electronic Properties of Si-Substituted Benzenes and Their Transition-Metal Complexes. *The Journal of Physical Chemistry Letters* **2010**, 1, (1), 136-140.
37. Valeev, E. F.; Coropceanu, V.; da Silva Filho, D. A.; Salman, S.; Brédas, J.-L., Effect of Electronic Polarization on Charge transport Parameters in Molecular Organic Semiconductors. *Journal of the American Chemical Society* **2006**, 128, (30), 9882-9886.
38. Chen, Z.; Wannere, C. S.; Corminboeuf, C.; Puchta, R.; Schleyer, P. v. R., Nucleus-Independent Chemical Shifts (NICS) as an Aromaticity Criterion. *Chemical Reviews* **2005**, 105, (10), 3842-3888.
39. Schleyer, P. v. R.; Maerker, C.; Dransfeld, A.; Jiao, H.; van Eikema Hommes, N. J. R., Nucleus-Independent Chemical Shifts: A Simple and Efficient Aromaticity Probe. *Journal of the American Chemical Society* **1996**, 118, (26), 6317-6318.
40. Wolinski, K.; Hinton, J. F.; Pulay, P., Efficient implementation of the gauge-independent atomic orbital method for NMR chemical shift calculations. *Journal of the American Chemical Society* **1990**, 112, (23), 8251-8260.
41. Rahalkar, A. Stanger, A., <https://chemistry.technion.ac.il/en/team/amnon-stanger/>
42. Stanger, A., Nucleus-Independent Chemical Shifts (NICS): Distance Dependence and Revised Criteria for Aromaticity and Antiaromaticity. *The Journal of Organic Chemistry* **2006**, 71, (3), 883-893.



43. Stanger, A., Obtaining Relative Induced Ring Currents Quantitatively from NICS. *The Journal of Organic Chemistry* **2010**, *75*, (7), 2281-2288.
44. Gershoni-Poranne, R.; Stanger, A., The NICS-XY-Scan: Identification of Local and Global Ring Currents in Multi-Ring Systems. *Chemistry – A European Journal* **2014**, *20*, (19), 5673-5688.
45. Geuenich, D.; Hess, K.; Köhler, F.; Herges, R., Anisotropy of the Induced Current Density (ACID), a General Method To Quantify and Visualize Electronic Delocalization. *Chemical Reviews* **2005**, *105*, (10), 3758-3772.
46. Yamaguchi, K.; Takahara, Y.; Fueno, T.; Nasu, K., Ab initio MO calculations of effective exchange integrals between transition-metal ions via oxygen dianions: nature of the copper-oxygen bonds and superconductivity. *Japanese journal of applied physics* **1987**, *26*, (8A), L1362.
47. Yamaguchi, K., The electronic structures of biradicals in the unrestricted Hartree-Fock approximation. *Chemical Physics Letters* **1975**, *33*, (2), 330-335.
48. Pérez-Guardiola, A.; Sandoval-Salinas, M. E.; Casanova, D.; San-Fabián, E.; Pérez-Jiménez, A.; Sancho-García, J.-C., The role of topology in organic molecules: origin and comparison of the radical character in linear and cyclic oligoacenes and related oligomers. *Physical Chemistry Chemical Physics* **2018**, *20*, (10), 7112-7124.
49. Neese, F., The ORCA program system. *Wiley Interdisciplinary Reviews: Computational Molecular Science* **2012**, *2*, (1), 73-78.
50. Tao, J.; Perdew, J. P.; Staroverov, V. N.; Scuseria, G. E., Climbing the density functional ladder: Nonempirical meta-generalized gradient approximation designed for molecules and solids. *Physical Review Letters* **2003**, *91*, (14), 146401.
51. Weigend, F.; Ahlrichs, R., Balanced basis sets of split valence, triple zeta valence and quadruple zeta valence quality for H to Rn: Design and assessment of accuracy. *Physical Chemistry Chemical Physics* **2005**, *7*, (18), 3297-3305.
52. Brooks, B. R.; Laidig, W. D.; Saxe, P.; Goddard, J. D.; Yamaguchi, Y.; Schaefer III, H. F., Analytic gradients from correlated wavefunctions via the two-particle density matrix and



## 2. Methodology

- the unitary group approach. *The Journal of Chemical Physics* **1980**, 72, (8), 4652-4653.
53. Krishnan, R.; Schlegel, H.; Pople, J., Derivative studies in configuration–interaction theory. *The Journal of Chemical Physics* **1980**, 72, (8), 4654-4655.
54. Pople, J. A.; Krishnan, R.; Schlegel, H. B.; Binkley, J. S., Derivative studies in hartree-fock and møller-pleeset theories. *International Journal of Quantum Chemistry* **1979**, 16, (S13), 225-241.
55. Pulay, P., Ab initio calculation of force constants and equilibrium geometries in polyatomic molecules: I. Theory. *Molecular Physics* **1969**, 17, (2), 197-204.
56. Wilson Jr, E. B., Decius, J. G., and Cross, P. G. Molecular vibrations. *American Journal of Physics*, **1955**, 23(8), 550-550.
57. Cornaton, Y., Ringholm, M., Louant, O., and Ruud, K. Analytic calculations of anharmonic infrared and Raman vibrational spectra. *Physical Chemistry Chemical Physics*, **2016**, 18(5), 4201-4215.
58. Ünal, Y., Nassif, W., Özeydin, B. C., and Sayin, K. Scale factor database for the vibration frequencies calculated in M06-2X, one of the DFT methods. *Vibrational Spectroscopy*, **2021**, 112, 103189.
59. Chemcraft - graphical software for visualization of quantum chemistry computations.  
<https://www.chemcraftprog.com>.
60. Pettersen, E. F.; Goddard, T. D.; Huang, C. C.; Couch, G. S.; Greenblatt, D. M.; Meng, E. C.; Ferrin, T. E., UCSF Chimera— a visualization system for exploratory research and analysis. *Journal of computational chemistry* **2004**, 25, (13), 1605-1612.
61. Marcus D Hanwell, Donald E Curtis, David C Lonie, Tim Vandermeersch, Eva Zurek and Geoffrey R Hutchison; “Avogadro: An advanced semantic chemical editor, visualization, and analysis platform” *Journal of Cheminformatics* **2012**, 4:17.





# SECTION 3. Results and discussion

## Table of contents

---

3.1 Chapter I: Evolution of the diradical character of dicyanomethylene substituted carbazole and indolocarbazole-based systems.

3.2 Chapter II: Cyclophane self-assembly from carbazole and indolocarbazole-based diradicals.

3.3 Chapter III: Photophysical and charge transport properties of carbazole-based macrocycles.

---





# CHAPTER I: Evolution of the diradical character of dicyanomethylene substituted carbazole and indolocarbazole-based systems.

## Table of contents

---

- 3.1.1 Introduction.
  - 3.1.2 Effect of substitution pattern and chain elongation on the diradical stability.
    - 3.1.2.1 Ground-state electronic structure.
    - 3.1.2.2 Optical properties.
    - 3.1.2.3 Relationship between diradical character and aromaticity.
  - 3.1.3 Influence of the structural isomerism on the diradical stability.
    - 3.1.3.1 Ground-state electronic structure.
    - 3.1.3.2 Relationship between diradical character and aromaticity.
  - 3.1.4 Conclusions.
  - 3.1.5 Bibliography.
-





### 3.1.1 Introduction.

Over the past few decades, diradicaloids have attracted remarkable attention due to their important role in understanding the nature of chemical bonds<sup>1-5</sup> and their wide range of promising applications as organic electronic devices, spintronics, non-linear optics, or chemical sensors, among others<sup>6-14</sup>. Theoretical chemistry investigations are vital to establish structure-property relationships for these molecules; for instance in the rationalization on how molecular properties change as a function of the degree of open-shell (OS) singlet nature<sup>15-22</sup>. Therefore, the quantitative estimation of diradical character by using theoretical methods is considered relevant since it enables a deeper understanding of the optical and electronic properties in OS molecular systems. More concretely, one of the most widely studied subject has been how the structural modifications influence the extent of diradical character<sup>23-30</sup>.

In this section, how the following chemical modifications affect the diradical character have been investigated: (i) substitution pattern<sup>31-37</sup>, (ii) the elongation of the conjugated backbone<sup>38-45</sup> and (iii) the structural isomerism<sup>46-50</sup>. To this end, we focus on carbazole (Cz) and indolocarbazole (ICz) diradicaloids (Figure 3.1) with dicyanomethylene (DCM) groups in para- or meta-positions. This investigation allows a deeper understanding of how the chemical reactivity and physical properties of  $\pi$ -conjugated diradicaloids are affected by these

three strategies (*i.e.*, substitution pattern, backbone elongation and structural isomerism).

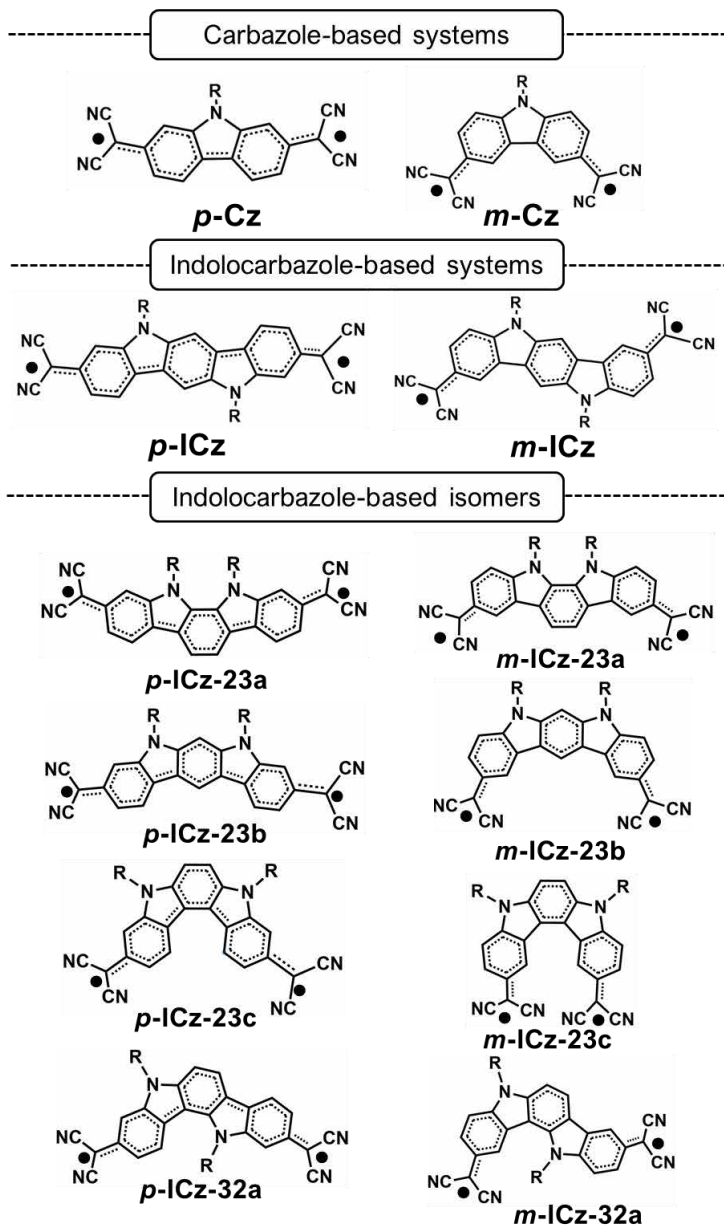


Figure 3.1 Whole set of DCM-substituted Cz and ICz-based systems studied in this section in their OS singlet state.

### 3.1.2 Effect of substitution pattern and chain elongation on the diradical stability.

Herein, we have studied the influence of chain elongation on the diradical character of Cz-based systems substituted with DCM groups via para (*p*-Cz and *p*-ICz) or meta (*m*-Cz and *m*-ICz) positions. The comparison of these four analogous molecules (Figure 3.2) represents a unique opportunity to evaluate how the  $\pi$ -delocalization and diradical character change with chain length and the different linkage positions.

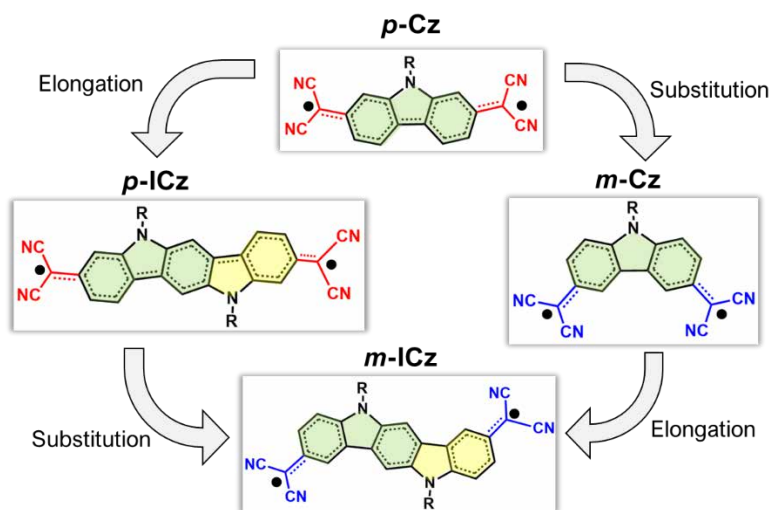


Figure 3.2 DCM-substituted diradicaloids under study.

#### 3.1.2.1 Ground-state electronic structure.

Firstly, we carried out a purely theoretical study of the ground-state electronic structure of the DCM-substituted diradicaloids at the DFT level. As Figure 3.3 shown, the HOMO-LUMO gap (HL gap) of these systems is quite small ( $\sim 3.1$ - $1.2$  eV) because of the strong stabilization of the LUMO upon the

insertion of the electron-withdrawing DCM groups when compared to the unsubstituted Cz and ICz molecules.

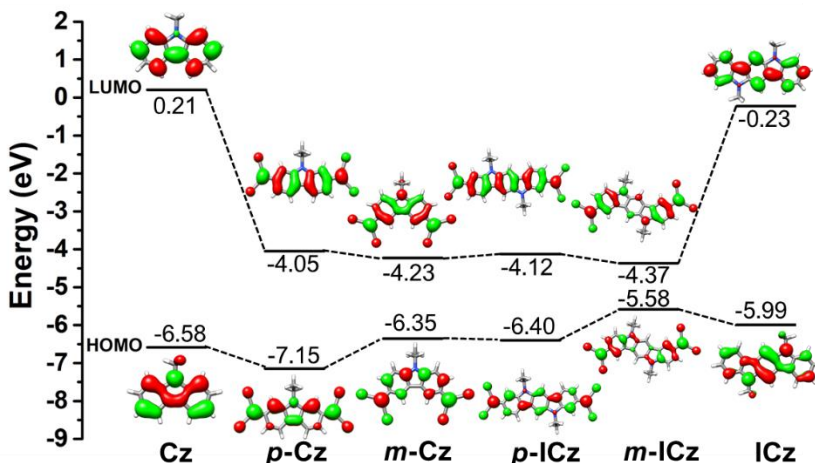


Figure 3.3. DFT-computed molecular orbital diagram for the DCM-substituted systems (*p*-Cz, *m*-Cz, *p*-ICz and *m*-ICz) and their unsubstituted homologues (Cz and ICz) at the M06-2X/6-31G\*\* level of theory. The topologies of the frontier molecular orbitals are also shown (isovalue 0.03 au).

Focusing on the DCM-substituted compounds, several important points should be highlighted: (i) the substitution of the DCM groups at the meta position shifts the  $E_{\text{HOMO}}$  to higher energy when compared to the para-substituted systems (*i.e.*, *m*-Cz and *m*-ICz vs. *p*-Cz and *p*-ICz, respectively). This is due to the fact that Cz and ICz units substituted at the para position display a longer conjugation path increasing the electronic delocalization meanwhile the meta position decreases the conjugation because of the interruption of the linear  $\pi$ -system<sup>51-55</sup>. (ii) Comparing the ICz compounds with their shorter Cz analogues, the increasing conjugation length causes a moderate  $E_{\text{HOMO}}$  destabilization together with a slight  $E_{\text{LUMO}}$  stabilization. This results in a HL gap



## Chapter I: Evolution of the diradical character

decreased of  $\sim 0.8$  eV on going from ***p*-Cz** to ***p*-ICz** (from 3.10 to 2.28 eV, respectively) and 0.9 eV from ***m*-Cz** to ***m*-ICz** (from 2.10 to 1.21 eV, respectively). As the HL gap decreases, the promotion of electrons from HOMO to LUMO is facilitated and therefore, the diradical character should be more pronounced<sup>41</sup>. (iii) The calculated frontier molecular orbitals (HOMO and LUMO) of the CS state are distributed on the whole  $\pi$ -conjugated core, with the DCM groups hosting a large electron density. However, in the case of the ***m*-ICz**, the electron density of the HOMO level is mainly localized at the external DCM groups and adjacent indole groups due to the less favourable conjugation with the ICz core exerted by the meta-substitution.

Secondly, the diradical stability of the compounds under study is also explored by means of different physical parameters: (i) the energy difference between OS singlet and CS singlet states ( $\Delta E_{OS-CS}$ ), (ii) the singlet-triplet energy gap ( $\Delta E_{S-T}$ ) and (iii) the effective electron exchange interaction ( $J_{ab}$ ) which reflects the overlap integral between the two nearly energetically degenerate molecular orbitals (following the equations described in methodology section). All these data are summarized in Table 3.1.



Table 3.1. Summarized DFT-calculated physical properties of compounds under study, at the (U)M062-X/6-31G\*\* level of theory.

	$\Delta E_{OS-CS}^a$	$\Delta E_{S-T}^b$	$J_{ab}^c$	HL gap <sup>d</sup>	$\langle S^2 \rangle^e$	
	(kcal·mol <sup>-1</sup> )	(kcal·mol <sup>-1</sup> )	(kcal·mol <sup>-1</sup> )	(eV)	OS	T
<b>p-Cz</b>	-3.27	-8.36	-4.10	3.10	0.79	2.04
<b>m-Cz</b>	-14.30	-2.32	-1.13	2.12	1.00	2.04
<b>p-ICz</b>	-10.92	-3.26	-1.59	2.28	1.01	2.04
<b>m-ICz</b>	-24.27	-0.37	-0.18	1.21	1.04	2.04

<sup>a</sup> The energy difference between OS singlet and CS singlet states. <sup>b</sup> The singlet-triplet energy gap. <sup>c</sup> The effective electron exchange interaction. <sup>d</sup> The HOMO-LUMO gap. <sup>e</sup> The spin contamination of the OS singlet and triplet state.

As seen in Table 3.1, the negative values of  $\Delta E_{OS-CS}$  reveals that all DCM-substituted systems are OS diradicals in the ground state, with this effect being more significant when the DCM groups are connected at the meta position. The  $\Delta E_{OS-CS}$  value is  $\sim -3$  kcal·mol<sup>-1</sup> for **p-Cz**, whereas this difference increases up to  $\sim -14$  kcal·mol<sup>-1</sup> in **m-Cz** homologue. Note that this difference is more significant for the ICz-based systems ( $\sim -11$  kcal·mol<sup>-1</sup> and  $\sim -24$  kcal·mol<sup>-1</sup> for **p-ICz** and **m-ICz**, respectively). Similarly, the  $\Delta E_{S-T}$  can be remarkably tuned upon chain elongation (*i.e.*, from -8.36 kcal·mol<sup>-1</sup> to -3.26 kcal·mol<sup>-1</sup> on going from **p-Cz** to **p-ICz**) and when going from para- to meta-substitution (*i.e.*, from -8.36 kcal·mol<sup>-1</sup> to -2.32 kcal·mol<sup>-1</sup> on going from **p-Cz** to **m-Cz**). Among all systems, the smallest  $\Delta E_{S-T}$  value is obtained for **m-ICz** compound (-0.37 kcal·mol<sup>-1</sup>). Note that small  $\Delta E_{S-T}$  values are generally accompanied by weak coupling of the unpaired electrons and thus, by large diradical character<sup>13, 56</sup>.





## Chapter I: Evolution of the diradical character

On the other hand, the OS singlet ground state of all molecules is supported by negative  $J_{ab}$  values. This parameter evaluated from the  $\Delta E_{S-T}$  indicates that the interaction between two unpaired electrons is smaller for ***p-ICz*** ( $-1.59 \text{ kcal}\cdot\text{mol}^{-1}$ ) with respect to ***p-Cz*** ( $-4.10 \text{ kcal}\cdot\text{mol}^{-1}$ ), and even lower values are predicted for the meta-substituted compounds ( $-1.13 \text{ kcal}\cdot\text{mol}^{-1}$  and  $-0.18 \text{ kcal}\cdot\text{mol}^{-1}$  for ***m-Cz*** and ***m-ICz***, respectively). Therefore, the OS diradical form should be favoured by increasing the chain length and when going from para to meta position.

Besides, the investigation of the frontier molecular orbitals of the OS singlet state is useful to get an additional insight into the electronic diradicaloid nature<sup>57, 58</sup>. As shown in Figure 3.4, the singly occupied molecular orbital (SOMO) profiles of the  $\alpha$  and  $\beta$  spins in the meta-substituted ***m-Cz*** and ***m-ICz*** systems can be classified as singlet disjoint diradicals where the two unpaired electrons reside on a different part of the molecule with almost no overlap between them (even more notably in the case of the ***m-ICz*** system). In contrast, the SOMOs of para-substituted compounds (***p-Cz*** and ***p-ICz***), exhibit some overlap at the central conjugated core indicating an extended delocalization.

Interestingly, the resulting spin density distribution of the ***p-Cz***, ***m-Cz*** and ***p-ICz*** compounds is highly delocalized over the entire core with a strong contribution from the DCM groups. In opposite, the ***m-ICz*** system is the only case where the spin density is located exclusively on the external parts of the

molecule with no overlap. Consequently, the two unpaired electrons in ***m*-ICz** are less electronically coupled because of the disruption of the effective  $\pi$ -conjugation<sup>43</sup>. This is in consonance with the rest of the physical parameters studied here which point out that ***m*-ICz** should display the strongest diradical character among the series, as will be shown below.

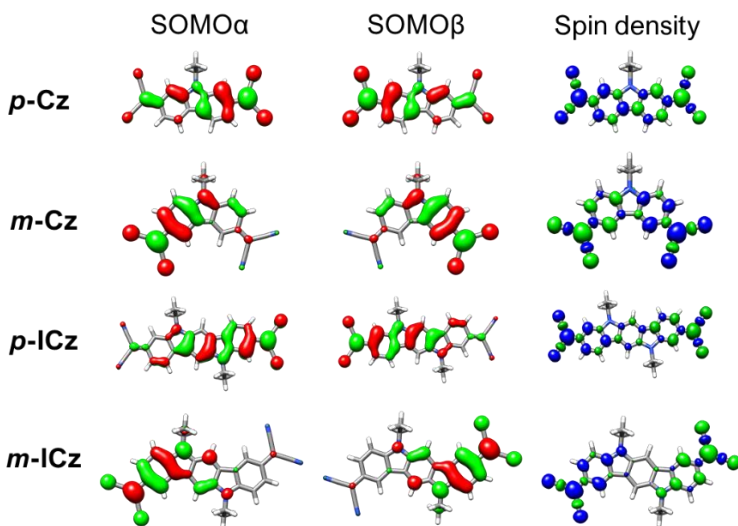


Figure 3.4. DFT-calculated singly occupied molecular orbital (SOMO) of  $\alpha$  and  $\beta$  electrons and spin density distribution of the four diradicaloid systems, at the UM06-2X/6-31G\*\* level of theory (isosurface value=0.03 au). The blue and green surfaces represent  $\alpha$  and  $\beta$  spin densities, respectively.

### 3.1.2.2 Optical properties.

Interestingly, a distinctive characteristic of OS singlet diradical systems is the presence of double exciton states (H,H-L,L) in low lying excited states<sup>27,59-62</sup>. Recently, several investigations have proved that this state can become the lowest singlet excited state for compounds with large diradical

character, a feature which has been experimentally supported for several conjugated diradicals and may influence their photo-response properties.

The quality of predictions can be appreciated in Figure 3.5 where the experimental and computed spectra of **p-ICz** are compared. As shown in Figure 3.5a, the experimental electronic spectrum of **p-ICz** shows a strong absorption at 1.76 eV together with two weak shoulders at lower energy (1.58 and 1.44 eV). Based on computed results, the first intense band is readily assigned to the H-L transition (determined from the broken-symmetry geometry is 1.72 eV) while the low energy shoulders are assigned to the double exciton state (two low lying excited states computed at TDUB3LYP level at 1.28 and 1.33 eV are dominated by the H,H-L,L excitations).

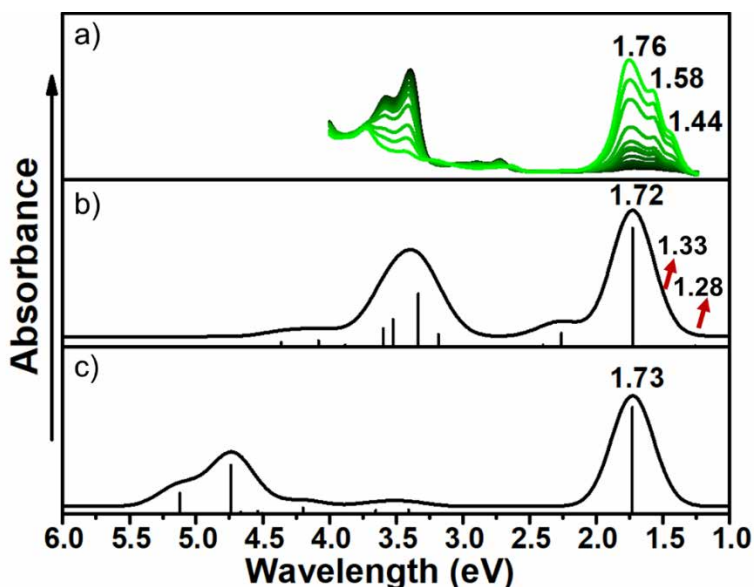


Figure 3.5 (a) UV/Vis-NIR absorption spectra of **p-ICz** compound in *o*-dichlorobenzene upon heating from 300 to 410 K. (b)



TDUDFT electronic absorption spectra (UB3LYP/6-31G\*\*) of **p-ICz** OS structure. The red arrows show the theoretical values of the one-photon forbidden (H,H → L,L) excited state. (c) TD-DFT electronic absorption spectra (B3LYP/6-31G\*\*) of **p-ICz** CS structure.

### 3.1.2.3 Relationship between diradical character and aromaticity.

For a better understanding of the key structure/diradical character relationship, the diradical character has been calculated using two methods. First, the diradical character  $y_0$  (CS structure has  $y_0=0$  and pure diradical state has  $y_0=1$ ) was calculated from the occupation numbers of the highest occupied natural orbital and the lowest unoccupied natural orbital using the spin-projected formalism<sup>63</sup>. This parameter is obtained by the equation described in methodology section.

Second, the fractional orbital density (FOD) method that incorporates a strong correlation effect has also been used to calculate the  $N^{\text{FOD}}$  values. The  $N^{\text{FOD}}$  values are the integrated number of electrons arising from the fractional occupation of orbitals and represent a very good estimation of the diradical character<sup>64</sup>. Following the trend reported before for a set of some polycyclic aromatic molecules where a linear relationship between the  $N^{\text{FOD}}$  values and the experimental diradical character is reported<sup>65</sup>,  $N^{\text{FOD}} \geq 1.5$  indicates a highly pronounced diradical character, whereas  $N^{\text{FOD}} < 1.5$  is associated with a slightly pronounced diradical character.

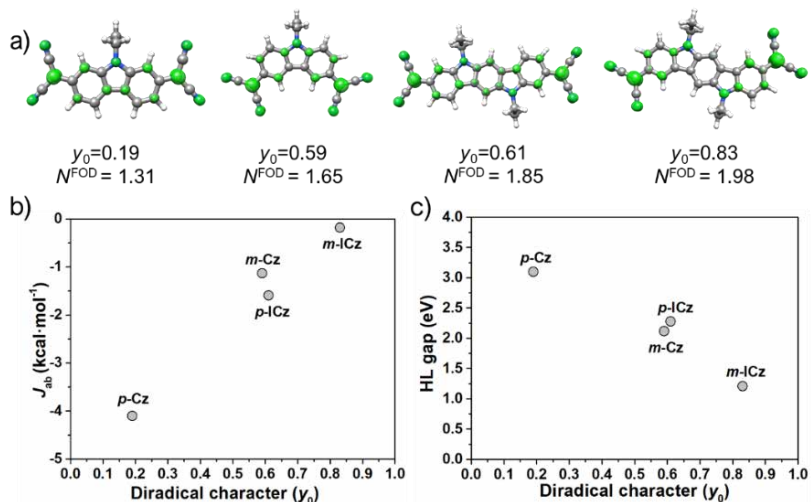


Figure 3.6. (a) Isocontour plot of the FOD density ( $\sigma = 0.005 \text{ e} \cdot \text{bohr}^{-3}$ ) and predicted  $N^{\text{FOD}}$  values together with the diradical character  $y_0$  values of four DCM-substituted diradicaloids. (b) Relationship between the diradical character  $y_0$  and  $J_{\text{ab}}$ . (c) Relationship between the diradical character  $y_0$  and the HL gap.

As Figure 3.6a displays, the diradical character can be remarkably tuned upon increasing the chain length elongation (*i.e.*, from  $y_0 = 0.19$  to  $y_0 = 0.61$  on going from ***p*-Cz** to ***p*-ICz**) and when going from para to meta-substitution (*i.e.*, from  $y_0 = 0.19$  to  $y_0 = 0.59$  on going from ***p*-Cz** to ***m*-Cz**). Among all systems, the highest diradical character is obtained for ***m*-ICz** compound ( $y_0 = 0.83$ ). Therefore, the extension of molecular size and the meta-substitution promote the diradical state. The FOD plots of the Cz and ICz-based systems show that the spatial distribution of the unpaired  $p$ -electrons is highly delocalized over the whole molecule with a strong contribution from the central carbon atoms of the DCM groups (see Figure 3.6a). The  $N^{\text{FOD}}$  values can be categorized as (i) mild for the ***p*-Cz** ( $N^{\text{FOD}} \sim 1.3$ ), (ii) moderate for



## Chapter I: Evolution of the diradical character

the ***m*-Cz** ( $N^{\text{FOD}} \sim 1.6$ ) and (iii) pronounce for the ***p*-ICz** and ***m*-ICz** ( $N^{\text{FOD}} \sim 1.9$  and 2, respectively). Thus, our calculations again suggest that the diradical character is strongly affected by the DCM-substitution position and the increase of the chain length. As seen in Figure 3.6b,c, the DFT-calculated diradical character values are in consonance with the trend predicted for the physical parameters ( $J_{\text{ab}}$  and HL gap values) along the series.

It is well-known in the literature that there is a correlation between the stabilization of the diradical and the (anti)aromaticity<sup>66-69</sup>. To explore this effect in more detail, we now discuss the NICS(0)<sup>70</sup> values calculated at the centre of the phenyl rings (see Table 3.2). Note that negative NICS values indicate aromaticity (diatropic ring current) while positive values indicate antiaromaticity (paratropic ring current); thus, an increase in the diatropic ring current is associated with a partial gain in aromatic character<sup>67, 68</sup>.

Table 3.2. NICS(0) values for Cz and ICz-based systems. The chemical structure of ***p*-Cz** and ***p*-ICz** are also shown.

Molecule	NICS <sub>A</sub> <sup>c</sup>		NICS <sub>B</sub> <sup>d</sup>		$y_0$
	CS	OS	CS	OS	
<b><i>p</i>-Cz</b>	0.3	-2.4	----	----	0.19
<b><i>m</i>-Cz</b>	-2.0	-5.1	----	----	0.59
<b><i>p</i>-ICz</b>	-0.5	-4.1	-0.9	-6.6	0.61
<b><i>m</i>-ICz</b>	-3.0	-5.3	-6.6	-9.5	0.83

<sup>a</sup> NICS<sub>A</sub> (0) values of the external phenyl rings at B3LYP/6-311+G\* level. <sup>b</sup> NICS<sub>B</sub> (0) values of the central phenyl ring of ICz-based systems at B3LYP/6-311+G\* level.



## Chapter I: Evolution of the diradical character

Focusing on the NICS(0) values, three key points should be highlighted: (i) The NICS(0) values calculated demonstrate that an increase in the aromatic degree is found when going from CS to OS state with this effect being more intense in the meta-substituted system and in the more extended systems. Therefore, the aromatization of the phenyl rings can be described as the driving force for the stabilization of the diradical species. (ii) Focusing on the CS state, slight differences are predicted in ***p*-ICz** when going from the external rings to the central core (with NICS values between -0.5 ppm and -0.9 ppm) whereas larger differences are found for ***m*-ICz** (with NICS values between -3.0 ppm and -6.6 ppm). Thus, the meta-connection leads to less conjugation between the external and central part of the ICz core in accordance with the increased diradical character.

### 3.1.3 Influence of the structural isomerism on the diradical stability.

Previously, we have demonstrated that the diradical character can be strongly modulated by increasing the chain length and the substitution pattern. Now, we explore how an additional structural change (*i.e.*, structural isomerism) affects the conjugation pattern in ICz-based systems, and thus the resulting diradical character<sup>47, 71-74</sup>. Note that it has been shown that the indenofluorene family<sup>75-80</sup>, which has the possibility to change the conjugation between the radical centres from para, to meta to ortho exhibits marked differences in magnetic properties by structural isomerism since the electronic ground state was found

to change from singlet to triplet character as a function of different topological changes<sup>76, 81</sup>.

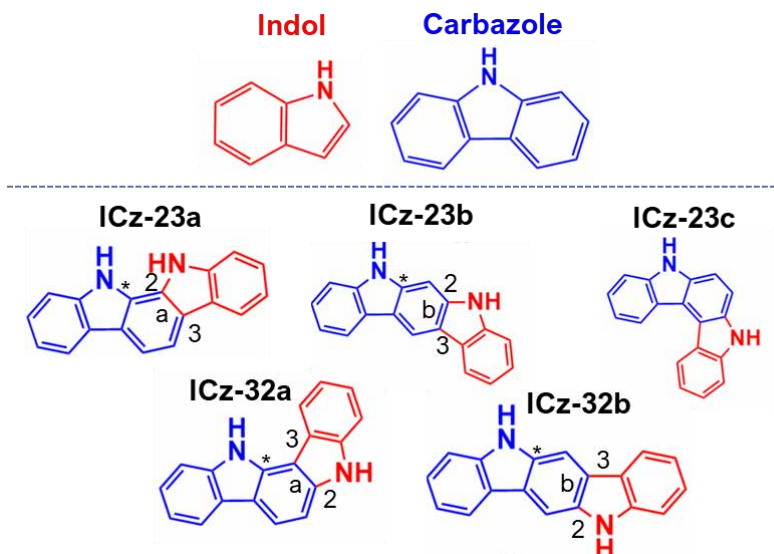


Figure 3.7 The five structural ICz isomers.

The ICz system possesses five structural isomers (Figure 3.7) with different phenyl linkages in ortho (**ICz-23c**), meta (**ICz-23b** and **ICz-32a**) and para (**ICz-23a** and **ICz-32b**) positions and different bridge structures (anti for **ICz-32a** and **ICz-32b** vs. syn conformation in **ICz-23a**, **ICz-23b** and **ICz-23c**). In addition, the insertion of DCM groups in para or meta-position with respect to the conjugated framework allows us to study a library of ten ICz isomers (Figure 3.8) that represent a truly good test to understand the consequences of the topological changes in the diradical character. In this way, we focus on elucidating how substitution position and structural isomerism modulate the diradical character, and thus the chemical reactivity and physical



properties aiming at building design guidelines for better efficient functional diradical systems.

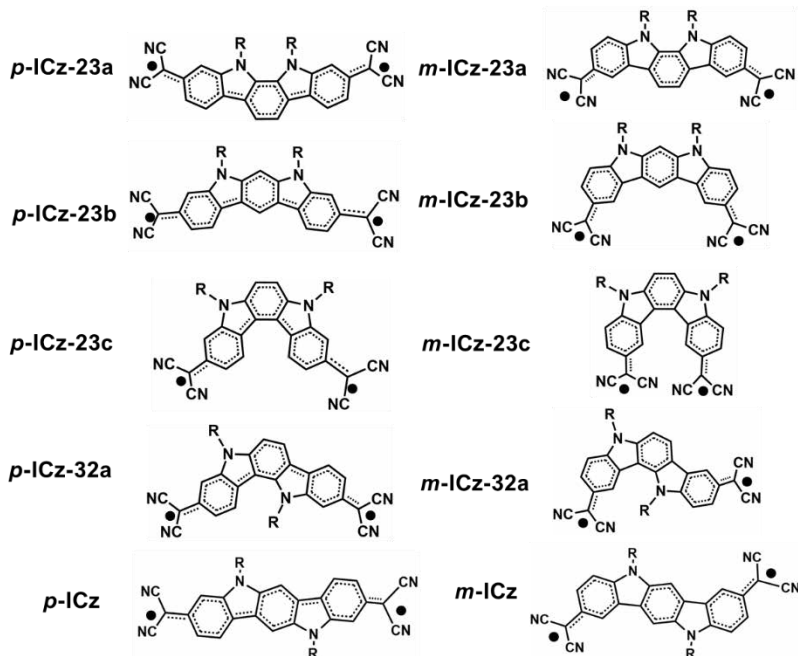


Figure 3.8. Ten ICz-based isomers studied in this section in their OS singlet state. Note that ***p*-ICz-32b** and ***m*-ICz-32b** isomers are denoted as ***p*-ICz** and ***m*-ICz** in order to be consistent with the previous section.

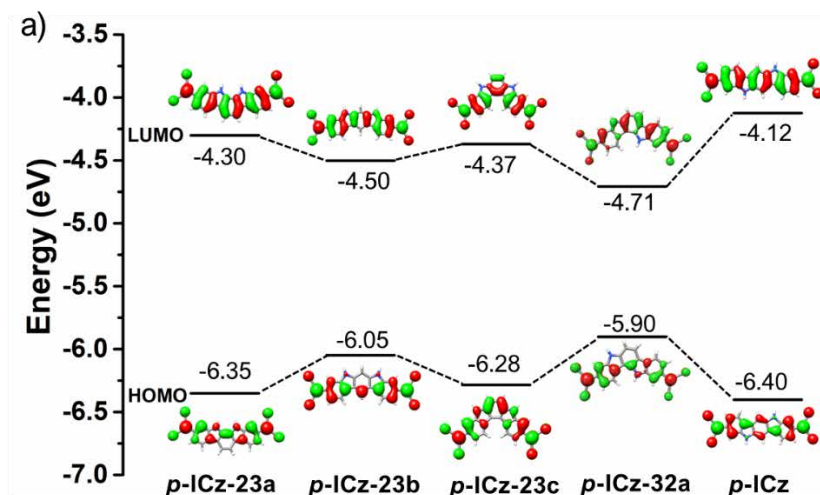
### 3.1.3.1 Ground-state electronic structure.

First of all, we performed a theoretical study of the ground-state electronic structure of the ten ICz-based isomers at the DFT level. Figure 3.9 shows the molecular orbital energy diagram and topologies for the whole set of isomers. As mentioned above, the HL gap decreased favours the HOMO to LUMO promotion of electrons and therefore, the diradical character should be more pronounced. At this point, we should highlight several important points: (i) focusing on the para-linked isomers, the HL gap values



## Chapter I: Evolution of the diradical character

for ***p*-ICz-23a**, ***p*-ICz-23c** and ***p*-ICz** compounds (2.05, 1.91 and 2.28 eV, respectively) are higher than for ***p*-ICz-23b** and ***p*-ICz-32a** analogues (1.55 and 1.19 eV, respectively). (ii) A HL gap decreased is found when compared the para-connected compounds with their meta-substituted analogues. The strongest reduction (of around 1 eV) is found when going from ***p*-ICz-23a** to ***m*-ICz-23a** (from 2.05 to 0.98 eV, respectively) and from ***p*-ICz** to ***m*-ICz** (from 2.28 to 1.21 eV, respectively). (iii) The frontier molecular orbital wavefunctions are delocalized over the whole conjugated core in the para-substituted systems, whereas in the meta-substituted compounds are predominantly located on the DCM groups and adjacent indole groups because of the less favourable conjugation at the meta-position.



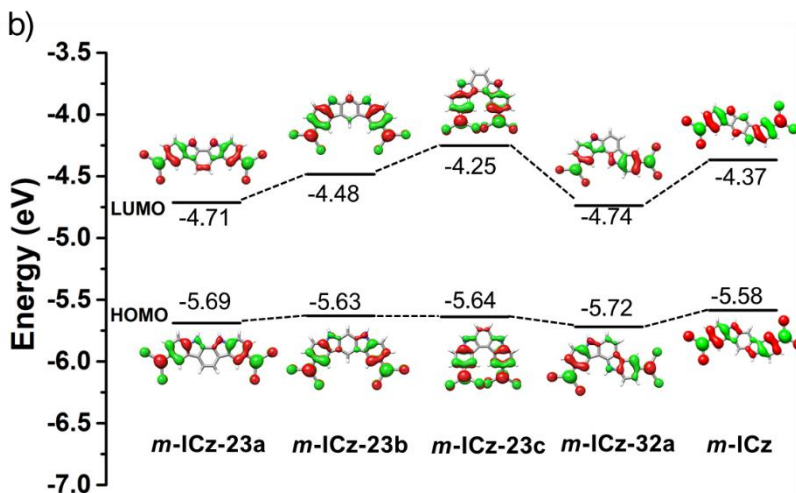


Figure 3.9. DFT-computed molecular orbital diagram for (a) the para-substituted systems (***p*-ICz-23a**, ***p*-ICz-23b**, ***p*-ICz-23c**, ***p*-ICz-32a** and ***p*-ICz**) and (a) the meta-connected homologues (***m*-ICz-23a**, ***m*-ICz-23b**, ***m*-ICz-23c**, ***m*-ICz-32a** and ***m*-ICz**) at the M06-2X/6-31G\*\* level of theory. The topologies of the frontier molecular orbitals are also shown (isovalue 0.03 au).

On the one hand, the diradical stability of the compounds under study is also explored by means of different physical parameters (*i.e.*, the  $\Delta E_{OS-CS}$ , the  $\Delta E_{S-T}$ , and the  $J_{ab}$ ). All these data are summarized in Table 3.3.



Table 3.3. Summarized DFT-calculated physical properties of compounds under study, at the (U)M062-X/6-31G\*\* level of theory.

	$\Delta E_{OS-CS}^a$ (kcal·mol <sup>-1</sup> )	$\Delta E_{S-T}^b$ (kcal·mol <sup>-1</sup> )	$J_{ab}^c$ (kcal·mol <sup>-1</sup> )	HL gap <sup>d</sup> (eV)	$\langle S^2 \rangle^e$	
					OS	T
<b>p-ICz-23a</b>	-13.74	-2.21	-1.08	2.05	1.02	2.05
<b>p-ICz-23b</b>	-19.73	-0.03	-0.01	1.55	1.04	2.06
<b>p-ICz-23c</b>	-16.85	-0.68	-0.33	1.91	1.04	2.05
<b>p-ICz-32a</b>	-25.25	0.74	0.36	1.19	1.04	2.05
<b>p-ICz</b>	-10.92	-3.26	-1.59	2.28	1.01	2.04
<b>m-ICz-23a</b>	-30.79	0.03	0.02	0.98	1.05	2.04
<b>m-ICz-23b</b>	-26.92	-0.07	-0.04	1.15	1.04	2.05
<b>m-ICz-23c</b>	-26.74	0.03	0.02	1.39	1.05	2.04
<b>m-ICz-32a</b>	-30.42	0.26	0.13	0.98	1.04	2.05
<b>m-ICz</b>	-24.27	-0.37	-0.18	1.21	1.04	2.04

<sup>a</sup> The energy difference between OS singlet and CS singlet states. <sup>b</sup> The singlet-triplet energy gap. <sup>c</sup> The effective electron exchange interaction. <sup>d</sup> The HOMO-LUMO gap. <sup>e</sup> The spin contamination of the singlet and triplet state.

As seen in Table 3.3, the negative values of  $\Delta E_{OS-CS}$  reveals that the whole set of ICz-based systems are OS singlet in their ground state, with this effect being more significant when the DCM groups are connected at the meta-position.  $\Delta E_{OS-CS}$  values in the range of  $\sim -11/-25$  kcal·mol<sup>-1</sup> are predicted for the para-substituted compounds, whereas this difference increases up to  $\sim -25/-31$  kcal·mol<sup>-1</sup> in the meta-connected homologues. Similarly, the  $J_{ab}$  and  $\Delta E_{S-T}$  parameters can be fine-tuned upon structural isomerism and substitution pattern. In fact, several isomers result in stable triplet ground states with positive  $\Delta E_{S-T}$  and  $J_{ab}$  values (*i.e.*, **p-ICz-32a**, **m-ICz-23a**, **m-ICz-23c** and **m-ICz-32a**). Thus, it could be expected that these compounds should display more pronounced diradical character.

Interestingly, it should be highlighted that all systems are characterized by planar backbone conformations except for **ICz-23c** isomers which display twisted structures (*i.e.*, with bay dihedral angle,  $\theta$ , of  $15^\circ$  in ***p*-ICz-23c** and  $22^\circ$  in ***m*-ICz-23c** observed in Figure 3.10). These distortions from planarity might be expected to involve remarkable modifications on the molecular conjugation and consequently, on the diradical character, as will be shown below<sup>82, 83</sup>.

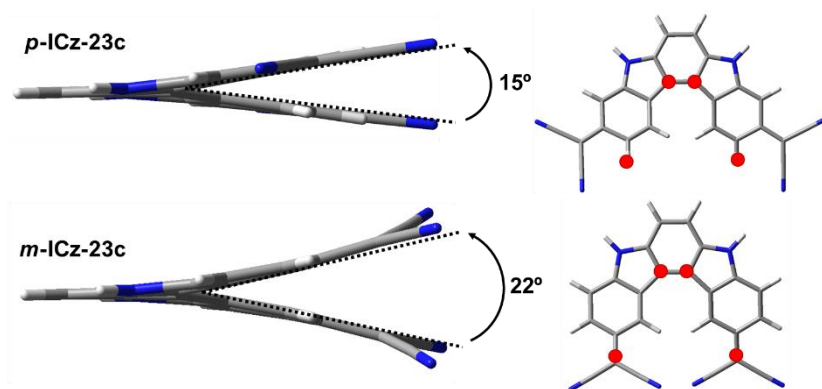


Figure 3.10. Top (right) and side (left) views of the optimized geometries for ***p*-ICz-23c** (up) and ***m*-ICz-23c** (down) calculated at the M06-2X/6-31G\*\* level of theory. The bay dihedral values ( $^\circ$ ) are also shown.

On the other hand, the investigation of the frontier molecular orbitals of the OS singlet state is useful to get an additional insight into the nature of the diradicaloids. As shown in Figure 3.11, the SOMO profiles in the meta-substituted compounds can be classified as singlet disjoint diradicals where the two unpaired electrons reside on a different part of the molecule with almost no overlap between them. In contrast, the SOMOs of para-substituted compounds are not separated but overlap at the

centre of the core displaying an extended delocalization, except for *p*-ICz-23b and *p*-ICz-32a compounds.

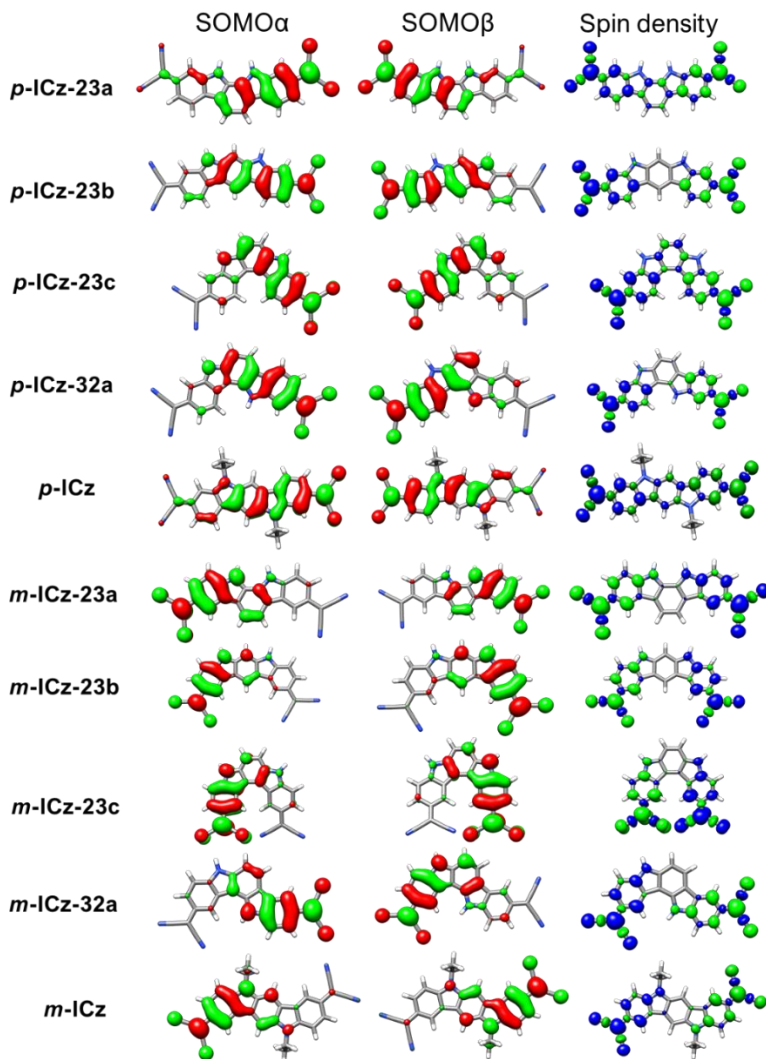


Figure 3.11. Frontier molecular orbitals and spin density distribution of ICz-based isomers computed by using the unrestricted BS method (isosurface value=0.03 au, blue for negative and green for positive sign).



## Chapter I: Evolution of the diradical character

Interestingly, the resulting spin density distribution of ICz isomers is localized over the external indole units and adjacent DCM groups, with the exception of ***p*-ICz-23a**, ***p*-ICz-23c** and ***p*-ICz** where the spin density distribution is delocalized over the entire  $\pi$ -conjugated core. Consequently, the two unpaired electrons in ***p*-ICz-23a**, ***p*-ICz-23c** and ***p*-ICz** compounds are electronically connected through the conjugated backbone while in the rest of isomers are less coupled because of the disruption of the effective  $\pi$ -conjugation. This is in consonance with the physical parameters previously reported here which point out that ***p*-ICz-23a**, ***p*-ICz-23c** and ***p*-ICz** display the lowest diradical character within the series.

### 3.1.3.2 Relationship between diradical character and aromaticity.

As Figure 3.12 shows, the diradical character can be remarkably tuned upon structural isomerism (*i.e.*, from  $y_0 = 0.65$  to  $y_0 = 0.93$  on going from ***p*-ICz-23a** to ***p*-ICz-32a**) and by varying the DCM connection (*i.e.*, from  $y_0 = 0.65$  to  $y_0 = 0.97$  on going from ***p*-ICz-23a** to ***m*-ICz-23a**). In addition, the FOD plots of the ICz-based isomers show that the spatial distribution of the unpaired electrons is highly localized over the central carbon atoms of the DCM groups (see Figure 3.12). The  $N^{\text{FOD}}$  values can be categorized as pronounce for all systems ( $N^{\text{FOD}} \sim 1.8/2.2$ ). Thus, our calculations again suggest that the diradical character is strongly affected by structural modifications.

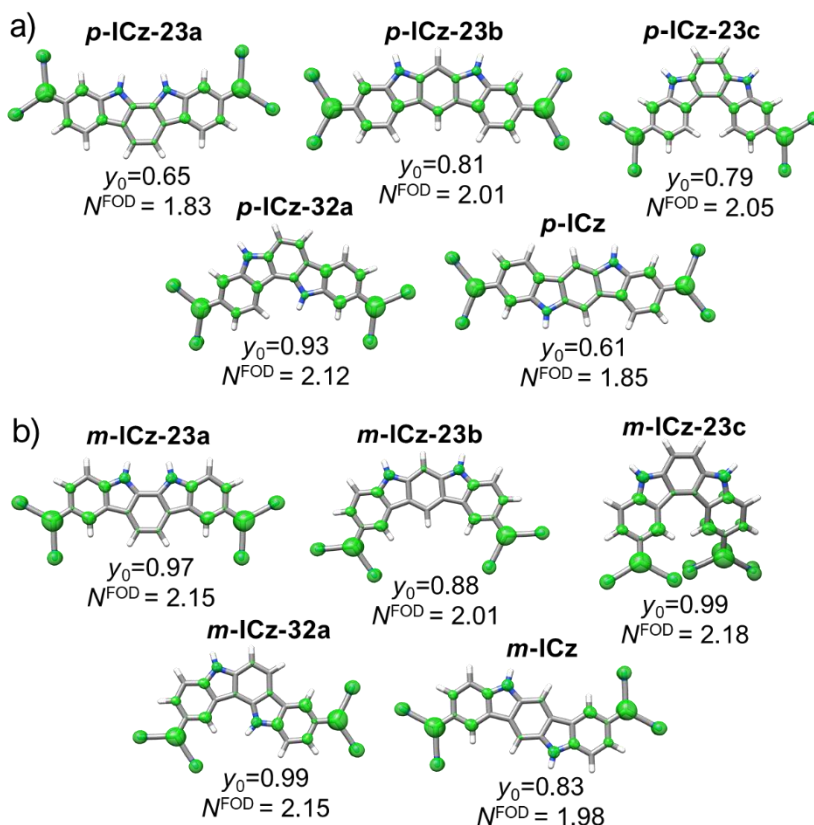


Figure 3.12. (a) Isocontour plot of the FOD density ( $\sigma = 0.005 \text{ e} \cdot \text{bohr}^{-3}$ ) and predicted  $N^{\text{FOD}}$  values together with the diradical character  $y_0$  values of the para-substituted (a) and meta-substituted (b) ICz-based isomers.

In addition, the molecules displaying the highest diradical character values are also those showing the largest  $\Delta E_{\text{OS-CS}}$  and the smallest  $\Delta E_{\text{S-T}}$ . Therefore, we are able to define a linear correlation between the diradical character  $y_0$  and these two factors ( $\Delta E_{\text{S-T}}$  and  $\Delta E_{\text{OS-CS}}$ ) for the whole set of isomers (Figure 3.13), suggesting that changes in the substitution pattern and



structural isomerism represent a very effective way to modulate the diradical properties.

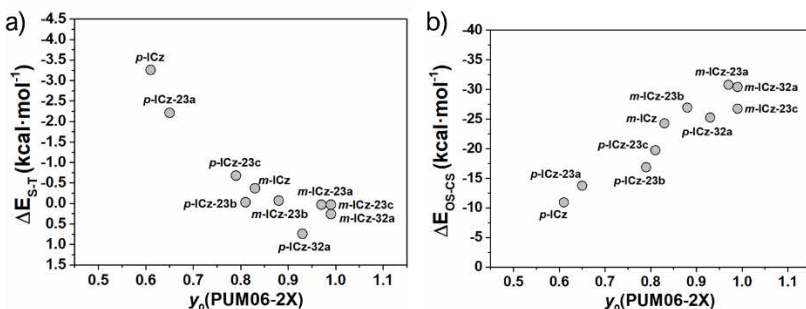


Figure 3.13. Correlation between the diradical character  $y_0$  calculated at projected UM06-2X and (a)  $\Delta E_{S-T}$  and (b)  $\Delta E_{OS-CS}$  for all ICz-based isomers

As in the previous section, we explore here the correlation between the diradical character and aromaticity. To this end, the ring currents were examined computationally with the nucleus independent chemical shift NICS(0)<sup>70</sup>, the NICS-XY scan<sup>84-86</sup>, and the anisotropy of the induced current density (ACID) method<sup>87,88</sup>.

The NICS (0) values of ten ICz-based isomers are summarized in Table 3.4. If we focus on the CS structures, several points should be highlighted: (i) In the case of the para-connection, the molecule displaying the highest diradical character value (*i.e.*,  $y_0=0.93$  for **p-ICz-32a**) is also that showing the largest differences in aromaticity between the external and central core (*i.e.*, -0.7 ppm for NICS<sub>A</sub>(0) and 13.1 ppm for NICS<sub>B</sub>(0), respectively). In contrast, the **p-ICz-23a** and **p-ICz** systems show similar values when going from the external rings to the central core allowing higher electronic delocalization over the whole conjugated backbone which is in line with the decrease of



## Chapter I: Evolution of the diradical character

the diradical character. (ii) On the other hand, much larger differences in the aromatic/antiaromatic character within the conjugated backbone are found in the peripheral meta-substituted systems when compared with the para-substituted analogues. As above-mentioned, this can be ascribed to a decreased in the conjugation upon DCM meta-substitution due to the interruption of the linear  $\pi$ -system which in turn promotes the diradical state. For instance, the external rings of ***m*-ICz-23c** and ***m*-ICz-32a** systems displays an increase in the paratropic ring current translating into antiaromatic rings while the central benzene ring retain the aromatic character.

Table 3.4. The calculated NICS(0) values of all ICz-based isomers.

Molecule	NICS <sub>A</sub> <sup>a</sup>		NICS <sub>B</sub> <sup>b</sup>		$y_0$
	CS	OS	CS	OS	
<b><i>p</i>-ICz-23a</b>	-1.6	-4.7	-1.8	-6.7	0.65
<b><i>p</i>-ICz-23b</b>	-0.5	-5.0	1.9	-6.8	0.81
<b><i>p</i>-ICz-23c</b>	-0.4	-4.9	2.8	-6.3	0.79
<b><i>p</i>-ICz-32a</b>	-0.7	-5.6	13.1	-6.6	0.93
<b><i>p</i>-ICz</b>	-0.5	-4.1	-0.9	-6.6	0.61
<b><i>m</i>-ICz-23a</b>	-0.6	-5.6	-7.5	-9.8	0.97
<b><i>m</i>-ICz-23b</b>	-3.1	-5.5	-6.8	-9.3	0.88
<b><i>m</i>-ICz-23c</b>	10.3	-5.6	-4.8	-9.5	0.99
<b><i>m</i>-ICz-32a</b>	20.6	-5.5	-0.9	-9.4	0.99
<b><i>m</i>-ICz</b>	-3.0	-5.3	-6.6	-9.5	0.83

<sup>a</sup> NICS<sub>A</sub> (0) values of the external phenyl rings at B3LYP/6-311+G\* level. <sup>b</sup> NICS<sub>B</sub> (0) values of the central phenyl ring of ICz-based systems at B3LYP/6-311+G\* level.

Interestingly, the ACID plots and NICS-XY scans shown in Figure 3.14 endorse the NICS (0) values, showing that an increase in the diradical character translates in the presence of antiaromatic rings which indicate less  $\pi$ -delocalization of the conjugated backbone allows the pair radicals being less coupled.

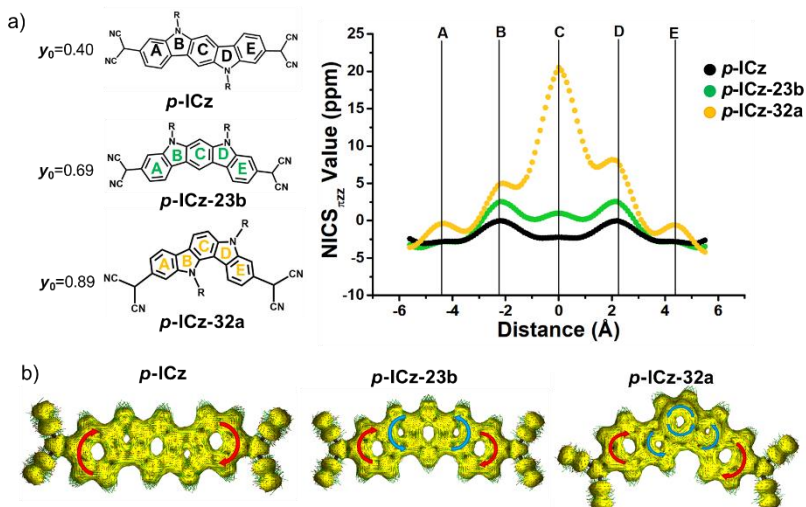


Figure 3.14. (a) NICS<sub>πz</sub>-XY scan values (B3LYP/6-311+G\* level) and chemical structures of *p*-ICz (black circle), *p*-ICz-23b (green circle) and *p*-ICz-32a (yellow circle). (b) ACID plots (B3LYP/6-311+G\* level) of the induced ring current at an isosurface value of 0.03 of *p*-ICz, *p*-ICz-23b and *p*-ICz-32a. The red arrows represent a diatropic (clockwise) ring current and the blue arrows correspond with a paratropic (counter-clockwise) ring current.

### 3.1.4 Conclusions.

❖ Our calculations have demonstrated that different structural modifications (*i.e.*, substitution pattern, elongation of the conjugated core and structural isomerism) represent a very effective way to modulate the diradical character in Cz and ICz-based systems.



## Chapter I: Evolution of the diradical character

❖ In comparison with the para-connection, the insertion of the DCM groups via meta results in stronger diradical character. Our data suggest that this is due to the fact that Cz and ICz units substituted at the para position display a longer conjugation path increasing the electronic delocalization meanwhile the meta position decreases the conjugation because of the interruption of the linear  $\pi$ -system.

❖ In addition, we demonstrated that the increase in the chain length (from Cz to ICz molecules) implies a remarkable increase in the diradical character. In other words, the elongation of the conjugated core provokes less interaction between the unpaired electrons (small  $J_{ab}$  and  $\Delta E_{S-T}$  values) resulting in a large diradical character.

❖ Our calculations based on ICz isomers suggest that the different degree of aromatization between the external and central parts of the backbone involves less  $\pi$ -delocalization resulting in an increase of the diradical character. In addition, the presence of double exciton states (H,H-L,L) has been successfully provided with a nice agreement found with the experimental absorption spectra of ***p*-ICz** and ***m*-ICz**. Besides, distortions from planarity could involve remarkable modifications on the molecular conjugation and consequently, on the diradical character.

### 3.1.5 Bibliography.

1. Abe, M., Diradicals. *Chemical Reviews* **2013**, 113, (9), 7011-7088.



2. Abe, M.; Ye, J.; Mishima, M., The chemistry of localized singlet 1,3-diradicals (biradicals): from putative intermediates to persistent species and unusual molecules with a  $\pi$ -single bonded character. *Chemical Society Reviews* **2012**, 41, (10), 3808-3820.
3. Salem, L.; Rowland, C., The Electronic Properties of Diradicals. *Angewandte Chemie International Edition in English* **1972**, 11, (2), 92-111.
4. Y. Gopalakrishna, T.; Zeng, W.; Lu, X.; Wu, J., From open-shell singlet diradicaloids to polyradicaloids. *Chemical Communications* **2018**, 54, (18), 2186-2199.
5. Zeng, Z.; Shi, X.; Chi, C.; López Navarrete, J. T.; Casado, J.; Wu, J., Pro-aromatic and anti-aromatic  $\pi$ -conjugated molecules: an irresistible wish to be diradicals. *Chemical Society Reviews* **2015**, 44, (18), 6578-6596.
6. Akdag, A.; Havlas, Z.; Michl, J., Search for a Small Chromophore with Efficient Singlet Fission: Biradicaloid Heterocycles. *Journal of the American Chemical Society* **2012**, 134, (35), 14624-14631.
7. Hu, X.; Wang, W.; Wang, D.; Zheng, Y., The electronic applications of stable diradicaloids: present and future. *Journal of Materials Chemistry C* **2018**, 6, (42), 11232-11242.
8. Kamada, K.; Ohta, K.; Kubo, T.; Shimizu, A.; Morita, Y.; Nakasuji, K.; Kishi, R.; Ohta, S.; Furukawa, S.-i.; Takahashi, H.; Nakano, M., Strong Two-Photon Absorption of Singlet Diradical Hydrocarbons. *Angewandte Chemie International Edition* **2007**, 46, (19), 3544-3546.
9. Lee, J.; Lee, E.; Kim, S.; Bang, G. S.; Shultz, D. A.; Schmidt, R. D.; Forbes, M. D. E.; Lee, H., Nitronyl Nitroxide Radicals as Organic Memory Elements with Both n- and p-Type Properties. *Angewandte Chemie International Edition* **2011**, 50, (19), 4414-4418.
10. Marshall, J. L.; Uchida, K.; Frederickson, C. K.; Schütt, C.; Zeidell, A. M.; Goetz, K. P.; Finn, T. W.; Jarolimek, K.; Zakharov, L. N.; Risko, C.; Herges, R.; Jurchescu, O. D.; Haley, M. M., Indacenodibenzothiophenes: synthesis, electronic properties and materials applications of molecules with strong antiaromatic character. *Chemical Science* **2016**, 7, (8), 5547-5558.
11. Muhammad, S.; Ito, S.; Nakano, M.; Kishi, R.; Yoneda, K.; Kitagawa, Y.; Shkir, M.; Irfan, A.; Chaudhry, A. R.; AlFaify, S.; Kalam, A.; Al-Sehemi, A. G., Diradical character and nonlinear



optical properties of buckyferrocenes: focusing on the use of suitably modified fullerene fragments. *Physical Chemistry Chemical Physics* **2015**, 17, (8), 5805-5816.

12. Okuno, K.; Shigeta, Y.; Kishi, R.; Nakano, M., Photochromic Switching of Diradical Character: Design of Efficient Nonlinear Optical Switches. *The Journal of Physical Chemistry Letters* **2013**, 4, (15), 2418-2422.

13. Zhang, D.; Song, X.; Cai, M.; Kaji, H.; Duan, L., Versatile Indolocarbazole-Isomer Derivatives as Highly Emissive Emitters and Ideal Hosts for Thermally Activated Delayed Fluorescent OLEDs with Alleviated Efficiency Roll-Off. *Advanced Materials* **2018**, 30, (7), 1705406.

14. Zhang, Y.; Zheng, Y.; Zhou, H.; Miao, M.-S.; Wudl, F.; Nguyen, T.-Q., Temperature Tunable Self-Doping in Stable Diradicaloid Thin-Film Devices. *Advanced Materials* **2015**, 27, (45), 7412-7419.

15. Das, S.; Herng, T. S.; Zafra, J. L.; Burrezo, P. M.; Kitano, M.; Ishida, M.; Gopalakrishna, T. Y.; Hu, P.; Osuka, A.; Casado, J.; Ding, J.; Casanova, D.; Wu, J., Fully Fused Quinoidal/Aromatic Carbazole Macrocycles with Poly-radical Characters. *Journal of the American Chemical Society* **2016**, 138, (24), 7782-7790.

16. Dias, J. R., Valence-Bond Determination of Diradical Character of Polycyclic Aromatic Hydrocarbons: From Acenes to Rectangular Benzenoids. *The Journal of Physical Chemistry A* **2013**, 117, (22), 4716-4725.

17. Lu, X.; Lee, S.; Hong, Y.; Phan, H.; Gopalakrishna, T. Y.; Herng, T. S.; Tanaka, T.; Sandoval-Salinas, M. E.; Zeng, W.; Ding, J.; Casanova, D.; Osuka, A.; Kim, D.; Wu, J., Fluorenyl Based Macrocyclic Polyradicaloids. *Journal of the American Chemical Society* **2017**, 139, (37), 13173-13183.

18. Morita, Y.; Suzuki, S.; Sato, K.; Takui, T., Synthetic organic spin chemistry for structurally well-defined open-shell graphene fragments. *Nature Chemistry* **2011**, 3, (3), 197-204.

19. Nakano, M.; Champagne, B., Diradical character dependences of the first and second hyperpolarizabilities of asymmetric open-shell singlet systems. *The Journal of Chemical Physics* **2013**, 138, (24), 244306.

20. Radenković, S.; Marković, S.; Kuč, R.; Stanković, N., The diradical character of polyacenequinododimethides. *Monatshefte für Chemie - Chemical Monthly* **2011**, 142, (10), 1013.



21. Yang, W.; Zhang, L.; Xiao, D.; Feng, R.; Wang, W.; Pan, S.; Zhao, Y.; Zhao, L.; Frenking, G.; Wang, X., A diradical based on odd-electron  $\sigma$ -bonds. *Nature Communications* **2020**, 11, (1), 3441.
22. Bendikov, M.; Duong, H. M.; Starkey, K.; Houk, K. N.; Carter, E. A.; Wudl, F., Oligoacenes: Theoretical Prediction of Open-Shell Singlet Diradical Ground States [J. Am. Chem. Soc. 2004, 126, 7416–7417]. *Journal of the American Chemical Society* **2004**, 126, (33), 10493-10493.
23. Dressler, J. J.; Haley, M. M., Learning how to fine-tune diradical properties by structure refinement. *Journal of Physical Organic Chemistry* **2020**, 33, (11), e4114.
24. Jung, Y.; Head-Gordon, M., How Diradicaloid Is a Stable Diradical? *ChemPhysChem* **2003**, 4, (5), 522-525.
25. da Silva Filho, A. J.; da Cruz Dantas, L.; de Santana, O. L., Diradicalar Character and Ring Stability of Mesoionic Heterocyclic Oxazoles and Thiazoles by Ab Initio Mono and Multi-Reference Methods. *Molecules* **2020**, 25, (19), 4524.
26. Scott, T.; Nieman, R.; Luxon, A.; Zhang, B.; Lischka, H.; Gagliardi, L.; Parish, C. A., A Multireference Ab Initio Study of the Diradical Isomers of Pyrazine. *The Journal of Physical Chemistry A* **2019**, 123, (10), 2049-2057.
27. Canola, S.; Casado, J.; Negri, F., The double exciton state of conjugated chromophores with strong diradical character: insights from TD-DFT calculations. *Physical Chemistry Chemical Physics* **2018**, 20, (37), 24227-24238.
28. Das, A.; Müller, T.; Plasser, F.; Lischka, H., Polyradical Character of Triangular Non-Kekulé Structures, Zethrenes, p-Quinodimethane-Linked Bisphenalenyl, and the Clar Goblet in Comparison: An Extended Multireference Study. *The Journal of Physical Chemistry A* **2016**, 120, (9), 1625-1636.
29. Pérez-Guardiola, A.; Sandoval-Salinas, M. E.; Casanova, D.; San-Fabián, E.; Pérez-Jiménez, A.; Sancho-García, J.-C., The role of topology in organic molecules: origin and comparison of the radical character in linear and cyclic oligoacenes and related oligomers. *Physical Chemistry Chemical Physics* **2018**, 20, (10), 7112-7124.
30. Yang, K.; Zhang, X.; Harbuzaru, A.; Wang, L.; Wang, Y.; Koh, C.; Guo, H.; Shi, Y.; Chen, J.; Sun, H.; Feng, K.; Ruiz Delgado, M. C.; Woo, H. Y.; Ortiz, R. P.; Guo, X., Stable Organic Diradicals



Based on Fused Quinoidal Oligothiophene Imides with High Electrical Conductivity. *Journal of the American Chemical Society* **2020**, 142, (9), 4329-4340.

31. Badía-Domínguez, I.; Pérez-Guardiola, A.; Sancho-García, J. C.; López Navarrete, J. T.; Hernández Jolín, V.; Li, H.; Sakamaki, D.; Seki, S.; Ruiz Delgado, M. C., Formation of Cyclophane Macrocycles in Carbazole-Based Biradicaloids: Impact of the Dicyanomethylene Substitution Position. *ACS Omega* **2019**, 4, (3), 4761-4769.

32. Jung, Y.; Head-Gordon, M., Controlling the Extent of Diradical Character by Utilizing Neighboring Group Interactions. *The Journal of Physical Chemistry A* **2003**, 107, (38), 7475-7481.

33. Kobashi, T.; Sakamaki, D.; Seki, S., N-Substituted Dicyanomethylphenyl Radicals: Dynamic Covalent Properties and Formation of Stimuli-Responsive Cyclophanes by Self-Assembly. *Angewandte Chemie International Edition* **2016**, 55, (30), 8634-8638.

34. Matsui, H.; Fukuda, K.; Takamuku, S.; Sekiguchi, A.; Nakano, M., Theoretical Study on the Relationship between Diradical Character and Second Hyperpolarizabilities of Four-Membered-Ring Diradicals Involving Heavy Main-Group Elements. *Chemistry – A European Journal* **2015**, 21, (5), 2157-2164.

35. Souri, M.; Kazemi, T., Substitution effect in 2-spiropropane-1,3-diyl derivatives: A DFT and CASSCF study. *Journal of Photochemistry and Photobiology A: Chemistry* **2018**, 353, 108-113.

36. Xue, G.; Hu, X.; Chen, H.; Ge, L.; Wang, W.; Xiong, J.; Miao, F.; Zheng, Y., Understanding the nature of quinoidal and zwitterionic states in carbazole-based diradicals. *Chemical Communications* **2020**, 56, (38), 5143-5146.

37. Zhang, R.; Peterson, J. P.; Fischer, L. J.; Ellern, A.; Winter, A. H., Effect of Structure on the Spin-Spin Interactions of Tethered Dicyanomethyl Diradicals. *Journal of the American Chemical Society* **2018**, 140, (43), 14308-14313.

38. Badía-Domínguez, I.; Peña-Álvarez, M.; Wang, D.; Pérez Guardiola, A.; Vida, Y.; Rodríguez González, S.; López Navarrete, J. T.; Hernández Jolín, V.; Sancho García, J. C.; García Baonza, V.; Nash, R.; Hartl, F.; Li, H.; Ruiz Delgado, M. C., Dynamic





Covalent Properties of a Novel Indolo[3,2-b]carbazole Diradical. *Chemistry – A European Journal* **2021**, 27, (17), 5509-5520.

39. Ito, S.; Nakano, M., Theoretical Molecular Design of Heteroacenes for Singlet Fission: Tuning the Diradical Character by Modifying  $\pi$ -Conjugation Length and Aromaticity. *The Journal of Physical Chemistry C* **2015**, 119, (1), 148-157.

40. Ponce Ortiz, R.; Casado, J.; Rodríguez González, S.; Hernández, V.; López Navarrete, J. T.; Viruela, P. M.; Ortí, E.; Takimiya, K.; Otsubo, T., Quinoidal Oligothiophenes: Towards Biradical Ground-State Species. *Chemistry – A European Journal* **2010**, 16, (2), 470-484.

41. Radenković, S.; Antić, M.; Đurđević, J.; Jeremić, S., Electronic structure study of the biradical pleiadene-like molecules. *Monatshefte für Chemie - Chemical Monthly* **2014**, 145, (2), 281-290.

42. Stuyver, T.; Zeng, T.; Tsuji, Y.; Geerlings, P.; De Proft, F., Diradical Character as a Guiding Principle for the Insightful Design of Molecular Nanowires with an Increasing Conductance with Length. *Nano Letters* **2018**, 18, (11), 7298-7304.

43. Zeng, Z.; Ishida, M.; Zafra, J. L.; Zhu, X.; Sung, Y. M.; Bao, N.; Webster, R. D.; Lee, B. S.; Li, R.-W.; Zeng, W.; Li, Y.; Chi, C.; Navarrete, J. T. L.; Ding, J.; Casado, J.; Kim, D.; Wu, J., Pushing Extended p-Quinodimethanes to the Limit: Stable Tetracyano-oligo(N-annulated perylene)quinodimethanes with Tunable Ground States. *Journal of the American Chemical Society* **2013**, 135, (16), 6363-6371.

44. Zeng, Z.; Lee, S.; Son, M.; Fukuda, K.; Burrezo, P. M.; Zhu, X.; Qi, Q.; Li, R.-W.; Navarrete, J. T. L.; Ding, J.; Casado, J.; Nakano, M.; Kim, D.; Wu, J., Push-Pull Type Oligo(N-annulated perylene)quinodimethanes: Chain Length and Solvent-Dependent Ground States and Physical Properties. *Journal of the American Chemical Society* **2015**, 137, (26), 8572-8583.

45. Zeng, Z.; Lee, S.; Zafra, J. L.; Ishida, M.; Bao, N.; Webster, R. D.; López Navarrete, J. T.; Ding, J.; Casado, J.; Kim, D.; Wu, J., Turning on the biradical state of tetracyano-perylene and quaterylenequinodimethanes by incorporation of additional thiophene rings. *Chemical Science* **2014**, 5, (8), 3072-3080.

46. Barker, J. E.; Dressler, J. J.; Cárdenas Valdivia, A.; Kishi, R.; Strand, E. T.; Zakharov, L. N.; MacMillan, S. N.; Gómez-García, C. J.; Nakano, M.; Casado, J.; Haley, M. M., Molecule Isomerism



Modulates the Diradical Properties of Stable Singlet Diradicaloids. *Journal of the American Chemical Society* **2020**, 142, (3), 1548-1555.

47. Hu, P.; Lee, S.; Park, K. H.; Das, S.; Heng, T. S.; Gonçalves, T. P.; Huang, K.-W.; Ding, J.; Kim, D.; Wu, J., Octazethrene and Its Isomer with Different Diradical Characters and Chemical Reactivity: The Role of the Bridge Structure. *The Journal of Organic Chemistry* **2016**, 81, (7), 2911-2919.

48. Romain, M.; Tondelier, D.; Vanel, J.-C.; Geffroy, B.; Jeannin, O.; Rault-Berthelot, J.; Métivier, R.; Poriel, C., Dependence of the Properties of Dihydroindenofluorene Derivatives on Positional Isomerism: Influence of the Ring Bridging. *Angewandte Chemie International Edition* **2013**, 52, (52), 14147-14151.

49. Konishi, A.; Okada, Y.; Nakano, M.; Sugisaki, K.; Sato, K.; Takui, T.; Yasuda, M., Synthesis and Characterization of Dibenzo[a,f]pentalene: Harmonization of the Antiaromatic and Singlet Biradical Character. *Journal of the American Chemical Society* **2017**, 139, (43), 15284-15287.

50. Kubo, T., Recent Progress in Quinoidal Singlet Biradical Molecules. *Chemistry Letters* **2015**, 44, (2), 111-122.

51. Gong, W.-L.; Wang, B.; Aldred, M. P.; Li, C.; Zhang, G.-F.; Chen, T.; Wang, L.; Zhu, M.-Q., Tetraphenylethene-decorated carbazoles: synthesis, aggregation-induced emission, photo-oxidation and electroluminescence. *Journal of Materials Chemistry C* **2014**, 2, (34), 7001-7012.

52. Marsal, P.; Avilov, I.; da Silva Filho, D. A.; Brédas, J. L.; Beljonne, D., Molecular hosts for triplet emission in light emitting diodes: A quantum-chemical study. *Chemical Physics Letters* **2004**, 392, (4), 521-528.

53. Skórka, Ł.; Kurzep, P.; Wiosna-Satyga, G.; Łuszczynska, B.; Wielgus, I.; Wróbel, Z.; Ulański, J.; Kulszewicz-Bajer, I., New diarylaminophenyl derivatives of carbazole: Effect of substituent position on their redox, spectroscopic and electroluminescent properties. *Synthetic metals* **2017**, 228, 1-8.

54. Wang, H.-Y.; Liu, F.; Xie, L.-H.; Tang, C.; Peng, B.; Huang, W.; Wei, W., Topological Arrangement of Fluorenyl-Substituted Carbazole Triads and Starbursts: Synthesis and Electronic Properties. *The Journal of Physical Chemistry C* **2011**, 115, (14), 6961-6967.



55. Zhang, N.; Hayer, A.; Al-Suti, M. K.; Al-Belushi, R. A.; Khan, M. S.; Köhler, A., The effect of delocalization on the exchange energy in meta- and para-linked Pt-containing carbazole polymers and monomers. *The Journal of Chemical Physics* **2006**, 124, (24), 244701.
56. Casado, J.; Ponce Ortiz, R.; López Navarrete, J. T., Quinoidal oligothiophenes: new properties behind an unconventional electronic structure. *Chemical Society Reviews* **2012**, 41, (17), 5672-5686.
57. Pozun, Z. D.; Su, X.; Jordan, K. D., Establishing the Ground State of the Disjoint Diradical Tetramethyleneethane with Quantum Monte Carlo. *Journal of the American Chemical Society* **2013**, 135, (37), 13862-13869.
58. Ravat, P.; Baumgarten, M., "Tschitschibabin type biradicals": benzenoid or quinoid? *Physical Chemistry Chemical Physics* **2015**, 17, (2), 983-991.
59. Canola, S.; Dai, Y.; Negri, F., The Low Lying Double-Exciton State of Conjugated Diradicals: Assessment of TDUDFT and Spin-Flip TD-DFT Predictions. *Computation* **2019**, 7, (4), 68.
60. Slipchenko, L. V.; Krylov, A. I., Singlet-triplet gaps in diradicals by the spin-flip approach: A benchmark study. *The Journal of Chemical Physics* **2002**, 117, (10), 4694-4708.
61. Bonačić-Koutecký, V.; Koutecký, J.; Michl, J., Neutral and charged biradicals, zwitterions, funnels in S<sub>1</sub>, and proton translocation: their role in photochemistry, photophysics, and vision. *Angewandte Chemie International Edition in English* **1987**, 26, (3), 170-189.
62. Di Motta, S.; Negri, F.; Fazzi, D.; Castiglioni, C.; Canesi, E. V., Biradicaloid and polyenic character of quinoidal oligothiophenes revealed by the presence of a low-lying double-exciton state. *The Journal of Physical Chemistry Letters* **2010**, 1, (23), 3334-3339.
63. Yamaguchi, K., The electronic structures of biradicals in the unrestricted Hartree-Fock approximation. *Chemical Physics Letters* **1975**, 33, (2), 330-335.
64. Grimme, S.; Hansen, A., A Practicable Real-Space Measure and Visualization of Static Electron-Correlation Effects. *Angewandte Chemie International Edition* **2015**, 54, (42), 12308-12313.



65. Bauer, C. A.; Hansen, A.; Grimme, S., The Fractional Occupation Number Weighted Density as a Versatile Analysis Tool for Molecules with a Complicated Electronic Structure. *Chemistry – A European Journal* **2017**, 23, (25), 6150-6164.
66. Li, Z.; Gopalakrishna, T. Y.; Han, Y.; Gu, Y.; Yuan, L.; Zeng, W.; Casanova, D.; Wu, J., [6]Cyclo-para-phenylmethine: An Analog of Benzene Showing Global Aromaticity and Open-Shell Diradical Character. *Journal of the American Chemical Society* **2019**, 141, (41), 16266-16270.
67. Motomura, S.; Nakano, M.; Fukui, H.; Yoneda, K.; Kubo, T.; Carion, R.; Champagne, B., Size dependences of the diradical character and the second hyperpolarizabilities in dicyclopenta-fused acenes: relationships with their aromaticity/antiaromaticity. *Physical Chemistry Chemical Physics* **2011**, 13, (46), 20575-20583.
68. Shi, X.; Quintero, E.; Lee, S.; Jing, L.; Heng, T. S.; Zheng, B.; Huang, K.-W.; López Navarrete, J. T.; Ding, J.; Kim, D.; Casado, J.; Chi, C., Benzo-thia-fused [n]thienoacenequinodimethanes with small to moderate diradical characters: the role of pro-aromaticity versus anti-aromaticity. *Chemical Science* **2016**, 7, (5), 3036-3046.
69. Kishi, R.; Dennis, M.; Fukuda, K.; Murata, Y.; Morita, K.; Uenaka, H.; Nakano, M., Theoretical Study on the Electronic Structure and Third-Order Nonlinear Optical Properties of Open-Shell Quinoidal Oligothiophenes. *The Journal of Physical Chemistry C* **2013**, 117, (41), 21498-21508.
70. Fallah-Bagher-Shaidaei, H.; Wannere, C. S.; Corminboeuf, C.; Puchta, R.; Schleyer, P. v. R., Which NICS Aromaticity Index for Planar  $\pi$  Rings Is Best? *Organic Letters* **2006**, 8, (5), 863-866.
71. Nandy, B. C., Gupta, A. K., Mittal, A., and Vyas, V., Carbazole: It's biological activity. *J. Biomed. Pharm. Res*, **2014** 3, 42-48.
72. Hacker, A. S.; Pavano, M.; Wood, J. E.; Hashimoto, H.; D'Ambrosio, K. M.; Frederickson, C. K.; Zafra, J. L.; Gómez-García, C. J.; Postils, V.; Ringer McDonald, A.; Casanova, D.; Frantz, D. K.; Casado, J., Fluoreno[2,1-a]fluorene: an ortho-naphthoquinodimethane-based system with partial diradical character. *Chemical Communications* **2019**, 55, (94), 14186-14189.



73. Kubo, T.; Sakamoto, M.; Nakasuji, K., Biradicaloid character of phenalenyl-based aromatic compounds with a small HOMO–LUMO gap. *Polyhedron* **2005**, 24, (16), 2522-2527.
74. Lu, R.-Q.; Wu, S.; Yang, L.-L.; Gao, W.-B.; Qu, H.; Wang, X.-Y.; Chen, J.-B.; Tang, C.; Shi, H.-Y.; Cao, X.-Y., Stable Diindeno-Fused Corannulene Regioisomers with Open-Shell Singlet Ground States and Large Diradical Characters. *Angewandte Chemie International Edition* **2019**, 58, (23), 7600-7605.
75. Chase, D. T.; Rose, B. D.; McClintock, S. P.; Zakharov, L. N.; Haley, M. M., Indeno[1,2-b]fluorenes: Fully Conjugated Antiaromatic Analogues of Acenes. *Angewandte Chemie International Edition* **2011**, 50, (5), 1127-1130.
76. Dressler, J. J.; Zhou, Z.; Marshall, J. L.; Kishi, R.; Takamuku, S.; Wei, Z.; Spisak, S. N.; Nakano, M.; Petrukhina, M. A.; Haley, M. M., Synthesis of the Unknown Indeno[1,2-a]fluorene Regioisomer: Crystallographic Characterization of Its Dianion. *Angewandte Chemie International Edition* **2017**, 56, (48), 15363-15367.
77. Frederickson, C. K.; Rose, B. D.; Haley, M. M., Explorations of the Indenofluorenes and Expanded Quinoidal Analogues. *Accounts of Chemical Research* **2017**, 50, (4), 977-987.
78. Shimizu, A.; Kishi, R.; Nakano, M.; Shiomi, D.; Sato, K.; Takui, T.; Hisaki, I.; Miyata, M.; Tobe, Y., Indeno[2,1-b]fluorene: A 20- $\pi$ -Electron Hydrocarbon with Very Low-Energy Light Absorption. *Angewandte Chemie International Edition* **2013**, 52, (23), 6076-6079.
79. Shimizu, A.; Nobusue, S.; Miyoshi, H.; Tobe, Y., Indenofluorene congeners: Biradicaloids and beyond. *Pure and Applied Chemistry* **2014**, 86, (4), 517-528.
80. Tobe, Y., Non-Alternant Non-Benzenoid Aromatic Compounds: Past, Present, and Future. *The Chemical Record* **2015**, 15, (1), 86-96.
81. Nakano, M., Electronic Structure of Open-Shell Singlet Molecules: Diradical Character Viewpoint. *Topics in Current Chemistry* **2017**, 375, (2), 47.
82. Sun, Z.; Zeng, Z.; Wu, J., Zethrenes, Extended p-Quinodimethanes, and Periacenes with a Singlet Biradical



## Chapter I: Evolution of the diradical character

- Ground State. *Accounts of Chemical Research* **2014**, 47, (8), 2582-2591.
83. Armon, A. M.; Bedi, A.; Borin, V.; Schapiro, I.; Gidron, O., Bending versus Twisting Acenes – A Computational Study. *European Journal of Organic Chemistry* **2021**, 2021, (39), 5424-5429.
84. Gershoni-Poranne, R.; Stanger, A., The NICS-XY-Scan: Identification of Local and Global Ring Currents in Multi-Ring Systems. *Chemistry – A European Journal* **2014**, 20, (19), 5673-5688.
85. Stanger, A., Nucleus-Independent Chemical Shifts (NICS): Distance Dependence and Revised Criteria for Aromaticity and Antiaromaticity. *The Journal of Organic Chemistry* **2006**, 71, (3), 883-893.
86. Stanger, A., Obtaining Relative Induced Ring Currents Quantitatively from NICS. *The Journal of Organic Chemistry* **2010**, 75, (7), 2281-2288.
87. Geuenich, D.; Hess, K.; Köhler, F.; Herges, R., Anisotropy of the Induced Current Density (ACID), a General Method To Quantify and Visualize Electronic Delocalization. *Chemical Reviews* **2005**, 105, (10), 3758-3772.
88. Herges, R.; Geuenich, D., Delocalization of Electrons in Molecules. *The Journal of Physical Chemistry A* **2001**, 105, (13), 3214-3220.







# CHAPTER II: Cyclophane self-assembly from carbazole and indolocarbazole-based diradicals.

## Table of contents

---

- 3.2.1 Introduction.
  - 3.2.2 Cyclophane structural features.
    - 3.2.2.1 Carbazole-based molecules.
    - 3.2.2.2 Indolocarbazole-based molecules.
  - 3.2.3 Interconversion between cyclophane and isolated monomer in solution.
    - 3.2.3.1 Carbazole-based molecules.
    - 3.2.3.2 Indolocarbazole-based molecules.
  - 3.2.4 Interconversion between cyclophane and isolated monomer in solid-state.
    - 3.2.4.1 Carbazole-based molecules.
    - 3.2.4.2 Indolocarbazole-based molecules.
  - 3.2.5 Conclusions.
  - 3.2.6 Bibliography.
-





### 3.2.1 Introduction.

A large body of information on diradicaloid molecules exists in the scientific literature<sup>1-9</sup>. In some cases, these molecules are found to form cyclophane structures through the formation of C-C  $\sigma$ -bonds between radical centres<sup>10-17</sup> which are longer than typical C(sp<sup>3</sup>)-C(sp<sup>3</sup>). Hence, these systems can show reversible association-dissociation behaviour giving rise to spin-switchable materials. Switching between closed-shell molecules to unpaired electron systems leads to significant changes in the molecular properties of these materials under external conditions which makes this spin switching feature a very attractive tool for the design of stimuli-responsive materials.

These electronic spin-state changes would result in chromism behaviour, that is, colour changes caused by an external stimulus. Owing to these properties, organic mono- and diradicals have emerged as essential building blocks in Dynamic Covalent Chemistry (DCC)<sup>18-24</sup>. Herein, we report an optical and vibrational study of a family of carbazole and indolocarbazole-based diradicaloids (Figure 3.1) with DCM groups incorporated via para (**p-Cz** and **p-ICz**) or meta positions (**m-Cz** and **m-ICz**) aiming to identify potential new building blocks for stimuli-responsive materials. These compounds contain long C-C single bonds between the bridgehead carbon atoms linked to the DCM groups that undergo bond dissociation in response to external stimuli such as heating, pressing, and grinding.

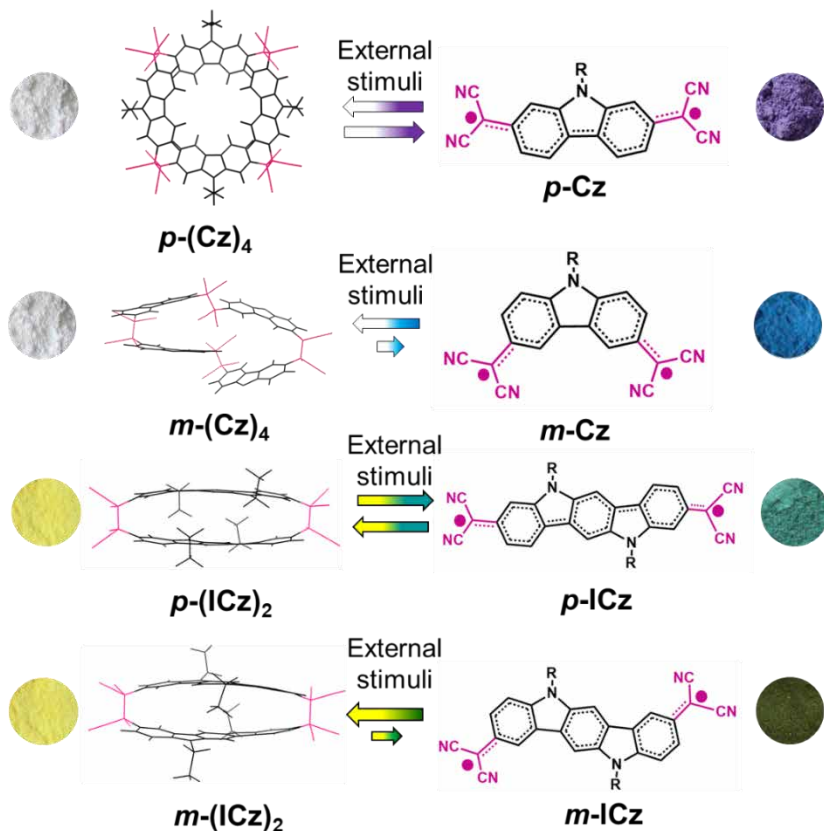


Figure 3.1. Equilibrium between the cyclophane-type oligomers and their corresponding isolated DCM-substituted diradicaloids in their open-shell (OS) singlet form.

### 3.2.2 Cyclophane structural features.

Interestingly, the four DCM-substituted diradicaloid systems under studied are able to form cyclophane structures by self-assembly of the unpaired electrons from the radical centres of the monomers (**Figure 3.1**). In fact, the structure of  $p\text{-Cz}$  was resolved by X-ray analysis showing that four different monomers were linked resulting in a tetramer cyclophane ( $p\text{-(Cz)}_4$ ), where the C-C bonds between the monomers (1.631 Å) were remarkably longer than typical  $\text{C}(\text{sp}^3)\text{-C}(\text{sp}^3)$  bonds (1.54 Å).



Unfortunately, it was not possible to obtain single crystals for the other systems, so we performed DFT calculations for different conformations to address the most favourable intermolecular arrangement for the cyclophane structures.

### 3.2.2.1 Carbazole-based molecules.

As above-mentioned, some diradicaloid systems are highly prone to form  $\sigma$ -bonded cyclophane structures through the formation of long C-C bonds between the carbon atoms linked to the CN groups. In fact, for the carbazole systems, it has already been proved that ***p*-Cz** monomers form a cyclic tetramer ***p*-(Cz)<sub>4</sub>**<sup>13</sup> and ***m*-Cz** monomers can build a cyclic trimer ***m*-(Cz)<sub>3</sub>** and a cyclic tetramer ***m*-(Cz)<sub>4</sub>**<sup>15</sup>. The single-crystal X-ray analysis revealed the structures of ***p*-(Cz)<sub>4</sub>** and ***m*-(Cz)<sub>3</sub>** where the C-C bonds between the monomers were unusually long (1.608–1.639 Å for ***m*-(Cz)<sub>3</sub>** and 1.631 Å for ***p*-(Cz)<sub>4</sub>**) regarding with ordinary C(sp<sup>3</sup>)-C(sp<sup>3</sup>) bonds (1.54 Å)<sup>13, 15</sup>.

Figure 3.2 shows the X-ray and DFT-computed global minima structures for ***p*-(Cz)<sub>4</sub>** and ***m*-(Cz)<sub>3</sub>**. A good agreement between the experimental and theoretical data is obtained. The cyclic tetramer ***p*-(Cz)<sub>4</sub>** is formed by four molecules extended in the cavity periphery (with negligible  $\pi$ - $\pi$  overlap) creating a ring-shaped structural cavity of 12.52 Å<sup>13</sup>. In contrast, a folded molecular shape conformation is obtained for the cyclic trimer ***m*-(Cz)<sub>3</sub>** resulting in labile  $\pi$ - $\pi$  interactions for the two **Cz** units pointing in the same direction<sup>17</sup>. Furthermore, the spontaneous

nature of the cyclophane macrocycles formation is supported by the negative relative Gibbs free energies calculated at 298 K.

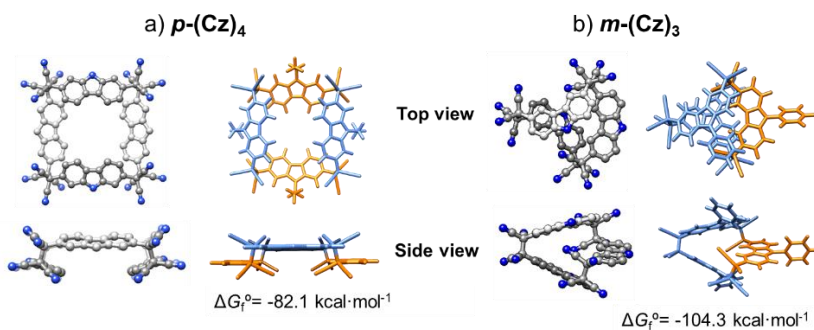


Figure 3.2. X-ray (left) and DFT-computed global minimum structure (right) for (a)  $p\text{-(Cz)}_4$  and (b)  $m\text{-(Cz)}_3$  cyclic oligomers. The N-substituents have been omitted for clarity. Free energy of formation ( $\Delta G_f^\circ$ ) values (at 298 K) calculated at the M06-2X/6-31G\*\* level are also shown.

Unfortunately, it was not possible to obtain single crystals of  $m\text{-(Cz)}_4$ . Thus, we performed DFT calculations for different conformations to address the most favourable intermolecular arrangement of this aggregate. To this end, three different conformations for the spatial disposition of the **Cz** fragments were considered: (i) a distorted-shaped conformation where one of the **Cz** fragments is twisted with its N-phenyl group pointed toward the inside of the ring cavity; (ii) a ring-shaped conformation, similarly to  $p\text{-(Cz)}_4$  structure, with the four **Cz** units extended over the periphery with the N-phenyl groups pointed outward of the cavity; (iii) a folded structure where the **Cz** units are co-facially reoriented in a pairwise conformation (Figure 3.3).

The computed free energies of formation (Figure 3.3) indicate that the folded-shape structure ( $\Delta G_f^\circ = -130.1 \text{ kcal}\cdot\text{mol}^{-1}$ )

is the most favourable one. This could be explained due by the presence of co-facially superimposed **Cz** units which results in favourable  $\pi$ - $\pi$  interactions of  $\sim 3.54$  Å between adjacent phenyl rings linked to the C-C  $\sigma$ -bonds in ***m*-(Cz)<sub>4</sub>**<sup>17</sup>.

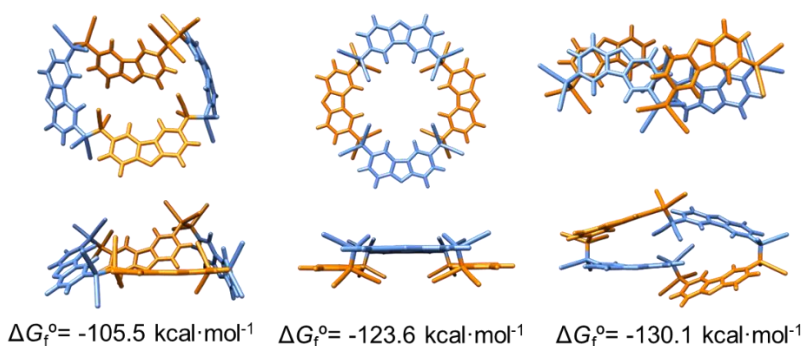


Figure 3.3. Top view (up) and side view (down) of DFT-computed global minimum structure for ***m*-(Cz)<sub>4</sub>** cyclophanes in three different conformations: distorted ring-shaped (left), ring-shaped (centre), and folded (right). The N-substituent groups have been omitted for clarity. Free energy of formation values (at 298 K) calculated at the M06-2X/6-31G\*\* level are also shown.

### 3.2.2.2 Indolocarbazole-based molecules.

Although, no X-ray data are available for the cyclophane structures derived from the ***p*-ICz** and ***m*-ICz** compounds, our collaborators carried out several experiments to discern their spatial arrangement (*i.e.*, HPLC, nitrogen adsorption-desorption isotherm or GPC, DOSY)<sup>25</sup>. The ***p*-ICz** compound and its brominated precursor (***p*-ICz-Br**) were examined by diffusion NMR techniques. Diffusion-ordered spectroscopy (DOSY) experiments were performed for ***p*-ICz** at concentrations below 2 mM, which corresponds to a dilute regime where the intermolecular separation avoids aggregate formation<sup>25-27</sup>. Larger

structures diffuse more slowly in solution, showing smaller diffusion coefficients ( $D$ ). As Table 3.1 displayed, ***p*-ICz** presents a smaller diffusion coefficient than ***p*-ICz-Br** and, in addition, a higher  $R_h$  (hydrodynamic radi) value. This indicates that the estimated size of the ***p*-ICz** compound is roughly more than twice larger than that of the ***p*-ICz-Br**, in line with the formation of a dominant dimeric structure.

Table 3.1. Diffusion coefficients ( $D$ ) and hydrodynamic radii ( $R_h$ ) determined by diffuse NMR experiments. The chemical structures are also shown.

Compound	$D$ ( $\text{m}^2 \cdot \text{s}^{-1}$ )	$R_h$ ( $\text{Å}$ )
<b><i>p</i>-ICz-Br</b>	$4.05 \times 10^{-10}$	10
<b><i>p</i>-ICz</b>	$1.76 \times 10^{-10}$	23

On the other hand, the retention time of the ***p*-ICz** peak, measured by the GPC technique, is close to the maximum peak of ***m*-ICz** suggesting similar chemical structures. Thereby, we assume the creation of a dimer-type cyclophane, both in the ***p*-ICz** and ***m*-ICz**, with the indolocarbazole units co-facially oriented in a pairwise conformation. As we previously investigated for the ***m*-(Cz)<sub>4</sub>** system, we proposed herein different dimeric models to predict the most favourable intermolecular arrangement for ***p*-ICz** and ***m*-ICz** cyclophanes. To this end, two different dimeric conformations have been tested: (i) an antiparallel disposition of the two **ICz** units and (ii) a parallel orientation with co-facially superimposed **ICz** units (Figure 3.4).



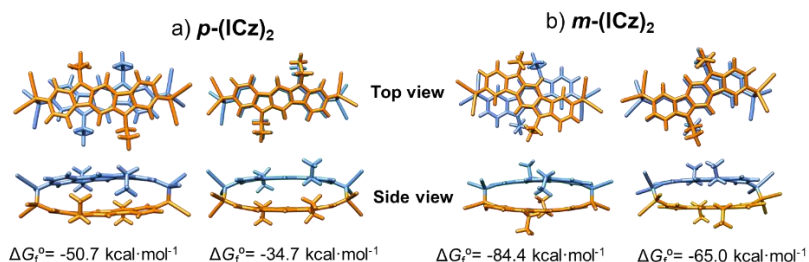


Figure 3.4. Antiparallel (left) and parallel (right) DFT-computed global minimum structures for (a)  $p\text{-(ICz)}_2$  and (b)  $m\text{-(ICz)}_2$ . Free energy of formation values (at 298 K, calculated at the M06-2X/6-31G\*\* level, are also shown.

In both systems, the calculated formation free energies revealed that the antiparallel structure is the most favourable one, with the cyclophane  $m\text{-(ICz)}_2$  being about  $34 \text{ kcal}\cdot\text{mol}^{-1}$  more stable than the para-substituted  $p\text{-(ICz)}_2$  homologue. In addition, the potential energy curve of the dimerization shows a little more pronounced well-defined minimum at  $1.65 \text{ \AA}$  for the meta-substituted compound (Figure 3.5). This is in line with the shortest C-C bonds calculated between the two radical centres and between two  $\text{ICz}$  units which indicates stronger  $\pi\text{-}\pi$  interactions on going from  $p\text{-(ICz)}_2$  to  $m\text{-(ICz)}_2$ ; thus, resulting in a higher stability of the meta-substituted cyclophane.

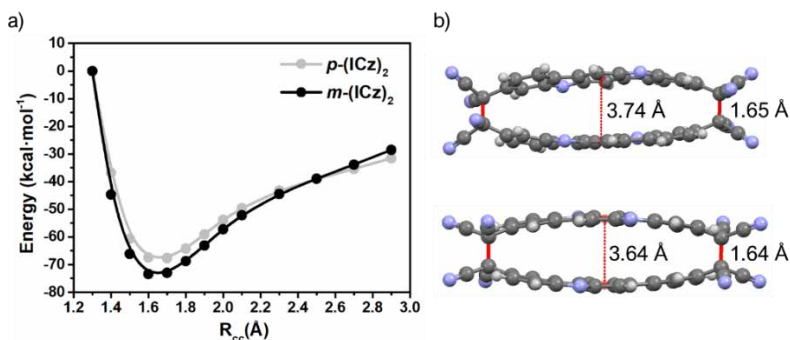


Figure 3.5. (a) Potential energy curve, computed at the M06-2X/6-31G\*\* level, for *p*-(ICz)<sub>2</sub> and *m*-(ICz)<sub>2</sub>. R<sub>CC</sub> is the length of the C-C σ-bonds formed between the two ICz units. (b) DFT-calculated global minimum structures for *p*-(ICz)<sub>2</sub> (up) and *m*-(ICz)<sub>2</sub> (down) displaying the closest π-π interactions between the co-facially oriented monomers and the C-C σ-bond lengths. The N-substituted alkyl groups have been omitted for clarity.

### 3.2.3 Interconversion between cyclophane and monomer in solution.

In this section, we now explore the optical properties of the cyclophanes structures and the possibility of C-C bond dissociation by external stimuli (*i.e.*, heat and time) in solution. Specifically, we put emphasis on the DCC properties linked to notable chromic effects in solution. To this end, we dissolved the carbazole and indolocarbazole-based cyclophanes in different solvents and measured their electronic absorption spectra as a function of time and temperature. Then, the nature and type of the electronic transition are assigned with the help of TD-DFT calculations.

#### 3.2.3.1 Carbazole-based molecules.

Note that we focus specifically on the comparison between *p*-(Cz)<sub>4</sub> and *m*-(Cz)<sub>4</sub> cyclophanes because of their structural

similarity. Figure 3.6a,b shows the UV/Vis-NIR absorption spectra at RT for  $p\text{-(Cz)}_4$  and  $m\text{-(Cz)}_4$  systems. Both compounds clearly exhibit a group of bands below  $\lambda = 400$  nm which correspond to the tetrameric cyclophane. Nevertheless, the colourless solution of the  $p\text{-(Cz)}_4$  system turned gradually purple with broad bands appearing between 500 and 850 nm which reveals the formation of the isolated diradicaloid monomers arising from the long C-C bond dissociation. In contrast, the solution of the white powder of  $m\text{-(Cz)}_4$  kept its initial transparent colour as a function of time and the spectrum showed only the bands corresponding to the cyclophane structure.

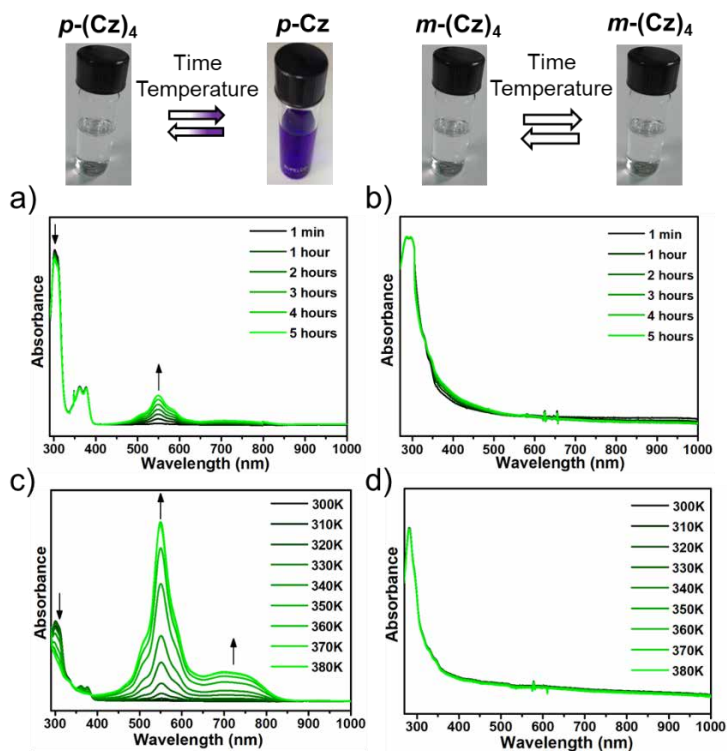


Figure 3.6. (a) UV/Vis-NIR absorption changes in chloroform accompanying transformation of cyclophane tetramer  $p\text{-(Cz)}_4$  to



## Chapter II: Cyclophane self-assembly

**p-Cz** monomer at RT as a function of time. (b) UV/Vis-NIR absorption of a freshly prepared solution in chloroform of **m-(Cz)<sub>4</sub>** at RT as a function of time. (c) UV/Vis-NIR spectral changes in toluene accompanying conversion of cyclophane tetramer **p-(Cz)<sub>4</sub>** to **p-Cz** monomer upon heating from 300 to 380 K. (d) UV/Vis-NIR absorption of **m-(Cz)<sub>4</sub>** in toluene as a function of temperature.

Analogously, we examined the tetramer–monomer dissociation in solution upon heating to facilitate the long C-C bonds breakdown. Figure 3.6c,d displays the UV/Vis–NIR absorption spectra in toluene at temperatures between 300 and 380 K. For **p-(Cz)<sub>4</sub>**, the intensities of the low-energy bands strongly increased upon heating, thus showing the formation of the isolated diradicaloid monomer. In contrast, C-C bond dissociation of **m-(Cz)<sub>4</sub>** was suppressed in solution state either upon heating or as a function of time.

This data reveals that substitution of the DCM groups at the meta-position of carbazole increases the stability of the tetrameric cyclophane. This may occur because of several factors: (i) the higher diradical character of **m-Cz** which implies a weak coupling of the unpaired electrons and, consequently, higher reactivity of the diradical resulting in stronger C-C  $\sigma$ -bonds; (ii) the higher spin density on the carbon atoms linked to the CN groups in **m-Cz** (-0.55) when compared to **p-Cz** (-0.46), hampering the cyclophane dissociation; (iii) the higher stability of the meta-substituted cyclophane structures when compared to the para-substituted systems, calculated both in gas-phase and solution (Table 3.2).



Table 3.2. Free energy of formation values (at 298 K) calculated at the M06-2X/6-31G\*\* level for **p-(Cz)<sub>4</sub>** and **m-(Cz)<sub>4</sub>** cyclic oligomers in gas-phase, toluene, chloroform and o-DCB.

Compound	$\Delta G_f^0$ (kcal·mol <sup>-1</sup> )			
	Gas-phase	Toluene ( $\epsilon=2.4$ )	Chloroform ( $\epsilon=4.7$ )	o-dichlorobenzene ( $\epsilon=9.9$ )
<b>p-(Cz)<sub>4</sub></b>	-82.1	-71.9	-66.7	-63.1
<b>m-(Cz)<sub>4</sub></b>	-130.1	-112.1	-102.1	-96.7

TD-DFT calculations support the experimental UV/Vis-NIR spectral evolution of the tetrameric cyclophanes towards the isolated monomers formation. As seen in Figure 3.7a, the **p-(Cz)<sub>4</sub>** tetrameric cyclophane exhibits a moderate electronic transition at 308 nm together with a more intense transition at 269 nm corresponding to the  $S_0 \rightarrow S_2/S_3$  and  $S_0 \rightarrow S_6/S_7$  transitions, respectively. Furthermore, two intense electronic transitions at 494 and 591 nm were predicted for the isolated **p-Cz** system associated with the  $S_0 \rightarrow S_1$  and  $S_0 \rightarrow S_2$  electronic transitions, respectively. In addition, an intense electronic transition at 248 nm is predicted for **m-(Cz)<sub>4</sub>** cyclophane corresponding to the  $S_0 \rightarrow S_{12}$  transition, whereas moderate transitions at 963 and 447 nm are predicted for **m-Cz** monomer, which are ascribed to the  $S_0 \rightarrow S_1$  and  $S_0 \rightarrow S_2$  transitions, respectively (Figure 3.7b).

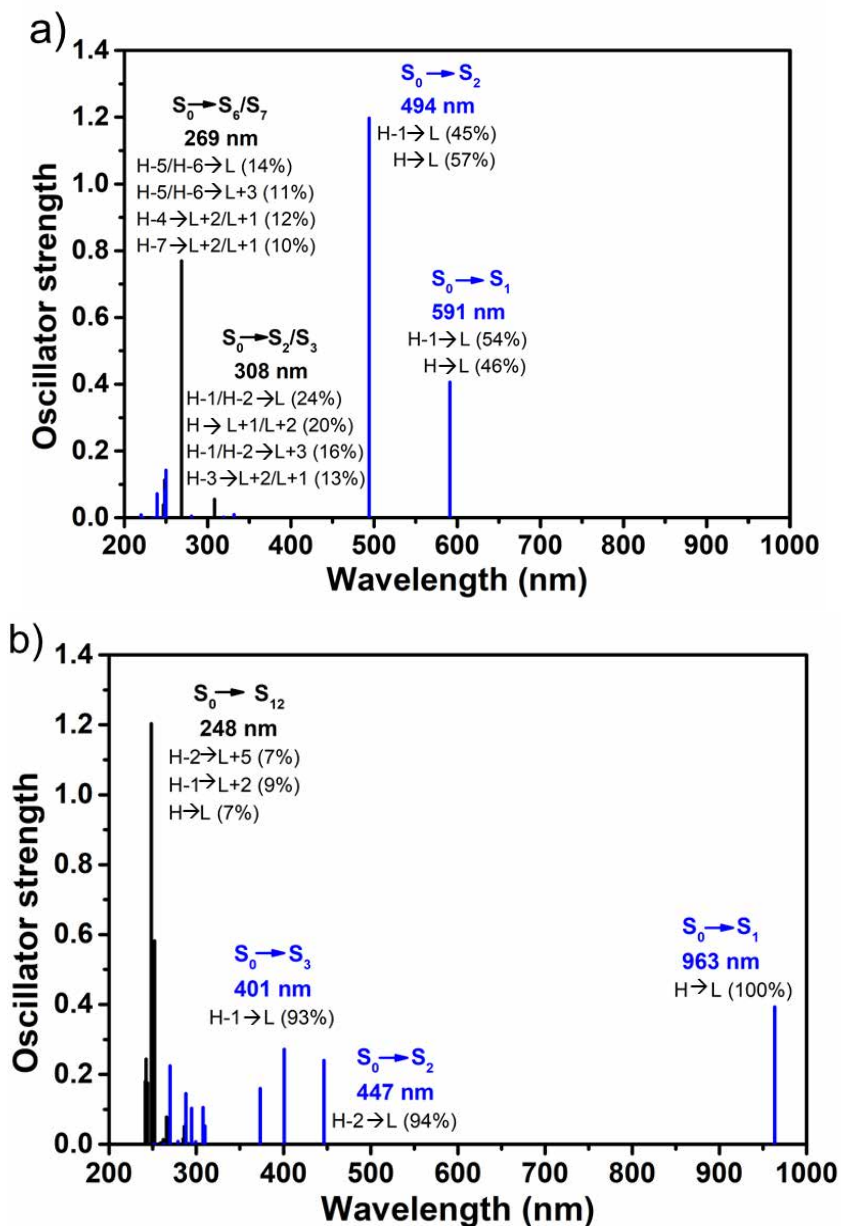


Figure 3.7. TD-DFT calculated vertical transition energies for closed-shell singlet monomer singlet (blue vertical lines) and tetrameric cyclophane (black vertical lines) of *p*-Cz (a) and *m*-Cz (b) at M06-2X/6-31G\*\* level of theory.



### 3.2.3.2 Indolocarbazole-based molecules.

Figure 3.8a shows the UV/Vis-NIR absorption spectra of *p*-(**ICz**)<sub>2</sub> (left) and *m*-(**ICz**)<sub>2</sub> (right) in chloroform as a function of time. For *p*-(**ICz**)<sub>2</sub>, the freshly prepared chloroform solution displays: (i) strong bands in the UV region and medium-weak bands below 500 nm, which correspond to the cyclophane structure, (ii) a small and broad absorption at around 700 nm which is ascribed to the isolated monomer, and (iii) negligible spectral changes as a function of time. In contrast, no bands above 500 nm are found for *m*-(**ICz**)<sub>2</sub> with no spectral changes found as a function of time.

Second, we investigated the cyclophane/monomer interconversion upon heating. To this end, we dissolved the compounds in toluene (Figure 3.8b) and heated the solution from 300 to 380 K. This induces an increase in the intensity of the band of the isolated monomer around 700 nm for the *p*-(**ICz**)<sub>2</sub> whereas the *m*-(**ICz**)<sub>2</sub> spectrum remained unchanged. Interestingly, the strongest intensity gains of the *p*-**ICz** low-energy visible band upon heating was achieved in *o*-dichlorobenzene (*o*-DCB) (Figure 3.8c). In fact, almost complete disappearance of the intense UV absorption corresponding to the cyclophane structure *p*-(**ICz**)<sub>2</sub> is achieved while the *p*-**ICz** monomer absorption dominates in the spectrum. The rupture of the long C-C  $\sigma$ -bonds in the dimer upon heating is accompanied by a gradual change of the solution colour from light yellow to blue-

green, which is fully reversed by cooling down the solution back to 300 K.

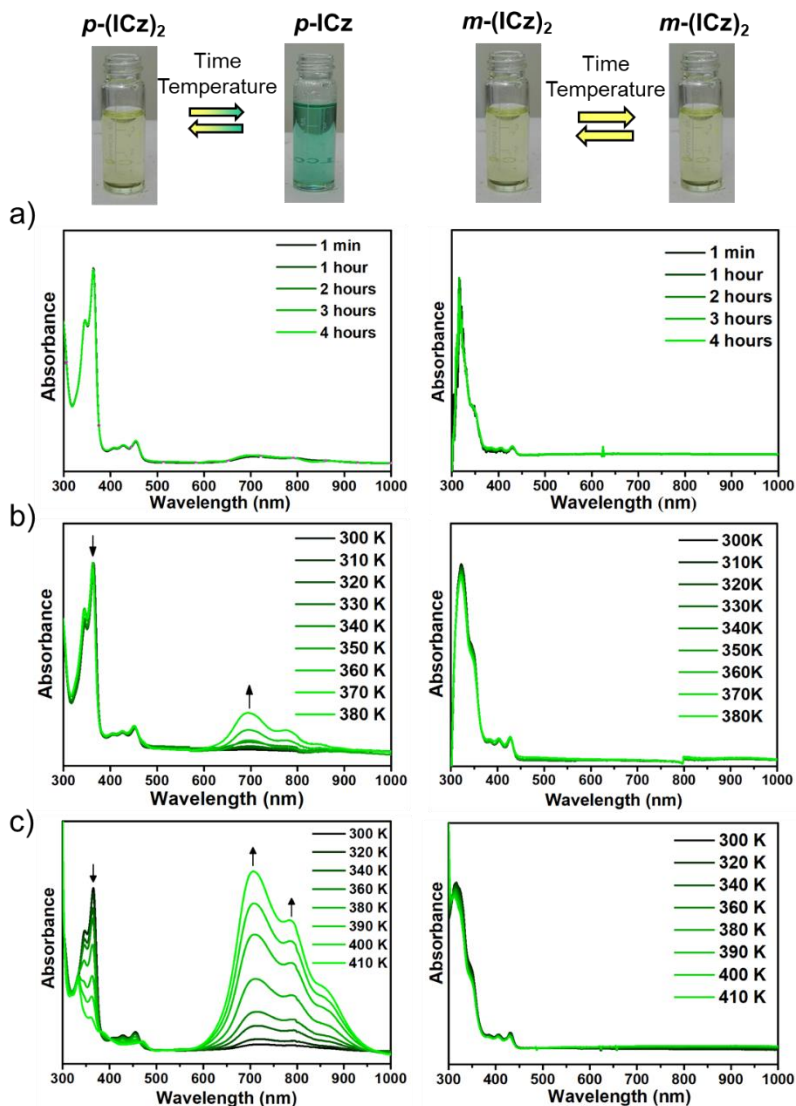


Figure 3.8. (a) UV/Vis-NIR absorption spectra in chloroform of  $p$ -(ICz)<sub>2</sub> (left) and  $m$ -(ICz)<sub>2</sub> (right) compounds as a function of time. (b) UV/Vis-NIR spectra in toluene of  $p$ -(ICz)<sub>2</sub> (left) and  $m$ -(ICz)<sub>2</sub> (right) upon heating from 300 to 380 K. (c) UV/Vis-NIR spectra in *o*-DCB of  $p$ -(ICz)<sub>2</sub> (left) and  $m$ -(ICz)<sub>2</sub> (right) as a function of temperature. The notable chromic effect is also shown.





## Chapter II: Cyclophane self-assembly

These results allow us to draw several conclusions. First, the elongation of the conjugation core when going from **Cz** to **ICz** systems involves a lower interaction between the two unpaired electrons. This fact leads to the domination of the contribution of the diradical form in the ground state which exhibits a higher propensity to form stronger  $\sigma$ -bonded cyclophanes. Second, the ***m*-(ICz)<sub>2</sub>** compound shows higher cyclophane stability due to the significant attractive  $\pi$ - $\pi$  interactions between the two indolocarbazole units. This is in accordance, DFT calculations predict that ***m*-(ICz)<sub>2</sub>** results in more stable cyclic oligomers than ***p*-(ICz)<sub>2</sub>**, both in solution and gas phase (Table 3.3).

Table 3.3. Free energy of formation values (at 298 K) calculated at the M06-2X/6-31G\*\* level for ***p*-(ICz)<sub>2</sub>** and ***m*-(ICz)<sub>2</sub>** cyclophanes in gas-phase, toluene, chloroform and *o*-DCB.

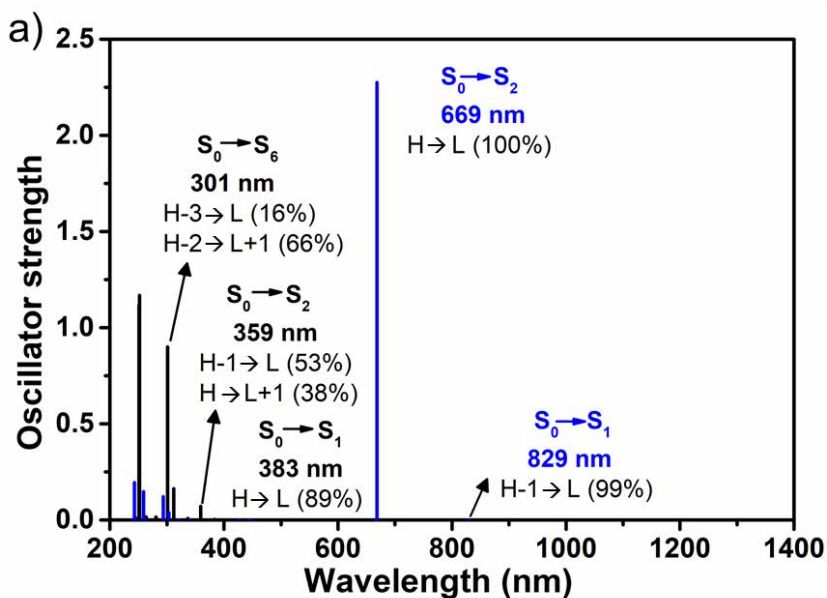
Compound	$\Delta G_f^0$ (kcal·mol <sup>-1</sup> )			
	Gas-phase	Toluene ( $\epsilon=2.4$ )	Chloroform ( $\epsilon=4.7$ )	<i>o</i> -dichlorobenzene ( $\epsilon=9.9$ )
<b><i>p</i>-(ICz)<sub>2</sub></b>	-50.7	-42.6	-38.9	-37.0
<b><i>m</i>-(ICz)<sub>2</sub></b>	-84.4	-60.1	-55.0	-51.2

As in the case of their short-chain analogues, TD-DFT calculations support the experimental evolution when going from dimeric cyclophanes to the isolated **ICz**-based monomers (Figure 3.9). In para-substituted system, we observe: (i) a moderate electronic transition predicted at 301 nm for ***p*-(ICz)<sub>2</sub>** together with two less intense transitions at 359 and 383 nm corresponding to the  $S_0 \rightarrow S_6$ ,  $S_0 \rightarrow S_2$  and  $S_0 \rightarrow S_1$  transitions, respectively, that involves orbitals with  $\pi$ -character delocalized



## Chapter II: Cyclophane self-assembly

through the two **ICz** moieties. (ii) An intense electronic transition predicted at 669 nm for the isolated monomer **p-ICz**, which is ascribed to the  $S_0 \rightarrow S_2$  transition with a strong  $\pi-\pi^*$  character (HOMO/LUMO). In line with this, the calculated spectrum of **m-(ICz)<sub>2</sub>** displays transitions at 292, 340 and 341 nm which are ascribed to the  $S_0 \rightarrow S_6$ ,  $S_0 \rightarrow S_2$  and  $S_0 \rightarrow S_1$  transitions, respectively, whereas the spectrum of **m-ICz** isolated monomer shows an intense electronic transition at 1263 nm corresponding to the  $S_0 \rightarrow S_1$  transition.



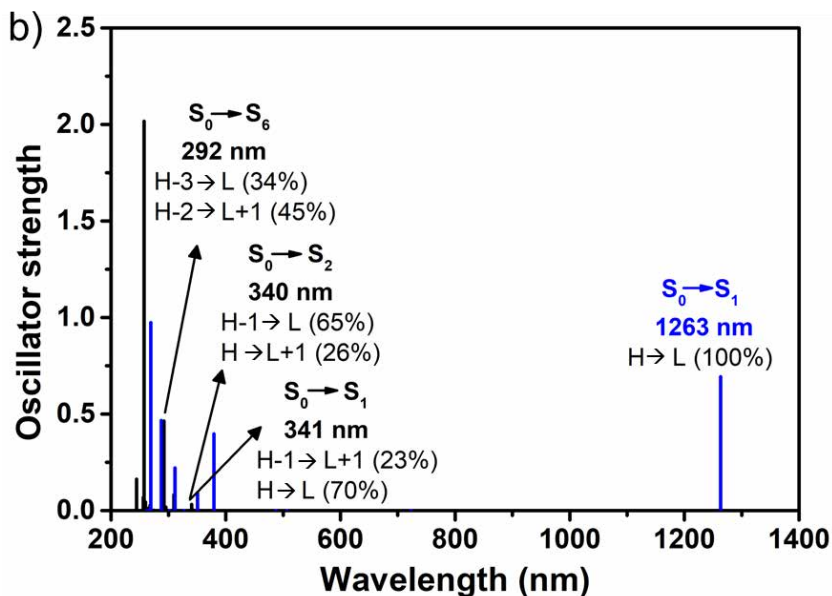


Figure 3.9. TD-DFT calculated vertical transition energies for closed-shell singlet monomer (blue vertical lines) and dimeric cyclophane (black vertical lines) of *p*-ICz (a) and *m*-ICz (b) at M06-2X/6-31G\*\* level of theory.

### 3.2.4 Interconversion between cyclophane and monomer in solid-state.

In this section, we attempt the C-C  $\sigma$ -bond dissociation in the solid-state by the application of external stimuli such as elevated temperature or pressure. To this end, we use IR and Raman spectroscopies to probe structural effects causing any mechanochromic changes<sup>13, 17, 28, 29</sup>.

#### 3.2.4.1 Carbazole-based molecules.

Figure 3.10 compares the IR spectra of *m*-(Cz)<sub>4</sub> and *p*-(Cz)<sub>4</sub> as a white powder and after grinding used to prepare the KBr pellet. Note that the colourless solid powder of *m*-(Cz)<sub>4</sub> compound turns to deep blue upon grinding demonstrating the



## Chapter II: Cyclophane self-assembly

C-C bond dissociation in solid-state. A similar chromic effect from white to purple was previously found in **p-(Cz)<sub>4</sub>** after grinding<sup>13</sup>. For the white powders, an intense band appears at 2253 cm<sup>-1</sup> related with the CN stretching,  $\nu(\text{CN})$ , which is very similar to that observed in nonconjugated nitriles (2252 cm<sup>-1</sup>)<sup>30</sup>. Interestingly, the samples colour change after grinding is accompanied by the appearance of a new very intense band at 2206 cm<sup>-1</sup> for the para-substituted compound. This indicates the cyclophane/monomer transformation which implies an increase of the conjugation of the CN groups with the core; note that the CN groups in  $\sigma$ -bonded cyclophane are connected to C atoms with sp<sup>3</sup> hybridization that evolve to sp<sup>2</sup> character in the monomer. Thus, the appearance of this new band indicates the predominant formation of isolated diradicaloid monomer upon pressure application in **p-Cz**.

On the other hand, after applying temperature of up to 523 K and then cooling to RT, the isolated diradicaloid monomer are preferentially formed in both the meta and para-substituted systems as suggested by the strong increase of the  $\nu(\text{CN})$  bands at 2219 and 2206 cm<sup>-1</sup>, respectively. Nevertheless, the pronounced prevalence of the  $\nu(\text{CN})$  band at 2253 cm<sup>-1</sup> in the meta-substituted system when compared to the para-substituted analogue indicates that  $\sigma$ -oligomers formed by **m-Cz** fragments are harder to dissociate.

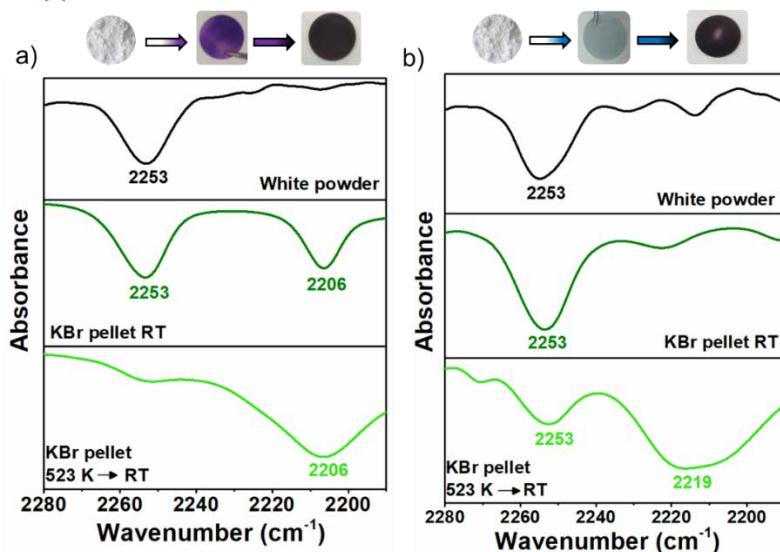


Figure 3.10. (a) IR spectrum of  $p\text{-(Cz)}_4$  as a white powder at RT (top); the purple KBr pellet containing a mixture of tetramer and isolated diradical  $p\text{-Cz}$  obtained after grinding at RT (middle); the KBr pellet with dominant isolated diradical  $p\text{-Cz}$  after heating and cooling to RT (bottom). (b) IR spectrum of  $m\text{-(Cz)}_4$  as a white powder at RT (top); the blue KBr pellet obtained after grinding at RT (middle); the KBr pellet containing a mixture of tetramer and isolated diradical  $m\text{-Cz}$  after heating and cooling to RT (bottom).

In addition, further analysis of the chromic behaviour of the carbazole-based compounds was performed by Raman spectroscopy, a sensitive tool to probe the diradicaloid character of quinoid systems<sup>31</sup>. Figure 3.11a shows the FT-Raman ( $\lambda=1064$  nm) spectra of  $p\text{-(Cz)}_4$  as a white powder and the Resonance Raman ( $\lambda=532$  nm) in dichloromethane solution. The most significant changes in Raman spectra occur in the range between 1700 and 1100  $\text{cm}^{-1}$ . The dichloromethane solution spectrum shows several changes with respect to the initial white powder spectra with a general shifting toward lower wavenumbers.



## Chapter II: Cyclophane self-assembly

Firstly, we observe an intense band at  $1634\text{ cm}^{-1}$  for the tetramer, which corresponds to a  $\nu(\text{C-C})$  mode of the **Cz** backbone; note that this mode appears at  $1626\text{ cm}^{-1}$  for an unsubstituted carbazole (Figure 3.11e). However, this band shifts to  $1598\text{ cm}^{-1}$  for the monomer *p*-**Cz**, suggesting an aromatic-to-quinoidal transformation of the **Cz** core upon the C-C  $\sigma$ -bond dissociation. Additionally, the spectrum also displayed the decrease of the Raman band related to C-C stretching vibrations and CH bending modes of the **Cz** (at  $1240\text{ cm}^{-1}$ ). This is good agreement with the DFT-computed Raman spectral evolution from tetrameric cyclophane to isolated monomer (Figure 3.11b).

Similarly, we measure the FT-Raman spectra of the white powder and KBr pellet for *m*-(**Cz**)<sub>4</sub> (Figure 3.11c). Both Raman spectra display intense bands in the  $1700\text{-}1100\text{ cm}^{-1}$  region. The most intense band of solid powder appears at  $1250\text{ cm}^{-1}$  belonging to the  $\nu(\text{C-C})$  and CH bending modes of **Cz** units which strongly decreases upon grinding. In the same context, the band at  $1634\text{ cm}^{-1}$  associated to a  $\nu(\text{C-C})$  mode of the **Cz** rings undergoes a downshifting in the Raman spectrum of the KBr pellet. Thus, the spectral trend is well reproduced by our theoretical calculations for the isolated diradical monomers and tetrameric cyclophane structures (Figure 3.11d).

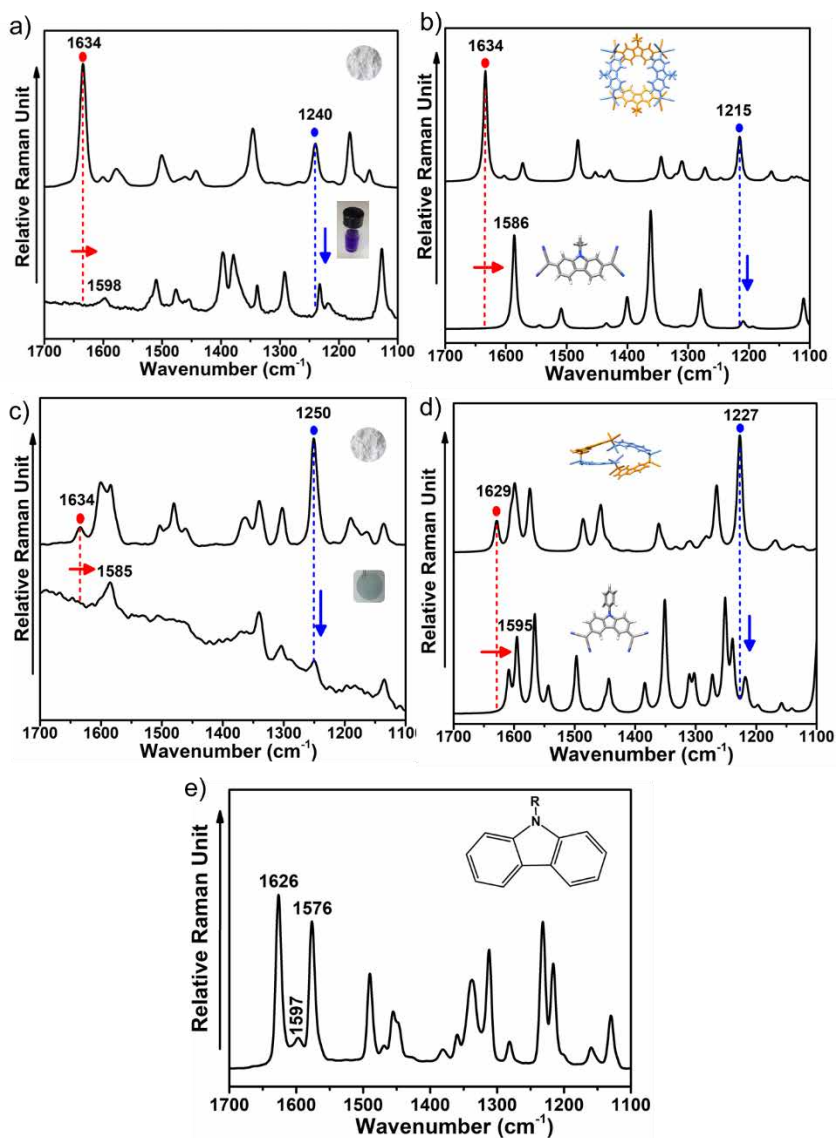
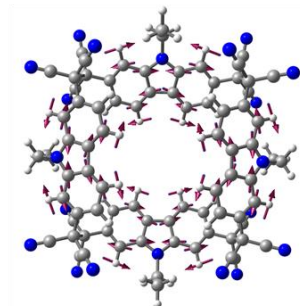


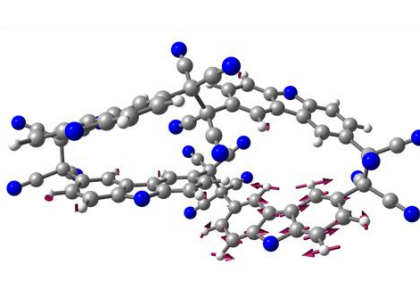
Figure 3.11. (a) FT-Raman ( $\lambda_{\text{exc}}=1064$  nm) spectrum of *p*-(Cz)<sub>4</sub> as a white powder at RT (up) and Resonance Raman spectrum ( $\lambda_{\text{exc}}=532$  nm, top) in dichloromethane solution of *p*-(Cz)<sub>4</sub> (down). (b) Theoretical Raman spectra (M06-2X/6-31G\*\*) of cyclophane tetramer (up) and monomer (down) for *p*-(Cz)<sub>4</sub>. (c) FT-Raman spectra of *m*-(Cz)<sub>4</sub> as a white powder at RT (up) and FT-Raman spectrum of blue KBr pellet (down). (d) Theoretical Raman

spectra (M06-2X/6-31G\*\*) of cyclophane tetramer (up) and monomer (down) for *m*-(Cz)<sub>4</sub>. (e) FT-Raman spectrum of Cz.

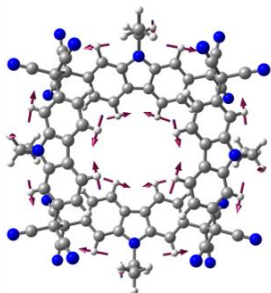
1634 cm<sup>-1</sup> (1634 cm<sup>-1</sup>)



1629 cm<sup>-1</sup> (1634 cm<sup>-1</sup>)



1215 cm<sup>-1</sup> (1240 cm<sup>-1</sup>)



1227 cm<sup>-1</sup> (1250 cm<sup>-1</sup>)

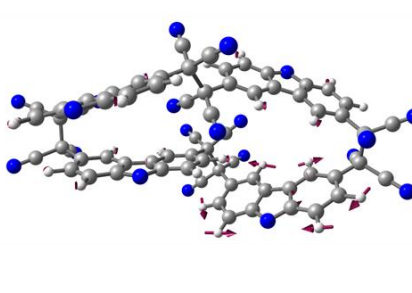


Figure 3.12. Eigenvectors (M06-2X/6-31G\*\* level) associated to the main Raman bands for *p*-(Cz)<sub>4</sub> (left) and *m*-(Cz)<sub>4</sub> (right). The theoretical and experimental (in parentheses) wavenumbers are also shown.

The transformation of conversion of *p*-(Cz)<sub>4</sub> to *p*-Cz in the solid state could also be monitored when applying mild pressures in a more controlled way<sup>32</sup>. To this end, we performed additional Raman spectroscopy experiments to pressures in the GPa range (Figure 3.13) seeking for further transformations. We observe that, at compressions of approximately 0.7 GPa, the tetramer is broken, and a monomeric conformation is favoured. The Raman spectrum of the sample reveals the vanishing of the bands at



2253 and 1634  $\text{cm}^{-1}$  belonging to the  $\nu(\text{CN})$  and  $\nu(\text{C-C})$  modes in the **Cz** rings, respectively. These bands are downshifting up to 2210 and 1600  $\text{cm}^{-1}$ , respectively, revealing the quinoid character of the Cz core in the monomer.

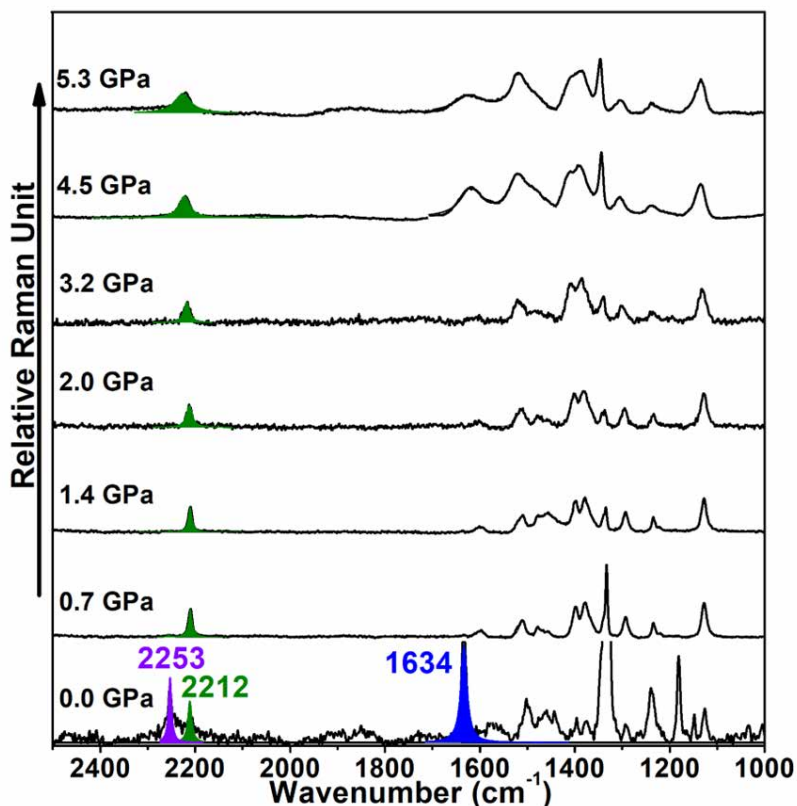


Figure 3.13 Raman spectra ( $\lambda_{\text{exc}}=532 \text{ nm}$ ) of  $p\text{-(Cz)}_4$  at selected pressures. Marked peaks correspond to: the  $\nu(\text{C-C})$  modes of the **Cz** rings, dark-blue area; the  $\nu(\text{CN})$  modes, green and purple areas. The shadowed region marks the band of the diamond chip used as pressure marker.

### 3.2.4.2 Indolocarbazole-based molecules.

Figure 3.14 displays the IR spectra of  $p\text{-(ICz)}_2$  and  $m\text{-(ICz)}_2$ . As we observe, the most intense  $\nu(\text{CN})$  band appears centred at

$\sim 2250\text{ cm}^{-1}$  for both compounds (similar to unconjugated nitriles). This band remains prominent in the IR spectrum of the corresponding KBr pellet recorded at 523 K and then cooled to RT, thus suggesting that the dimer cyclophane structure is always prevalent. Nevertheless, an additional weak  $\nu(\text{CN})$  band appears after grinding at around  $2224\text{ cm}^{-1}$  which is attributed to the formation of monomer *p-ICz*. This band appears with a larger intensity (at  $2219\text{ cm}^{-1}$ ) for the KBr pellet of the meta-substituted system; thus, suggesting that the *m-(ICz)<sub>2</sub>* dimeric cyclophane dissociates easier in the solid-state than its para-substituted analogue which is contrast to the situation in the solution-state.

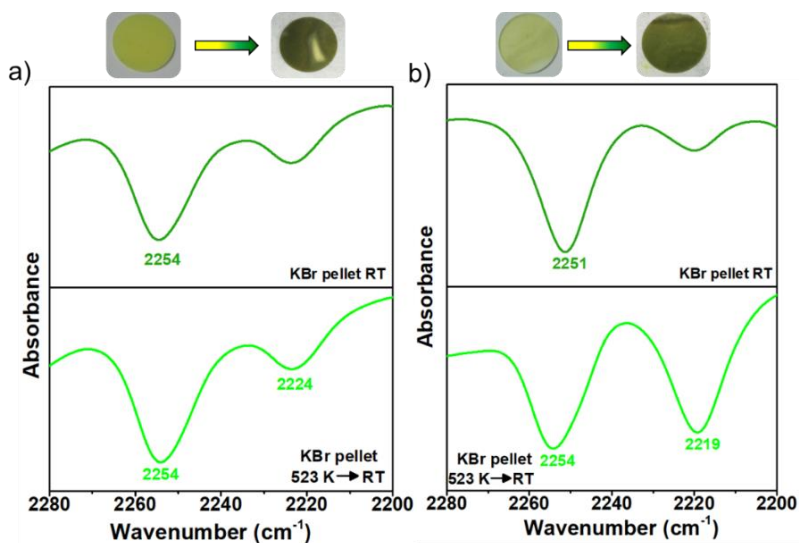


Figure 3.14. (a) IR spectrum of *p-(ICz)<sub>2</sub>* as a yellow KBr pellet obtained after grinding at RT (up) and a KBr pellet after heating and cooling to RT (down). (b) IR spectrum of *m-(ICz)<sub>2</sub>* as a yellow KBr pellet at RT (up) and a KBr pellet containing a mixture of dimer and isolated diradical *m-ICz* after heating and cooling to RT (down).



## Chapter II: Cyclophane self-assembly

We now use Raman spectroscopy in order to analyse in more detail the molecular structure evolution associated with the cyclophane/monomer transformation in solid-state. Figure 3.15a exhibits the FT-Raman spectrum of the light-yellow powder of **p-ICz**<sub>2</sub> and the Resonance Raman spectrum of isolated diradicaloid **p-ICz** in *o*-DCB at 363 K. When comparing the two spectra, the following spectral changes are found: (i) While the most intense band of the dimeric structure appears at 1640 cm<sup>-1</sup>, assigned to a  $\nu(\text{C-C})$  mode (Figure 3.16) of the **ICz** units (note that it bears resemblance to that assigned to its aromatic precursor **p-ICz-Br** at 1634 cm<sup>-1</sup>); this  $\nu(\text{C-C})$  mode appears at 1580 cm<sup>-1</sup> in the isolated monomer; thus, suggesting a change in the molecular structure from an aromatic to a more quinoidal character. (ii) The band at 1252 cm<sup>-1</sup> related to C-C stretching vibrations and CH bending modes of the external phenyl rings of the **ICz** units (Figure 3.16) disappears in the spectrum of the hot solution while a new band at 1191 cm<sup>-1</sup> appears which is ascribed to the CH bending of the central phenylene ring, giving further support to the presence of the isolated **p-ICz** monomer structure. This experimental spectral evolution is in a very good agreement with the theoretical Raman spectra (Figure 3.15b).

Analogously, the FT-Raman spectrum of **m-ICz**<sub>2</sub> was recorded together with its brominated precursor **m-ICz-Br**. As the Figure 3.15c shown, both spectra present a similar aromatic spectral profile (the most intense band appear at 1641 cm<sup>-1</sup> for **m-ICz**<sub>2</sub> and 1637 cm<sup>-1</sup> for **m-ICz-Br**). The Resonance Raman

spectra of  $m$ -(**ICz**)<sub>2</sub> yellow powder were recorded upon heating to favour the formation of the isolated monomer at solid-state. As previously found in the para-substituted compound, two characteristic new bands appear: (i) a  $\nu$ (C-C) mode at 1580 cm<sup>-1</sup> which is ascribed to the isolated monomer, suggesting a partially quinoidization upon the cyclophane/monomer transformation, and (ii) a CH bending mode at 1191 cm<sup>-1</sup> localized in the central phenyl ring which is hindered in the dimeric unit due to the neighbouring connecting units, confirming the presence of the isolated monomer.

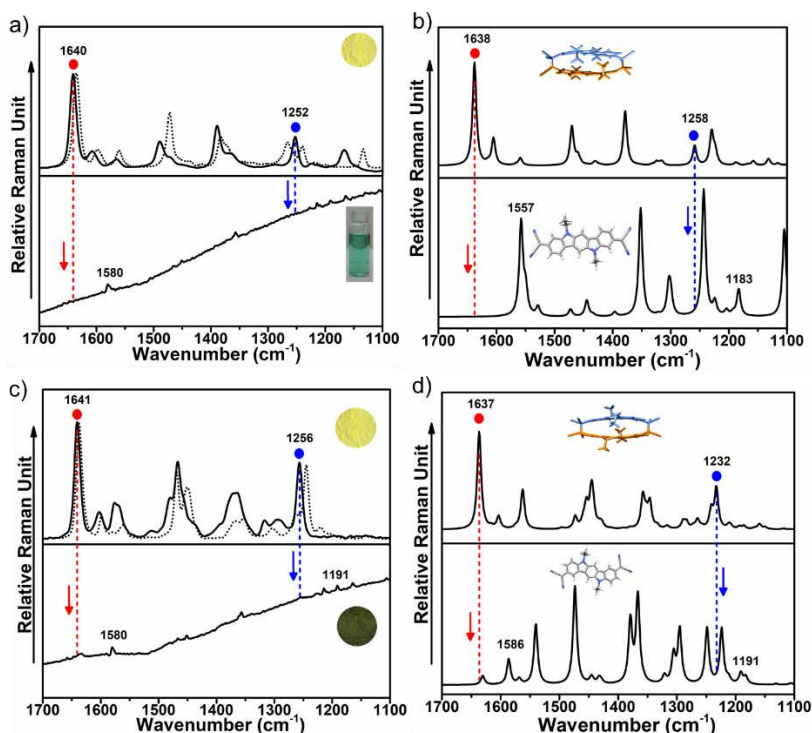


Figure 3.15. (a) FT-Raman spectra of the solid yellow powder of  $p$ -(**ICz**)<sub>2</sub> (black line), a brominated precursor  $p$ -**ICz**-Br plotted as grey dots (top) and the Resonance Raman spectrum ( $\lambda_{\text{exc}}=785$  nm) of isolated diradical  $p$ -**ICz** in *o*-DCB at 363 K (bottom). (b)

Theoretical Raman spectra (M06-2X/6-31G\*\*) of the dimeric cyclophane structure (up) and monomer (down) for  $p$ -(ICz)<sub>2</sub>. (c) FT-Raman spectra of the solid yellow powder of  $m$ -(ICz)<sub>2</sub> (black line), a brominated precursor  $m$ -ICz-Br plotted as grey dots (top) and the Resonance Raman spectrum ( $\lambda_{exc}=785$  nm) of diradical  $m$ -ICz at 413 K (bottom). (d) Theoretical Raman spectra (M06-2X/6-31G\*\*) of the dimeric cyclophane structure (up) and monomer (down) for  $m$ -(ICz)<sub>2</sub>.

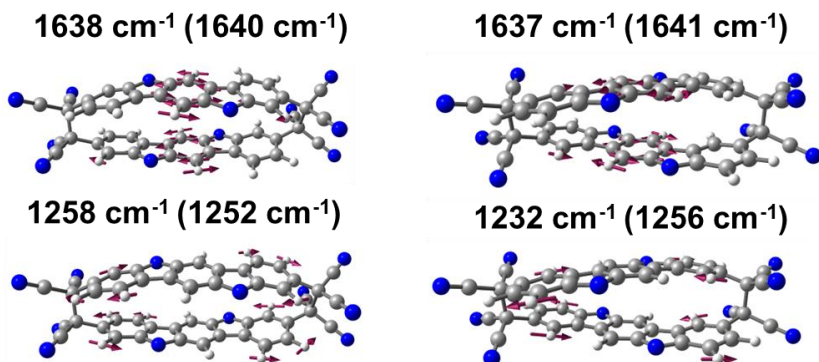


Figure 3.16. Eigenvectors (M06-2X/6-31G\*\* level) associated to the main Raman bands for (left)  $p$ -(ICz)<sub>2</sub> and (right)  $m$ -(ICz)<sub>2</sub>. The theoretical and experimental (in parentheses) wavenumbers are also shown.

As in the case of the  $p$ -(Cz)<sub>4</sub> compound, the transformation of the  $p$ -(ICz)<sub>2</sub> into the isolated monomer in the solid-state was also monitored upon pressures raising well above 0.1 GPa in a more controlled way. As seen in Figure 3.17, the Raman spectrum reveals several differences on going from ambient pressure to 2.2 GPa compressions, suggesting that the dimer C-C bonds are broken, and a monomer conformation is favoured. This assignment is supported by the appearance of new Raman bands at 1585 cm<sup>-1</sup> and 1140 cm<sup>-1</sup> which are ascribed to the appearance of the monomer as previously mentioned. This effect can be ascribed to the fact that the compression hinders the  $\pi$ -

electron delocalization within complex and large molecular skeletons and the radical forms become more dominant.

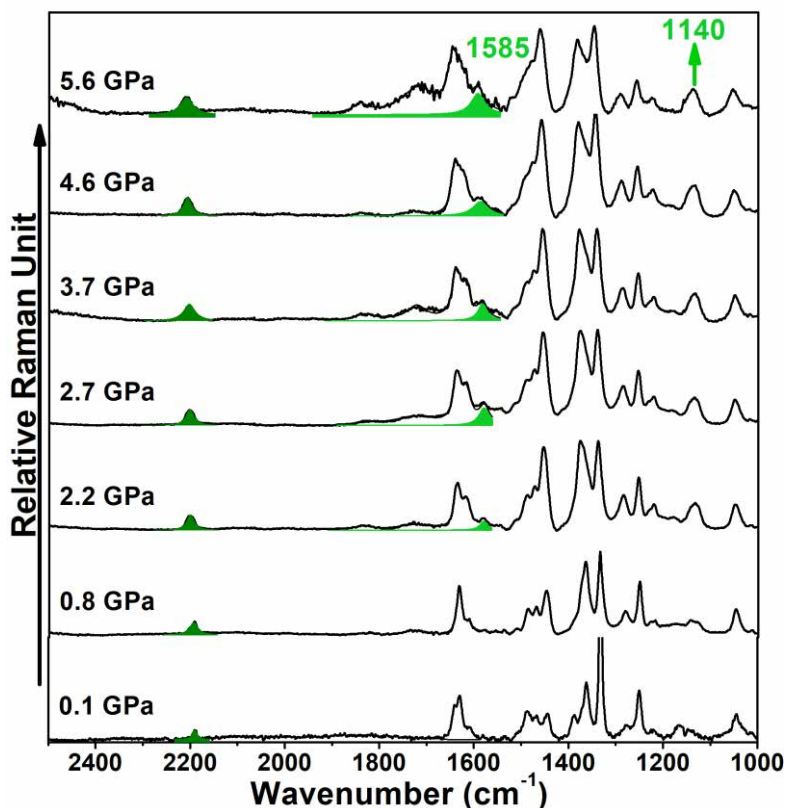


Figure 3.17 Raman spectra ( $\lambda_{\text{exc}}=785$  nm line of excitation) of the solid yellow powder of  $p\text{-(ICz)}_2$  at high pressures. Marked peaks correspond to: the  $\nu(\text{C-C})$  modes of the carbazole rings, light-green area; the  $\nu(\text{CN})$  modes, deep-green area. The shadowed region marks the band of the diamond chip used as pressure marker.

### 3.2.5 Conclusions.

❖ We demonstrate here the potential of DCM-substituted Cz and ICz-based diradicals in the field of the dynamic covalent chemistry. All these systems are able to form cyclophane structures with the formation of long C-C bonds between



## Chapter II: Cyclophane self-assembly

unpaired electrons from the radical centres (located on the bridgehead carbons of the DCM groups). While Cz-based diradicals are able to form macrocyclic tetramers, ICz analogues can build  $\sigma$ -stacked dimers. On the other hand, the substitution pattern position is also found to strongly modulate the oligomerization behaviour with meta-substitution resulting in more stable aggregates with stronger C-C bonds and remarkable  $\pi$ - $\pi$  interactions than para-substitution, which is related with the stronger diradical character predicted for the meta-substituted systems.

❖ For Cz-based systems, a dynamic monomer/cyclophane transformation is shown both in solution and solid state for ***p*-Cz**, whereas the C-C bond dissociation by external stimuli in ***m*-(Cz)<sub>4</sub>** is suppressed in solution. Therefore, the strong chromic effect from white to purple/deep blue found for these Cz-based diradicals in response to external stimuli (*i.e.*, temperature, grinding) can be adequately modulated upon appropriate changes in the substitution pattern position.

❖ The longer ICz-based systems are able to form more stable aggregates when compared to the Cz-based analogues, thus resulting in a less reversible cyclophane/monomer transformation in comparison with the shorter analogues. When compared the different substitution pattern, while ***p*-(ICz)<sub>2</sub>** shows a dynamic cyclophane/monomer transformation both in solution and solid state, the C-C bond dissociation by external stimuli in ***m*-(ICz)<sub>2</sub>** is suppressed in solution although favoured in solid-state. A major difference between solution-state and solid-state



is that the diradical is free to sample conformational space in solution whereas the solid-state experiments a confinement situation.

❖ In summary, our results demonstrate that cyclophane behaviour is strongly modulated by the DCM-substitution and the chain elongation thus considerably affecting their properties. Therefore, the strong chromic effects in response to external stimuli (*i.e.*, temperature or grinding) can be adequately modulated upon appropriate changes in the chemical structure. We believe that this study helps to identify new potential design strategies for stimuli-responsive materials.

### 3.2.6 Bibliography.

1. Kubo, T., Recent Progress in Quinoidal Singlet Biradical Molecules. *Chemistry Letters* **2015**, 44, (2), 111-122.
2. Y. Gopalakrishna, T.; Zeng, W.; Lu, X.; Wu, J., From open-shell singlet diradicaloids to polyradicaloids. *Chemical Communications* **2018**, 54, (18), 2186-2199.
3. Barker, J. E.; Dressler, J. J.; Cárdenas Valdivia, A.; Kishi, R.; Strand, E. T.; Zakharov, L. N.; MacMillan, S. N.; Gómez-García, C. J.; Nakano, M.; Casado, J.; Haley, M. M., Molecule Isomerism Modulates the Diradical Properties of Stable Singlet Diradicaloids. *Journal of the American Chemical Society* **2020**, 142, (3), 1548-1555.
4. Salem, L.; Rowland, C., The Electronic Properties of Diradicals. *Angewandte Chemie International Edition in English* **1972**, 11, (2), 92-111.
5. Abe, M.; Ye, J.; Mishima, M., The chemistry of localized singlet 1,3-diradicals (biradicals): from putative intermediates to persistent species and unusual molecules with a  $\pi$ -single bonded character. *Chemical Society Reviews* **2012**, 41, (10), 3808-3820.
6. Rudebusch, G. E.; Zafra, J. L.; Jorner, K.; Fukuda, K.; Marshall, J. L.; Arrechea-Marcos, I.; Espejo, G. L.; Ponce Ortiz, R.; Gómez-García, C. J.; Zakharov, L. N.; Nakano, M.; Ottosson, H.;





Casado, J.; Haley, M. M., Diindeno-fusion of an anthracene as a design strategy for stable organic biradicals. *Nature Chemistry* **2016**, 8, (8), 753-759.

7. Abe, M., Diradicals. *Chemical Reviews* **2013**, 113, (9), 7011-7088.

8. Ueda, A.; Nishida, S.; Fukui, K.; Ise, T.; Shiomi, D.; Sato, K.; Takui, T.; Nakasuji, K.; Morita, Y., Three-Dimensional Intramolecular Exchange Interaction in a Curved and Nonalternant  $\pi$ -Conjugated System: Corannulene with Two Phenoxy Radicals. *Angewandte Chemie International Edition* **2010**, 49, (9), 1678-1682.

9. Dressler, J. J.; Cárdenas Valdivia, A.; Kishi, R.; Rudebusch, G. E.; Ventura, A. M.; Chastain, B. E.; Gómez-García, C. J.; Zakharov, L. N.; Nakano, M.; Casado, J.; Haley, M. M., Diindenoanthracene Diradicaloids Enable Rational, Incremental Tuning of Their Singlet-Triplet Energy Gaps. *Chem* **2020**, 6, (6), 1353-1368.

10. Zhang, R.; Peterson, J. P.; Fischer, L. J.; Ellern, A.; Winter, A. H., Effect of Structure on the Spin-Spin Interactions of Tethered Dicyanomethyl Diradicals. *Journal of the American Chemical Society* **2018**, 140, (43), 14308-14313.

11. Peterson, J. P.; Zhang, R.; Winter, A. H., Effect of Structure on the Spin Switching and Magnetic Bistability of Solid-State Aryl Dicyanomethyl Monoradicals and Diradicals. *ACS Omega* **2019**, 4, (8), 13538-13542.

12. Peterson, J. P.; Geraskina, M. R.; Zhang, R.; Winter, A. H., Effect of Substituents on the Bond Strength of Air-Stable Dicyanomethyl Radical Thermochromes. *The Journal of Organic Chemistry* **2017**, 82, (12), 6497-6501.

13. Wang, D.; Capel Ferrón, C.; Li, J.; Gámez-Valenzuela, S.; Ponce Ortiz, R.; López Navarrete, J. T.; Hernández Jolín, V.; Yang, X.; Peña Álvarez, M.; García Baonza, V.; Hartl, F.; Ruiz Delgado, M. C.; Li, H., New Multiresponsive Chromic Soft Materials: Dynamic Interconversion of Short 2,7-Dicyanomethylenecarbazole-Based Biradicaloid and the Corresponding Cyclophane Tetramer. *Chemistry – A European Journal* **2017**, 23, (55), 13776-13783.

14. Okino, K.; Hira, S.; Inoue, Y.; Sakamaki, D.; Seki, S., The Divergent Dimerization Behavior of N-Substituted Dicyanomethyl Radicals: Dynamically Stabilized versus Stable Radicals.



*Angewandte Chemie International Edition* **2017**, 56, (52), 16597-16601.

15. Kobashi, T.; Sakamaki, D.; Seki, S., N-Substituted Dicyanomethylphenyl Radicals: Dynamic Covalent Properties and Formation of Stimuli-Responsive Cyclophanes by Self-Assembly. *Angewandte Chemie International Edition* **2016**, 55, (30), 8634-8638.

16. Hartzler, H. D., Polycyano Radicals. *The Journal of Organic Chemistry* **1966**, 31, (8), 2654-2658.

17. Badía-Domínguez, I.; Pérez-Guardiola, A.; Sancho-García, J. C.; López Navarrete, J. T.; Hernández Jolín, V.; Li, H.; Sakamaki, D.; Seki, S.; Ruiz Delgado, M. C., Formation of Cyclophane Macrocycles in Carbazole-Based Biradicaloids: Impact of the Dicyanomethylene Substitution Position. *ACS Omega* **2019**, 4, (3), 4761-4769.

18. Yuan, L.; Han, Y.; Tao, T.; Phan, H.; Chi, C., Formation of a Macrocycles-in-a-Macrocycle Superstructure with All-gauche Conformation by Reversible Radical Association. *Angewandte Chemie International Edition* **2018**, 57, (29), 9023-9027.

19. Schaufelberger, F.; Timmer, B. J. J.; Ramström, O., Principles of Dynamic Covalent Chemistry. In *Dynamic Covalent Chemistry*, 2017; pp 1-30.

20. Sakamaki, D.; Ghosh, S.; Seki, S., Dynamic covalent bonds: approaches from stable radical species. *Materials Chemistry Frontiers* **2019**, 3, (11), 2270-2282.

21. Oda, K.; Hiroto, S.; Shinokubo, H., NIR mechanochromic behaviours of a tetracyanoethylene-bridged hexa-perihexabenzocoronene dimer and trimer through dissociation of C-C bonds. *Journal of Materials Chemistry C* **2017**, 5, (22), 5310-5315.

22. Imato, K.; Nishihara, M.; Kanehara, T.; Amamoto, Y.; Takahara, A.; Otsuka, H., Self-Healing of Chemical Gels Cross-Linked by Diarylbibenzofuranone-Based Trigger-Free Dynamic Covalent Bonds at Room Temperature. *Angewandte Chemie International Edition* **2012**, 51, (5), 1138-1142.

23. Furgal, J. C.; Dunn, M.; Wei, T.; Scott, T. F., Emerging Applications of Dynamic Covalent Chemistry from Macro- to Nanoscopic Length Scales. In *Dynamic Covalent Chemistry*, 2017; pp 389-434.



24. Beaudoin, D.; Levasseur-Grenon, O.; Maris, T.; Wuest, J. D., Building Giant Carbocycles by Reversible C–C Bond Formation. *Angewandte Chemie International Edition* **2016**, *55*, (3), 894-898.
25. Badía-Domínguez, I.; Peña-Álvarez, M.; Wang, D.; Pérez Guardiola, A.; Vida, Y.; Rodríguez González, S.; López Navarrete, J. T.; Hernández Jolín, V.; Sancho García, J. C.; García Baonza, V.; Nash, R.; Hartl, F.; Li, H.; Ruiz Delgado, M. C., Dynamic Covalent Properties of a Novel Indolo[3,2-b]carbazole Diradical. *Chemistry – A European Journal* **2021**, *27*, (17), 5509-5520.
26. van Dongen, M. A.; Orr, B. G.; Banaszak Holl, M. M., Diffusion NMR Study of Generation-Five PAMAM Dendrimer Materials. *The Journal of Physical Chemistry B* **2014**, *118*, (25), 7195-7202.
27. Jiménez, V. A.; Gavín, J. A.; Alderete, J. B., Scaling trend in diffusion coefficients of low generation G0–G3 PAMAM dendrimers in aqueous solution at high and neutral pH. *Structural Chemistry* **2012**, *23*, (1), 123-128.
28. González-Cano, R. C.; Di Motta, S.; Zhu, X.; López Navarrete, J. T.; Tsuji, H.; Nakamura, E.; Negri, F.; Casado, J., Carbon-Bridged Phenylene-Vinylens: On the Common Diradicaloid Origin of Their Photonic and Chemical Properties. *The Journal of Physical Chemistry C* **2017**, *121*, (41), 23141-23148.
29. Mosca, S.; Milani, A.; Peña-Álvarez, M.; Yamaguchi, S.; Hernández, V.; Ruiz Delgado, M. C.; Castiglioni, C., Mechanochromic Luminescent Tetrathiazolylthiophenes: Evaluating the Role of Intermolecular Interactions through Pressure and Temperature-Dependent Raman Spectroscopy. *The Journal of Physical Chemistry C* **2018**, *122*, (30), 17537-17543.
30. Smith, B., Organic Nitrogen Compounds IV: Nitriles. *Spectroscopy* **2019**, *34*, (7), 18–21, 44.
31. Canesi, E. V.; Fazzi, D.; Colella, L.; Bertarelli, C.; Castiglioni, C., Tuning the Quinoid versus Biradicaloid Character of Thiophene-Based Heteroquaterphenoquinones by Means of Functional Groups. *Journal of the American Chemical Society* **2012**, *134*, (46), 19070-19083.
32. Baonza, V. G.; Taravillo, M.; Arencibia, A.; Cáceres, M.; Núñez, J., Diamond as pressure sensor in high-pressure Raman



## Chapter II: Cyclophane self-assembly

spectroscopy using sapphire and other gem anvil cells. *Journal of Raman Spectroscopy* **2003**, 34, (4), 264-270.





# CHAPTER III: Photophysical and charge transport properties of carbazole-based macrocycles.

## Table of contents

---

- 3.3.1 Introduction.
  - 3.3.2 Structural and photophysical properties of tetracarbazole-based macrocycles.
    - 3.3.2.1 Effect of the substitution pattern (ortho, meta and para positions)
      - 3.3.2.1.1 Cyclophane structural features.
      - 3.3.2.1.2 Ground-state molecular and electronic structure.
    - 3.3.2.2 Effect of cyclization on the photophysical properties.
  - 3.3.3 Charge transport properties of tetracarbazole-based macrocycles.
    - 3.3.3.1 Tetracarbazole-based macrocycles: Influence of the insertion of ethylene group.
      - 3.3.3.1.1 Cyclophane structural features.
      - 3.3.3.1.2 Ground-state molecular and electronic structure.
      - 3.3.3.1.3 Charge transport properties.
    - 3.3.3.2 Coronoid carbazole-based macrocycles: Influence of isomerism.
      - 3.3.3.2.1 Cyclophane structural features.
      - 3.3.3.2.2 Ground-state electronic structure.
      - 3.3.3.2.3 Charge transport properties.
  - 3.3.4 Conclusions.
  - 3.3.5 Bibliography.
-







### 3.3.1 Introduction.

In the field of organic electronics, organic conjugated systems based on Cz units have been recognized as “essential structures” due to their good electro- and photoactive properties, such as high hole-transporting mobilities, with respect to other heterocycles<sup>1-7</sup>. For instance, Cz-based compounds have been implemented in organic solar cells, organic light-emitting diodes (OLEDs) or organic field-effect transistors (OFETs), etc<sup>8-14</sup>. In this sense, the investigation of structure-properties relationships is critically important and allows the development of novel materials with enhanced performance.

Recently, there has been a great interest in the synthesis of Cz-based compounds with tuneable electronic and optical properties as a function of the molecular structural features such as size, shape symmetry, or cyclicity, allowing to obtain improved electronic devices<sup>15-21</sup>. While the majority of our previously studies had been focused on small and lineal Cz-based materials, macrocyclic  $\pi$ -conjugated compounds will be addressed in this chapter as novel two-dimensional topological materials. Thus, different  $\pi$ -conjugated Cz-based macrocycles have been investigated here to understand their electronic and photophysical properties in order to explore new materials with great potential for electronic applications<sup>22-26</sup>.

### 3.3.2 Structural and photophysical properties of tetracarbazole-based macrocycles.

In the two previous chapters, we have discussed the electronic, molecular, and optical properties of small and lineal Cz-based molecules. In this section, we would like to explore how the cyclization with different connection (*i.e.*, ortho, meta and para) affects the system properties to establish structure-properties relationships. To carry out this investigation, we present the comparison of three different tetracarbazole-based macrocycles (*i.e.*, named as **o-CyCz**, **m-CyCz** and **p-CyCz**, see Figure 3.1) with distinct structural features, which determine their spatial arrangement and supramolecular assembly, as well as afford them some unique physicochemical properties.

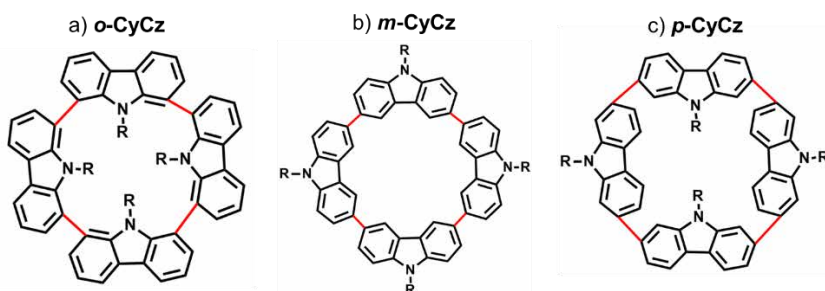


Figure 3.1. Chemical structures of the tetracarbazole-based macrocycles studied in this section.

#### 3.3.2.1 Effect of the substitution pattern (ortho, meta and para positions).

##### 3.3.2.1.1 Cyclophane structural features.

Figure 3.2 compared the DFT-calculated and experimental X-ray structures of **p-CyCz** and **m-CyCz**. While **p-CyCz** is formed by four Cz units creating a belt-shaped possessing

radially oriented  $\pi$  orbitals, a ring-shaped with the four Cz units extended with the *N*-alkyl groups pointed outward of the cavity is obtained for ***m*-CyCz** macrocycle.

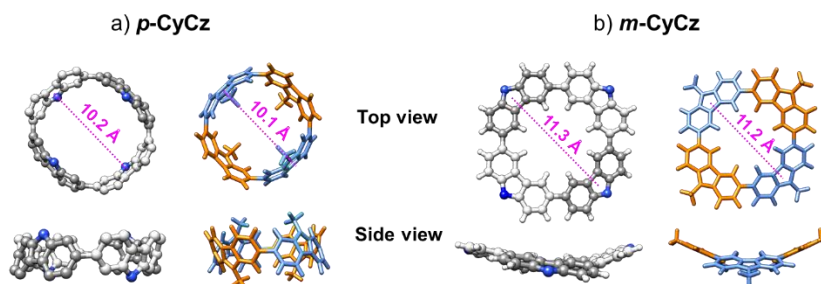


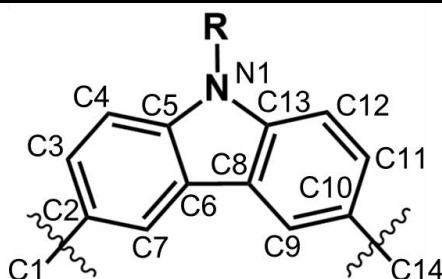
Figure 3.2 X-ray (left) and DFT-computed (M06-2X/6-31G\*\* level) global minimum structure (right) for (a) ***p*-CyCz** and (b) ***m*-CyCz** macrocycles. The *N*-substituents have been omitted for clarity.

To replicate adequately the single-crystal X-ray experimental structures, DFT-calculations with different hybrid functionals were performed. The comparison between theoretical and experimental bond distances for ***m*-CyCz** are summarized in Table 3.1.

Table 3.1. Comparison of the experimental and calculated bond length values [ $\text{\AA}$ ] determined for ***m*-CyCz**.

Bond length ( $\text{\AA}$ )	Exp.	DFT		
		B3LYP	$\omega$ B97XD	M06-2X
C1-C2	1.474	1.486	1.485	1.484
C2-C3	1.409	1.415	1.409	1.410
C3-C4	1.376	1.393	1.388	1.388
C4-C5	1.372	1.398	1.395	1.396
C5-N1	1.387	1.392	1.386	1.385

C5-C6	1.405	1.419	1.410	1.412
C6-C7	1.392	1.394	1.390	1.391
C7-C2	1.394	1.402	1.395	1.395
C6-C8	1.449	1.448	1.446	1.447
C8-C13	1.412	1.419	1.410	1.412
C13-N1	1.381	1.392	1.386	1.385
C8-C9	1.389	1.394	1.390	1.391
C9-C10	1.395	1.402	1.395	1.395
C10-C11	1.416	1.415	1.409	1.410
C11-C12	1.366	1.393	1.388	1.388
C12-C13	1.384	1.398	1.395	1.396
C10-C14	1.486	1.486	1.485	1.484



According to these values, M06-2X functional was found to provide the best quantitative agreement with the experimental data. These results confirm that M06-2X functional seems appropriate for evaluating the structural and vibrational properties of tetracarbazole-based macrocycles under study. In addition, Figure 3.2 confirms that the macrocycle spatial arrangements predicted by theoretical calculations are in good agreement with the experimental data.

Unfortunately, suitable single crystals of **o-CyCz** for X-ray analysis were not obtained. Thus, we performed DFT calculations for different conformations to address the most favourable molecular arrangement of this macrocycle (Figure 3.3). To this end, two different conformations for the spatial disposition of the Cz fragments were considered: (i) a double-decker ring-shaped with the *N*-alkyl groups pointed inward of the cavity where the Cz units are co-facially oriented in a pairwise conformation; (ii) a distorted chair-shaped with two Cz units pointed outward of the cavity. DFT calculations indicated that the double-decker ring-shaped structure is the most favourable one, with much lower energy ( $\sim 98$  kcal·mol<sup>-1</sup>) than the distorted chair-shaped structure.

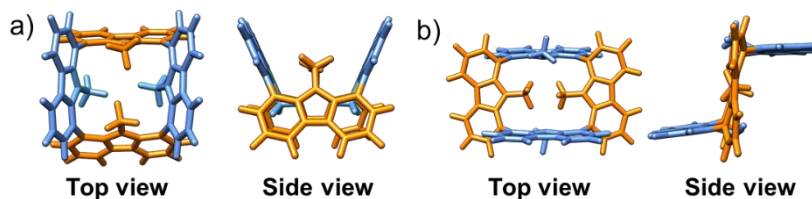


Figure 3.3. Top view (left) and side view (right) of DFT-computed global minimum structure for **o-CyCz** macrocycle in two different configurations: a double-decker ring-shaped (a) and a distorted chair-shaped (b).

### 3.3.2.1.2 Ground-state molecular and electronic structure.

In this section, we carried out a combined experimental and theoretical approach that links electronic and vibrational spectroscopies with DFT calculations. Figure 3.4 shows the DFT-computed molecular orbital diagram for three tetracarbazole-based macrocycles together with the topologies of their frontier molecular orbitals. It is noteworthy that both HOMO and LUMO

orbitals are completely delocalized in all tetracarbazole units. Nevertheless, HOMO and LUMO have preferential localization sites as a function of the substitution pattern (*i.e.*, ortho, meta and para) resulting in notable differences among them that we will discuss below.

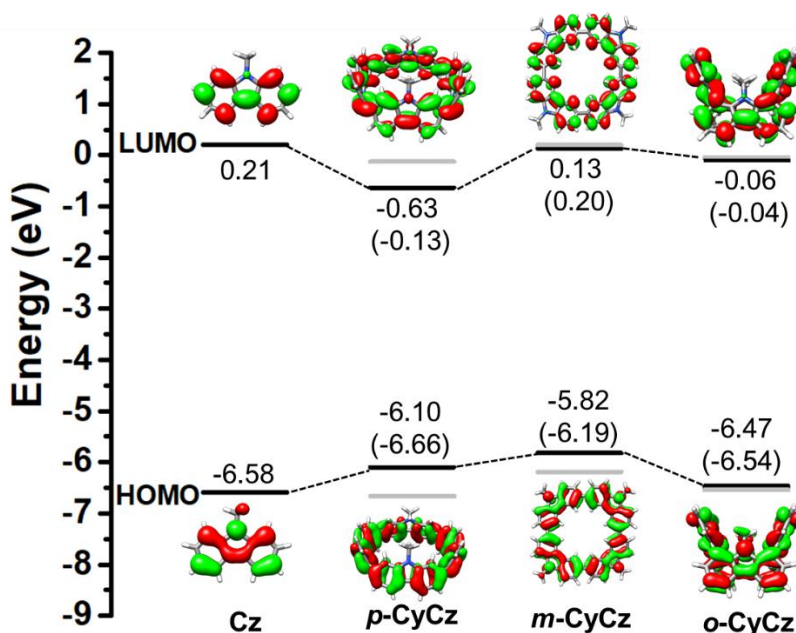


Figure 3.4 DFT-computed molecular orbital diagram for the tetracarbazole-based macrocycles (*p*-CyCz, *m*-CyCz and *o*-CyCz) and the isolated Cz unit at the M06-2X/6-31G\*\* level. The topologies of the frontier molecular orbitals are also shown (isovalue 0.02 au). The values in parenthesis and gray lines are ascribed to the HOMO-1 and LUMO+1 levels.

For *p*-CyCz, HOMO and LUMO are delocalized through the whole ring with a radial geometry. Indeed, the HOMO density resembles that of [8]cycloparaphenylene (8CPP)<sup>27-28</sup>, with no participation of the nitrogen atoms, whereas the LUMO density resembles that of isolated Cz itself, with no participation of the



carbon atom in para position with respect to the nitrogen atom. These wavefunctions reflect a good conjugation between the Cz units and, consequently, the **p-CyCz** macrocycle exhibits the lowest HL gap (5.47 eV). In contrast, the change in the substitution position from para to meta causes a moderate  $E_{\text{HOMO}}$  destabilization together with a strong  $E_{\text{LUMO}}$  destabilization since the LUMO topologies display a node in meta position, and hence remains close in energy to that isolated **Cz** system<sup>29</sup>. Therefore, **m-CyCz** compound shows higher HL gap (5.95 eV) than its para-substituted analogue.

On the other hand, **o-CyCz** macrocycle shows the largest HL gap (6.41 eV) within the series, probably due to the large deviation of inter-ring dihedral angles from planarity. This affirmation can be explained because the HOMO has antibonding interactions located on the inter-ring C-C bonds. Thus, the HOMO is stabilized with an increasing inter-ring dihedral angle removing the antibonding interactions. The reverse situation applies to the LUMO, which has bonding interactions located on inter-ring bonds. Therefore, larger dihedral angles disturb the inter-ring bonding interactions which result in the destabilization of the LUMO. Thus, the change of substitution pattern leads to a significant increase in the HL gap when going from para to meta to ortho as a result of the decrease of the conjugation between the Cz units; this is especially relevant in the case of **o-CyCz** due to the large torsion angles between the Cz units.

Secondly, the UV/Vis absorption spectra were measured in order to elucidate the photophysical properties of the



macrocycles under study. Figure 3.5 shows a comparison of the electronic absorption spectra of three macrocycles in chloroform together with their theoretical spectra. Curiously, ***p*-CyCz** compound exhibits a band tail at 397 nm, which is due, according to TD-DFT calculations, to a symmetry forbidden ( $f=0$ ) HOMO  $\rightarrow$  LUMO electronic transition predicted at 340 nm associated with a  $S_0 \rightarrow S_1$  transition. The appearance of this symmetry forbidden band in the experimental absorption spectrum might be associated with a macrocycle distortion caused by the solvent resulting in an increase of their intensity band. A parallel situation is found for ***m*-CyCz** where a weak band is observed at 372 nm associated with the  $S_0 \rightarrow S_1$  electronic transition predicted at 305 nm. However, a different absorption spectral pattern is found for ***o*-CyCz** with a moderate double-peak band at 347 and 334 nm associated with the degenerated  $S_0 \rightarrow S_1$  and  $S_0 \rightarrow S_2$  transitions and the  $S_0 \rightarrow S_4$  transition predicted at 290 and 288 nm, respectively. Therefore, the electronic absorption spectra exhibit a blue-shift ongoing from ***p*-CyCz** ( $\lambda = 397$  nm) to ***m*-CyCz** ( $\lambda = 372$  nm) to ***o*-CyCz** ( $\lambda = 347$  nm) indicating that the linking via para position is a more efficient way to improve the  $\pi$ -conjugation. As seen in Figure 3.5, TD-DFT calculations support the blue-shift of the experimental UV/Vis spectra when going from para to meta to ortho connection.

On the other hand, ***p*-CyCz** and ***m*-CyCz** display a strong absorbance band at 340 and 303 nm, respectively. Finally, ***o*-CyCz** shows moderate absorption double-peak bands at 291 and



300 nm. Again, TD-DFT calculations support the experimental spectra predicting intense electronic transitions at 287 nm and 257 nm for *p*-CyCz and *m*-CyCz, respectively, and a weak transition at 241 nm for *o*-CyCz fulfilling the experimental trend.

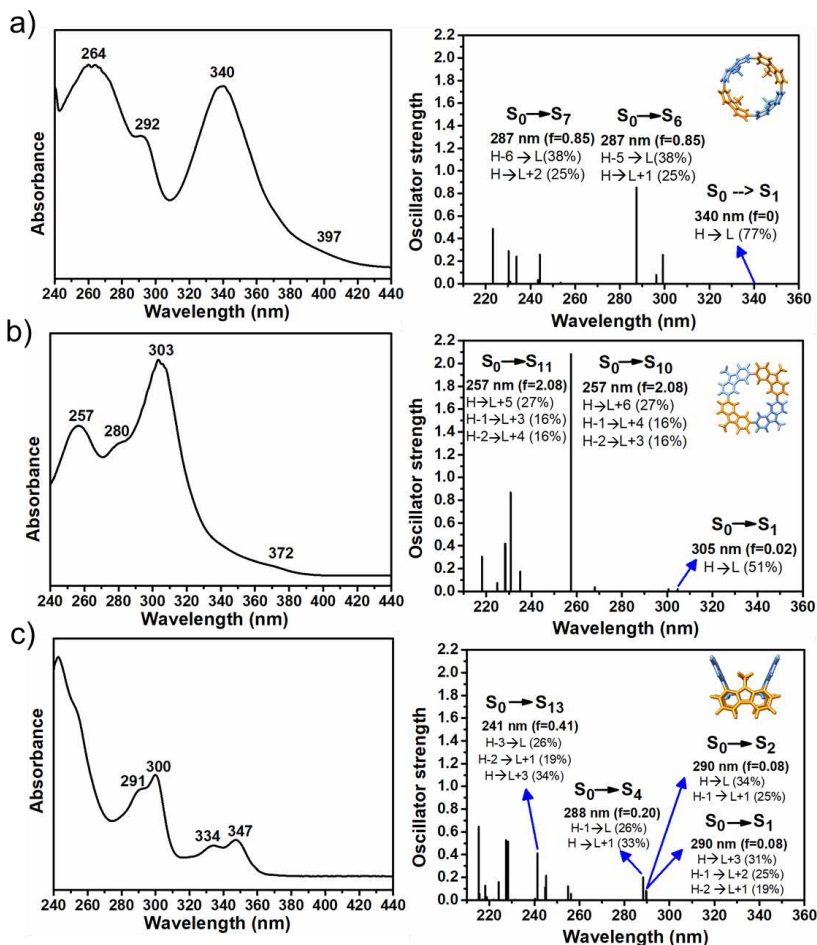


Figure 3.5. Left: Experimental UV/Vis absorption of a freshly prepared solution in chloroform of (a) *p*-CyCz, (b) *m*-CyCz and (c) *o*-CyCz at RT. Right: TD-DFT calculated vertical transition energies for tetracarbazole-based macrocycles of (a) *p*-CyCz, (b) *m*-CyCz and (c) *o*-CyCz at M06-2X/6-31G\*\*.



Thirdly, we make use of Raman spectroscopy as a rich source of information on the molecular structural changes that might occur upon the different substitution pattern. Figure 3.6 shows the FT-Raman ( $\lambda_{\text{exc}}=1064$  nm) spectra of isolated **Cz** molecule and the macrocycles under study. We focus on the 1700-1400  $\text{cm}^{-1}$  region since the most significant Raman spectral changes occur in this region. The FT-Raman spectrum of isolated **Cz** molecule is characterized by three main bands at 1626  $\text{cm}^{-1}$  (blue point), 1597  $\text{cm}^{-1}$  (pink point) and 1576  $\text{cm}^{-1}$  (green point), which are ascribed to symmetric and antisymmetric CC stretching modes and CC breathing of the pyrrole ring vibrational stretches, respectively (Figure 3.7). When comparing the tetracarbazole-based macrocycles, we observe that the para-position led to a remarkable downshifting of these three main bands (*i.e.*, 1610, 1588 and 1564  $\text{cm}^{-1}$  for **p-CyCz** macrocycle) which agrees with the increase of the electronic delocalization in this system. The opposite occurs in the **o-CyCz** case, in which the 1597 and 1576  $\text{cm}^{-1}$  bands suffer an upshifting to 1604 and 1587  $\text{cm}^{-1}$ , respectively, due to its notable distortional shape which results in a less conjugation. Finally, similar frequencies to isolated **Cz** are shown for **m-CyCz** thanks to its ring-shape conformation resulting in an analogous electronic delocalization (1628, 1601 and 1574  $\text{cm}^{-1}$ ). This is good agreement with the DFT-computed eigenvectors and Raman spectra for tetracarbazole-based macrocycles (Figures 3.6-3.8).

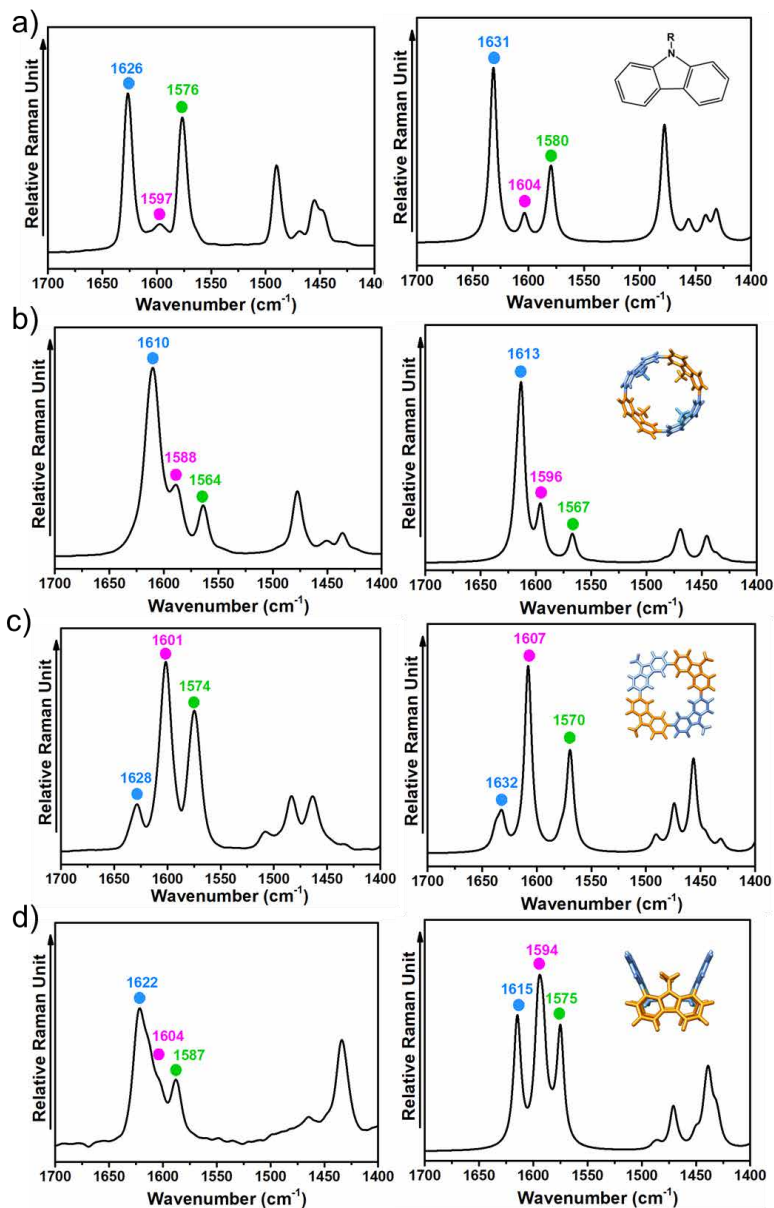


Figure 3.6 Left: FT-Raman spectra ( $\lambda_{\text{exc}}=1064$  nm) of (a) **Cz**, (b) **p-CyCz**, (c) **m-CyCz** and (d) **o-CyCz** as a white powder at RT. Right: Theoretical Raman spectra (M06-2X/6-31G\*\*) for (a) **Cz**, (b) **p-CyCz**, (c) **m-CyCz** and (d) **o-CyCz**.

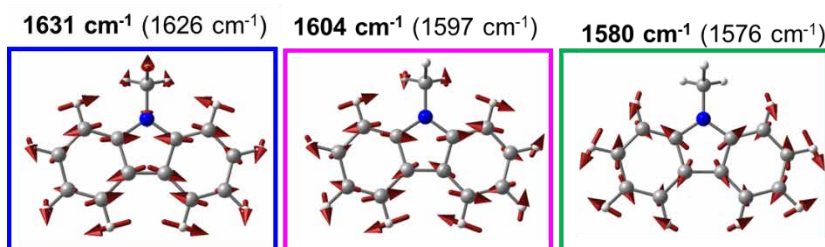


Figure 3.7. Eigenvectors (M06-2X/6-31G\*\* level) associated to the main Raman bands for isolated **Cz**. The theoretical and experimental (in parentheses) wavenumbers are also shown.

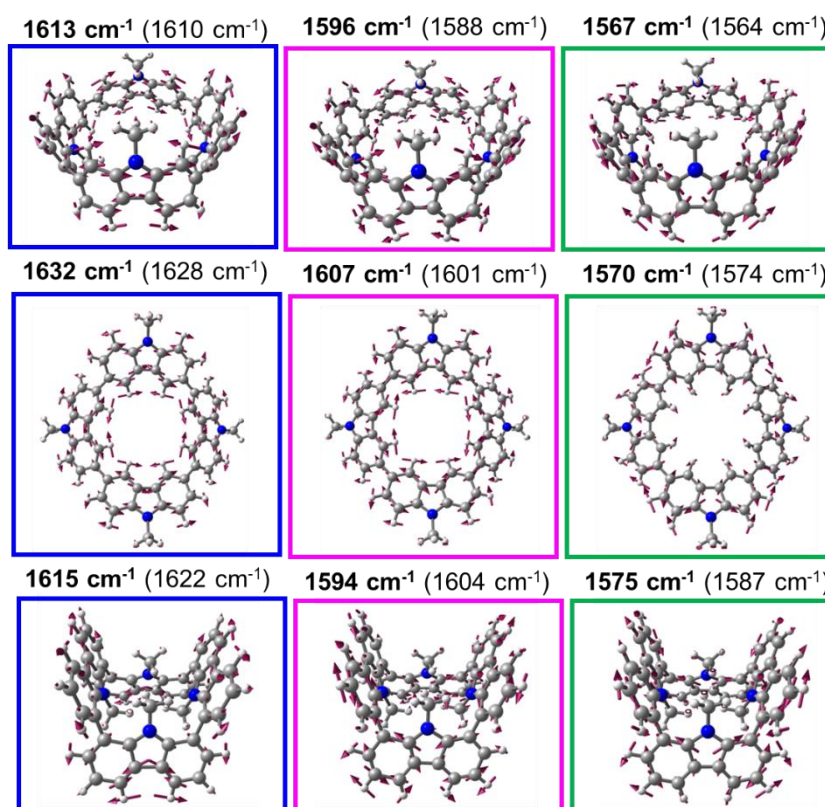


Figure 3.8. Eigenvectors (M06-2X/6-31G\*\* level) associated to the main Raman bands for (up) **p-CyCz**, (middle) **m-CyCz** and (down) **o-CyCz**. The theoretical and experimental (in parentheses) wavenumbers are also shown.

### 3.3.2.2 Effect of cyclization on the photophysical properties.

In addition to our initial interest in the structural diversity of Cz-based macrocycles, we were intrigued by the potential of these macrocycles in advanced optical devices since Cz derivatives have been found to inherit persistent phosphorescent lifetimes ( $\tau_p$ ) because their lowest triplet excited state<sup>30-33</sup>. In this section, we explore whether we could further promote  $\tau_p$  as well as the phosphorescence efficiency by cyclization. To this end, the photophysical properties of the ***m-CyCz*** macrocycle were investigated to get deeper understanding about how the cyclization (and thus, cyclic conjugation) influences the phosphorescence behaviour in comparison with its linear counterpart ***m-LCz*** (Figure 3.9)<sup>20</sup>.

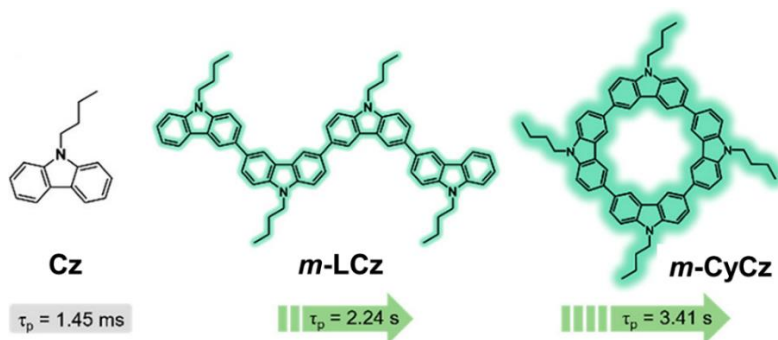


Figure 3.9. Chemical structures of isolated **Cz**, ***m-LCz***, and ***m-CyCz***. The phosphorescent lifetimes ( $\tau_p$ ) are also shown.

The photophysical data of all these three Cz-based systems are shown in Table 3.2. It has been demonstrated that isolated **Cz** held a weak and short phosphorescence with a  $\tau_p$  of 1.45 ms at 77 K in solution with low phosphorescence quantum yield ( $\Phi_p$ ). To improve the phosphorescence process, a linear conjugated backbone with four Cz units (***m-LCz***) was studied aiming to



investigate how the linear polymerization influenced the phosphorescence behaviour. Interestingly, **m-LCz** displayed improved phosphorescence with a  $\tau_p$  of 2.24 s at 77 K in solution. Analogously, we decided to investigate the cyclic conjugated molecule with four Cz units (**m-CyCz**). Compared with their linear analogue, **m-CyCz** exhibited a more efficient ultralong phosphorescence with a longer lifetime of 3.41 s in the same condition. These results support the enhanced phosphorescence behaviour (*i.e.*, upgraded phosphorescence lifetime and phosphorescence efficiency) upon elongation of the linear conjugation from one to four Cz units and even more by cyclization demonstrating that the cyclic conjugation is a more effective way to promote the phosphorescence process than linear conjugation. These results can be well-reflected by the images taken with and without UV irradiation (Figure 3.10).

Table 3.2. Photophysical properties of **Cz**, **m-LCz**, and **m-CyCz** in the solution state.

Molecule	T (K)	Emission (nm) <sup>a</sup>	PL	$\tau$
<b>Cz</b>	298	353	Fluorescence	10.08 ns
	77	366	Fluorescence	---- <sup>b</sup>
		440	Phosphorescence	1.45 ms
<b>m-LCz</b>	298	421	Fluorescence	----
	77	428	Fluorescence	----
		470, 504	Phosphorescence	2.24 s, 2.22 s
<b>m-CyCz</b>	298	428	Fluorescence	6.38 ns
	77	428	Fluorescence	13.24 ns
		472, 494	Phosphorescence	3.41 s, 3.33 s

<sup>a</sup>Only main peaks are shown here. <sup>b</sup> $\tau_p$  is not determined because it is fluorescence, proved by time-resolved PL spectrum.

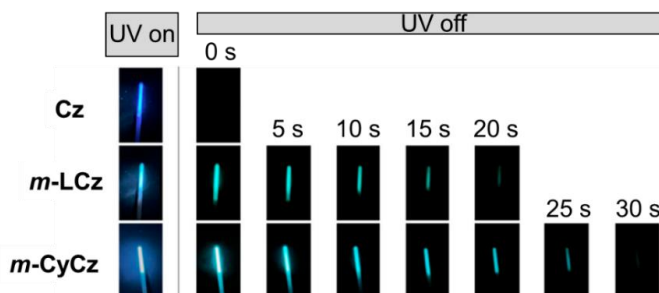


Figure 3.10 Photographs of low temperature THF solutions of **Cz**, **m-LCz** and **m-CyCz** in NMR tubes to present phosphorescence.

At this point, we decided to carry out theoretical calculations in order to understand why the phosphorescence behaviour is improved by linear conjugation and further pushed forward by cyclization. All theoretical data are listed in Table 3.3 and Figure 3.11 displays the energy level diagrams for all three systems.

Table 3.3 TD-DFT calculated (B3LYP/6-31G\*\*) energy levels of  $S_1$  ( $E_{S1}$ ) and  $T_1$  ( $E_{T1}$ ) excited states, singlet-triplet energy gap ( $\Delta E_{ST}$ ), energy gaps for the most favourable ISC channels ( $E_{ISC}$ ) and the reorganization energy of the  $S_1$  to  $S_0$  ( $\lambda_{S1 \rightarrow S0}$ ) transition and the one from  $T_1$  to  $S_0$  ( $\lambda_{T1 \rightarrow S0}$ ) transition of **Cz**, **m-LCz** and **m-CyCz**.

	<b>Cz</b>	<b>m-LCz</b>	<b>m-CyCz</b>
$E_{S1}$	4.04	3.60	3.33
$E_{T1}$	3.18	2.96	2.77
$\Delta E_{ST}$	0.86	0.64	0.55
$E_{ISC}^a$	0.70	0.38	0.04
$\lambda_{S1 \rightarrow S0}$	---	0.16	0.06
$\lambda_{T1 \rightarrow S0}$	---	0.47	0.07

<sup>a</sup> $E_{ISC}$  represents the energy gap between  $S_1$  and the specific  $T_n$  excited states with transition configurations with high similarity. However, note that it would be necessary to go beyond qualitative rules to study in more detail the mechanisms of ISC process; thus, a more exhaustive study involving spin-orbit coupling are currently under way in our group.

First, we calculated the intersystem crossing (ISC) energy gap ( $E_{ISC}$ ) for all three studied compounds. For the isolated **Cz**, the  $E_{ISC}$  between  $S_1$  and  $T_2$  was defined to be 0.70 eV worsening the ISC channel. On the other hand, the linear structure **m-LCz** improved the problem of inadequate channels with decreased  $E_{ISC}$  between the  $S_1$  and  $T_n$  states (*i.e.*,  $E_{ISC}$  value of 0.38 eV between  $S_1$  and  $T_8$ ) thereby helping the ISC process and further phosphorescence<sup>34</sup>. By cyclization, the  $E_{ISC}$  dramatically decreased to 0.04 eV, which further promoted the ultralong phosphorescence.

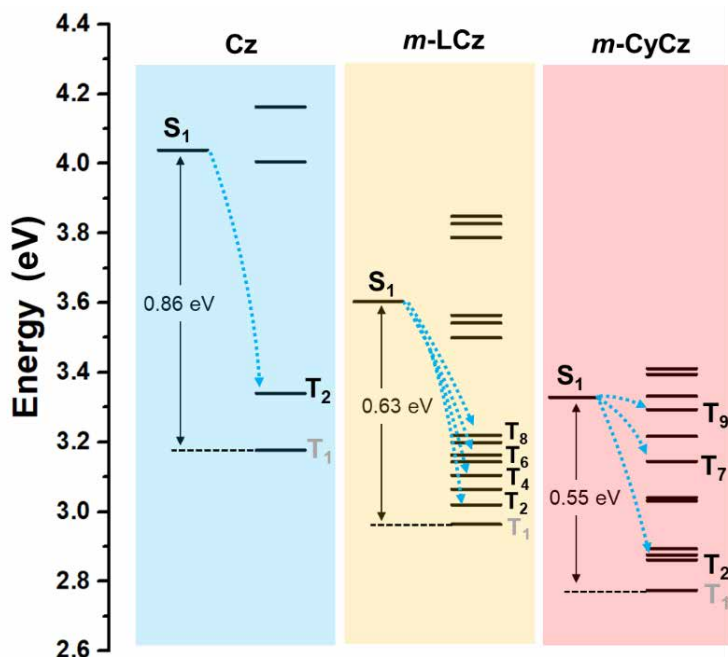


Figure 3.11 TD-DFT calculated (B3LYP/6 31G\*\*) energy level diagrams of **Cz**, **m-LCz** and **m-CyCz**. The  $\Delta E_{ST}$  values together with the ISC possible channels (indicated by dash arrows) are also shown.





Second, we also computed the energy gap between the  $S_1$  and  $T_1$  excited states ( $\Delta E_{ST}$ ). This energy decreased when going from isolated **Cz** to **m-LCz** and **m-CyCz** (from 0.86 to 0.64 and 0.55 eV, respectively, see Table 3.3 and Figure 3.11). It should be highlight that the  $\Delta E_{ST}$  of **m-CyCz** is large enough to prevent the reversible ISC, but it is also moderate enough to decrease the nonradiative decay. Therefore, the proper  $\Delta E_{ST}$  value together with the favourable ISC process endowed **m-CyCz** with excellent phosphorescence properties.

Finally, the structural changes upon  $T_1 \rightarrow S_0$  and  $S_1 \rightarrow S_0$  transitions were also tested based on the reorganization energies. Lower reorganization energies occurred in **m-CyCz** during these two processes when compared with **m-LCz** (*i.e.*, 0.06 eV vs. 0.16 eV for  $S_1 \rightarrow S_0$  transition and 0.07 eV vs. 0.47 eV for  $T_1 \rightarrow S_0$  transition, respectively) indicating that the rigidification effect is more profound in **m-CyCz**, which synergistically suppresses the nonradiative decay and promotes the long-lived phosphorescence.

In summary, by comparing the isolated **Cz**, the linear tetramer **m-LCz**, and the corresponding macrocycle **m-CyCz**, we found a relationship between the conjugated structure and the excited state energy levels that could dramatically influence the phosphorescence characteristics. This study demonstrates that cyclization-promoted phosphorescence may further act as a guideline for designing novel pure organic phosphorescent molecules.



### 3.3.3 Charge transport properties of Cz-based macrocycles.

Efficient charge transport in  $\pi$ -conjugated organic systems is one of the most important requirements for the development of high-performance electronic devices<sup>35,36</sup>. In this sense, important scientific progress has been achieved towards better understanding of intrinsic charge transport phenomena in these materials<sup>37-39</sup>. In fact, extensive effort has been directed toward the elucidation of the relationship between the molecular arrangement and the charge transport properties<sup>40</sup>. Here, we aim to investigate how different chemical structural changes (*i.e.*, insertion of ethylene groups between neighbouring Cz units in ***m*-CyCz** or the effect of structural isomerism in fully-fused cycles) affect the charge transport properties of Cz-based macrocycles

#### 3.3.3.1 Tetracarbazole-based macrocycles: insertion of ethylene group.

The tetracarbazole-based macrocycles studied in the previous section (***p*-CyCz**, ***m*-CyCz** and ***o*-CyCz**) are too flexible because of the rotation around the adjacent biphenyl units which might worsen the charge transport properties<sup>24,41,42</sup>. In this section, we want to explore the effect of the insertion of ethylene moiety between the neighbouring Cz units of ***m*-CyCz**, which can minimize the distortion angle between the Cz units improving the charge transport properties, see Figure 3.12. In fact, it has been demonstrated in previous studies that the insertion of an ethylene spacer enhances the  $\pi$ -conjugation playing a crucial role in the electronic coupling between neighbouring units and thereby, in the charge transport<sup>43,44</sup>.

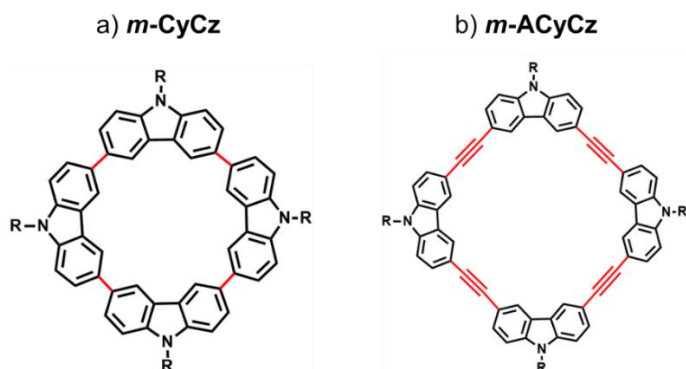


Figure 3.12. Chemical structures of the tetracarbazole-based macrocycles studied in this section.

### 3.3.3.1.1 Cyclophane structural features.

As described above, the single-crystal X-ray analysis for *m*-CyCz reveal that four Cz molecules are linked creating a ring cavity with a moderate distortional dihedral angle of  $\sim 30^\circ$  between the Cz units, see Figure 3.13. The DFT-calculated structure exhibits a similar distortion with a moderate twist ( $\sim 35^\circ$  dihedral angles) between the Cz units, demonstrating that the theoretical calculations are in good agreement with the experimental data due to the similarity of the macrocycle spatial arrangement. Although, the X-ray structure of *m*-ACyCz macrocycle was not obtained. According to the DFT calculations, the insertion of ethylene groups diminishes the steric repulsion between the adjacent Cz units and results in a more planar macrocycle structure minimizing the distortion of the dihedral angle between Cz units (from  $35^\circ$  to  $0.2^\circ$  for *m*-CyCz and *m*-ACyCz, respectively). Hence, this increase in the planarity could influence their electronic and molecular structure, as well as

optical properties since it favours the  $\pi$ -conjugation through the macrocycle.

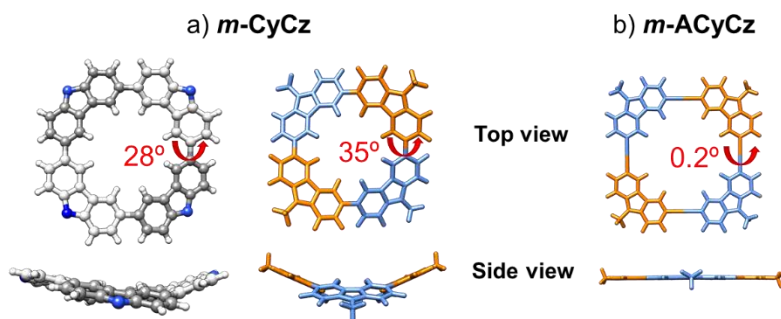


Figure 3.13 (a) X-ray (left) and DFT-computed (M06-2X/6-31G\*\*) global minimum structure (right) for ***m-CyCz*** macrocycle. The *N*-substituents have been omitted for clarity. (b) Top and side view of DFT-calculated structure for ***m-ACyCz*** macrocycle at the M06-2X/6-31G\*\* level.

### 3.3.3.1.2 Ground-state molecular and electronic structure.

Figure 3.14 displays the frontier molecular orbitals together with the energy diagram for ***m-CyCz*** and ***m-ACyCz*** macrocycles. Focusing on the comparison between the isolated **Cz** and its macrocycle analogous ***m-CyCz***, we observed that the elongation and further cyclization of the conjugated core induces more efficient conjugation resulting in smaller HL gap (*i.e.*, 6.79 eV in **Cz** and 5.95 eV in ***m-CyCz***). An additional HL gap decrease of  $\sim 0.4$  eV is also found when comparing the ***m-CyCz*** with the ***m-ACyCz*** homologue (*i.e.*, 5.95 eV and 5.60 eV, respectively) due to the stabilization of the  $E_{\text{LUMO}}$  upon the insertion of electron-withdrawing ethylene groups.

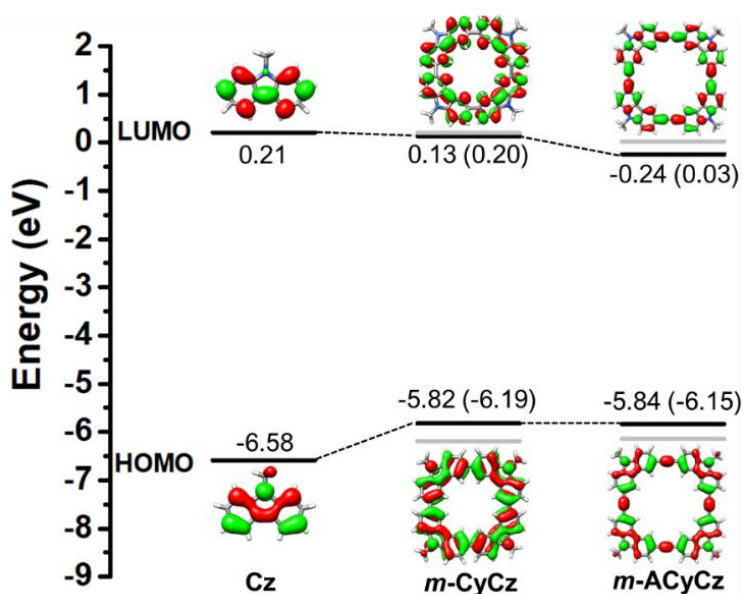


Figure 3.14 DFT-computed molecular orbital diagram for the tetracarbazole-based macrocycles (*m*-CyCz and *m*-ACyCz) and the isolated Cz unit at the M06-2X/6-31G\*\* level. The topologies of the frontier molecular orbitals are also shown (isovalue 0.02 au). The values in parenthesis and gray lines are ascribed to the HOMO-1 and LUMO+1 levels.

The optical properties of the target samples were monitored by UV/Vis absorption spectroscopy. Figure 3.15 exhibits the experimental absorption spectra in dichloromethane solution at RT together with their simulated spectra obtained with TD-DFT at M06-2X/6-31G\*\* level. As above-mentioned, *m*-CyCz display a weak band at 372 nm associated with the  $S_0 \rightarrow S_1$  electronic transition predicted at 305 nm together with a strong absorbance band at 303 nm (theoretically predicted at 257 nm which corresponds to the  $S_0 \rightarrow S_{10}$  and  $S_0 \rightarrow S_{11}$  degenerated electronic transitions). A parallel situation is observed for *m*-ACyCz macrocycle with a weak band at 382 nm, which is due, according

to TD-DFT calculations, to a HOMO  $\rightarrow$  LUMO one-electron excitation corresponding to the  $S_0 \rightarrow S_1$  electronic transition predicted at 332 nm. In addition, a strong double-peak absorbance band is observed for ***m*-ACyCz** at 323 and 333 nm, which corresponds to the  $S_0 \rightarrow S_6$  and  $S_0 \rightarrow S_7$  degenerated electronic transitions predicted at 294 nm. Therefore, the absorption spectra exhibit a red-shift when going from ***m*-CyCz** to ***m*-ACyCz** indicating that the insertion of ethylene groups improves the  $\pi$ -conjugation.

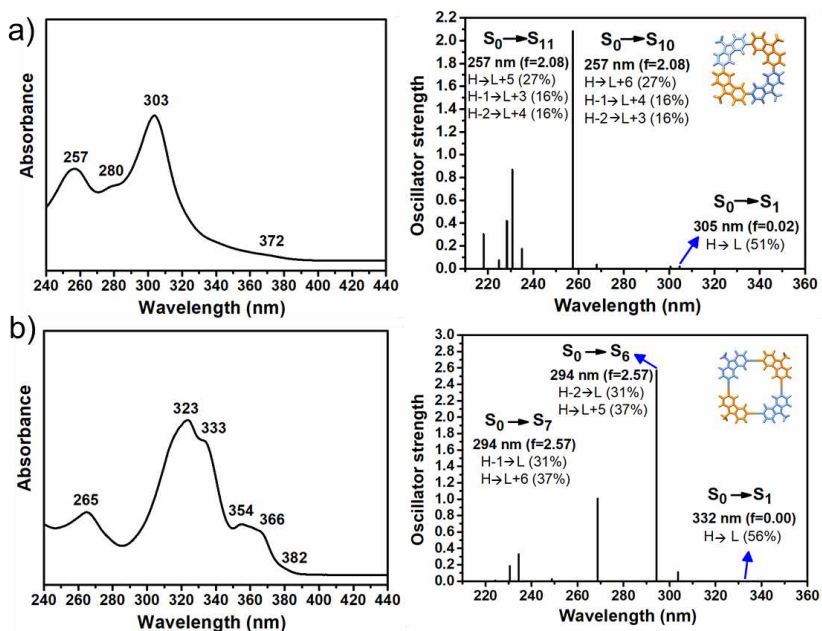


Figure 3.15. Left: UV/Vis absorption of a freshly prepared solution in dichloromethane of (a) ***m*-CyCz** and (b) ***m*-ACyCz** at RT. Right: TD-DFT calculated (M06-2X/6-31G\*\*) vertical transition energies of (a) ***m*-CyCz** and (b) ***m*-ACyCz**.



At this point, we make use of Raman spectroscopy to analyse how the insertion of ethylene groups affects the molecular structure. Figure 3.16 compares the FT-Raman spectra ( $\lambda_{\text{exc}}=1064$  nm) of **Cz** and the two macrocycles in solid-state at RT. The most significant changes in the Raman spectra occur in the range between  $1700$  and  $1400$   $\text{cm}^{-1}$ , where the C-C/C=C stretching vibrations of the  $\pi$ -conjugated core are found. As we found earlier in this chapter, the FT-Raman spectrum of isolated **Cz** molecule is characterized by three main bands at  $1626$ ,  $1597$  and  $1576$   $\text{cm}^{-1}$  (the eigenvectors associated to the main Raman bands for **Cz** are shown in Figure 3.7). When comparing the spectra of **Cz** molecule with its macrocycle analogous (**m-CyCz**), similar frequencies are shown. However, a frequency downshifting is found upon the insertion of ethylene units (**m-ACyCz**) acting as spacer groups between the Cz units, as a result of the  $\pi$ -conjugation extension. Specifically, the most intense Raman band observed at  $1601$   $\text{cm}^{-1}$  in **m-CyCz** downshifts up to  $1595$   $\text{cm}^{-1}$  in **m-ACyCz**.

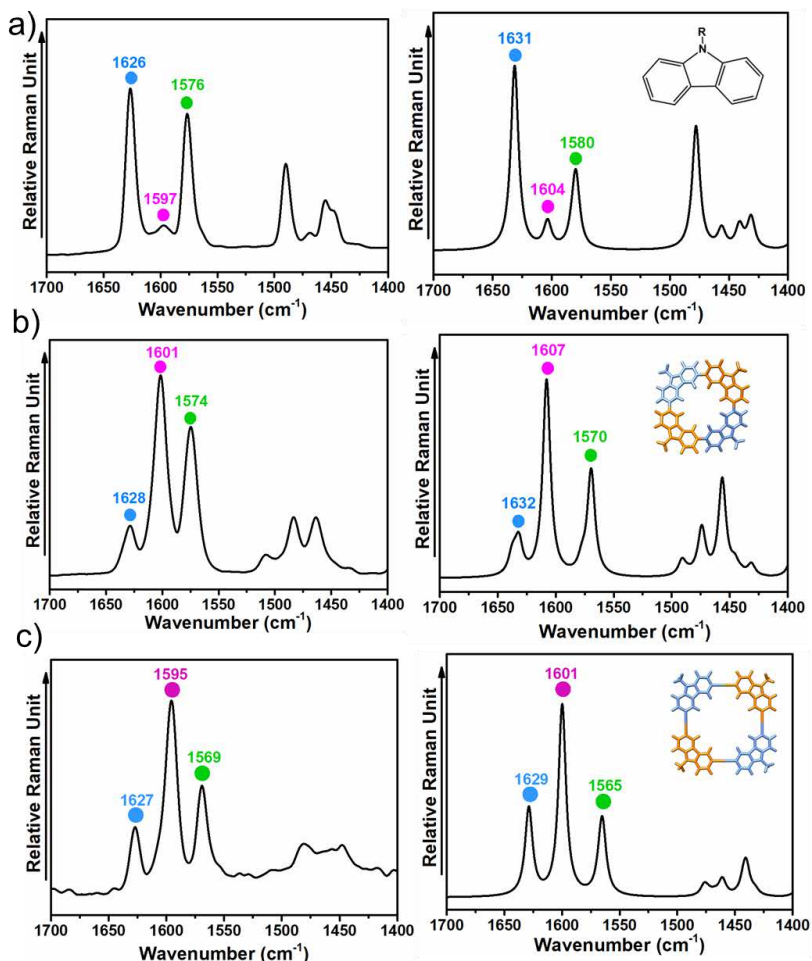


Figure 3.16 Left: FT-Raman spectra ( $\lambda_{\text{exc}}=1064$  nm) of (a) **Cz**, (b) **m-CyCz** and (c) **m-ACyCz** as solids at RT. Right: Theoretical Raman spectra (M06-2X/6-31G\*\*) for (a) isolated **Cz** (b) **m-CyCz** and (c) **m-ACyCz**.

### 3.3.3.1.3 Charge transport properties.

In this section, we considered two key molecular charge transport parameters that have an impact on the charge mobility: i) the hole transfer integral ( $t_h$ ) which gauges the electronic coupling between adjacent molecules and ii) the reorganization





energy associated with hole ( $\lambda_h$ ) and electron ( $\lambda_e$ ) transfer, which reflects the geometrical changes needed to accommodate a positive (or negative) charge, respectively. It is interesting to note that small  $\lambda$  values and large  $t$  values result in larger mobility. For instance, Andrienko and co-workers<sup>26</sup> studied the charge transport properties of several Cz-based structures and they demonstrated that the  $\lambda$  decreases when going from an isolated **Cz** molecule ( $\lambda=100$  meV) to a macrocycle consisting of twelve Cz units ( $\lambda=60$  meV) leading to an increase in mobility by at least an order of magnitude.

The calculated  $\lambda$  values of ***m*-CyCz** and ***m*-ACyCz** macrocycles are collected in Table 3.4. As we can observe, the  $\lambda$  values obtained by using different functionals are in the same range. In principle, it would be expected that the further extension of the  $\pi$ -conjugation and most planar molecular structure of ***m*-ACyCz** should result in smaller  $\lambda$  values<sup>45,46</sup>. As seen in Table 3.4, both  $\lambda_h$  and  $\lambda_e$  values are lower for ***m*-ACyCz** than its homologue macrocycle (*i.e.*,  $\lambda_h=102$  meV and  $\lambda_h=68$  meV for ***m*-CyCz** and ***m*-ACyCz**, respectively, at the B3LYP-D3/6-31G\*\* level). Interestingly, both Cz-based macrocycles present lower  $\lambda_h$  values than  $\lambda_e$  which should provide high hole mobilities (p-type typical semiconductors).

Table 3.4. Calculated hole ( $\lambda_h$ ) and electron ( $\lambda_e$ ) reorganization energies (in meV) by using different functionals.

Molecule	M06-2X-D3/6-31G**		M06-D3/6-31G**		B3LYP-D3/6-31G**	
	$\lambda_h$ (meV)	$\lambda_e$ (meV)	$\lambda_h$ (meV)	$\lambda_e$ (meV)	$\lambda_h$ (meV)	$\lambda_e$ (meV)
<b><i>m</i>-CyCz</b>	133	158	105	138	102	132
<b><i>m</i>-ACyCz</b>	90	105	70	89	68	86

Nevertheless, it is well-known that the charge mobility is not only affected by the inherent molecular nature but also by the supramolecular arrangement of the isolated molecules. At this stage, understanding how the intermolecular packing influences the charge transport parameters is crucial to modulate the electronic coupling (or transfer integral). The first step was to carry out detailed research on dimeric theoretical models to elucidate which molecular orientations are more favourable in order to maximize charge transport.

As a starting point, we calculated the potential energy surface (PES) for a co-facially superimposed model dimer as a function of the intermolecular distance (see Figure 3.17a) which shows a well-defined minimum at 3.6 Å for both compounds. In addition, we inspected the influence of the rotation for a co-facial dimer ***m*-(ACyCz)<sub>2</sub>**. To this end, a rotation scan was calculated by rotating one molecule over the other in a co-facial dimeric structure with an intermolecular distance of 3.6 Å obtaining a minimum at 10° (see Figure 3.17b).

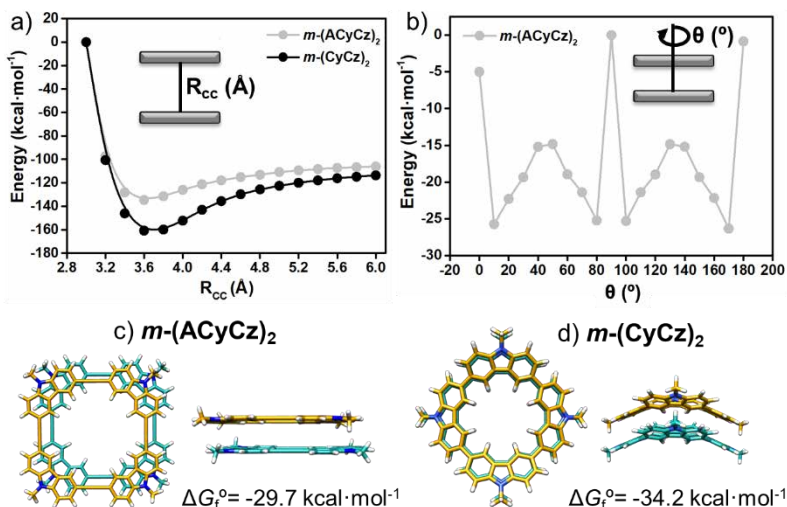


Figure 3.17. (a) PES for co-facial structures based on  $m$ -(CyCz)<sub>2</sub> and  $m$ -(ACyCz)<sub>2</sub> at M06-2X-D3/6-31G\*\* level, as a function of the intermolecular distance ( $R_{cc}$ ) between the two tetracarbazole units. (b) Rotation scan for a co-facial  $m$ -(ACyCz)<sub>2</sub> dimer at M06-2X-D3/6-31G\*\* level. Here  $\theta$  is the rotation degree between two isolated monomers. DFT-calculated global minimum structures for (c)  $m$ -(ACyCz)<sub>2</sub> and (d)  $m$ -(CyCz)<sub>2</sub>. The nitrogen atoms are depicted in blue and hydrogen atoms in white. The values of the free energy of formation ( $\Delta G_f^0$ ) are also shown.

Thus, two different theoretical dimer models were built up and optimized at the M06-2X-D3/6-31G\*\* level of theory. The spatial arrangement of the minimum-energy calculated dimeric structures together with their negative free energy of formation values are displayed in Figure 3.17c-d.

Table 3.5. Calculated transfer integrals (in meV) for hole ( $t_h$ ) and ( $t_e$ ) electron transfer for  $m$ -(**ACyCz**)<sub>2</sub> and  $m$ -(**CyCz**)<sub>2</sub> dimers.

Molecule	Centre of mass distance (Å)	Rotation degree ( $\theta$ )	$t_h$ (meV)	$t_e$ (meV)
$m$ -( <b>ACyCz</b> ) <sub>2</sub>	3.5	0°	353	44
		10°	203	415
$m$ -( <b>CyCz</b> ) <sub>2</sub>	3.5	0°	12	233 <sup>b</sup>

<sup>a</sup> For this molecule, LUMO and LUMO<sup>+1</sup> orbitals were degenerated. Hence, the transfer integrals for electrons ( $t_e$ ) were calculated by considering both the transfer integrals for LUMO ( $t_{LUMO,LUMO}$ ) and LUMO<sup>+1</sup> ( $t_{LUMO+1,LUMO+1}$ ).

Table 3.5 shows the transfer integrals ( $t$ ) calculated for the predicted dimers. The highest values for hole transport ( $t_h$ ) are found for the  $m$ -**ACyCz** dimeric system. These results are consistent so far as the transfer integral depends on the wavefunction overlap, and therefore, the electronic coupling is expected to be larger at higher orbitals overlap. For instance, much lower transfer integral for holes is predicted for co-facial dimeric structures based on  $m$ -**CyCz** ( $t_h=12$  meV) than for the ethylene-based analogue cyclic system ( $t_h=353$  meV); this can be ascribed to the deviations from planarity observed for  $m$ -**CyCz** with torsional angle of 35° between the Cz units which causes a decrease in the orbitals overlap. It is also interesting to highlight that a 40% reduction of the  $t_h$  values are predicted when molecules are slightly rotated (*i.e.*, from 353 meV for  $m$ -(**ACyCz**)<sub>2</sub> to 203 meV for  $m$ -(**ACyCz10**)<sub>2</sub> where the molecules are rotated by 10°). Thus, the different columnar stacking behaviour that the molecules would exhibit in the films might play a key role in their performance as electronic devices<sup>47</sup>.



In addition, organic field-effect transistors (OFETs) with a standard top-contact/bottom-gate (TC/BG) configuration were fabricated to evaluate the charge transport properties of the two Cz-based macrocycles. The optimization of the device fabrications steps suggests that both substrate treatment (*i.e.*, octadecyltrichlorosilane (OTS) and hexamethyldisilazane (HMDS)) and thermal annealing play a relevant role in the resultant device performance. As shown in Figure 3.18, ***m-CyCz*** and ***m-ACyCz***-based devices exhibited typical unipolar p-channel characteristics with moderately good transfer and output curves measured under vacuum conditions. The main device performance parameters, including hole charge carrier mobilities ( $\mu_h$ ), threshold voltages ( $V_T$ ) and intensities ratios ( $I_{on}/I_{off}$ ) extracted from the transfer plots in the saturation regime, are summarized in Table 3.6.

Table 3.6. OFET performance parameters of the ***m-CyCz*** and ***m-ACyCz*** semiconductors measured under vacuum.

	Deposition conditions	$\mu_h$ (cm <sup>2</sup> V <sup>-1</sup> s <sup>-1</sup> )	$V_T$ (V)	$I_{ON}/I_{OFF}$
<b><i>m-CyCz</i></b>	OTS at RT	$5.2 \cdot 10^{-6}$	-5	20
<b><i>m-ACyCz</i></b>	OTS at RT	$2.3 \cdot 10^{-4}$	-33	24

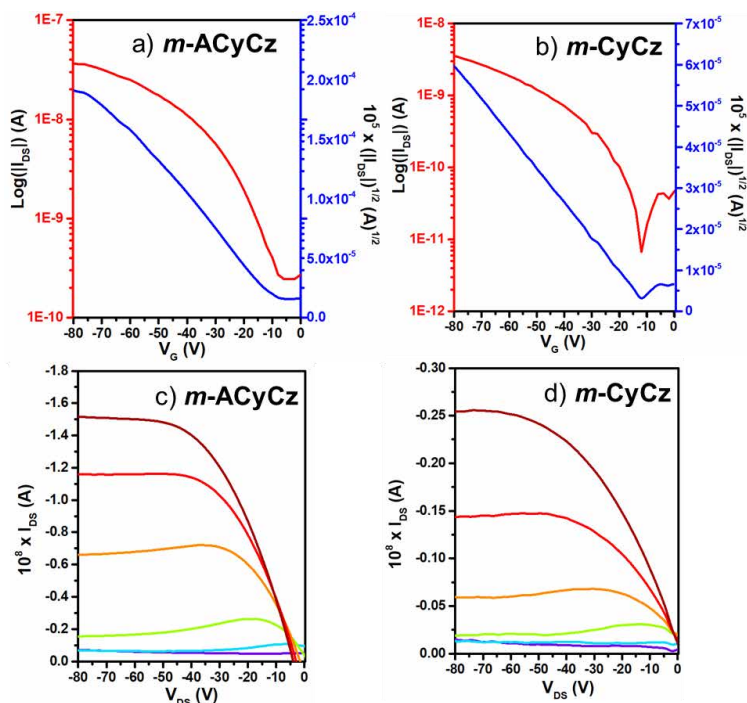


Figure 3.18 TFT transfer (a-b) and output (c-d) characteristics of *m*-ACyCz (a,c) and *m*-CyCz (b,d). The transfer characteristics were measured at a constant source–drain voltage of -80 V. The gate voltage range in the output plots going from 0 to -80 V in steps of 20 V.

As seen in Table 3.6, *m*-ACyCz semiconductor shows the highest hole mobility of  $2.3 \times 10^{-4} \text{ cm}^2 \text{V}^{-1} \text{s}^{-1}$ , which is nearly 2 orders of magnitude higher than that of device based on *m*-CyCz ( $5.2 \times 10^{-6} \text{ cm}^2 \text{V}^{-1} \text{s}^{-1}$ ). This can be ascribed to the more planar molecular structure of *m*-ACyCz, leading to a more efficient molecular packing, which results in a larger overlap between the HOMO orbitals and, thus higher electronic couplings, which is generally beneficial for charge transport in OFETs devices. In addition, the increase of the  $\pi$ -conjugation length going from *m*-CyCz to *m*-ACyCz could also facilitate the intramolecular charge

transport. Comparable threshold voltages (-5 and -33 V for **m-CyCz** and **m-ACyCz**, respectively) and low  $I_{ON}/I_{OFF}$  current ratios for the two macrocycles were observed.

### 3.3.3.2 Coronoid carbazole-based macrocycles: Influence of the isomerism.

In this section, we performed a theoretical investigation of different ICz-based coronoid molecules based on **ICz-23a**, **ICz-23b** and **ICz-32b** isomers shown in Figure 3.19. Coronoid systems consist of a macrocycle enclosed by a fully fused periphery of  $\pi$ -conjugated rings<sup>48-53</sup>. The results of this study might help to identify macrostructures with interesting physicochemical properties as well as to display the usefulness of the theoretical tools to advance knowledge in the organic electronics field<sup>54</sup>.

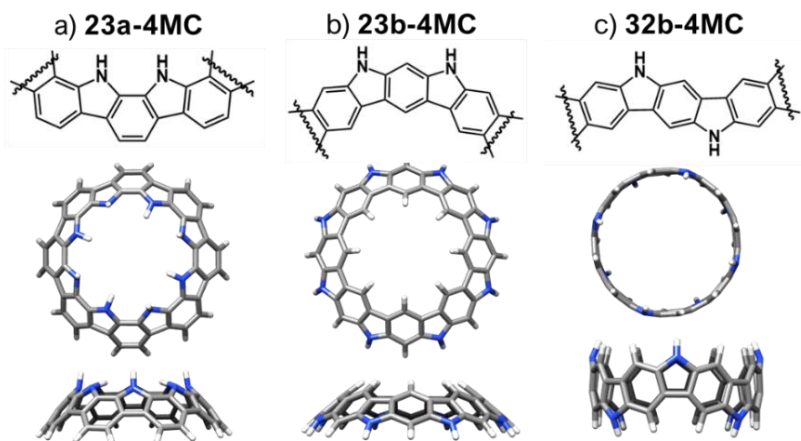


Figure 3.19. Chemical structures of the three macrocycles (a) **23a-4MC**, (b) **23b-4MC** and (c) **32b-4MC**, which contain four ICz units.



### 3.3.3.2.1 Cyclophane structural features.

In this section, we carried out a detailed computational study to explore the most favourable conformations of each isomer. To this end, molecular geometries (and associated molecular point group) of **23a-4MC**, **23b-4MC** and **32b-4MC** are analysed at the M06-2X/6-31G\*\* level (Figure 3.20).

First, the minimum energy conformation for **23a-4MC** isomer displays a bowl-like structure with fully conjugated structure ( $C_{4v}$ ) suggesting a large delocalization over the whole conjugated backbone. On the contrary, the planar structure obtained using the  $D_{8h}$  point groups displays a strained configuration and appears at much higher energies ( $> 110 \text{ kcal}\cdot\text{mol}^{-1}$ ) indicating that  $C_{4v}$  form is the most stable conformations. A similar situation is found for the **23b-4MC** macrocycle since the minimum energy configuration displays a bowl-like structure with an isoenergetic  $C_{4v}$  and  $C_{8v}$  forms whereas their planar configuration,  $D_{8h}$ , is predicted at higher energies ( $> 60 \text{ kcal}\cdot\text{mol}^{-1}$ ). In contrast to the bowl-like structures found for **23a-4MC** and **23b-4MC** isomers, **32b-4MC** macrocycle shows a belt-type shape with an isoenergetic  $C_{4v}$  and  $D_{4d}$  structures (see Figure 3.20c).



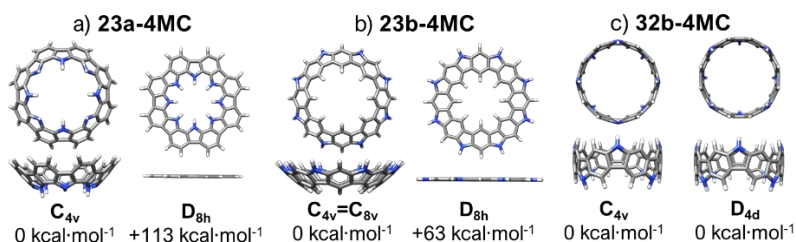


Figure 3.20. DFT-optimized structures of (a) **23a-4MC**, (b) **23b-4MC** and (c) **32b-4MC**, at the M06-2X/6-31G\*\* level. The relative energies respect to the most stable conformation are also shown.

### 3.3.3.2.2 Ground-state electronic structure.

The energy diagram and the frontier molecular orbitals of the three macrostructures are displayed in Figure 3.21. The HL gap values of **23a-4MC**, **23b-4MC**, and **32b-4MC** are found to be 5.33, 5.94, and 4.52 eV, respectively. Thus, the HL gap decreases as the electronic delocalization improves as a consequence of the radial conjugation in the belt-shaped **32b-4MC** isomer. This reduction in the HL gap is mainly caused by a significant stabilization of the  $E_{\text{LUMO}}$  which is also accompanied by a slight destabilization of the  $E_{\text{HOMO}}$ . Focusing on the frontier MOs topologies, the **23a-4MC** and **32b-4MC** compounds are delocalized through the whole ring with a radial geometry similar to **p-CyCz**. Interestingly, the HOMO density resembles that of **8CPP** (and **p-CyCz**), with no participation of the nitrogen atoms while the LUMO density resembles that of **p-CyCz**, with no participation of the carbon atom in para position of the nitrogen atom. These results reflect the efficient conjugation between the Cz units in these two isomers resulting in lower HL gap when compared to the **23b-4MC** isomer analogue. In contrast, the

wavefunction of **23b-4MC** is different with respect to their **23a-4MC** and **32b-4MC** homologous because of the meta linking position between de Cz units which leads to an interruption of the conjugation pattern, and therefore, an increase of the HL gap (5.94 eV).

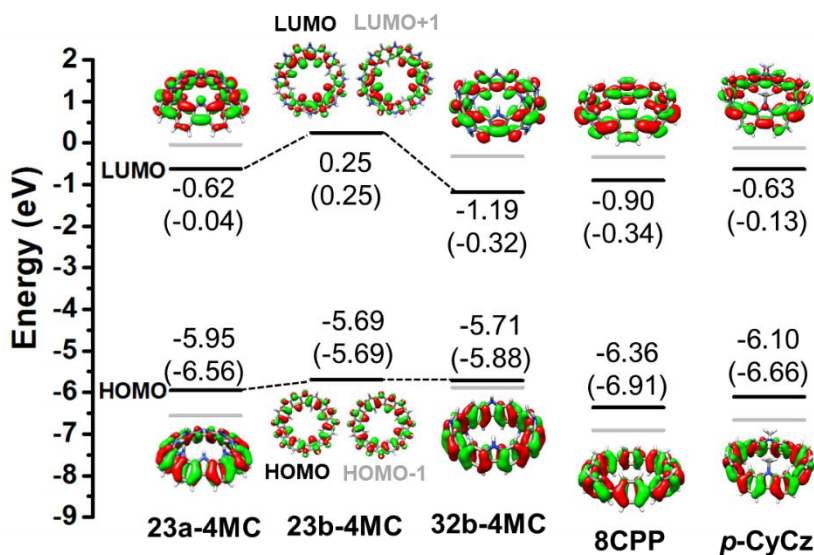


Figure 3.21 DFT-computed molecular orbital energy diagram of **23a-4MC**, **23b-4MC** and **32b-4MC** at the M06-2X/6-31G\*\* level. The topologies of the frontier molecular orbitals are also shown (isovalue 0.02 au). The values in parenthesis and gray lines are ascribed to the HOMO-1 and LUMO+1 levels. For comparison reasons, the molecular topologies of **8CPP** and **p-CyCz** are also shown.

### 3.3.3.2.3 Charge transport properties.

The calculated reorganization energies of the three studied macrostructures are collected in Table 3.7. Independently of the functional used, very similar  $\lambda_h$  and  $\lambda_e$  values are found for the bucky-bowl **23a-4MC** and **23b-4MC** molecules; however, for the



belt-shaped **32b-4MC** isomer, larger  $\lambda_h$  values are predicted together with lower  $\lambda_e$  values.

Table 3.7. Calculated hole ( $\lambda_h$ ) and electron ( $\lambda_e$ ) reorganization energies (in meV) by using different functionals.

Molecule	M06-2X-D3/6-31G**		M06-2X/6-31G**		B3LYP-D3/6-31G**	
	$\lambda_h$	$\lambda_e$	$\lambda_h$	$\lambda_e$	$\lambda_h$	$\lambda_e$
<b>23a-4MC</b>	244	211	189	167	180	165
<b>23b-4MC</b>	259	261	161	171	162	173
<b>32b-4MC</b>	350	192	210	159	201	152

We now explore the effect of intermolecular interactions on the charge transport properties. To this end, we carry out a detailed research on model theoretical dimers and then the electronic couplings are computed to discern which molecular orientations are more favourable to maximize charge transport.

On the one hand, three different co-facial dimer models were defined and optimized for each bucky-bowl system (**23a-4MC** and **23b-4MC**). As Figure 3.22a-b displays, the co-facial structure where the convex cavity of one monomer and the concave surface of the other monomer is matched (Co1) is the most favourable configuration for both **23a-4MC** and **23b-4MC** molecules ( $\Delta G_f^0 \cong -22$  kcal·mol<sup>-1</sup> and  $\Delta G_f^0 \cong -25$  kcal·mol<sup>-1</sup>, respectively).

In the case of the **32b-4MC** isomer, three different disposition are considered (Figure 3.22c): (i) a co-facial dimeric structure (Co1) where two molecules are fitted one above the other, (ii) a T-shaped conformation (T1) where a monomer is oriented into the cavity of a neighbouring molecule and (iii) a lateral arrangement (L1) where two molecules are situated one

in front of the other. As Figure 3.22c shown, the **(32b-4MC)<sub>2</sub>-T1** is the most favourable dimeric model due to the radial conjugation in the belt-shaped.

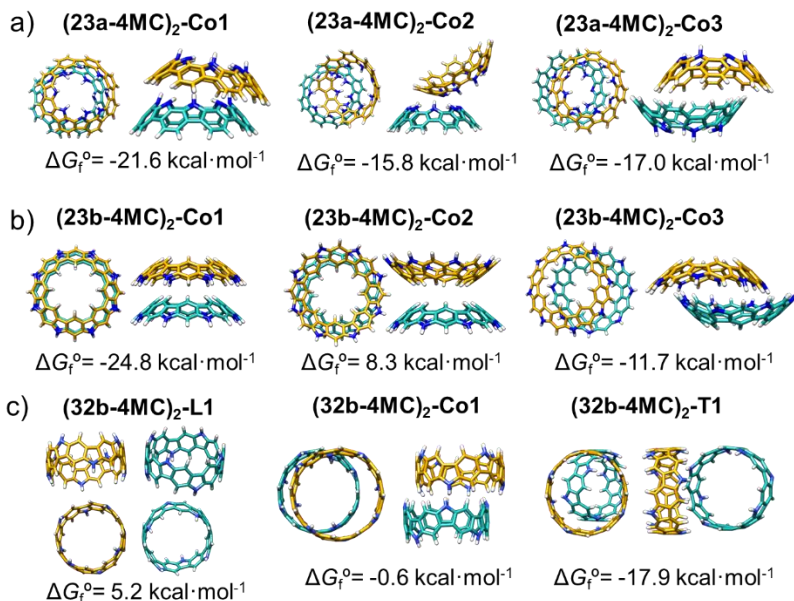


Figure 3.22. Minimum-energy dimeric structures computed for 23a-based (a), 23b-based (b) and 32b-based (c) macrocycles at the M06-2X-D3/6-31G\*\* level of theory. The free energies of formation are also shown.

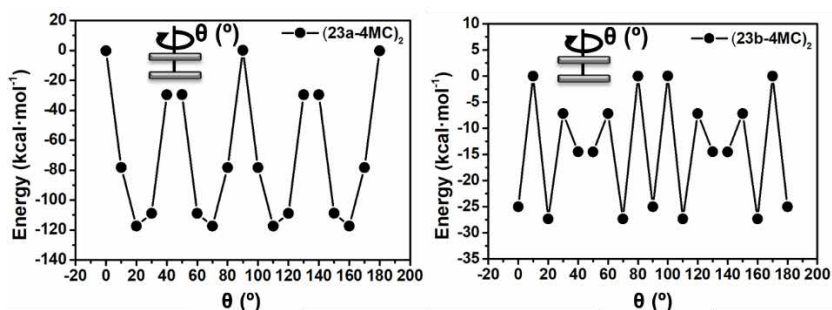


Figure 3.23. PES for **(23a-4MC)<sub>2</sub>** and **(23b-4MC)<sub>2</sub>** as a function of the rotational angle ( $\theta$ ) of the top molecule at M06-2X-D3/6-31G\*\* level. The intermolecular distance between the two adjacent molecules in the model dimer is set at 3.5Å.



In addition, we checked the effect of the rotation degree between two isolated molecules by calculating the PES. As we can observe in Figure 3.23, a well-defined minimum is predicted at  $20^\circ$  for both **23a-4MC** and **23b-4MC** macrocycles therefore we also decided to compute the integral transfer values associated with this rotation degree as will be shown below.

All transfer integral data are summarized in Table 3.8. Note that the highest values for hole and electron transport are found for **23a-4MC** (*i.e.*,  $t_h=590$  meV and  $t_e=620$ , respectively) although **23b-4MC** co-facial structures also show moderate values (*i.e.*,  $t_h=100$  meV and  $t_e=98$ ). It is also interesting to highlight that moderate changes in  $t_h$  values are predicted when molecules are rotated  $20^\circ$ , thus, demonstrating again the important role of the spatial arrangement in the electronic coupling. On the other hand, the dimeric structures based on **32b-4MC** isomer exhibit the lowest  $t$  values because of small orbital overlap between the adjacent molecules.

Table 3.8. Calculated transfer integrals (in meV) for hole ( $t_h$ ) and electron ( $t_e$ ) transfer considering degenerated orbitals.

Molecule	Dimer structure	Centre of mass distance (Å)	Rotation degree ( $\theta$ )	$t_h$ (meV)	$t_e$ (meV)
<b>23a-4MC</b>	Co1	3.5	$0^\circ$	590	620
			$20^\circ$	660	332
<b>23b-4MC</b>	Co1	3.5	$0^\circ$	100 <sup>a</sup>	98 <sup>b</sup>
			$20^\circ$	42 <sup>a</sup>	280 <sup>b</sup>
<b>32b-4MC</b>	Co1	6.5	$0^\circ$	0	34
	T1	8	$0^\circ$	5	2

<sup>a</sup> For this molecule, HOMO and HOMO<sup>-1</sup> orbitals were degenerated. Hence, the transfer integrals for electrons ( $t_h$ ) were calculated by considering both the transfer integrals for HOMO ( $t_{\text{HOMO,HOMO}}$ ) and HOMO<sup>-1</sup> ( $t_{\text{HOMO-1,HOMO-1}}$ ). <sup>b</sup> For this molecule, LUMO and LUMO<sup>+1</sup> orbitals were degenerated so the transfer



integrals for electrons ( $t_e$ ) were calculated by considering both the transfer integrals for LUMO ( $t_{LUMO,LUMO}$ ) and LUMO<sup>+1</sup> ( $t_{LUMO+1,LUMO+1}$ ).

These results reveal that the bucky-bowl structures (**23a-4MC** and **23b-4MC**) exhibit lower  $\lambda_h$  values and higher  $t_h$  values than the **32b-4MC** macrocycle demonstrating their potential as charge carrier transporting materials. In addition to their applicability to organic electronic devices<sup>55</sup>, the interest in bucky-bowl-shaped structures is growing up owing to the multidiscipline applications such as coordination with metal ions<sup>56</sup> or encapsulation of fullerenes<sup>57</sup>, among others.

### 3.3.4 Conclusions.

❖ Our results demonstrated that the different connectivity between the Cz units in tetracarbazole-based macrocycles provoke an enormous molecular structural diversity going from a belt-shape structure in **p-CyCz** with radial conjugation to a ring-shaped conformation in **m-CyCz** and a double-decker ring-shaped structure in **o-CyCz**. This structural conformation variety strongly modulates the  $\pi$ -conjugation and HL gap as demonstrated by UV-Vis and Raman spectroscopies; thus, allowing us to develop new classes of systems with attractive structures and unique electronic properties.

❖ Our data reveal a novel strategy to improve the phosphorescence behaviour by cyclization. By comparing the monomer, the linear tetramer, and the corresponding macrocycle, we found a relationship between the conjugated structure and the excited state energy levels that could dramatically influence the phosphorescence characteristics. The



cyclization-promoted phosphorescence may further act as a guideline for designing novel pure organic phosphorescent molecules.

❖ The insertion of an ethylene group between neighbouring Cz units in a tetracarbazole macrocycle leads to an increase of the planarity enhancing the  $\pi$ -conjugation and the intermolecular electronic coupling between adjacent units. As a result, the experimental hole field-effect mobility is two orders of magnitude higher when going from *m*-CyCz to *m*-ACyCz, thus resulting in high-performance OFET devices.

❖ Our theoretical results based on coronoid macrocycles predict bowl-like structures for **23a-4MC** and **23b-4MC** isomers, while **32b-4MC** macrocycle shows a belt-type shape structure. This different spatial arrangement is demonstrated to strongly impact the columnar packing, thus affecting the charge transport properties. Indeed, significant *t* values are found for **23a-4MC** and **23b-4MC** dimeric structures thanks to the favourable wave function overlap between adjacent molecules in contrast to the low values reported for **32b-4MC** dimeric analogues.

### 3.3.5 Bibliography.

1. Nayana, V.; Kandasubramanian, B., Polycarbazole and its derivatives: progress, synthesis, and applications. *Journal of Polymer Research* **2020**, 27, (9), 285.
2. Li, J.; Grimsdale, A. C., Carbazole-based polymers for organic photovoltaic devices. *Chemical Society Reviews* **2010**, 39, (7), 2399-2410.



3. Tomkeviciene, A.; Bartiuk, T.; Grazulevicius, J. V., Synthesis and properties of 2-(10,11-dihydrodibenz[b,f]azepine-5-yl)carbazole-based monomers and polymers. *Polymer Bulletin* **2012**, 68, (2), 453-464.
4. Hlel, A.; Mabrouk, A.; Chemek, M.; Ben Khalifa, I.; Alimi, K., A DFT study of charge-transfer and opto-electronic properties of some new materials involving carbazole units. *Computational Condensed Matter* **2015**, 3, 30-40.
5. Jenekhe, S. A.; Lu, L.; Alam, M. M., New Conjugated Polymers with Donor–Acceptor Architectures: Synthesis and Photophysics of Carbazole–Quinoline and Phenothiazine–Quinoline Copolymers and Oligomers Exhibiting Large Intramolecular Charge Transfer. *Macromolecules* **2001**, 34, (21), 7315-7324.
6. Peng, F.; Wang, X.; Guo, T.; Xiong, J.; Ying, L.; Cao, Y., Realizing efficient bipolar deep-blue light-emitting poly (2, 7-carbazole) derivatives by suppressing intramolecular charge transfer. *Organic Electronics* **2019**, 67, 34-42.
7. Strahan, J.; Popere, B. C.; Khomein, P.; Pointer, C. A.; Martin, S. M.; Oldacre, A. N.; Thayumanavan, S.; Young, E. R., Modulating absorption and charge transfer in bodipy-carbazole donor–acceptor dyads through molecular design. *Dalton Transactions* **2019**, 48, (23), 8488-8501.
8. Nandy, B. C., Gupta, A. K., Mittal, A., & Vyas, V., Carbazole: It's biological activity. *J. Biomed. Pharm. Res*, **2014** 3, 42-48.
9. Bahy, A.; Chemli, M.; Hassine, B. B., Synthesis and characterization of new carbazole-based materials for electronic applications. *Tetrahedron Letters* **2013**, 54, (31), 4026-4029.
10. Higginbotham, H. F.; Karon, K.; Ledwon, and Data, P. Carbazoles in Electronic Applications, *Disp. Imaging* **2017**, 2, (3-4), 207-216.
11. Hu, M.; Xu, Q.; Jiang, Y.; Mu, H.; Gao, L.; Hu, P.; Huang, J.; Su, J., Bipolar carbazole/quinoxaline-based host materials for efficient red PhOLEDs. *Dyes and Pigments* **2018**, 150, 185-192.





12. Su, Y.; Lin, H.; Li, W., The Applications of Carbazole and Carbazole-Related Compounds in Blue Emitting Organic Light-Emitting Diodes. *Progress in Chemistry* **2015**, 27, 1384-1399.
13. Wex, B.; Kaafarani, B. R., Perspective on carbazole-based organic compounds as emitters and hosts in TADF applications. *Journal of Materials Chemistry - C* **2017**, 5, (34), 8622-8653.
14. Sathiyam, G.; Sivakumar, E.; Ganesamoorthy, R.; Thangamuthu, R.; Sakthivel, P., Review of carbazole based conjugated molecules for highly efficient organic solar cell application. *Tetrahedron Letters* **2016**, 57, (3), 243-252.
15. Brunner, K.; van Dijken, A.; Börner, H.; Bastiaansen, J. J.; Kigger, N. M.; Langeveld, B. M., Carbazole compounds as host materials for triplet emitters in organic light-emitting diodes: tuning the HOMO level without influencing the triplet energy in small molecules. *Journal of the American Chemical Society* **2004**, 126, (19), 6035-6042.
16. Gong, W.-L.; Wang, B.; Aldred, M. P.; Li, C.; Zhang, G.-F.; Chen, T.; Wang, L.; Zhu, M.-Q., Tetraphenylethene-decorated carbazoles: synthesis, aggregation-induced emission, photo-oxidation and electroluminescence. *Journal of Materials Chemistry C* **2014**, 2, (34), 7001-7012.
17. Skórka, Ł.; Kurzep, P.; Wiosna-Sałyga, G.; Łuszczynska, B.; Wielgus, I.; Wróbel, Z.; Ulański, J.; Kulszewicz-Bajer, I., New diarylamino-phenyl derivatives of carbazole: Effect of substituent position on their redox, spectroscopic and electroluminescent properties. *Synthetic metals* **2017**, 228, 1-8.
18. Tomkeviciene, A.; Grazulevicius, J. V.; Kazlauskas, K.; Gruodis, A.; Jursenas, S.; Ke, T.-H.; Wu, C.-C., Impact of linking topology on the properties of carbazole trimers and dimers. *The Journal of Physical Chemistry C* **2011**, 115, (11), 4887-4897.
19. Venkateswararao, A.; Thomas, K. R. J.; Lee, C.-P.; Li, C.-T.; Ho, K.-C., Organic Dyes Containing Carbazole as Donor and  $\pi$ -Linker: Optical, Electrochemical, and Photovoltaic Properties. *ACS Applied Materials & Interfaces* **2014**, 6, (4), 2528-2539.



20. Zhu, H.; Badía-Domínguez, I.; Shi, B.; Li, Q.; Wei, P.; Xing, H.; Ruiz Delgado, M. C.; Huang, F., Cyclization-promoted ultralong low-temperature phosphorescence via boosting intersystem crossing. *Journal of the American Chemical Society* **2021**, 143, (4), 2164-2169.
21. Sutanto, A. A.; Joseph, V.; Igci, C.; Syzgantseva, O. A.; Syzgantseva, M. A.; Jankauskas, V.; Rakstys, K.; Quelo, V. I. E.; Huang, P.-Y.; Ni, J.-S.; Kinge, S.; Asiri, A. M.; Chen, M.-C.; Nazeeruddin, M. K., Isomeric Carbazole-Based Hole-Transporting Materials: Role of the Linkage Position on the Photovoltaic Performance of Perovskite Solar Cells. *Chemistry of Materials* **2021**, 33, (9), 3286-3296.
22. Mao, L.; Zhou, M.; Niu, Y.-F.; Zhao, X.-L.; Shi, X., Aryl carbazole-based macrocycles: synthesis, their remarkably stable radical cations and host-guest complexation with fullerenes. *Organic Chemistry Frontiers* **2021**, 8, (17), 4678-4684.
23. Schweighauser, L., Häussinger, D., Neuburger, M., and Wegner, H. A. Symmetry as a new element to control molecular switches. *Organic & Biomolecular Chemistry* **2014**, 12, (21), 3371-3379.
24. Lucas, F.; Sicard, L.; Jeannin, O.; Rault-Berthelot, J.; Jacques, E.; Quinton, C.; Poriol, C., [4]Cyclo-N-ethyl-2,7-carbazole: Synthesis, Structural, Electronic and Charge Transport Properties. *Chemistry – A European Journal* **2019**, 25 (32), 7740-7748.
25. Manickam, M., Iqbal, P., Belloni, M., Kumar, S., and Preece, J. A. A Brief Review of Carbazole-Based Photorefractive Liquid Crystalline Materials. *Israel Journal of Chemistry* **2012**, 52, (10), 917-934.
26. Vehoff, T., Baumeier, B., & Andrienko, D. Charge transport in columnar mesophases of carbazole macrocycles. *The Journal of chemical physics*, **2010**, 133(13), 134901.
27. Graham, C., Moral, M., Muccioli, L., Olivier, Y., Pérez-Jiménez, Á. J., and Sancho-García, J. C. N-doped cycloparaphenylenes: Tuning electronic properties for



applications in thermally activated delayed fluorescence. *International Journal of Quantum Chemistry* **2018**, 118(12), e25562.

28. Segawa, Y., Fukazawa, A., Matsuura, S., Omachi, H., Yamaguchi, S., Irle, S., & Itami, K. Combined experimental and theoretical studies on the photophysical properties of cycloparaphenylenes. *Organic & biomolecular chemistry* **2012**, 10, (30), 5979-5984.

29. Marsal, P., Avilov, I., da Silva Filho, D. A., Brédas, J. L., and Beljonne, D. Molecular hosts for triplet emission in light emitting diodes: A quantum-chemical study. *Chemical physics letters*, **2004**, 392, (4-6), 521-528.

30. Thomas, K. R.; Lin, J. T.; Tao, Y.T. and Ko, C.W. Light-Emitting Carbazole Derivatives: Potential Electroluminescent Materials. *Journal of the American Chemical Society* **2001**, 123, 9404-9411.

31. Chen, C.; Chi, Z.; Chong, K. C.; Batsanov, A. S.; Yang, Z.; Mao, Z.; Yang, Z. and Liu, B. Carbazole isomers induce ultralong organic phosphorescence. *Nature materials*, **2021**, 20, (2), 175-180.

32. Mu, Y.; Yang, Z.; Chen, J.; Yang, Z.; Li, W.; Tan, X.; Mao, Z.; Yu, T.; Zhao, J.; Zheng, S.; Liu, S.; Zhang, Y.; Chi, Z.; Xu, J. and Aldred, M. P. Mechano-induced persistent room-temperature phosphorescence from purely organic molecules. *Chemical Science* **2018**, 9, (15), 3782-3787.

33. Paul, L.; Chakrabarti, S. and Ruud, K. Origin of dual-peak phosphorescence and ultralong lifetime of 4,6-diethoxy-2-carbazolyl-1,3,5-triazine. *The Journal of Physical Chemistry Letters* **2017**, 8, (6), 1253-1258.

34. Beljonne, D.; Shuai, Z.; Pourtois and G.; Bredas, J. L. Spin-orbit coupling and intersystem crossing in conjugated polymers: A configuration interaction description. *The Journal of Physical Chemistry A* **2001**, 105, (15), 3899-3907.

35. Yao, Y.; Dong, H.; Hu, W. Charge Transport in Organic and Polymeric Semiconductors for Flexible and Stretchable Devices. *Advanced Materials* **2016**, 28, (22), 4513-4523.



36. Blakesley, J. C.; Castro, F. A.; Kylberg, W.; Dibb, G. F. A.; Arantes, C.; Valaski, R.; Cremona, M. and Kim, J. S. Towards Reliable Charge-Mobility Benchmark Measurements for Organic Semiconductors. *Organic Electronics* **2014**, 15, (6), 1263-1272.
37. Fratini, S., Nikolka, M., Salleo, A., Schweicher, G., and Sirringhaus, H. Charge transport in high-mobility conjugated polymers and molecular semiconductors. *Nature materials* **2020**, 19, (5), 491-502.
38. Podzorov, V., Menard, E., Borissov, A., Kiryukhin, V., Rogers, J. A., and Gershenson, M. E. Intrinsic charge transport on the surface of organic semiconductors. *Physical review letters* **2004**, 93, (8), 086602.
39. Pramanik, A., Biswas, S., Pal, S., and Sarkar, P. Charge transport and transfer phenomena involving conjugated acenes and heteroacenes. *Bulletin of Materials Science* **2019**, 42, (3), 1-20.
40. Lemaur, V., da Silva Filho, D. A., Coropceanu, V., Lehmann, M., Geerts, Y., Piris, J., Debije M.G., Van de Craets A.M., Senthilkumar K., Siebbeles L.D., Warman J.M., Brédas J.L. and Cornil, J. Charge transport properties in discotic liquid crystals: a quantum-chemical insight into structure– property relationships. *Journal of the American Chemical Society* **2004**, 126, (10), 3271-3279.
41. Ball, M. L., Zhang, B., Xu, Q., Paley, D. W., Ritter, V. C., Ng, F., Steigerwald M.L. and Nuckolls, C. Influence of molecular conformation on electron transport in giant, conjugated macrocycles. *Journal of the American Chemical Society* **2018**, 140, (32), 10135-10139.
42. Lucas, F., Mcintosh, N., Jacques, E., Lebreton, C., Heinrich, B., Donnio, B., Jeannin O., Rault-Berthelot J., Quinton J. and Poriel, C. [4] Cyclo-N-alkyl-2, 7-carbazoles: Influence of the alkyl chain length on the structural, electronic, and charge transport properties. *Journal of the American Chemical Society*, **2021**, 143, (23), 8804-8820.



43. Gámez-Valenzuela, S., Echeverri, M., Gómez-Lor, B., Martínez, J. I., and Delgado, M. C. R. In silico design of 2D polymers containing truxene-based platforms: insights into their structural and electronic properties. *Journal of Materials Chemistry C*, **2020**, 8, (43), 15416-15425.
44. Volpi, R., Camilo, A. C. S., da Silva Filho, D. A., Navarrete, J. T. L., Gómez-Lor, B., Delgado, M. C. R., and Linares, M. Modelling charge transport of discotic liquid-crystalline triindoles: the role of peripheral substitution. *Physical Chemistry Chemical Physics*, **2017**, 19, (35), 24202-24208.
45. Coropceanu, V., Malagoli, M., da Silva Filho, D. A., Gruhn, N. E., Bill, T. G., and Brédas, J. L. Hole- and electron-vibrational couplings in oligoacene crystals: intramolecular contributions. *Physical review letters* **2002**, 89, (27), 275503.
46. Pablo-Pedro, R., Lopez-Rios, H., Mendoza-Cortes, J. L., Kong, J., Fomine, S., Van Voorhis, T., and Dresselhaus, M. S. Exploring low internal reorganization energies for silicene nanoclusters. *Physical Review Applied* **2018**, 9, (5), 054012.
47. Arrechea-Marcos, I.; de Echegaray, P.; Mancheño, M. J.; Ruiz Delgado, M. C.; Ramos, M. M.; Quintana, J. A.; Villalvilla, J. M.; Díaz-García, M. A.; López Navarrete, J. T.; Ponce Ortiz, R.; Segura, J. L., Molecular aggregation of naphthalimide organic semiconductors assisted by amphiphilic and lipophilic interactions: a joint theoretical and experimental study. *Physical Chemistry Chemical Physics* **2017**, 19 (8), 6206-6215.
48. Stępień, M. An aromatic riddle: decoupling annulene conjugation in coronoid macrocycles. *Chem* **2018**, 4, (7), 1481-1483.
49. Prajapati, B., Dang, D. K., Chmielewski, P. J., Majewski, M. A., Lis, T., Gómez-García C.J, Zimmerman P.M. and Stępień, M. An Open-Shell Coronoid with Hybrid Chichibabin-Schlenk Conjugation. *Angewandte Chemie (International ed. in English)* **2021**, 60, (41), 22496-22504.
50. Das, S., Heng, T. S., Zafra, J. L., Burrezo, P. M., Kitano, M., Ishida, M., Gopalakrishna T.Y., Osuka, A., Casado, J., Ding, J.,



- Casanova, D., and Wu, J. Fully fused quinoidal/aromatic carbazole macrocycles with poly-radical characters. *Journal of the American Chemical Society* **2016**, 138, (24), 7782-7790.
51. Liu, C., Sandoval-Salinas, M. E., Hong, Y., Gopalakrishna, T. Y., Phan, H., Aratani, N., Heng, T.S., Ding, J., Yamada, H., Kim, D., Casanova, D., and Wu, J. Macrocyclic polyradicaloids with unusual super-ring structure and global aromaticity. *Chem*, **2018**, 4, (7), 1586-1595.
52. Lu, X., Gopalakrishna, T. Y., Han, Y., Ni, Y., Zou, Y., and Wu, J. Bowl-shaped carbon nanobelts showing size-dependent properties and selective encapsulation of C70. *Journal of the American Chemical Society* **2019**, 141,(14), 5934-5941.
53. Lu, X., An, D., Han, Y., Zou, Y., Qiao, Y., Zhang, N., Chang, D., Wu, J. and Liu, Y. A cyclopenta-fused dibenzo [b, d] thiophene-co-phenanthrene macrocyclic tetraradicaloid. *Chemical science* **2021**, 12, (11), 3952-3957.
54. Ghosh, S., Rolland, N., and Zozoulenko, I. Electronic structure, optical properties, morphology and charge transport in naphthalenediimide (NDI)-based n-type copolymer with altered  $\pi$ -conjugation: A theoretical perspective. *Applied Physics Letters* **2021** 118,(22), 223302.
55. Shi, K., Lei, T., Wang, X. Y., Wang, J. Y., & Pei, J. A bowl-shaped molecule for organic field-effect transistors: crystal engineering and charge transport switching by oxygen doping. *Chemical Science* **2014** 5, (3), 1041-1045.
56. Petrukhina, M. A. Coordination of Buckybowls: The First Concave - Bound Metal Complex. *Angewandte Chemie International Edition* **2008**, 47, (9), 1550-1552.
57. Filatov, A. S., Ferguson, M. V., Spisak, S. N., Li, B., Campana, C. F., and Petrukhina, M. A. Bowl-shaped polyarenes as concave-convex shape complementary hosts for C60-and C70-fullerenes. *Crystal growth & design* **2014**, 14, (2), 756-762.







# **SECTION 4. Concluding observations**





### Section 4: Concluding observations.

The present Thesis aims to perform an exhaustive study of the electronic and structural properties of Cz and ICz based systems using a combined experimental and theoretical approach that links electronic and vibrational spectroscopy (infrared and Raman) together with quantum-chemical calculations based on DFT theory. The main conclusions obtained from the results section are reported here as follows.

---

#### **Chapter I: Evolution of the diradical character of dicyanomethylene substituted carbazole and indolocarbazole-based systems.**

---

In this chapter, our calculations have demonstrated that different structural modifications (*i.e.*, substitution pattern, elongation of the conjugated core and structural isomerism) represent a very effective way to modulate the diradical character in Cz and ICz-based systems.

In section 3.1.2, we demonstrated that the insertion of the DCM groups via meta results in stronger diradical character in comparison with the para-connection. Our data suggest that this is due to the fact that Cz and ICz units substituted at the para position display a longer conjugation path increasing the electronic delocalization meanwhile the meta position decreases the conjugation because of the interruption of the linear  $\pi$ -system. In addition, we demonstrated that the increase in the chain length (from Cz to ICz molecules) implies a remarkable increase in the diradical character. In other words, the elongation



#### 4. Concluding observations

of the conjugated core provokes less interaction between the unpaired electrons (small  $J_{ab}$  and  $\Delta E_{S-T}$  values) resulting in a large diradical character.

In section 3.1.3, our calculations based on ICz isomers suggest that the different degree of aromatization between the external and central parts of the backbone involves less  $\pi$ -delocalization resulting in an increase of the diradical character. Besides, the presence of double exciton states (H,H-L,L) has been successfully provided with a nice agreement found with the experimental absorption spectra of *p*-ICz and *m*-ICz. Interestingly, distortions from planarity could involve remarkable modifications on the molecular conjugation and consequently, on the diradical character.

---

### **Chapter II: Cyclophane self-assembly from carbazole and indolocarbazole-based diradicals.**

---

In this chapter, we demonstrated the potential of DCM-substituted Cz and ICz-based diradicals in the field of the dynamic covalent chemistry. All these systems are able to form cyclophane structures with the formation of long C-C bonds between unpaired electrons from the radical centres (located on the bridgehead carbons of the DCM groups). While Cz-based diradicals are able to form macrocyclic tetramers, ICz analogues can build  $\sigma$ -stacked dimers. On the other hand, the substitution pattern position is also found to strongly modulate the oligomerization behaviour with meta-substitution resulting in more stable aggregates with stronger C-C bonds and remarkable



#### 4. Concluding observations

$\pi$ - $\pi$  interactions than para-substitution, which is related with the stronger diradical character predicted for the meta-substituted systems.

For Cz-based systems, a dynamic monomer/cyclophane transformation is shown both in solution and solid state for **p-Cz**, whereas the C-C bond dissociation by external stimuli in **m-(Cz)<sub>4</sub>** is suppressed in solution. Therefore, the strong chromic effect from white to purple/deep blue found for these Cz-based diradicals in response to external stimuli (*i.e.*, temperature, grinding) can be adequately modulated upon appropriate changes in the substitution pattern position.

The longer ICz-based systems are able to form more stable aggregates when compared to the Cz-based analogues, thus resulting in a less reversible cyclophane/monomer transformation in comparison with the shorter analogues. When compared the different substitution pattern, while **p-(ICz)<sub>2</sub>** shows a dynamic cyclophane/monomer transformation both in solution and solid state, the C-C bond dissociation by external stimuli in **m-(ICz)<sub>2</sub>** is suppressed in solution although favoured in solid-state. A major difference between solution-state and solid-state is that the diradical is free to sample conformational space in solution whereas the solid-state experiments a confinement situation.

Therefore, our results demonstrate that cyclophane behaviour is strongly modulated by the DCM-substitution and the chain elongation, thus considerably affecting their properties.



#### 4. Concluding observations

Therefore, the strong chromic effects in response to external stimuli (*i.e.*, temperature or grinding) can be adequately modulated upon appropriate changes in the chemical structure. We believe that this study helps to identify new potential design strategies for stimuli-responsive materials.

---

### Chapter III: Photophysical and charge transport properties of carbazole-based macrocycles.

---

In the first part of the chapter, our results demonstrated that the different connectivity between the Cz units in tetracarbazole-based macrocycles provoke an enormous molecular structural diversity going from a belt-shape structure in ***p*-CyCz** with radial conjugation to a ring-shaped conformation in ***m*-CyCz** and a double-decker ring-shaped structure in ***o*-CyCz**. This structural conformation variety strongly modulates the  $\pi$ -conjugation and HL gap as demonstrated by UV-Vis and Raman spectroscopies; thus, allowing us to develop new classes of systems with attractive structures and unique electronic properties.

In section 3.3.2.2, our data reveal a novel strategy to improve the phosphorescence behaviour by cyclization. By comparing the monomer, the linear tetramer, and the corresponding macrocycle, we found a relationship between the conjugated structure and the excited state energy levels that could dramatically influence the phosphorescence characteristics. The cyclization-promoted phosphorescence may further act as a guideline for designing novel pure organic phosphorescent molecules.



#### 4. Concluding observations

In section 3.3.3.1, the insertion of an ethylene group between neighbouring Cz units in a tetracarbazole macrocycle leads to a planarity increase enhancing the  $\pi$ -conjugation and the intermolecular electronic coupling between adjacent units. As a result, the experimental hole field-effect mobility is two orders of magnitude higher when going from *m-CyCz* to *m-ACyCz*, thus resulting in high-performance OFET devices.

Finally, our theoretical results based on coronoid macrocycles predict bowl-like structures for **23a-4MC** and **23b-4MC** isomers, while **32b-4MC** macrocycle shows a belt-type shape structure. This different spatial arrangement is demonstrated to strongly impacts the columnar packing, thus affecting the charge transport properties. Indeed, significant  $t$  values are found for **23a-4MC** and **23b-4MC** dimeric structures thanks to the favourable wave function overlap between adjacent molecules in contrast to the low values reported for **32b-4MC** dimeric analogues.









# **SECTION 5. Resumen y Conclusiones**





### Section 5: Resumen y conclusiones

#### 5.1 Introducción y objetivos.

En la actualidad, vivimos en un mundo en el que los dispositivos electrónicos son parte esencial de nuestra vida cotidiana. Por tanto, en las últimas décadas, una parte de la comunidad científica se ha dedicado al estudio y a la caracterización de nuevos materiales con objeto de diseñar mejores dispositivos electrónicos. En este sentido, el uso de materiales orgánicos conjugados se ha incrementado, ya que combinan las propiedades intrínsecas de los sistemas moleculares (gran versatilidad sintética, flexibilidad, baja densidad, procesabilidad o biocompatibilidad, entre otros) con las propiedades eléctricas (conductividad, superconductividad, etc.) y ópticas (electrocromismo, electroluminiscencia, óptica no lineal, emisión estimulada, etc.) de los semiconductores y de los metales. Hasta ahora, la síntesis orgánica ha proporcionado un amplio abanico de materiales orgánicos conjugados para electrónica orgánica. La Figura 5.1 muestra algunos ejemplos de materiales comerciales que ya han sido implementados en dispositivos electrónicos. Sin embargo, la síntesis supone una ardua tarea y requiere estudios intensivos sobre las relaciones estructura/propiedad de los sistemas, ya que sus propiedades no solo se ven afectadas por los cambios en la estructura química sino también en su organización supramolecular.

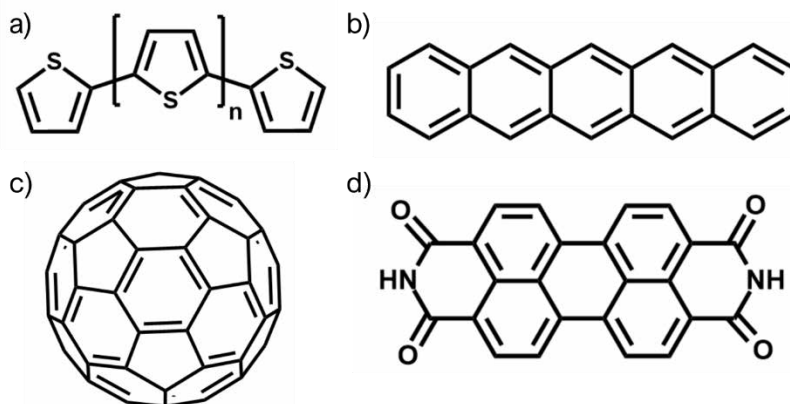


Figura 5.1. Ejemplos de materiales orgánicos comercialmente disponibles para su uso en electrónica orgánica: (a) oligotiofenos con estructuras definidas, (b) pentaceno de la familia de los hidrocarburos aromáticos policíclicos, (c) derivados del fullereno y (d) derivados de la perilenobisimida.

Concretamente, los materiales orgánicos conjugados basados en Carbazol (Cz) presentan importantes ventajas con respecto a otros heterociclos:

- ❖ La unidad de 9H-Cz es un material de partida bastante barato.
- ❖ El Cz presenta una alta estabilidad química gracias a la presencia de anillos completamente aromáticos.
- ❖ El átomo de nitrógeno se puede funcionalizar fácilmente con una gran variedad de sustituyentes que permiten un aumento de solubilidad y que confieren al sistema distintas propiedades eléctricas y ópticas. Además, también es posible la inserción de estos sustituyentes en el esqueleto conjugado, modificando las propiedades fisicoquímicas del sistema.
- ❖ El Cz es un buen transportador de huecos.

Todas estas características hacen que los compuestos basados en Cz sean sistemas propicios para aplicaciones en el campo de la electrónica orgánica, entre otros.

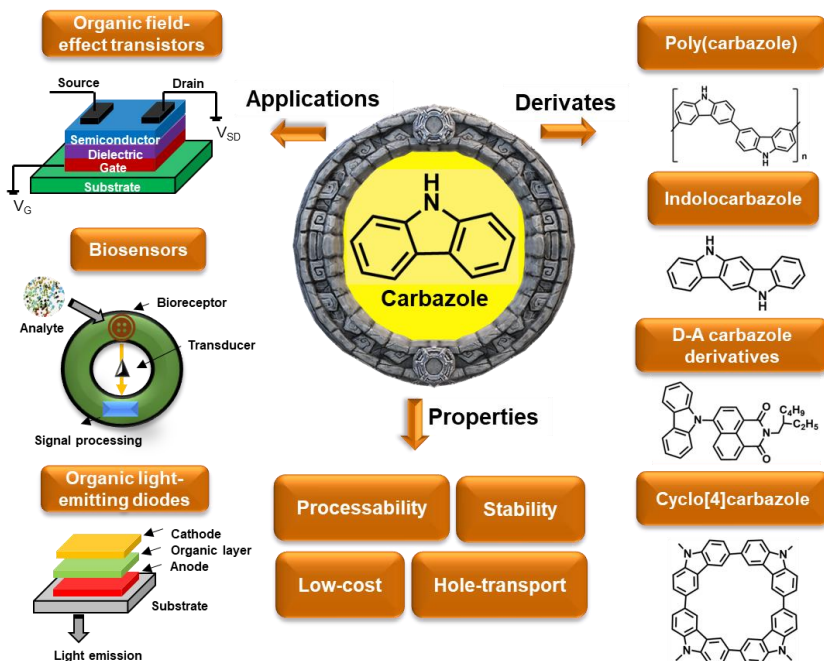


Figura 5.2 Esquema de las aplicaciones, derivados y propiedades de los sistemas basados en Cz.

Por otro lado, en el campo de los materiales orgánicos conjugados, el desarrollo de la química de especies dirradicales  $\pi$ -conjugadas ha atraído especial interés en los últimos años. Estos sistemas ofrecen características mecánicas y electrónicas únicas que los hacen enormemente prometedores en aplicaciones relacionadas con la nanotecnología y con la electrónica y fotónica orgánica<sup>1-4</sup>. El estudio de moléculas que presentan una capa de valencia que no está completamente llena, también conocidas como sistemas de capa abierta, se ha



## 5. Resumen y conclusiones

centrado sobre todo en conferirles estabilidad para su síntesis y posterior caracterización, ya que al disponer de electrones desapareados son susceptibles de formar nuevos enlaces.

En los sistemas dirradicalarios, en los que la interacción inter-electrónica es tan despreciable como para dar lugar a dos estados de espín, singlete y triplete, elucidar qué configuración electrónica se presentaría como estado fundamental sería esencial para entender sus propiedades estructurales y electrónicas<sup>5-7</sup>. Sin embargo, es posible que los dos centros radicalarios interaccionen significativamente y, en ese caso, estas especies se definirían como sistemas dirradicaloides donde existe un equilibrio entre una estructura quinoide de capa cerrada y una estructura diradical de capa abierta<sup>8,9</sup>.

Además, estudios recientes han demostrado que existen sistemas dirradicales capaces de formar enlaces C-C largos entre dos pares de electrones desapareados, resultando en distintas estructuras, ya sean macrociclos<sup>10</sup>, oligómeros en escalera<sup>11</sup> o incluso polímeros<sup>12</sup>, todo ello a partir de especies radicales. Gracias a esta propiedad, los compuestos dirradicales  $\pi$ -conjugados han llegado a ser “*building blocks*” esenciales en la química dinámica covalente (DCC)<sup>13</sup>. Este campo se focaliza, principalmente, en la creación de estructuras basadas en componentes químicos que interaccionen a través de enlaces covalentes pero que, a su vez, sean capaces de romperse o formarse dependiendo de las condiciones externas a las que se les someta. De hecho, se ha demostrado que la





## 5. Resumen y conclusiones

formación/disociación de estos nuevos enlaces C-C largos va acompañada con un cambio gradual de color, dando lugar a lo que se conoce como sistemas cromóactivos<sup>14-16</sup>. Por tanto, es de vital importancia elucidar cómo las propiedades de los sistemas dirradicales están determinadas por factores intramoleculares tales como la naturaleza del esqueleto conjugado, el perfil de sustitución o requerimientos estéricos, así como por factores intermoleculares que, a su vez, están controlados por las restricciones intramoleculares<sup>17</sup>.

El objetivo principal de esta Tesis es llevar a cabo un estudio exhaustivo de las propiedades electrónicas y estructurales de ciertos sistemas basados en Cz y su homólogo de cadena larga llamado Indolcarbazol (ICz), combinando estudios experimentales (espectroscopía electrónica y vibracional) y teóricos (cálculos químico-cuánticos basados en la teoría DFT).

En los capítulos I y II, se han estudiado diferentes modificaciones estructurales, como el cambio de sustitución<sup>14</sup>, el aumento del esqueleto conjugado<sup>15</sup> o la isomería<sup>17</sup> de sistemas dirradicales basados en Cz e ICz con grupos dicianometilenos (DCM) terminales con el fin de descubrir la conexión entre los cambios estructurales y el carácter dirradical. Además, como se ha comentado anteriormente, estos sistemas dirradicales son capaces de formar nuevos enlaces C-C dando lugar a estructuras de mayor tamaño, llamadas ciclofanos. Por tanto, nuestra investigación también se ha centrado en explorar la relación entre el carácter dirradical y la formación/disociación del



## 5. Resumen y conclusiones

ciclofano, así como estudiar si esta transformación es reversible o no.

En el capítulo III, hemos realizado un estudio en profundidad de las propiedades estructurales, fotofísicas y de transporte de carga de diferentes familias de macrociclos basados en Cz que muestran características prometedoras en el campo de la electrónica orgánica<sup>18</sup>.

Para hacer una discusión de resultados clara, hemos clasificado esta Tesis en dos bloques distintos:

### **Bloque A. Compuestos dirradicales basados en Cz e ICz.**

Este primer bloque está dividido en dos capítulos.

Capítulo I, denominado “*Evolution of the diradical character of dicyanomethylene substituted carbazole and indolocarbazole-based systems*”. En este capítulo, se lleva a cabo un estudio puramente teórico donde el principal objetivo es entender la relación entre el carácter diradical y las modificaciones estructurales. Para ello, se han explorado tres cambios estructurales diferentes:

1) El efecto del patrón de sustitución: aquí nos hemos centrado en la comparativa entre un Cz con grupos DCM sustituidos en para y un Cz con grupos DCM sustituidos en meta (ver Figura 5.3a).

2) El efecto del aumento de la cadena: aquí nos hemos centrado en la comparativa entre los Cz mencionados en el punto

anterior y sus respectivos homólogos basados en ICz (ver Figura 5.3b).

3) El efecto de la isomería: aquí nos hemos centrado en el estudio de los cinco isómeros que presenta el sistema ICz. Además, hemos incluido grupos DCM tanto en posición meta como para, dando lugar a una serie de diez isómeros (ver Figura 5.3c).

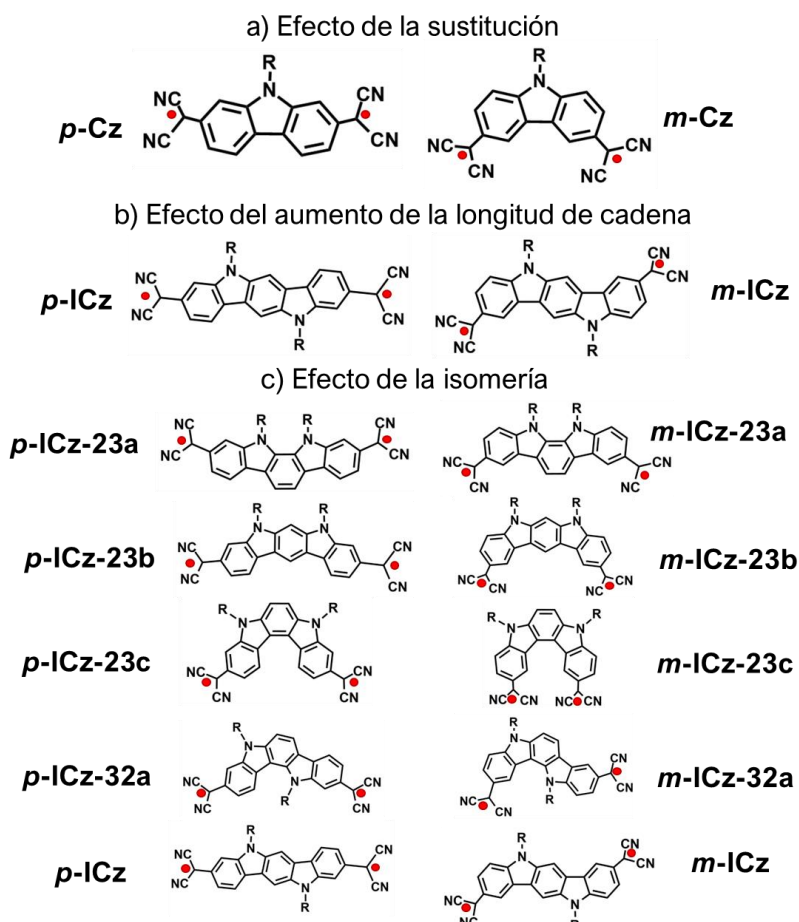


Figura 5.3 Conjunto completo de sistemas basados en Cz e ICz sustituidos por DCM estudiados en este capítulo. Se ha clasificado en base a diferentes modificaciones estructurales

como (a) el efecto de la sustitución de DCM, (b) el efecto del aumento de la cadena y (c) el efecto de la isomería.

Capítulo 2, denominado “*Cyclophane self-assembly from carbazole and indolocarbazole-based diradicals.*” En este capítulo, el principal objetivo es estudiar como las condiciones externas afectan a las propiedades y a la organización supramolecular de sistemas basados en Cz e ICz. En concreto, nos hemos centrado en la formación/disociación de ciclofanos que responden a estímulos, y exploraremos la transformación dinámica y reversible entre las estructuras de ciclofano y sus dirradicales monoméricos aislados ante estímulos (presión, temperatura, etc). Con este fin, llevamos a cabo un estudio experimental de una familia de dirradicales basados en Cz e ICz con grupos DCM terminales (ver Figura 5.4).

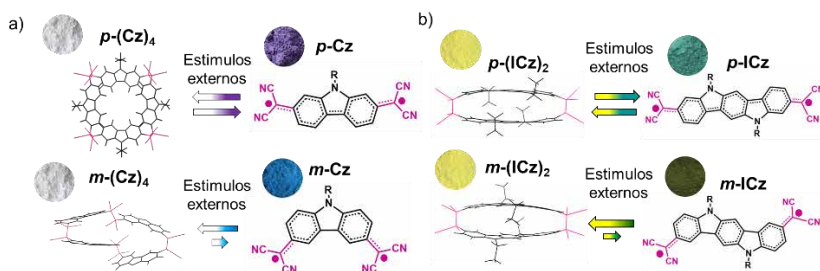


Figura 5.4 Equilibrio entre los ciclofanos y sus correspondientes monómeros dirradicales sustituidos con DCM.

### Bloque B. Macrociclos basados en Cz para electrónica orgánica.

En el bloque anterior, nos enfocamos en cómo la reactividad química y las propiedades físicas de sistemas dirradicales basados en Cz e ICz se ven afectados por los cambios estructurales. Sin embargo, los sistemas orgánicos conjugados



## 5. Resumen y conclusiones

basados en Cz también han sido reconocidos como “estructuras esenciales” en electrónica orgánica debido a sus buenas propiedades electrónicas, como altas movilidades de transporte de huecos, con respecto a otros heterociclos.

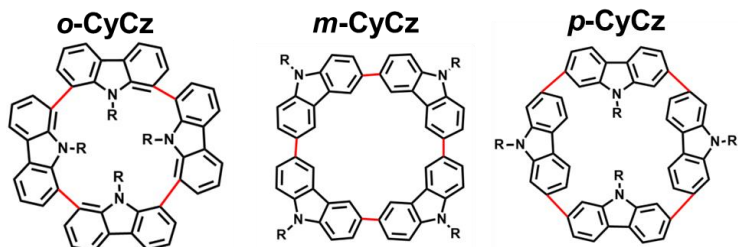
En los últimos años se ha demostrado que la ciclación de sistemas orgánicos conjugados tiene numerosos beneficios para el desarrollo de dispositivos electrónicos. Así, los macrociclos conjugados basados en Cz aparecen en este escenario como una familia emergente de materiales con gran potencial para aplicaciones electrónicas. Por esa razón, el Capítulo III, denominado “*Photophysical and charge transport properties of carbazole-based macrocycles*”, se centra en los macrociclos basados en Cz con el objetivo de explorar sus propiedades electrónicas, fotofísicas y de transporte de carga. Para ello, este capítulo se ha organizado en tres secciones diferentes (Figura 5.5):

1) Una primera sección en la que exploramos el efecto de las posiciones de enlace orto, meta y para entre las unidades Cz en macrociclos basados en tetra-carbazol.

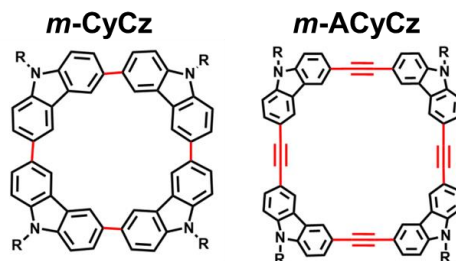
2) Una segunda sección en la que investigamos cómo afecta al sistema la inserción de un grupo etileno entre las unidades de Cz en un macrociclo basado en tetra-carbazol y, por lo tanto, como cambian sus propiedades de transporte de carga.

3) Un tercer apartado donde realizamos un estudio puramente teórico de una familia de macrociclos fusionados basados en Cz para probar la utilidad de estas macroestructuras en el campo de la electrónica orgánica.

a) Efecto de la posición de enlace



b) Efecto de la inserción de etileno



c) Efecto de la fusión y la isomería

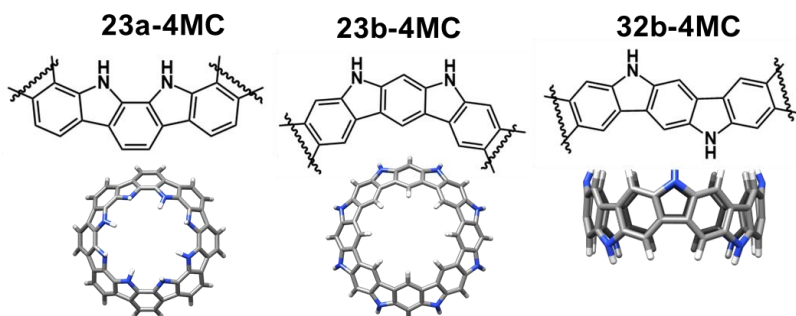


Figura 5.5 Conjunto completo de los macrociclos basados en Cz estudiados en el bloque B. Se ha clasificado en base a diferentes cambios estructurales como (a) el efecto de la posición de enlace (orto, meta o para), (b) el efecto de la inserción de un grupo etileno y (c) el efecto de la fusión y de la isomería.

## 5.2 Metodología

Para llevar a cabo esta Tesis, se han empleado técnicas espectroscópicas de absorción electrónica UV-Vis-NIR, infrarrojo (IR) y Raman (resonante y no resonante), tanto a temperatura



## 5. Resumen y conclusiones

ambiente como a temperatura variable. También se ha realizado espectroscopía Raman a presión variable. En algunos casos concretos, se ha usado espectroscopía de orden difusional (DOSY NMR) enfocado a los ciclofanos basados en ICz. Además, se han realizado cálculos químico-cuánticos basados en la teoría DFT, que nos han permitido la interpretación de los espectros y nos han aportado mayor información sobre el papel que juegan las interacciones inter e intramoleculares en nuestros sistemas.

### 5.3 Resultados y discusión.

A continuación, detallaremos los resultados más relevantes obtenidos de los sistemas derivados de Cz estudiados en esta Tesis Doctoral.

#### **Capítulo I: Evolución del carácter dirradical de los sistemas basados en carbazol e indolcarbazol sustituidos con dicianometileno.**

*Chapter I: Evolution of the diradical character of dicyanomethylene substituted carbazole and indolocarbazole-based systems.*

Dentro de este capítulo, llevamos a cabo un estudio puramente teórico donde el objetivo principal fue comprender la relación entre el carácter dirradical y las modificaciones estructurales. Con este fin, se exploraron tres cambios estructurales diferentes:

❖ Efectos del patrón de sustitución en la estabilidad de los dirradicales (Figura 5.3a). Los resultados obtenidos demostraron que el cambio de sustitución de los grupos DCM terminales



## 5. Resumen y conclusiones

desde la posición -para a la -meta propicia un aumento del carácter dirradical, ya que los sistemas sustituidos en -meta disminuyen la deslocalización electrónica debido a la interrupción de la conjugación lineal, dando lugar a centros radicalarios con menor interacción entre sí y promocionando la forma dirradical.

❖ Efectos del aumento de la longitud de cadena en la estabilidad de los dirradicales (Figura 5.3b). Los resultados de este estudio demostraron que, al aumentar la longitud de la cadena, existe un menor acoplamiento entre los electrones desapareados, lo que se traduce en un incremento del carácter dirradical. Este incremento fue todavía más acusado en el caso del ICz sustituido en -meta como consecuencia de lo expuesto en el punto anterior.

❖ Efectos de la isomería en la estabilidad de los dirradicales (Figura 5.3c). En este estudio, investigamos teóricamente cómo la isomería estructural y la sustitución afectan a las propiedades ópticas y electrónicas de los sistemas basados en ICz. Los diez isómeros resultantes se dividieron en dos subgrupos en función de la posición de sustitución de DCM: los sistemas para-sustituidos con valores de carácter dirradical que abarcan un amplio rango ( $\sim 0.4-0.9$ ) y sus homólogos meta-sustituidos que muestran valores mayores en un rango más estrecho ( $\sim 0.7-0.95$ ). Además, los resultados mostraron grandes diferencias en el carácter aromático y/o anti-aromático lo que modifica la conjugación lineal de los sistemas y, por ende, el carácter dirradical.





## 5. Resumen y conclusiones

En general, estos resultados demuestran cómo pequeños cambios estructurales afectan las propiedades de los sistemas estudiados.

### **Capítulo II: Autoensamblaje de ciclofanos a partir de dirradicales basados en carbazol e indolcarbazol.**

*Chapter II: Cyclophane self-assembly from carbazole and indolocarbazole-based diradicals.*

En este capítulo se llevó a cabo un estudio experimental para entender cómo las condiciones externas afectan la estructura molecular y la organización supramolecular de una familia de sistemas basados en Cz e ICz. Como se expuso anteriormente, este estudio se centró en la formación/disociación de ciclofanos sensibles a estímulos, y exploramos la transformación dinámica y reversible ante estímulos externos (como la presión o la temperatura) entre el ciclofano y su correspondiente monómero aislado. Con este propósito, presentamos un estudio óptico y vibracional de una familia de dirradicales basados en Cz e ICz (Figura 5.6 y 5.7) con grupos DCM incorporados a través de posiciones -para (***p*-Cz** y ***p*-ICz**) o -meta (***m*-Cz** y ***m*-ICz**). La síntesis de los sistemas ***p*-Cz**, ***p*-ICz** y ***m*-ICz** ha sido realizada por el grupo del Prof. Hongxiang Li, del Instituto de Química Orgánica de Shanghai de la Academia de Ciencias de China (Shanghai, China). La síntesis del sistema ***m*-Cz** ha sido realizada por el grupo del profesor Shu Seki, de la escuela de ingeniería de la Universidad de Kyoto (Kyoto, Japón).

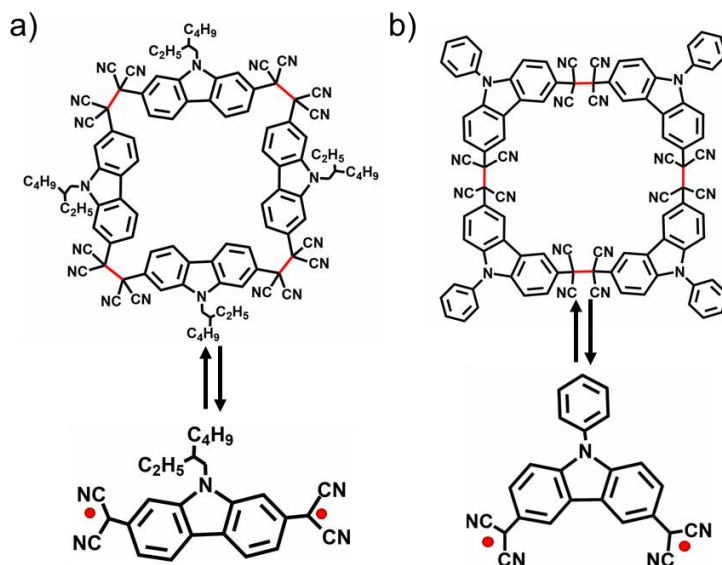


Figura 5.6 Equilibrio entre las estructuras tetraméricas y sus correspondientes dirradicales aislados sustituidos con grupos DCM terminales para el compuesto ***p*-Cz** (a) y ***m*-Cz** (b).

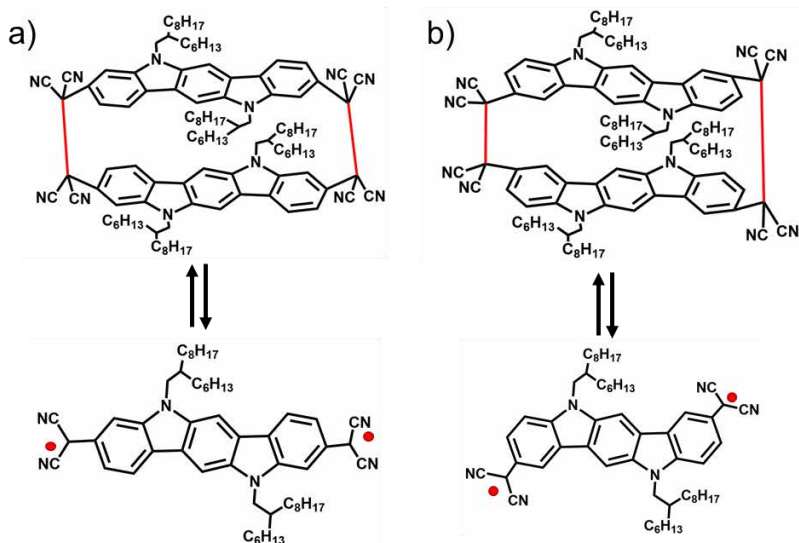


Figura 5.7 Equilibrio entre las estructuras diméricas y sus correspondientes dirradicales aislados sustituidos con grupos DCM terminales para el compuesto ***p*-ICz** (a) y ***m*-ICz** (b).



## 5. Resumen y conclusiones

Los resultados de este capítulo demostraron que todos estos sistemas son capaces de formar enlaces C-C entre electrones desapareados dando lugar a ciclofanos tetraméricos para el caso de los sistemas más cortos y ciclofanos diméricos en el caso de los compuestos ICz.

Por un lado, se llevó a cabo un estudio en disolución donde se registraron los espectros electrónicos de los cuatro compuestos. En ellos se observó un grupo de bandas por debajo de los 500 nm, correspondiente con la estructura del ciclofano, presentes en los cuatro compuestos. Sin embargo, en el caso del compuesto **p-Cz**, se observó que, al medir una disolución de cloroformo con el tiempo, aparecía un conjunto de bandas entre 500-700 nm, correspondientes a la formación del monómero dirradical aislado. La aparición de esta banda se intensificaba al aumentar la temperatura, asociada con un cambio gradual de color de transparente a morado.

En el caso del compuesto **p-ICz**, el tiempo no era un estímulo suficiente para dar lugar a la formación del monómero aislado por lo que su espectro se mantenía prácticamente igual. Sin embargo, al someterlo a condiciones más extremas (preparación de una disolución de *orto*-diclorobenceno y calentamiento hasta temperaturas de 410 K) se obtenía la aparición de un conjunto de bandas entre 600-900 nm asociada al monómero dirradical, junto con un cambio de color de amarillo a azul-verdoso.

A diferencia de los sistemas para-sustituídos, los compuestos que tienen los grupos DCM en meta no mostraban



## 5. Resumen y conclusiones

ningún cambio al ser sometidos a condiciones externas similares, cuando se encuentra en disolución. Estos resultados demostraron que tanto el perfil de sustitución como el aumento de la longitud de la cadena son capaces de condicionar en gran medida el comportamiento de los sistemas dando lugar a ciclofanos más estables y con fuertes interacciones  $\pi$ - $\pi$  en el caso de los meta-sustituidos.

De cara a estudiar cómo actúan estos sistemas en estado sólido, se utilizaron técnicas espectroscópicas como Raman o IR. Además, también se emplearon condiciones externas como temperatura (hasta 520 K) o presión (hasta 5.6 GPa).

En el caso de los sistemas basados en Cz, se observó que al molturar los compuestos ***p*-Cz** y ***m*-Cz** se producía un cambio de color de blanco a morado y a azul oscuro, respectivamente, demostrando la ruptura del enlace C-C en estado sólido. Haciendo uso de la espectroscopía IR, se registró el espectro del sólido blanco inicial y se vio que en ambos sistemas aparecía una banda intensa a  $2253\text{ cm}^{-1}$  relacionada con la vibración de tensión de CN,  $\nu(\text{CN})$ , que es muy similar a la observada en los nitrilos no conjugados ( $2252\text{ cm}^{-1}$ ), demostrando la presencia del ciclofano aromático.

En el caso del sistema ***p*-Cz**, el cambio de color, producido al preparar una pastilla de bromuro potásico (KBr), se acompaña de la aparición de una nueva banda muy intensa a  $2206\text{ cm}^{-1}$ , indicando una transformación entre el ciclofano aromático y el monómero dirradical. Esto ocurre porque en el ciclofano aromático, los grupos CN, están conectados a átomos de C con



## 5. Resumen y conclusiones

hibridación  $sp^3$  que cambian a  $sp^2$  en el monómero quinoide. Por tanto, la aparición de esta nueva banda, junto con la banda a  $2253\text{ cm}^{-1}$ , indica la presencia tanto de monómero aislado como de ciclofano tras la aplicación de presión en ***p-Cz***. Sin embargo, al calentar la pastilla de KBr, obtuvimos la desaparición completa de la banda asociada al ciclofano. Para el caso del compuesto ***m-Cz***, después de calentar la pastilla se obtiene la banda asociada al monómero aislado, pero siempre con la presencia de la banda a  $2253\text{ cm}^{-1}$ . Por tanto, estos resultados demuestran que la meta-sustitución en los sistemas más cortos dificulta la disociación del ciclofano en estado sólido.

En el caso de los sistemas más largos, se observó que los ciclofanos son más difíciles de disociar ya que es necesario someterlos a presiones mucho más extremas para conseguir un cambio de color como se obtuvo en los sistemas basados en Cz. Sin embargo, a alta temperatura, la formación del monómero aislado en estado sólido se ve significativamente favorecida en el compuesto ***m-ICz***, mientras que la presencia del ciclofano siempre prevalece en su homólogo sustituido en -para.

Por lo tanto, la cromo-actividad en respuesta a estímulos externos (como la temperatura o la presión) puede modularse adecuadamente con cambios apropiados en la estructura química. Así, este estudio ayuda a identificar nuevas estrategias de diseño potenciales para materiales sensibles a estímulos.



### Capítulo III: Propiedades fotofísicas y de transporte de carga de macrociclos basados en carbazol.

*Chapter III: Photophysical and charge transport properties of carbazole-based macrocycles.*

En los dos capítulos anteriores, se han estudiado las propiedades electrónicas y moleculares de sistemas dirradicales basadas en Cz e ICz. Sin embargo, como se expuso anteriormente, se ha demostrado que la ciclación de sistemas orgánicos conjugados tiene numerosos beneficios para el desarrollo de dispositivos electrónicos. Por tanto, en este capítulo hemos querido hacer un estudio de macrociclos basados en Cz con un gran potencial para aplicaciones electrónicas. Gracias al estudio desarrollado aquí, podremos comprender cómo se ve afectado el sistema para distintos macrociclos y, de esa forma, conocer en mayor profundidad la química que hay detrás de estos compuestos. Con este fin, se exploraron tres patrones diferentes:

❖ Influencia de la posición de enlace entre unidades de Cz vecinas (Figura 5.5a). Los resultados obtenidos demostraron que el cambio en la posición de enlace (-orto, -meta o -para) conduce una enorme diversidad estructural que va desde una estructura en forma de cinturón en **p-CyCz** con conjugación radial a una conformación en forma de anillo en **m-CyCz** y una estructura en forma de anillo de dos pisos en **o-CyCz**. Esta gran variedad estructural se traduce en un aumento significativo del HL gap al pasar de -para a -meta a -orto como resultado de la disminución



## 5. Resumen y conclusiones

de la conjugación entre las unidades de Cz; esto es especialmente relevante en el caso de **o-CyCz**, debido a los grandes ángulos de torsión entre las unidades Cz. Esta afirmación se vio reforzado con los experimentos hechos mediante espectroscopía electrónica de absorción, en los que las bandas sufrían un desplazamiento hipsocrómico desde **p-CyCz** ( $\lambda = 397$  nm) a **m-CyCz** ( $\lambda = 372$  nm) y a **o-CyCz** ( $\lambda = 347$  nm), lo que indica que la conexión -para es la forma más eficiente de mejorar la conjugación  $\pi$ . Además, nuestros resultados muestran que la ciclación puede ser una nueva estrategia para mejorar la fosforescencia en los sistemas. De hecho, al comparar la molécula aislada de Cz con su homólogo tetra-lineal y su correspondiente macrociclo (**m-CyCz**), encontramos una relación entre la estructura conjugada y los niveles de energía del estado excitado que podría influir drásticamente en las características de la fosforescencia. La fosforescencia promovida por la ciclación puede actuar además como guía para diseñar nuevas moléculas fosforescentes orgánicas puras.

La síntesis de los sistemas **p-CyCz**, **m-CyCz** y **o-CyCz** ha sido realizada por el grupo del Prof. Cyril Poriel, de la Universidad de Rennes (Rennes, Francia), por el grupo de Prof. Feihe Huang del centro de “*Chemistry of High-Performance & Novel materials*” (Hangzhou, China) y por el grupo del Prof. Shuhei Higashibayashi del instituto de ciencia molecular (Okazaki, Japón), respectivamente.

❖ Influencia de la inserción de un grupo etileno entre unidades de Cz vecinas (Figura 5.5b). Los resultados



## 5. Resumen y conclusiones

experimentales (obtenidos mediante espectroscopía UV-Vis y Raman) y teóricos mostrados en este capítulo demostraron que la planarización del sistema, gracias a la inserción de grupos etilenos, provoca un incremento de la conjugación y una mejora en las interacciones intermoleculares, favoreciendo el transporte de carga. De hecho, en esta sección, se fabricaron OFETs para evaluar las propiedades de transporte de carga de los dos macrociclos basados en Cz a nivel experimental. El compuesto ***m*-CyCz** exhibió movilidades de huecos de  $\sim 5.5 \cdot 10^{-6} \text{ cm}^2\text{V}^{-1}\text{s}^{-1}$ , mientras que el sistema ***m*-ACyCz** mostró movilidades de alrededor de  $\sim 1.5 \cdot 10^{-4} \text{ cm}^2\text{V}^{-1}\text{s}^{-1}$ . Esto confirma que el aumento de conjugación facilita el transporte de carga intramolecular y, por lo tanto, mejora la movilidad en los dispositivos OFETs. La síntesis del compuesto ***m*-ACyCz** ha sido realizada por el grupo del Prof. Jeffrey Moore de la universidad de Illinois (Illinois, USA).

❖ Influencia de la fusión y la isomería (Figura 5.5c). De cara a probar la utilidad de ciertas macroestructuras basadas en Cz en el campo de la electrónica orgánica, llevamos a cabo en esta sección un estudio puramente teórico de diferentes coronoides basados en tres isómeros ICz. Nuestros resultados teóricos predicen estructuras en forma de cuenco para los isómeros **23a-4MC** y **23b-4MC**, mientras que el macrociclo **32b-4MC** muestra una estructura en forma de cinturón. Se han estudiado las energías de reorganización de las tres macroestructuras y se observó que los valores más bajos de energía de reorganización de huecos ( $\lambda_h$ ) se obtienen para las moléculas en forma de cuenco **23a-4MC** y **23b-4MC**; sin embargo, para el isómero **32b-**





## 5. Resumen y conclusiones

**4MC** con forma de cinturón, se predicen valores de  $\lambda_h$  más grandes, lo que afecta al transporte de carga. De hecho, se encuentran valores significativos de integral de transferencia de huecos ( $t_h$ ) para las estructuras diméricas **23a-4MC** y **23b-4MC**, mientras que los valores disminuyen para los modelos diméricos basados en el sistema **32b-4MC**.

### 5.4 Conclusiones.

El objetivo principal de esta Tesis es llevar a cabo un estudio exhaustivo de las propiedades electrónicas y estructurales de ciertos sistemas basados en Cz y su homólogo de cadena larga llamado Indolcarbazol (ICz), combinando estudios experimentales (espectroscopia electrónica y vibracional) y teóricos (cálculos químico-cuánticos basados en la teoría DFT). A continuación, se presentan las principales conclusiones obtenidas en el apartado de resultados.

---

Capítulo I: Evolución del carácter dirradical de los sistemas basados en carbazol e indolcarbazol sustituidos con dicianometileno.

---

En este capítulo, nuestros cálculos han demostrado que diferentes modificaciones estructurales (como el patrón de sustitución, el aumento de la longitud de cadena o la isomería) representan una forma muy efectiva de modular el carácter dirradical en sistemas basados en Cz e ICz.

En la sección 3.1.2, demostramos que, en comparación con la conexión -para, la inserción de los grupos DCM vía -meta da como resultado un mayor carácter dirradical. Nuestros



## 5. Resumen y conclusiones

resultados sugieren que esto se debe al hecho de que las unidades Cz e ICz sustituidas en la posición -para muestran una ruta de conjugación más larga que aumenta la deslocalización electrónica, mientras que la posición -meta disminuye la deslocalización debido a la interrupción de la conjugación lineal. Además, demostramos que el aumento en la longitud de la cadena (de moléculas Cz a ICz) implica un aumento notable en el carácter dirradical. En otras palabras, el aumento de la longitud de cadena provoca una menor interacción entre los electrones no apareados (valores pequeños de  $J_{ab}$  y  $\Delta E_{S-T}$ ), lo que da como resultado un gran carácter dirradical.

En la sección 3.1.3, nuestros cálculos basados en los isómeros ICz sugieren que el diferente grado de aromatización entre las partes externa y central de la columna vertebral implica una menor deslocalización, lo que resulta en un aumento del carácter dirradical. Además, se ha demostrado la presencia de estados de doble excitón (H,H-L,L) con una gran semejanza con el espectro de absorción experimental del sistema **p-ICz**. Curiosamente, las distorsiones por planaridad podrían implicar modificaciones notables en la conjugación molecular y, en consecuencia, en el carácter dirradical.

---

Capítulo II: Autoensamblaje de ciclofanos a partir de dirradicales a base de carbazol e indolcarbazol.

---

En este capítulo, demostramos el potencial de los dirradicales basados en Cz y ICz sustituidos con DCM en el campo de la química dinámica covalente. Todos estos sistemas



## 5. Resumen y conclusiones

pueden formar estructuras de ciclofano con la formación de enlaces C-C largos entre electrones no apareados de los centros radicales. Mientras que los dirradicales basados en Cz pueden formar tetrámeros macrocíclicos, los análogos de ICz pueden construir dímeros tipo sándwich. Por otro lado, también se encuentra que el patrón de sustitución afecta en gran medida a la estabilidad del ciclofano, dando como resultado, agregados más estables con enlaces C-C más fuertes y notables interacciones  $\pi$ - $\pi$  para la sustitución -meta. De hecho, en el sistema ***p-Cz*** se da una transformación dinámica entre el monómero aislado y el ciclofano, tanto en disolución como en estado sólido, mientras que la disociación del enlace C-C, en disolución, no se produce en el compuesto ***m-Cz***.

Los sistemas basados en ICz son capaces de formar agregados más estables en comparación con sus homólogos de cadena corta. Por ejemplo, comparado con el compuesto ***p-Cz***, el sistema ***p-ICz*** requiere aplicar estímulos externos más agresivos para conseguir la ruptura del ciclofano con la consiguiente formación del monómero aislado.

Por lo tanto, nuestros resultados demuestran que el comportamiento del ciclofano está fuertemente modulado por la sustitución de los grupos DCM y del incremento del tamaño de la cadena. Además, la cromo-actividad en respuesta a estímulos externos (como la temperatura o la presión) puede modularse adecuadamente con cambios apropiados en la estructura química. Creemos que este estudio ayuda a identificar nuevas



estrategias de diseño potenciales para materiales sensibles a estímulos.

---

### Capítulo III: Propiedades fotofísicas y de transporte de carga de macrociclos basados en carbazol.

---

En la primera parte de este capítulo, nuestros resultados demostraron que la conectividad entre unidades vecinas de Cz en los macrociclos provocan una enorme variedad estructural, dando lugar a conformaciones de tipo cinturón con conjugación radial (como el sistema ***p-CyCz***), de tipo anillo (como el sistema ***m-CyCz***), o en forma de doble silla (como el sistema ***o-CyCz***). Esta amplia variedad de disposiciones espaciales tiene una gran influencia en parámetros como la p-conjugación o el HL gap, medibles mediante espectroscopía UV-Vis y Raman. Todo esto, nos permite desarrollar nuevos sistemas con propiedades electrónicas únicas.

En la sección 3.3.2.2, nuestros datos revelan una novedosa estrategia para mejorar la fosforescencia mediante la ciclación. Comparando una unidad de Cz aislado con su tetrámero lineal y su correspondiente macrociclo, se ha encontrado una relación entre la conjugación en las estructuras y los niveles energético de los estados excitados, que podrían tener una gran influencia en la fosforescencia. Esto hace que el término “*cyclization-promoted phosphorescence*” o fosforescencia promovida por la ciclación actúe como guía para el diseño de moléculas fosforescentes totalmente orgánicas.



## 5. Resumen y conclusiones

En la sección 3.3.3.1, la inserción de grupos etilenos entre unidades de Cz vecinas en un tetra-ciclo lleva a un incremento en la planaridad del sistema y, por ende, a una mejora de la interacción electrónica intermolecular. Como resultado, la movilidad de huecos experimental es dos órdenes de magnitud mayor en el caso del sistema ***m*-CyCz**, dando lugar a dispositivos más eficientes

En la sección 3.3.3.2, nuestros resultados teóricos basados en macrociclos totalmente fusionados predijeron estructuras tipo cuenco para los isómeros **23a-4MC** y **23b-4MC**, mientras que el macrociclo **32b-4MC** muestra una estructura con forma de cinturón. Esta diferencia tiene un gran impacto en la agrupación de moléculas afectando las propiedades de transporte de carga. De hecho, gracias al solapamiento más favorable entre moléculas adyacentes, los sistemas diméricos **23a-4MC** y **23b-4MC** han mostrado considerables valores de integral de transferencia, a diferencia de su análogo dimérico **32b-4MC**.

### 5.5 Referencias.

1. Cui, Z., Abdurahman, A., Ai, X., & Li, F, Stable luminescent radicals and radical-based LEDs with doublet emission. *CCS chemistry* **2020**, 2, (4), 1129-1145.
2. Hu, X.; Wang, W.; Wang, D.; Zheng, Y., The electronic applications of stable diradicaloids: present and future. *Journal of Materials Chemistry C* **2018**, 6, (42), 11232-11242.
3. Juetten, M. J.; Buck, A. T.; Winter, A. H., A radical spin on viologen polymers: organic spin crossover materials in water. *Chemical Communications* **2015**, 51, (25), 5516-5519.



## 5. Resumen y conclusiones

4. Jin, Y.; Yu, C.; Denman, R. J.; Zhang, W., Recent advances in dynamic covalent chemistry. *Chemical Society Reviews* **2013**, 42, (16), 6634-6654.
5. Takashi, K.; Akihiro, S.; Maki, S.; Mikio, U.; Kyuya, Y.; Masayoshi, N.; Daisuke, S.; Kazunobu, S.; Takeji, T.; Yasushi, M.; Kazuhiro, N., Synthesis, Intermolecular Interaction, and Semiconductive Behavior of a Delocalized Singlet Diradical Hydrocarbon. *Angewandte Chemie* **2005**, 117 (40), 6722-6726;
6. Kolc, J.; Michl, J.,  $\pi$ -Biradicaloid hydrocarbons. Pleiadene family. I. Photochemical preparation from cyclobutene precursors. *Journal of the American Chemical Society* **1973**, 95 (22), 7391-7401;
7. Abe, M., Diradicals. *Chemical Reviews* **2013**, 113 (9), 7011-7088.
8. Dewar, M. J. S.; Healy, E. Ab initio study of the chair cope rearrangement of 1,5-hexadiene. *Chemical Physics Letters*, **1987**, 141, 521-524.
9. Li, Z.; Hou, Y.; Li, Y.; Hinz, A.; Chen, X. Biradicaloid and Zwitterion Reactivity of Dicarbondiphosphide Stabilized with NHeterocyclic Carbenes. *Chemistry - European Journal* **2018**, 24, 4849-4855
10. Thomas, H. M.; Kumari, H.; Maddalena, J.; Mayhan, C. M.; Ellis, L. T.; Adams, J. E.; Deakyne, C. A., Conformational preference and dynamics of pyrogallol[4]arene: stability, interconversion, and solvent influence. *Supramolecular Chemistry* **2018**, 30 (5-6), 520-532.
11. Huang, J.; Kertesz, M., Intermolecular Covalent  $\pi$ - $\pi$  Bonding Interaction Indicated by Bond Distances, Energy Bands, and Magnetism in Biphenalenyl Diradicaloid Molecular Crystal. *Journal of the American Chemical Society* **2007**, 129 (6), 1634-1643.
12. Zafra, J. L.; Qiu, L.; Yanai, N.; Mori, T.; Nakano, M.; Alvarez, M. P.; Navarrete, J. T. L.; Gómez-García, C. J.; Kertesz, M.; Takimiya, K.; Casado, J., Reversible Dimerization and Polymerization of a Janus Diradical To Produce Labile C-C



## 5. Resumen y conclusiones

Bonds and Large Chromic Effects. *Angewandte Chemie International Edition* **2016**, 55 (47), 14563-14568.

13. Rowan, S. J.; Cantrill, S. J.; Cousins, G. R. L.; Sanders, J. K. M.; Stoddart, J. F. Dynamic Covalent Chemistry. *Angewandte Chemie International Edition*, **2002**, 41, 898–952.

14. Badía-Domínguez, I.; Peña-Álvarez, M.; Wang, D.; Pérez Guardiola, A.; Vida, Y.; Rodríguez González, S.; López Navarrete, J. T.; Hernández Jolín, V.; Sancho García, J. C.; García Baonza, V.; Nash, R.; Hartl, F.; Li, H.; Ruiz Delgado, M. C., Dynamic Covalent Properties of a Novel Indolo[3,2-b]carbazole Diradical. *Chemistry – A European Journal* **2021**, 27, (17), 5509-5520.

15. Badía-Domínguez, I.; Pérez-Guardiola, A.; Sancho-García, J. C.; López Navarrete, J. T.; Hernández Jolín, V.; Li, H.; Sakamaki, D.; Seki, S.; Ruiz Delgado, M. C., Formation of Cyclophane Macrocycles in Carbazole-Based Biradicaloids: Impact of the Dicyanomethylene Substitution Position. *ACS Omega* **2019**, 4, (3), 4761-4769.

16. Wang, D., Capel Ferron, C., Li, J., Gámez-Valenzuela, S., Ponce Ortiz, R., Lopez Navarrete, J. T., Hernández Jolín V., Yang X., Peña-Álvarez M., García Baonza V., Hartl F., Ruiz Delgado M.C. and Li, H. New Multiresponsive Chromic Soft Materials: Dynamic Interconversion of Short 2,7-Dicyanomethylenecarbazole-Based Diradicaloid and the Corresponding Cyclophane Tetramer. *Chemistry – A European Journal* **2017**, 23 (55), 13776-13783.

17. Badía-Domínguez I., Canola S., Hernández Jolín V., López Navarrete J.T., Sancho-García J.C., Negri F. and Ruiz Delgado M.C., Tuning the Diradical Character of Indolocarbazoles: Impact of Structural Isomerism and Substitution Position. *Journal of physical chemistry letters*, **2022**, 13, 6003-6010.

18. Zhu H., Badía-Domínguez I., Shi B., Li Q., Wei P., Xing H., Ruiz Delgado MC, and Huang F., Cyclization-Promoted Ultralong Low-Temperature Phosphorescence via Boosting Intersystem Crossing. *Journal of the American Chemical Society*, **2021**, 143, 2164–2169.









# SECTION 6. Appendix

## Table of contents

---

- A. List of abbreviations and symbols
- B. List of publications





## Section 6: Appendix

### Appendix A. List of abbreviations and symbols.

#### Acronyms

BS-UDFT	Broken-Symmetry Unrestricted Density Functional Theory
CPs	Conducting polymers
CS	Closed-shell
CT	Charge transport
Cz	Carbazole
D	Diffusion coefficient
D-A	Donor-Acceptor
DCC	Dynamic Covalent Chemistry
DCM	Dicyanomethylene
DFT	Density Functional Theory
DOSY	Diffusion-Order Spectroscopy
FT-IR	Fourier Transform Infrared
GPC	Gel Permeation Chromatography
HF	Hartree-Fock
HL gap	HOMO-LUMO gap
HOMO	Highest Occupied Molecular Orbital
HPLC	High Performance Liquid Chromatography
ICz	Indolocarbazole
IICz	Diindolocarbazole
ISC	Intersystem Crossing



K	Kelvin
KBr	Potassium Bromide
LUMO	Lowest Unoccupied Molecular Orbital
MOFs	Metal-Organic Frameworks
NICS	Nucleus Independent Chemical Shifting
NIR	Near Infrared
NO	Natural Orbital
OFET	Organic Field-Effect Transistor
OLED	Organic Light-Emitting Diode
OS	Open-shell
OTS	Octadecyltrichlorosilane
PCM	Polarizable Continuum Model
RT	Room Temperature
SOMO	Singly Occupied Molecular Orbital
T	Triplet
TCBG	Top Contact-Bottom Gate
TD-DFT	Time Dependent Density Functional Theory
UV-Vis	Ultraviolet-Visible

### **Symbols**

$\mu_h$	Hole field-effect mobility
$E_{ISC}$	Energy gap of ISC channels
$I_{DS}$	Drain-source current
$I_{on}/I_{off}$	Intensities on/off current ratio
$J_{ab}$	Effective electron exchange interaction



$N^{\text{FOD}}$	Fractional occupation number of hot electrons
$S_0$	Ground electronic state
$\langle S^2 \rangle$	Spin contamination
$S_n$	Excited electronic state
$t$	Transfer integral
$R_h$	Hydrodynamic radio
$V_{\text{DS}}$	Drain-source voltage
$V_{\text{GS}}$	Gate-source voltage
$V_{\text{T}}$	Threshold voltages
$y_0$	Diradical character
$\Delta E_{\text{OS-CS}}$	Energy difference between OS and CS singlet states
$\Delta E_{\text{S-T}}$	Singlet-Triplet energy gap
$\Delta G_f^0$	Gibbs free energy of formation
$\epsilon$	Dielectric constant
$\theta$	Rotation degree
$\lambda_e$	Electron reorganization energy
$\lambda_{\text{exc}}$	Excitation line
$\lambda_h$	Hole reorganization energy
$\Phi_p$	Phosphorescence quantum yield
$\tau_p$	Phosphorescent lifetime

## Appendix B. List of publications.

The research work developed during my PhD has resulted in six publications, four of them directly linked to this Thesis and two additional papers related to parallel investigations.

### **Publications directly linked to the PhD Thesis**

- 1. Formation of Cyclophane Macrocycles in Carbazole-Based Biradicaloids: Impact of the Dicyanomethylene Substitution Position;** Irene Badía-Domínguez, Andrés Pérez-Guardiola, Juan Carlos Sancho-García, Juan T. López Navarrete, Víctor Hernández Jolín, Hongxiang Li, Daisuke Sakamaki, Shu Seki and M. Carmen Ruiz Delgado; ACS omega 2019, 4, 4761-4769.
- 2. Dynamic Covalent Properties of a Novel Indolo[3,2-b]carbazole Diradical;** Irene Badía-Domínguez, Miriam Peña-Álvarez, Deliang Wang, Andrés Pérez-Guardiola, Yolanda Vida, Sandra Rodríguez González, Juan T. López Navarrete, Víctor Hernández Jolín, Juan Carlos Sancho-García, Valentín García Baonza, Rosie Nash, Frantisek Hartl, Hongxiang Li, and M. Carmen Ruiz Delgado; Chem. Eur. J. 2021, 27, 1-13 (*hot paper*).
- 3. Cyclization-Promoted Ultralong Low-Temperature Phosphorescence via Boosting Intersystem Crossing;** Huangtianzhi Zhu, Irene Badía-Domínguez, Bingbing Shi, Qi





Li, Peifa Wei, Hao Xing, M. Carmen Ruiz Delgado, and Feihe Huang; *J. Am. Chem. Soc.* 2021, 143, 2164-2169.

- 4. Tuning the Diradical Character of Indolocarbazoles: Impact of Structural Isomerism and Substitution Position;** Irene Badía-Domínguez, Sofia Canola, Víctor Hernández Jolín, Juan T. López Navarrete, J. Carlos Sancho-García, Fabrizia Negri and M. Carmen Ruiz Delgado; *J. Phys. Chem. Lett.* 2022, 13, 6003–6010.

#### Other publications

- 1. Sigmoidally hydrochromic molecular porous crystal with rotatable dendrons;** Hiroshi Yamagishi, Sae Nakajima, Jooyoung Yoo, Masato Okazaki, Youhei Takeda, Satoshi Minakata, Ken Albrecht, Kimihisa Yamamoto, Irene Badía-Domínguez, Maria Moreno Oliva, M. Carmen Ruiz Delgado, Yuka Ikemoto, Hiroyasu Sato, Kenta Imoto, Kosuke Nakagawa, Hiroko Tokoro, Shin-ichi Ohkoshi and Yohei Yamamoto; *Comm. Chem.* 2020, 3, 1-8.
- 2. Probing the nature of donor–acceptor effects in conjugated materials: a joint experimental and computational study of model conjugated oligomers;** Trent E. Anderson, Evan W. Culver, Irene Badía-Domínguez, Wyatt D. Wilcox, Claire E. Buysse, M. Carmen Ruiz Delgado and Seth C. Rasmussen; *Phys. Chem. Chem. Phys.* 2021, 23, 26534-26546.



- 3. Molecular Tuning in Diaryl-Capped Pyrrolo[2,3-d:5,4-d']bisthiazoles: Effects of Terminal Aryl Unit and Comparison to Dithieno[3,2-b:2',3'-d]pyrrole Analogues;**  
Eric J. Uzelac, Irene Badía-Domínguez, Spencer J. Gilman, M. Carmen Ruiz Delgado and Seth C. Rasmussen; *Molecules* 2022, 27, 6638.



## Formation of Cyclophane Macrocycles in Carbazole-Based Biradicaloids: Impact of the Dicyanomethylene Substitution Position

Irene Badía-Domínguez,<sup>1</sup> Andrés Pérez-Guardiola,<sup>2</sup> Juan Carlos Sancho-García,<sup>1,3</sup> Juan T. López Navarrete,<sup>1</sup> Víctor Hernández Jolin,<sup>1</sup> Hongxiang Li,<sup>3</sup> Daisuke Sakamaki,<sup>4</sup> Shu Seki,<sup>4</sup> and M. Carmen Ruiz Delgado\*<sup>1</sup>

<sup>1</sup>Department of Physical Chemistry, University of Malaga, Campus de Teatinos s/n, 29071 Malaga, Spain

<sup>2</sup>Department of Physical Chemistry, University of Alicante, 03080 Alicante, Spain

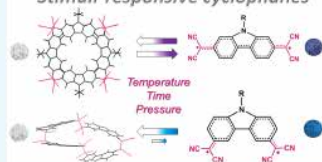
<sup>3</sup>Key Laboratory of Synthetic and Self-Assembly Chemistry for Organic Functional Materials, Shanghai Institute of Organic Chemistry, Chinese Academy of Sciences, No. 345 Lingling Road, Shanghai 200032, China

<sup>4</sup>Department of Molecular Engineering, Graduate School of Engineering, Kyoto University, Nishikyo-ku, Kyoto 615-8510, Japan

### Supporting Information

**ABSTRACT:** We have recently demonstrated that carbazole-based biradicaloids are promising building blocks in dynamic covalent chemistry. To elucidate their intriguing dynamic covalent chemical properties, it is necessary to understand the physical origin of their biradical nature. To this end, here we focus on two quinoid carbazole systems substituted with dicyanomethylene (DCM) groups via para (*p*-Cz-alkyl) or meta positions (*m*-Cz-ph), which are able to form cyclophane macrocycles by the formation of long C–C bonds between the bridgehead carbon atoms linked to the DCM groups. We aim at exploring the following questions: (i) How is the biradicaloid character of a quinoid carbazole affected by the substitution position of the DCM groups? (ii) How is the stability of the resulted cyclophane aggregate attained? (iii) How is the dynamic interconversion between the carbazole-based monomers and cyclophane aggregates affected by this subtle change in the substitution pattern position? Density functional theory-based calculations reveal that both *p*-Cz-alkyl and *m*-Cz-ph are open-shell biradicaloids in the ground electronic state, with the DCM substitution in the meta position resulting in a more pronounced biradical character. In contrast, the derivatization via the nitrogen of the carbazole unit is not predicted to affect the biradicaloid character. The spontaneous nature of the cyclophane-based macrocycle formation (i.e., the cyclic tetramer in *p*-Cz-alkyl and the cyclic trimer and the tetramer in *m*-Cz-ph) is supported by the negative relative Gibbs free energies calculated at 298 K. Interestingly, cyclic oligomers in which the DCM groups are inserted in the meta position tend to adopt folded conformations with attractive  $\pi$ – $\pi$  interactions resulting in more stable aggregates; in contrast, note that an extended ring-shaped conformation is acquired for (*p*-Cz-alkyl)<sub>n</sub>. In addition, the larger spin density on the bridgehead carbon atom in the meta-substituted system strengthens the bridging C–C bond in the aggregate forms, hampering its dissociation. In fact, the C–C bond dissociation of (*m*-Cz-ph)<sub>n</sub> and (*m*-Cz-ph)<sub>n</sub> was suppressed in solution state, although it was achieved in solid state in response to soft external stimuli (i.e., temperature and grinding). In summary, we report a very comprehensive study aiming at elucidating the challenging chemical properties of carbazole-based biradicaloid systems.

### Stimuli-responsive cyclophanes



## 1. INTRODUCTION

Recently, the development of the chemistry of  $\pi$ -conjugated biradical species has attracted much interest because of their unique optical,<sup>1</sup> electronic,<sup>2</sup> and magnetic properties.<sup>3</sup> According to IUPAC, a biradical is described as a molecular entity with two radical centers (possibly delocalized), which act nearly independently of each other.<sup>4</sup> In other words, systems characterized by two unpaired electrons with a long distance between them would result in distinct singlet and triplet electronic states because of the negligible interelectronic interaction. The elucidation of the electronic configuration of

these systems is fundamental to understand their electronic and structural properties.<sup>5</sup> However, it is possible that two radical centers interact significantly, and in this case, these species are better defined as biradicaloids according to the IUPAC Gold Book.<sup>6</sup> These species have two representative resonance forms in the ground states: (i) a closed-shell (CS)

Received: December 5, 2018

Accepted: February 19, 2019

Published: March 4, 2019



## Stimuli-Responsive Materials | Hot Paper

 Dynamic Covalent Properties of a Novel Indolo[3,2-*b*]carbazole Diradical

 Irene Badía-Domínguez,<sup>[a]</sup> Miriam Peña-Álvarez,<sup>[b,1]</sup> Deliang Wang,<sup>[c]</sup>  
 Andrés Pérez Guardiola,<sup>[d]</sup> Yolanda Vida,<sup>[e,1]</sup> Sandra Rodríguez González,<sup>[a]</sup>  
 Juan T. López Navarrete,<sup>[a]</sup> Víctor Hernández Jolin,<sup>[a]</sup> Juan C. Sancho García,<sup>[d]</sup>  
 Valentín García Baonza,<sup>[g]</sup> Rosie Nash,<sup>[h]</sup> František Hartl,<sup>[i]</sup> Hongxiang Li,<sup>[e,2]</sup> and  
 M. Carmen Ruiz Delgado<sup>[a,2]</sup>

**Abstract:** This work describes the synthesis and properties of a dicyanomethylene-substituted indolo[3,2-*b*]carbazole diradical ICz-CN. This quinoidal system dimerises almost completely to (ICz-CN)<sub>2</sub>, which contains two long C(sp<sup>2</sup>)–C(sp<sup>2</sup>)  $\sigma$ -bonds between the dicyanomethylene units. The minor open-shell ICz-CN component in the solid-state mixture was identified by EPR spectroscopy. Cyclic voltammetry and UV–visible spectroelectrochemical data, as well as comparison with reference monomer ICz-Br reveal that the nature of the one-electron oxidation of (ICz-CN)<sub>2</sub> at ambient temperature and ICz-CN at elevated temperature is very similar in all these compounds due to the prevailing localization of their HOMO on the ICz backbone. The peculiar cathodic behaviour reflects the co-existence of (ICz-CN)<sub>2</sub> and ICz-CN.

The involvement of the dicyanomethylene groups stabilizes the close-lying LUMO and LUMO+1 of (ICz-CN)<sub>2</sub> and especially ICz-CN compared to ICz-Br, resulting in a distinctive cathodic response at low overpotentials. Differently from neutral ICz-CN, its radical anion and dianion are remarkably stable under ambient conditions. The UV/Vis–(NIR) electronic transitions in parent (ICz-CN)<sub>2</sub> and ICz-CN and their different redox forms have been assigned convincingly with the aid of TD-DFT calculations. The  $\sigma$ -bond in neutral (ICz-CN)<sub>2</sub> is cleaved in solution and in the solid-state upon soft external stimuli (temperature, pressure), showing a strong chromism from light yellow to blue–green. Notably in the solid state, the monomeric diradical species is predominantly formed under high hydrostatic pressure (> 1 GPa).

## Introduction

Chromo-active materials have attracted much interest of the scientific community in different fields as they are able to reversibly change colour when 1) exposed to certain light energies (photochromic switches),<sup>[1,2]</sup> 2) slightly deformed with

small compressive strain<sup>[3,4]</sup> or 3) lightly heated/cooled.<sup>[5–7]</sup> Reversible homolytic covalent bond cleavage/formation involving radical species has been recently demonstrated to be an efficient strategy to obtain multi-responsive chromic soft materials.<sup>[8–10]</sup> Owing to this property, organic mono- and diradicals have emerged as essential building blocks in dynamic covalent

[a] I. Badía-Domínguez, Dr. S. Rodríguez González, Prof. J. T. López Navarrete, Prof. V. Hernández Jolin, Prof. M. C. Ruiz Delgado  
 Department of Physical Chemistry, University of Málaga  
 Campus de Teatinos s/n, 29071, Málaga (Spain)  
 E-mail: camend@uma.es

[b] Dr. M. Peña-Álvarez  
 Present address: Centre for Science at Extreme Conditions & School of Physics and Astronomy, University of Edinburgh, Edinburgh EH9 3FD (UK)

[c] Dr. D. Wang, Prof. H. Li  
 Key Laboratory of Synthetic and Self-assembly Chemistry for Organic Functional Materials, Shanghai Institute of Organic Chemistry, Chinese Academy of Sciences, Shanghai, 200032 (China)  
 E-mail: hli@sioc.ac.cn

[d] A. Pérez Guardiola, Prof. J. C. Sancho García  
 Department of Physical Chemistry, University of Alicante  
 03080 Alicante (Spain)

[e] Prof. Y. Vida  
 Departamento de Química Orgánica, Universidad de Málaga—IBIMA  
 Campus de Teatinos s/n, 29071 Málaga (Spain)

[f] Prof. Y. Vida  
 Centro Andaluz de Nanomedicina y Biotecnología-IBANAND  
 Parque Tecnológico de Andalucía, C/ Severo Ochoa 35  
 29590 Campanillas, Málaga (Spain)

[g] Prof. V. García Baonza  
 MALTA Consolider Team and Instituto de Geociencias IGEO (CSIC-UCM)  
 University Complutense of Madrid, 28040 Madrid (Spain)

[h] R. Nash, Prof. F. Hartl  
 Department of Chemistry of Reading  
 Whiteknights, Reading RG6 6DX (UK)  
 E-mail: f.hartl@reading.ac.uk

[i] Dr. M. Peña-Álvarez  
 MALTA Consolider Team, Department of Physical Chemistry I  
 Chemistry Faculty, University Complutense of Madrid  
 28040 Madrid (Spain)

Supporting Information and the ORCID identification numbers for the authors of this article can be found under:  
<https://doi.org/10.1002/chem.202005211>.

## Cyclization-Promoted Ultralong Low-Temperature Phosphorescence via Boosting Intersystem Crossing

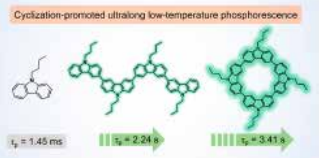
Huangtianzhi Zhu, Irene Badia-Domínguez, Bingbing Shi, Qj Li, Peifa Wei, Hao Xing\*, M. Carmen Ruiz Delgado,\* and Feihe Huang\*

 Cite This *J. Am. Chem. Soc.* 2021, 143, 2164–2169

Read Online

ACCESS | Metrics &amp; More | Article Recommendations | Supporting Information

**ABSTRACT:** Ultralong organic phosphorescence holds great promise as an important approach for optical materials and devices. Most of phosphorescent organic molecules with long lifetimes are substituted with heavy atoms or carbonyl groups to enhance the intersystem crossing (ISC), which requires complicated design and synthesis. Here, we report a cyclization-promoted phosphorescence phenomenon by boosting ISC. *N*-butyl carbazole exhibits a phosphorescence lifetime ( $\tau_p$ ) of only 1.45 ms and a low phosphorescence efficiency in the solution state at 77 K due to the lack of efficient ISC. In order to promote its phosphorescence behavior, we explored the influence of conjugation. By linear conjugation of four carbazole units, possible ISC channels are increased so that a longer  $\tau_p$  of 2.24 s is observed. Moreover, by cyclization, the energy gap between the singlet and triplet states is dramatically decreased to 0.04 eV for excellent ISC efficiency accompanied by increased rigidification to synergistically suppress the nonradiative decay, resulting in satisfactory phosphorescence efficiency and a prolonged  $\tau_p$  to 3.41 s in the absence of any heavy atom or carbonyl group, which may act as a strategy to prepare ultralong phosphorescent organic materials by enhancing the ISC and rigidification.



### INTRODUCTION

Organic luminogens encompassing fluorescent and phosphorescent molecules are highly desirable because of their wide applications ranging from fundamental research such as sensing and imaging to practical fields including organic light-emitting diodes, data storage, and other advanced optical devices.<sup>1</sup> Especially, long-lived or ultralong phosphorescence of luminous molecules, which is also called afterglow or persistent luminescence, has received considerable attention since the first artificial material with ultralong phosphorescence was acquired in 1866.<sup>2</sup> Broad applications of long-lived phosphorescence in the cases of displays, diagnostic agents, and anticounterfeiting attract lots of scientists, and many excellent examples have been developed with high efficiency and long lifetimes.<sup>3</sup> However, the ultralong-phosphorescent luminogens are mainly limited to transition-metal-doped molecules.<sup>4</sup> Owing to flaws of metal-dope molecules such as intrinsic insulated nature, high costs, and harsh preparation conditions, preparing pure organic molecules with long-lived phosphorescence is of great significance.

Compared with transition-metal-doped complexes, metal-free organic molecules usually exhibit weak phosphorescence that is caused by an insufficient intersystem crossing (ISC) from singlet to triplet state and the rapid nonradiative decay of triplet excitons.<sup>5</sup> In order to achieve ultralong phosphorescence

of metal-free organic molecules, promoting ISC and rigidifying molecular motion to suppress nonradiative decay seem to be indispensable. By crystallization, freezing, host–guest doping, fixed in framework materials, mixed with polymers, etc, numerous metal-free systems with ultralong organic phosphorescence (UOP) have been established.<sup>6</sup> Most of the molecules with UOP contain substitutions like carbonyls, heteroatoms, and halogens to facilitate the spin–orbital coupling (SOC).<sup>7</sup> However, these functional groups tend to increase the rates of  $S_1-T_1$  and  $T_1-S_0$  transitions simultaneously. As such, an inherent dilemma exists that increasing phosphorescence efficiency always leads to decreased lifetime.<sup>8</sup> Developing novel strategies to increase phosphorescence property in the absence of carbonyls and heavy atoms will provide new guidelines to design phosphorescent molecules and more approaches for preparing optical materials.

Carbazole derivatives have been found to inherit persistent phosphorescent lifetimes ( $\tau_p$ ) due to their lowest triplet excited

 Received: December 5, 2020  
 Published: January 14, 2021


## Tuning the Diradical Character of Indolocarbazoles: Impact of Structural Isomerism and Substitution Position

Irene Badía-Domínguez, Sofía Canola, Víctor Hernández Jolín, Juan T. López Navarrete, Juan C. Sancho-García, Fabrizia Negri,\* and M. Carmen Ruiz Delgado\*

 Cite This: *J. Phys. Chem. Lett.* 2022, 13, 6003–6010

Read Online

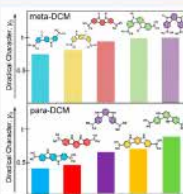
ACCESS |

Metrics &amp; More

Article Recommendations

Supporting Information

**ABSTRACT:** In this study, a set of 10 positional indolocarbazole (IC<sub>2</sub>) isomers substituted with dicyanomethylene groups connected via *para* or *meta* positions are computationally investigated with the aim of exploring the efficiency of structural isomerism and substitution position in controlling their optical and electronic properties. Unrestricted density functional theory (DFT), a spin-flip time-dependent DFT approach, and the multireference CASSCF/NEVPT2 method have been applied to correlate the diradical character with the energetic trends (i.e., singlet–triplet energy gaps). In addition, the nucleus-independent chemical shift together with ACID plots and Raman intensity calculations were used to strengthen the relationship between the diradical character and (anti)aromaticity. Our study reveals that the substitution pattern and structural isomerism represent a very effective way to tune the diradical properties in IC<sub>2</sub>-based systems with *meta*-substituted systems with a V-shaped structure displaying the largest diradical character. Thus, this work contributes to the elucidation of the challenging chemical reactivity and physical properties of diradicaloid systems, guiding experimental chemists to produce new molecules with desirable properties.



Diradical systems present two unpaired electrons localized at two different regions with a non-negligible interaction. The coupling interaction between the radical centers determines (i) the open-shell (OS) singlet or triplet (T) ground state and (ii) the degree of diradical character of a molecule fluctuating from pure diradical ( $y_0 = 1$ ) to closed-shell (CS) electronic structure ( $y_0 = 0$ ). Particularly interesting is the case of OS singlet diradical molecules, which feature a large number of relevant properties compared to CS systems, for instance, a small HOMO–LUMO gap (H–L gap), largely improved two-photon absorption (TPA) toward the near-infrared (near-IR) region, or a remarkable magnetic activity emerging from thermally populated triplet states.<sup>1–3</sup> However, diradicals share a complicated electronic structure; one configuration dominates the electronic wave function, and several possess equal or similar weights. In fact, although OS and CS notations for singlet states are frequently used in the literature, some alternative terms also exist (i.e., “disjoint” or “joint” diradicals based on a delocalized to localized orbital transformation that interchanges CS and OS descriptions), as has been shown in a recent review.<sup>4</sup>

In the past several decades, the chemistry of diradical systems, mainly the preparation of stable long-lived OS molecules, has been greatly developed to exploit these systems in many promising applications in the fields of organic electronics and spintronics and to design nonlinear optical devices.<sup>5–12</sup> Quantum chemical (QC) investigations are essential for determining structure–property relationships for these molecules and for rationalizing the variations of

electronic and geometrical properties as a function of the degree of OS singlet nature.<sup>13–16</sup> Among others, the quantitative estimation of diradical character with QC approaches is remarkably relevant because it enables a deeper understanding of the nature of chemical bonds, thereby illuminating the best structure–property relationships in OS molecular systems. A widely used diradical character descriptor is the  $y_0$  parameter, defined as twice the weight of the doubly excited configuration,<sup>17–20</sup> and it can be calculated via spin-unrestricted approaches.<sup>21</sup> More recently, other descriptors have been proposed, such as the  $N^{\text{ROD}}$  parameter, based on finite-temperature density functional theory (FT-DFT) and measuring the appearance of “hot” or strongly correlated electrons.<sup>21,23</sup>

In the past few years, there has been more interest in the rationalization of how the extent of diradical character is influenced by structural changes introduced to stabilize (or destabilize) the diradical system. Because of the tremendous effort of organic chemists, more stable singlet diradical molecules with controllable amounts of diradical character have been synthesized and characterized.<sup>24,25</sup>

 Received: May 3, 2022  
 Accepted: June 20, 2022